La collana della Scuola di Alta Formazione Dottorale accoglie le migliori tesi di dottorato dell'Università degli Studi di Bergamo, insignite della dignità di stampa e sottoposte a procedura di *blind peer review*.

Additive Manufacturing (AM) is progressively consolidating its role within high value-added sectors such as healthcare, driving the transformation of contemporary medicine toward patient-specific and technologically advanced solutions. Within this evolving landscape, this work investigates Material Extrusion (MEX). Through controlled feedstock deposition, this versatile and scalable technology enables the fabrication of complex and customised geometries that remain scarcely attainable through conventional processes. The research unfolds along two parallel and complementary lines, focusing on polymer-based and metal-based applications to critically assess the technological maturity and medical potential of MEX.

Francesca Sala earned her PhD in Technology, Innovation and Management (37th cycle), a joint Engineering doctoral program between the University of Bergamo and the University of Naples Federico II. Her research developed along two complementary and strategically significant directions: the application of process simulation approaches to industrial and healthcare workflows, and the investigation of Advanced Manufacturing techniques, especially within the medical field. She currently works in the industrial sector as a Process Engineer.

ISBN: 978-88-97253-52-5
DOI: 10.13122/978-88-97253-52-5

Francesca Sala
ADDITIVE MANUFACTURING IN HEALTHCARE

97

Collana della Scuola di Alta Formazione Dottorale
- 97 -

Francesca Sala

ADDITIVE MANUFACTURING APPLICATIONS IN HEALTHCARE

UNIVERSITÀ DEGLI STUDI DI BERGAMO

2026

Collana della Scuola di Alta Formazione Dottorale

Diretta da Paolo Cesaretti

Ogni volume è sottoposto a *blind peer review*.

ISSN: 2611-9927

Sito web: https://aisberg.unibg.it/handle/10446/130100

Francesca Sala

EXPLORING ADDITIVE MANUFACTURING
Applications in the Healthcare Sector

Università degli Studi di Bergamo

2026

Exploring Additive Manufacturing Applications in the Healthcare Sector.
/ Francesca Sala. – Bergamo :
Università degli Studi di Bergamo, 2026.
(Collana della Scuola di Alta Formazione Dottorale; 97)

ISBN: 978-88-97253-52-5
DOI: 10.13122/978-88-97253-52-5

Progetto grafico: Servizi Editoriali – Università degli Studi di Bergamo
© 2018 Università degli Studi di Bergamo
via Salvecchio, 19
24129 Bergamo
Cod. Fiscale 80004350163
P. IVA 01612800167

https://aisberg.unibg.it/handle/10446/330906

Table of contents

Introduction

Additive Manufacturing (AM), also known as 3D printing, is considered one of the most advanced and promising production techniques in the industrial landscape. In recent years, the availability of accessible technologies and biocompatible materials promoted a significant deployment of these methodologies in high-value industrial segments, among which the medical field.

Nowadays, the healthcare sector keeps evolving, moving from a one-fit-all therapeutic approach towards strategies prioritising the differences between patients. Concurrently, progresses in AM and its supporting systems contribute to the trend of personalised medicine by realising medical applications able to meet the needs of each individual diagnostic case.

The adoption of 3D printing processes and products requires a balance between scientific advancements, regulatory compliance and practical implementation considerations, such as production efficiency, cost-effectiveness and alignment with clinical needs and trends. Hence, there is the necessity to invest in research to facilitate and streamline the integration of AM technologies into those areas of medical practice that strongly benefit from their utilisation. In this framework, the present document intends to study AM methodologies, offering an interdisciplinary assessment of the factors that influence the applicability of these technologies within the medical setting. Starting from the identification of specific clinical issues, the analysis examines their medical context and traditional practices to understand how AM can establish itself and transform this environment. Diverse perspectives, such as medical, technological, process and economic aspects, are covered.

To accomplish the objectives of the research, the current document relies on a specific AM methodology and technology, Material Extrusion (MEX). The technique fabricates elements by heating and depositing a feedstock material, usually thermoplastic polymer, from an extrusion head.

The primary focus of the research delves into the adoption of MEX technology for the development of patient-specific orthoses, namely external medical devices designed to support and correct impaired physiological abilities of the musculoskeletal system. This research topic involves devising an innovative manufacturing methodology to address the criticalities deriving from the traditional techniques. The study proposes a multi-step procedure, based on three integrated activities: capturing patient data, processing it into a digital model and, subsequently, 3D printing the medical device. A dedicated software program, based on Python language, is developed to assist healthcare professionals in the digital modelling process of the device. The procedure generates wrist orthosis for joint immobilisation and, furthermore, it is adaptable for producing orthoses for various anatomical regions, demonstrating its efficiency in terms of reliability and flexibility. Alongside,

these positive outcomes encourage the exploration towards innovative orthosis design solutions, characterised by an increased level of customisation, improved lightweight for equivalent strength and durability and greater comfort too. Particularly, the studies evaluate different design techniques, ranging from simpler methods, able to be combined within the developed software, to more complex approaches, requiring in-depth mechanical behaviour analysis of the developed orthoses. A comparative schema, showcasing a collection of distinct orthosis models with varying technical and clinical features, is elaborated to provide healthcare professionals with a valuable tool to guide therapeutic decisions when employing this novel methodology. Also, particular attention is paid to the competitiveness and sustainability of both the AM process and its resulting products, including observations on the economic and production time dimension.

Recent improvements and increased knowledge in MEX processes have broadened its application to metal manufacturing too. This emerging technique, known as Metal Material Extrusion (metal MEX), combines MEX technology with fine metal powders to produce full metal components. The approach tries to fit into the metal AM industry as a simple, affordable, low-energy consumption and safer alternative to those already established in the market. Hence, the secondary research topic provides an insight into the suitability of MEX technology for the production of metal medical components. This research evaluates the production of AISI 316L metal components via MEX, adapting the processing strategies from the established AM metal technologies, such as Powder Bed Fusion (PBF) technologies, to provide knowledge on the MEX-produced samples for medical use.

Chapter 1. Introduction to Additive Manufacturing

1.1 General concepts about Additive Manufacturing

Additive Manufacturing (AM), commonly known as 3D printing, is a relatively new manufacturing methodology that, integrating advanced technologies, fits into the context of Industry 4.0 to address the challenges of the fourth industrial revolution [1].

The term Additive Manufacturing (AM) is used to describe a cluster of technologies, whose manufacturing technique is based on the principle of creating three-dimensional components by depositing layers of material, one on the top of the other. This distinct production mechanism, known as layer-based manufacturing, revolutionises the concept of traditional machining and production processes, that remove/subtract material from a block of raw material or form/cast material into the desired shape.

Historically, AM was conceived and realised for rapid prototyping and tooling. Indeed, its dissemination and adoption in the manufacturing industry is typical only of the latest years [2]. Some of these technologies already existed in the 1950s, but it was not until the 1980s that their advancement enabled the development of the earliest 3D printing technologies. In fact, the roots of the very first AM system dates back to the 1980s: the first technology was developed by Charles 'Chuck' Hull and consisted of polymerisation of thin layers of photosensitive liquid polymer using a UV laser. This methodology is known as stereolithography (SLA) and inspired further different AM approaches and technologies. In the 1990s, Steven Scott Crump developed and patented a process based on the extrusion of polymeric filament, Fused Deposition Modelling (FDM). This technology stood out for its low-cost approach and operational simplicity, making 3D printing accessible to a wider audience. In the same years, Carl Deckard, Joe Beaman e Paul Forderhase developed Selective Laser Sintering (SLS), an approach based on polymer powder (nylon). This innovation paved the way for processes involving the use of metal powders, shifting the research towards systems that would enable to achieve elements with mechanical properties comparable to those obtained using traditional manufacturing techniques.

The fast growth of AM prompted the diffusion and integration of 3D printed parts even in highly regulated industrial sectors, such as military, aerospace, automotive, biomedical and, even, food field. In 2019, the automotive and manufacturing sectors emerged as the most profitable AM segments on a global scale (Figure 1). In particular, around 40% of the global AM market turnover was generated by automotive and manufacturing industries, while aerospace industry accounted for 18% of the total

turnover [3]. This demonstrates how, nowadays, in certain sectors, the utilisation of AM techniques has evolved far beyond rapid prototyping. These methodologies are being exploited in various industries with the aim of achieving significant improvements in process and product performance. In these fields, some AM applications are already at the highest level of technology readiness level (TRL), thus, including low and/or full rate production.

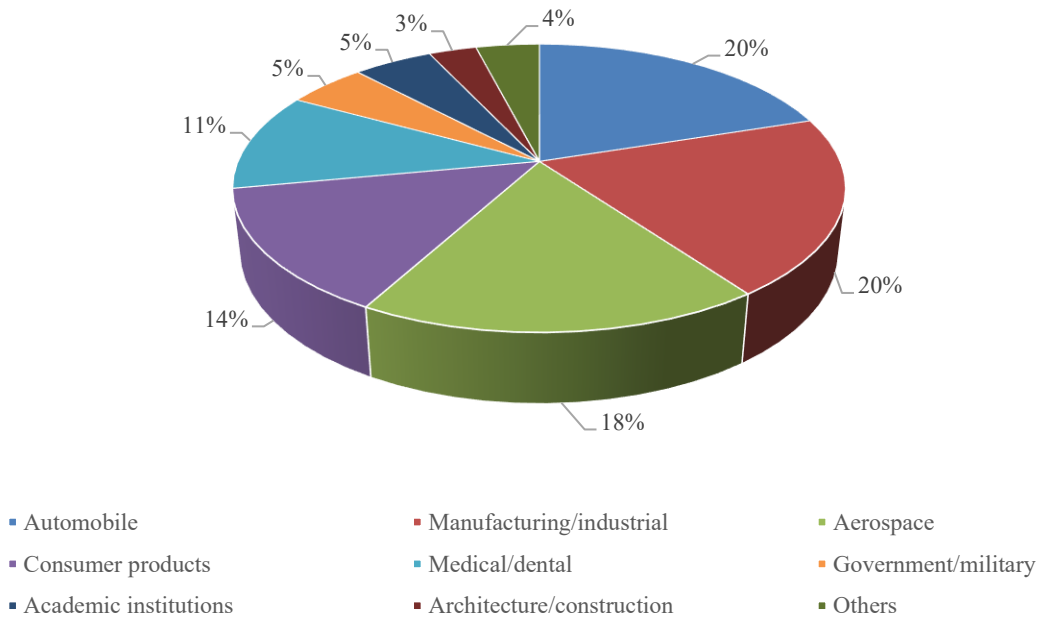

Figure 1. Global AM market revenue distribution by industry, 2019 [3].

As technology keeps progressing, AM systems are radically transforming product design, supply chains and production processes, globally. The increasing spread and adoption of these advanced manufacturing methodologies for the fabrication of small volumes of products, characterised by enhanced complexity and geometric customisation, transform the economies of scale into economies of scope. The industrial landscape is witnessing a transition from the supply chains, designed for traditional high-volume production and cost optimisation, to the so-called demand chains, oriented towards mass customisation [4].

Key concepts related to this transition are described in Figure 2. The left-hand graph (a) of Figure 2 highlights how, for small volume production, AM is more cost-effective than traditional manufacturing techniques, such as forming and subtractive manufacturing methodologies. Although production costs may vary considerably depending on the specific AM technology employed, the costs associated to small production volumes still remain significantly low. This substantial economic advantage partly derives from the elimination of the need to use dedicated moulds and equipment for the production of the part. Specifically, AM avoids additional tooling costs, which in traditional

manufacturing tend to increase with the complexity, intricacy and size of the components being produced. Conversely, the cost of the parts produced via AM remains constant regardless of the geometric and dimensional complexity. Hence, the utilisation of AM techniques suggests the possibility and affordability of realising extremely customised and articulated geometries that, with traditional production methodologies, would be prohibitive. This second aspect is pictured in the right-hand graph (b) of Figure 2.

Looking back to Figure 2a, in contrast to subtractive and forming manufacturing techniques, the cost per AM unit does not decrease significantly as the number of units increases. This is due to the fact that, even eliminating the need for initial mould and tooling, the economic benefits of AM do not change on large production scale owing to process limitation. In this respect, process constraints are mainly related to speed and build capacity. AM is precluded from benefitting from economies of scale.

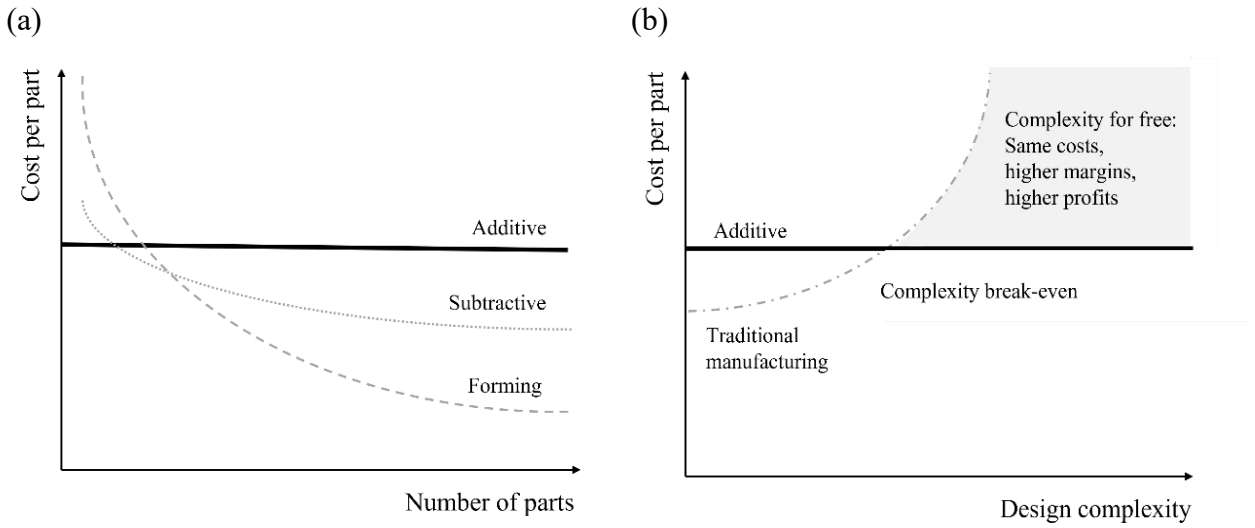

Figure 2. Cost analysis as a function of manufacturing unit (a) and design complexity (b): a comparison between AM and traditional manufacturing (forming and subtractive techniques).

Hence, the decision on the adoption of the most appropriate production process depends on the specific requirements of the project in terms of complexity, volume and cost. In essence, AM distinguishes itself for its ability to create complex and customised geometries, making it ideal for the production of prototypes. Also, AM is suitable for the development of high value and technologically advanced products. Furthermore, AM speeds up manufacturing time and reduces time to market for small production series by preventing unnecessary investment in tooling. In contrast, mass production of standardised parts is obviously not the domain of AM technologies.

Figure 3 denotes the positioning of AM technologies compared to conventional production models. Furthermore, Table 1 summarises and compares the major distinctive features between the AM and conventional manufacturing techniques.

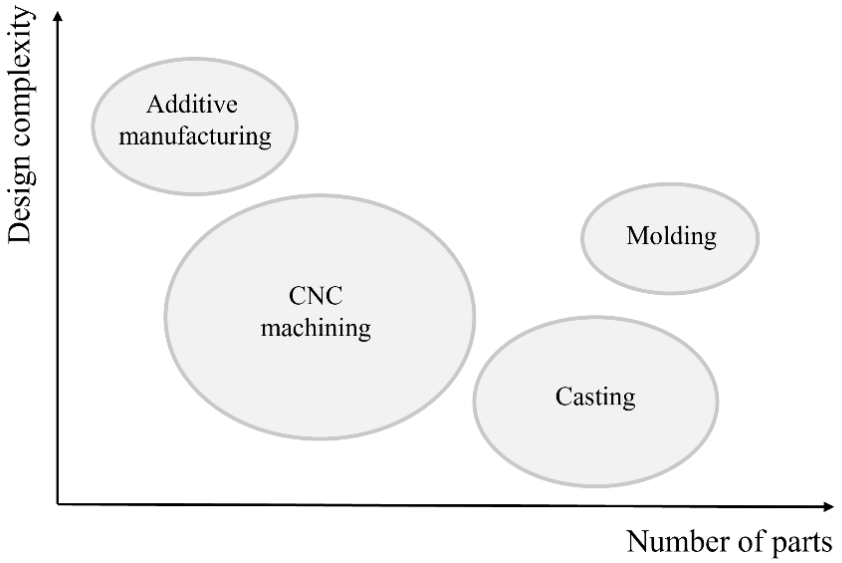

Figure 3. Positioning matrix of the different manufacturing methodologies, among which the AM, as a function of the number of produced parts and design complexity.

	Additive Manufacturing	Traditional Manufacturing
Tooling	Not required	Required
Resource consumption	Resource-efficient	Resource-consuming
Material consumption	Minimal, material is added only where it is needed	Higher, material is removed and discarded
Inventory	Small hands-on inventory	Wide hands-on inventory
Geometry	No limitations, flexible and complex designs are allowed	Limited
Customization	Rapid and easy small one-off production runs	Need for several initial tooling
Production volume	Low volume	High volume
Profitability	Independent of the number of units, efficient for low volume	High volume-based
Production objective	Mass customisation	Mass production

Table 1. Key characteristics distinguishing AM from traditional manufacturing [5].

Over the past decade, AM has grown in notoriety and this optimistic trend is expected to last. Indeed, between 2020 and 2026, the AM market size is estimated to almost triple (Figure 4) [6]. Figure 5 highlights the projected percentages of annual growth rate of AM market from 2020 to 2026. Between 2020 and 2023, the AM industry raised at a compound annual growth rate of about 17%. In the years 2023-2025 and 2025-2026, the global AM market is projected to grow by almost 24% and 20%, respectively [7]. In parallel, innovative materials continue to be developed on a rapid basis: among the fastest-growing materials are metals and metal alloys. In particular, metals are likely to drive the growth of the market, which is currently dominated by polymeric materials. The market for AM materials is expected to rise and reach just below four billion U.S. dollars by 2026.

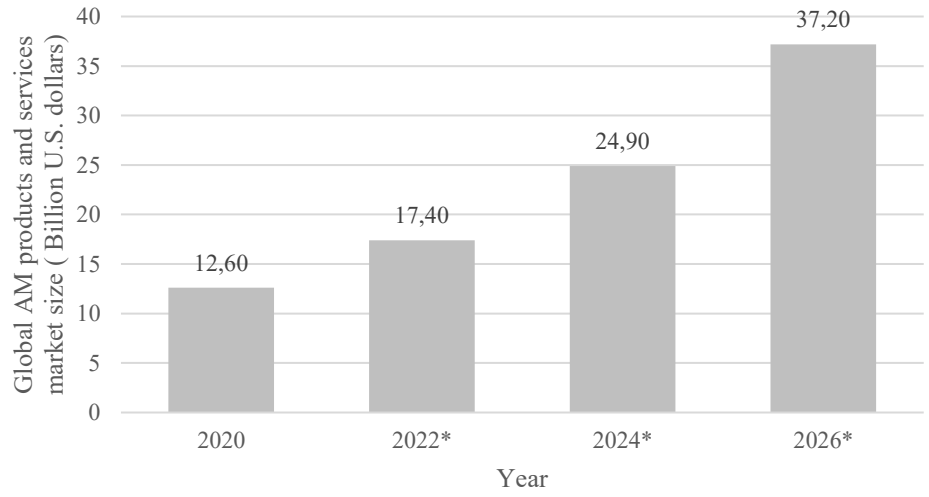

Figure 4. Global AM products and services market size (Billion U.S. dollars), 2020-2026 [6].

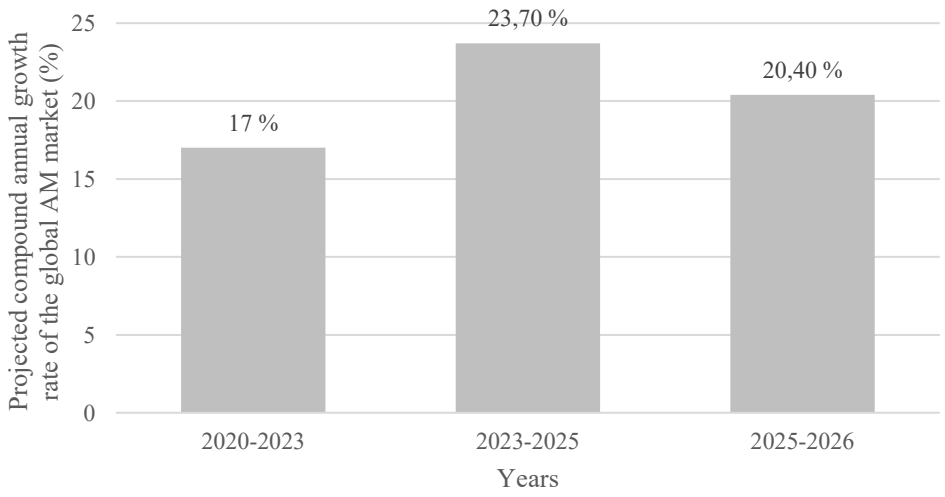

Figure 5. Projected compound annual growth rate of the global AM market, 2020-2026 [7].

1.2 Additive Manufacturing workflow

The process chain for the fabrication of 3D printed elements comprises several activities, each of which contributes to the quality and functionality of the final product (Figure 6). Regardless of the selected 3D printing technology, a number of shared activities to all AM processes, with the purpose of transforming a digital model into its physical prototype, are identified and described hereafter.

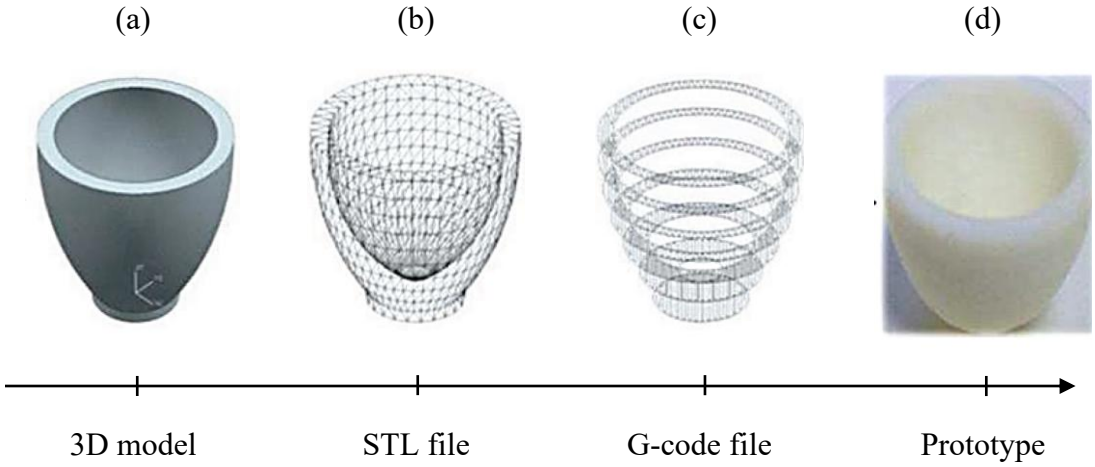

Figure 6. Workflow of the AM activities. (a) Design and modelling of the digital model of the manufacturing part; (b) conversion of the 3D model to STL file format; (c) processing of the digital model with rapid prototyping software; (d) manufacturing of the prototype and post-processing treatments [8].

1. Generation of the digital model of the manufacturing element

   The development of a CAD model is based on the reproduction of the three-dimensional features and characteristics that describe the external geometry of the manufacturing element. The model is created using 3D CAD modelling software, such as AutoCAD, SolidWorks, or Fusion360. Alternatively, if an existing physical model is available, Reverse Engineering (RE) techniques might be used. In this case, the geometry of the physical model is acquired through 3D imaging and scanning techniques, relying on laser scanners, photogrammetry, or Computed Tomography (CT) systems. Generally, the data collected through 3D scanning devices are processed to generate a point cloud, which entails the spatial coordinates describing the surface of the physical model, and, then, data are further elaborated to achieve a watertight solid model and refined to obtain the desired tolerance and shape.
2. Conversion of the digital model to STL file format

   The digital model of the manufacturing element is converted into a file format which is compatible with rapid prototyping software. The most commonly used format is STL (Standard Tessellation Language), a binary or ASCII file format, describing only the

geometric information. This format discretises the continuous surface of the solid part using a network of triangles (tessellation or triangulation): each polygon is characterised by three vertices and a normal indicating the outer surface direction. The discrepancy between the exact geometry of a physical model and its digital approximation introduces discretisation errors [9]. Hence, the STL conversion influences the quality of the resulting digital model: the density of the mesh and the distribution of the grid nodal points are the factors that determine the degree of accuracy and precision with which the digital model approximates the physical one [10].

3. Digital model processing with rapid prototyping software

   The STL file is transferred to a rapid prototyping software, responsible for arranging the digital model for its manufacturing. Commercially available rapid prototyping software packages include Cura, Slic3r or PrusaSlicer.

   In the software environment, the model is positioned and oriented on the building platform to improve the adhesion of the part to the building platform and ensure the successful manufacturing of the part. Orientation influences mechanical performances of the resulting parts, including tensile strength, hardness, surface roughness and dimensional accuracy. Indeed, it is well known that by applying a tensile load parallel to the layers' direction, vice versa, by applying a compression load perpendicular to the layers' direction, the specimen has a higher strength compared to that bearing the same loads in the opposite direction [11]. Moreover, part orientation plays a key role in the trade-off between product accuracy and process time [12]. Also, the correct positioning of the part on the building platform affects material usage and consumption, impacting on manufacturing times and costs.

   Besides part positioning and orientation, the model is subjected to a process known as slicing: the element is segmented into a series of horizontal slices (whose thickness may be either constant either variable), each representing a deposition layer of material. The approximation of sloped surfaces by small vertical steps might prompt the edges of each layer to be visible. This step-like pattern on the surface of the 3D printed element is known as staircase effect (Figure 7) [13]: it is a topographical defect inherent to all AM methodologies. This effect induces a geometrical and dimensional deviation between the digital model and the manufactured prototype [14]. Right from the beginning, significant advancements were made in the development of slicing algorithms capable of varying and adapting layer thicknesses based on the inclination of external surfaces (Figure 8) [15].

   Besides, the software allows to configure and select the process parameters, thereby tailoring the manufacturing activity and the resulting prototype. Depending on the specific AM

technology employed, a unique set of printing parameters is defined. Nevertheless, regardless of the specific AM methodology, common parameters might be identified: profile settings (i.e., layer height and width, infill density and pattern), temperature (i.e., printing temperature and building plate temperature), speed (i.e., printing speed of each line category), cooling, material and support (i.e., overhang angle) and build plate adhesion settings. Once parameters configuration and slicing are completed, the software generates a G-code format file, containing the machine instructions to additively manufacture the part.

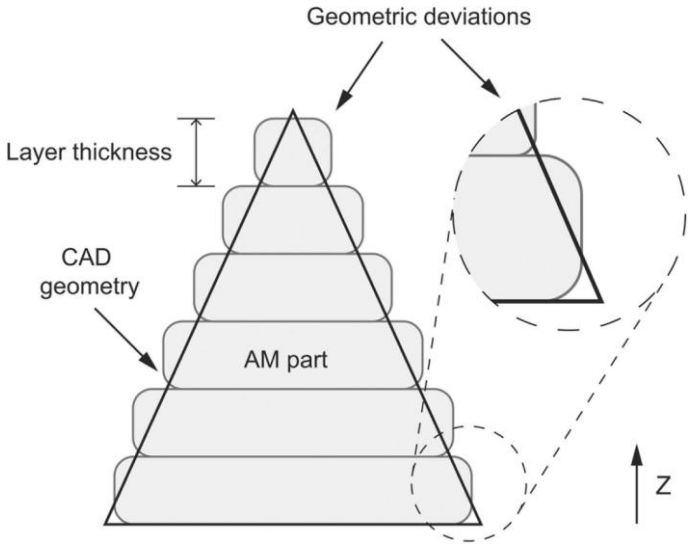

Figure 7. Schematic representation of the staircase effect: topographical error resulting from the mismatch between the digital model and the manufactured prototype [14].

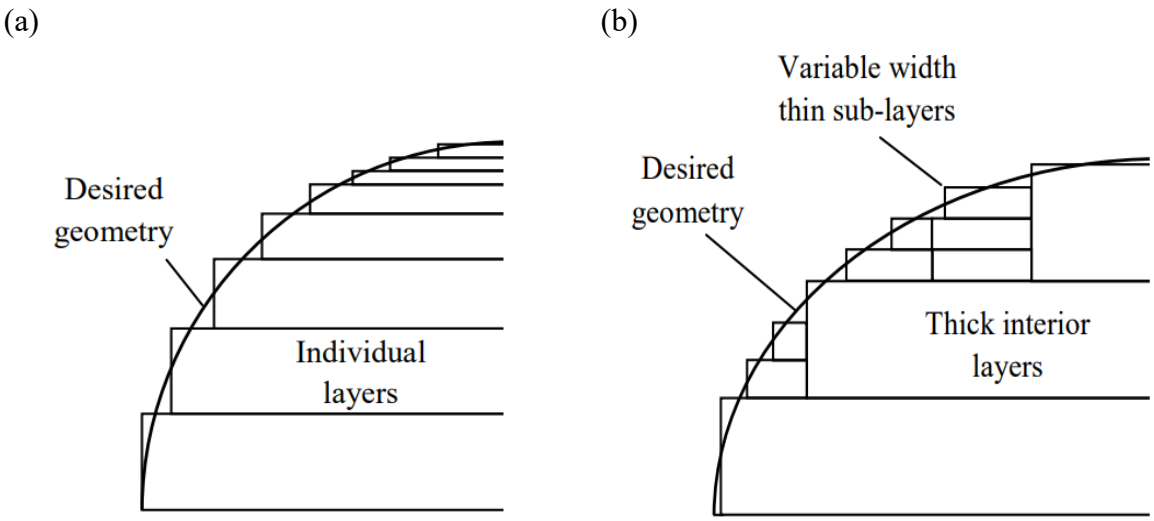

Figure 8. Strategies for minimising the staircase effect: improvement of the surface accuracy through the employment of variable layer thickness (a) and adaptive layer thickness (b)[15].

4. Machine set-up and 3D printing

   Completed the configuration of the process parameters on the slicing software, the actual manufacturing activity takes place. The machine builds the part, layer-by-layer, according to the instructions provided by G-code file. Although the manufacturing process is fully automated, it is advisable to monitor the 3D printing activity to prevent, detect and correct the potential issues that may arise during the process. The timely and efficient detection of defects during the manufacturing process contributes to the optimisation of material consumption and manufacturing times and costs. Lately, advances in Artificial Intelligence (AI) algorithm and cameras, sensors and imaging techniques automated process monitoring to assess the quality of 3D printed parts and prevent the necessity of re-manufacturing the elements [16].

5. Removal of the manufactured model and post-processing activities

   Upon completion of the manufacturing process, the part is removed from the building platform. Before the element is put in place, post-processing activities may be necessary. Usually, these tasks involve removal of the support material, sanding, cleaning, polishing, coatings and other techniques to improve the surface finish. Often, heat or chemical treatments are essential to improve the desired mechanical properties of the manufactured element.

1.2.1 Design for Additive Manufacturing (DfAM)

The intrinsic nature of AM virtually allows the creation of complex geometries without the limitations typically imposed by conventional tooling and manufacturing methods. Nonetheless, this geometric freedom does not translate into the ability of fabricating any shape without criteria. Indeed, to successfully achieve the generation of cost-effective parts characterised by improved performance, it is essential to account for the characteristics of AM processes. Design for Additive Manufacturing (DfAM) represents a fundamental approach, entailing common rules and best practices, to harness the full potential of AM.

A critical aspect, already emerged from the previous section, concerns the positioning and orientation of the part with respect to the printing platform. The building direction, defined along the Z-axis, often differs from the height of the part. In fact, the component might be printed lying down or rotated by an angle with respect to its intended operating configuration. This is particularly relevant with complex geometries, whose orientation might not be trivial, and the choice of their positioning, inevitably, falls into a trade-off between surface quality, mechanical performance, production cost and time and the need to use support structures.

Another key factor is the use of supporting structures. Their role consists in providing support during the printing of critical geometries, such as when the inclination of walls is less than 45° with respect

to the build plate, or with downward surfaces. Generally, it is preferable to minimise the use of support material as an excessive use may hinder their removal in post-processing. So, it is advisable to rethink part characteristics as self-supporting geometries. Another function of these structures consists in the ability to mitigate the risk of distortion and residual stresses (Figure 9). Specifically, in AM systems relying on high-power energy sources, residual stresses might cause deformation of the part, causing a curling or warping of the edges and inducing delamination of the part from the substrate (Figure 10). In more severe cases, these stresses exceed the strength of the part causing catastrophic cracks. Furthermore, in AM methodologies leveraging on high-intensity energy sources, support structures serve to dissipate heat by transferring it away from surface areas to avoid burning, over-melting, distortion and discoloration.

In essence, although the nature of AM systems makes them incredibly flexible in terms of feasible geometries, the characteristics of these processes need to be considered so that manufacturing efficiency, quality and design intents are not compromised.

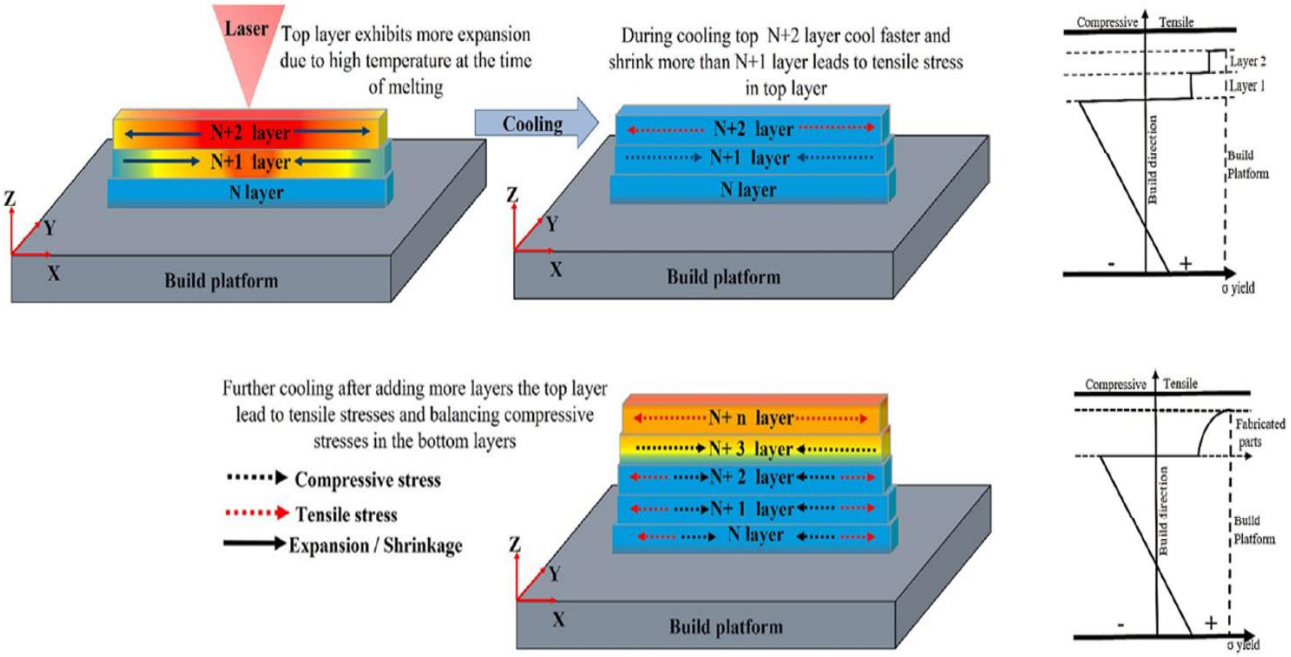

Figure 9. Schematic representation of the mechanism of residual stress formation in AM-produced parts (LPBF) [17].

(a) (b)

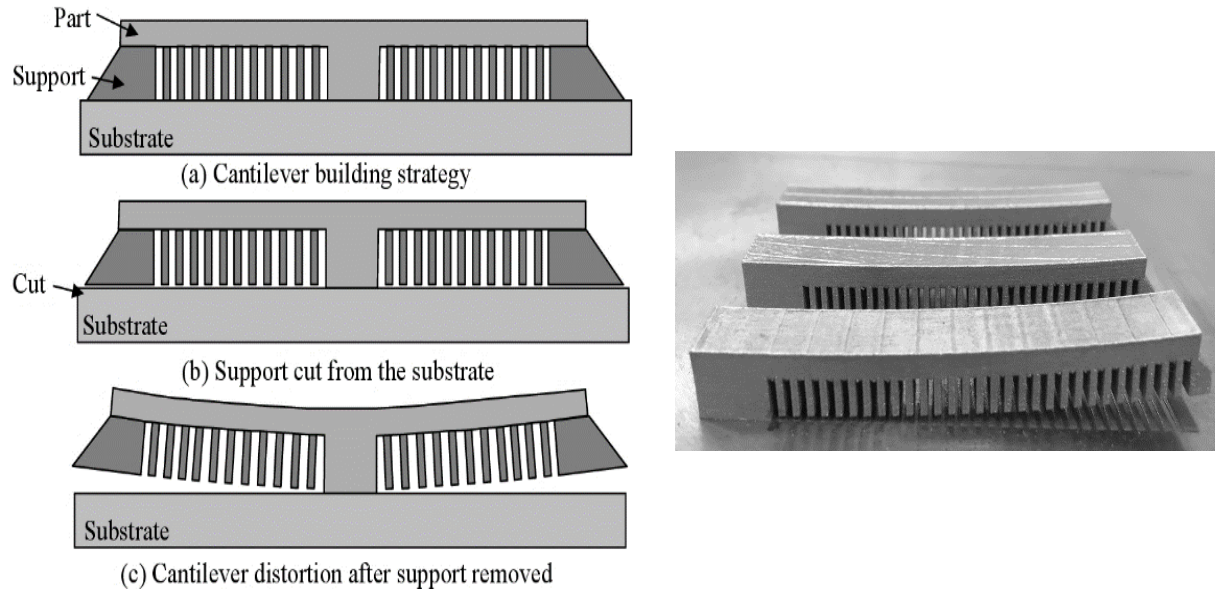

Figure 10. Schematic representation of an AM-produced cantilever building structure before and after support removal from the building platform (a); AM-produced samples characterised by residual stress-induced distortion (b) [18].

1.3 Additive Manufacturing processes

The classification of AM processes has been debated since early systems were introduced onto the market, to the extent that scientific literature presents various classification about the available techniques [19].

According to the UNI EN ISO/ASTM 52900:2022 regulation [20], AM technologies are classified into seven main categories: VAT Photopolymerization (VPP), Material Extrusion (MEX), Powder Bed Fusion (PBF), Binder Jetting (BJT), Material Jetting (MJT), Sheet Lamination (SHL) and Directed Energy Deposition (DED). This classification reflects the variety of each unique and distinct technical approach used to manufacture three-dimensional elements, following a layer-by-layer methodology.

The subsequent sections discuss in detail each technology identified by the normative. Table 2 summarises the key characteristics of each AM principle.

AM Process	Description	Related technologies	Materials
Vat Photo-polymerization (VPP)	Curing of light-reactive liquid material (or resin), collected inside a vat	• Stereolithography (SLA) • Digital Light Processing (DLP) • Continuous Liquid Interface Printing (CLIP) or Continuous Digital Light Processing (CDLP)	Light-curable polymer
Material Extrusion (MEX)	Heating and deposition of material through extrusion nozzles	• Fused Deposition Modelling (FDM)	Polymer, metal, ceramic
Powder Bed Fusion (PBF)	Selective fusion (or sintering) of powder particles in a powder bed through thermal energy sources	• Selective Laser Sintering (SLS) • Selective Laser Melting (SLM) • Direct Metal Laser Sintering (DMLS) • Electron Beam Melting (EBM)	Polymer, metal, ceramic
Binder Jetting (BJT)	Selective deposition of liquid binder to bond powder particles		Polymer, metal, ceramic, sand
Material Jetting (MJT)	Selective deposition of light-reactive droplets and curing	• Continuous inkjet (CIJ) • Drop-On-Demand (DOD)	Light-curable polymer, wax
Sheet Lamination (SHL)	Forming and bonding of sheets of material	• Laminated Object Manufacturing (LOM) • Ultrasonic Additive Manufacturing (UAM)	Polymer, metal, paper
Directed Energy Deposition (DED)	Selective deposition of material as it is melted by a focused thermal energy	• Laser Additive Manufacturing DED (LAM-DED) • Wire Arc Additive Manufacturing (WAAM) • Plasma Arc Additive Manufacturing • Wire Laser or Electron Additive Manufacturing (WLAM or WEAM)	Metal

Table 2. Overview of AM process category, principles and materials according to UNI EN ISO/ASTM 52900:2022 regulation [19].

1.3.1 VAT Photopolymerization

VAT photopolymerization (VPP) technique consists of a chemical reaction of bonding, enabling the fabrication of 3D elements from the curing or solidification of liquid-state material. The photopolymerization process is catalysed by the energy provided through irradiation by a light source (either visible or UV), striking the surface layer of light-curable resin contained within a transparent tank (vat).

The starting material, under the form of resin, contains a specific combination of:

- light-reactive monomers and oligomers which, upon exposure to a light source, form covalent bonds, leading to cross-linking of the molecular structure;
- initiators that, under photochemical and photophysical actions, release radicals and ions, facilitating and accelerating the polymerization reaction [21].

The photopolymerization process, depicted in Figure 11, is irreversible as polymer cannot be traced back to its initial liquid molecular composition.

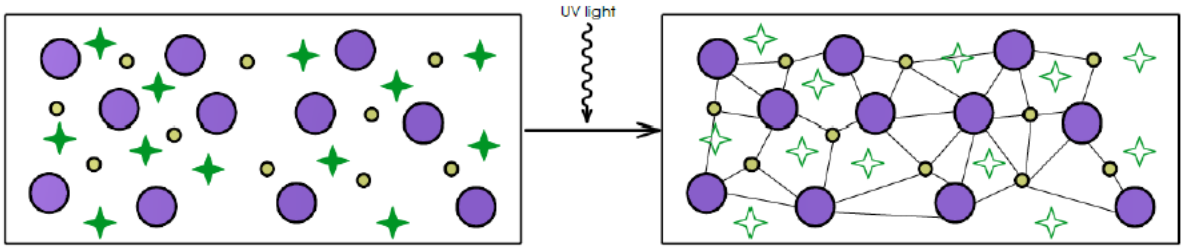

Figure 11. Schematic representation of the photopolymerization process. On the left, the photosensitive liquid composed by monomers (small circles), oligomers (large circles) and photo-initiators (stars). On the right, the activation of the polymerization process and formation of the desired polymer structure following the light beam interaction [22].

In VPP systems, the 3D printed part is grown layer upon layer on a building platform, immersed in a transparent tank filled with resin. Whenever a layer of resin is cured, the building platform lowers or raises along the Z direction of a constant quantity equal to the layer height (average values are in the range of 0.025-0.5 mm [23]). The motion direction depends on whether the building mechanism is top-down or bottom-up. Between the curing of one layer and the succeeding one, some technologies use a blade, whose movement smooths and homogenises the remaining resin. The process of photopolymerization is repeated for the subsequent layers until the printing is completed.

According to the curing system, different classes of VPP can be distinguished [24]:

- Stereolithography (SLA) (Figure 12a) was the first AM process to be developed. It is a vector scanning-based process: a focused laser beam and galvano-mirrors are used to cure the

footprint of a layer in a point-by-point manner (Figure 13a). The accuracy of the SLA parts is high and it is associated with the diameter of the laser beam. Typically, the spot dimension is around 100 µm, although size may vary depending on the manufacturer. The fine accuracy of the curing system inevitably affects the building speed.

- Digital Light Processing (DLP) (Figure 12b) is a mask projection-based process: a digital micromirror device (DMD) projects a mask of light to cure the footprint of a layer all at once (Figure 13b). Thus, DLP systems are characterised by an increased scanning speed. Part accuracy depends on the DMD pixel size, whose minimum dimension is greater than the SLA laser spot size, thereby making the technology less accurate compared to SLA.
- Continuous Digital Light Processing (CDLP) or Continuous Liquid Interface Production (CLIP) is a technology based on DLP principle (Figure 13b). Polymerization is achieved through an oxygen-permeable window that creates a persistent liquid interface (dead zone) preventing the polymerization between the window itself and the polymerizing part. The CDLP / CLIP part is continuously drawn out of the resin tank, unlike SLA and DLP processes, in which the curing of each layer occurs in discrete steps. Compared to DLP, the continuous polymerization minimises the staircase effect and improves the isotropic behaviour of the CDLP / CLIP parts. As a result, the CDLP / CLIP technology is extremely fast [25].

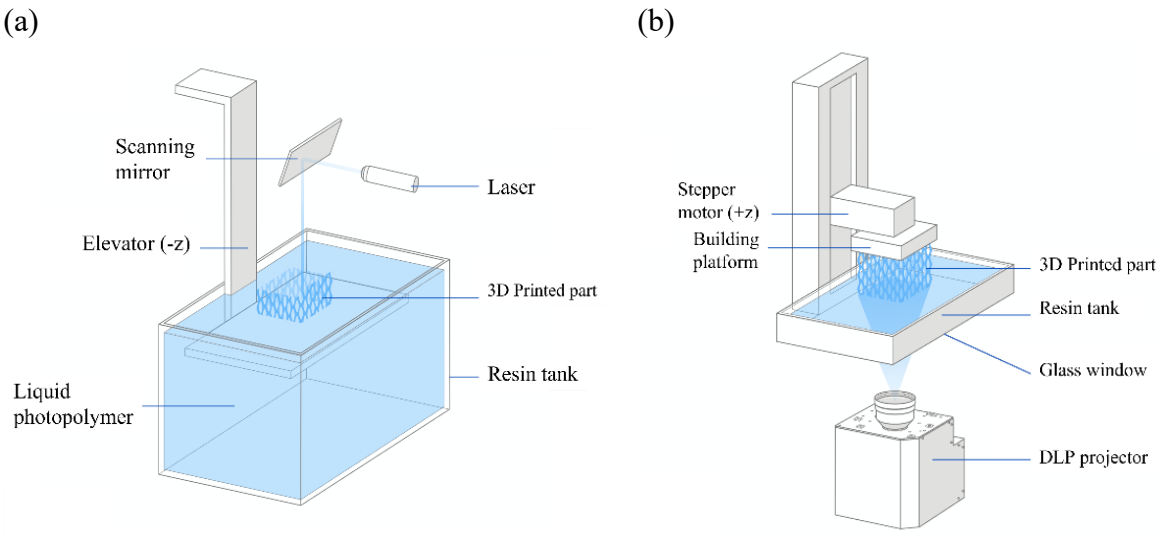

Figure 12. Schematic representation of VAT photopolymerization technologies: SLA with top-down configuration (a) and DLP (b).

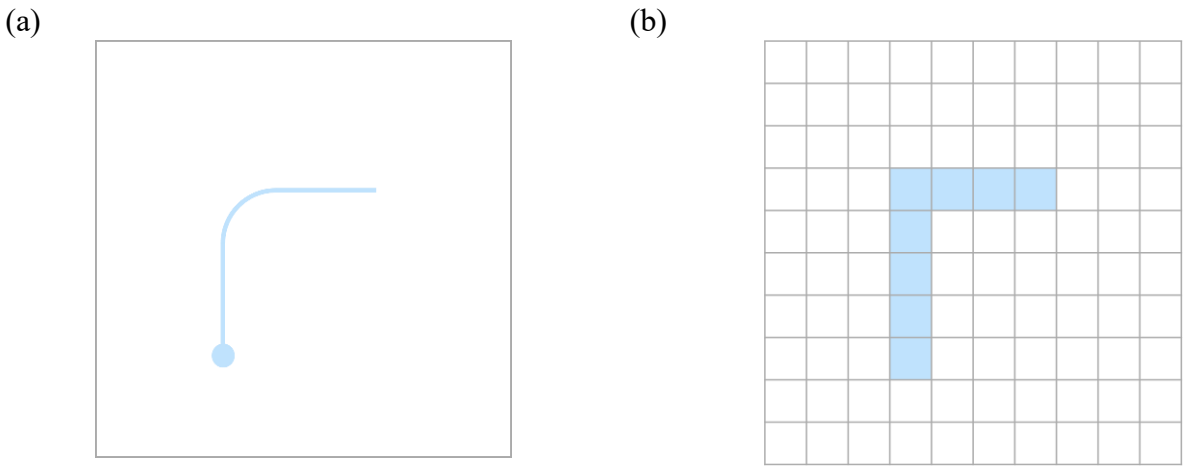

Figure 13. Accuracy comparison of SLA (a) vs DLP, CDLP/CLIP (b). The accuracy of DLP and CDLP/CLIP footprint is limited by the pixel network.

Once 3D printed, the VPP part might be subjected to various post-processing activities. The treatments involve the removal of unreacted resin elements, part drying (in air or vacuum) and UV post-curing to ensure full solidification and strengthen of the part.

1.3.2 Material Extrusion

In Material Extrusion (MEX) processes, the production of 3D elements is based on a thermal reaction bonding. The feedstock material, usually thermoplastic polymer, is fed into the technology and it is drawn to an extrusion head, where it is melted by a heated liquefier.

Depending on the type of the extrusion head [26,27], MEX mechanism is classified in:

- Plunger-based extrusion, in which the feedstock (rods) is softened, collected into a reservoir and extruded via mechanical drive system (i.e., plunger).
- Filament-based, the most popular extrusion approach. Feedstock (filament, with a typical diameter of 1.75 or 2.85 mm), pulled by drive wheels, is softened and extruded.
- Screw-based extrusion, designed for the extrusion of feedstocks other than rods and filaments. Feedstock (pellets or granules) is softened in a melting zone and a rotating screw forces the molten material to a feeding zone to be extruded.

The extrusion nozzle, able to move in the X-Y plane, builds the initial layer by depositing the melted material onto a heated building platform. Suddenly, the material cools down from the glass transition temperature to the chamber temperature. Once the deposition of a slice is completed, the platform moves downward to deposit the following layers by an amount equal to the height of the slice. A schematic representation of the MEX manufacturing process is illustrated in Figure 14.

Fused Deposition Modelling (FDM) and Fused Filament Fabrication (FFF) are common examples of prototyping technologies that leverage on MEX principle. FDM was developed by S. Scott Crump and patented by Stratasys in 1989. In 2009, as the Stratasys patent expired, FFF was developed. Beyond the legal perspective, FDM and FFF technologies do not differ in technical features.

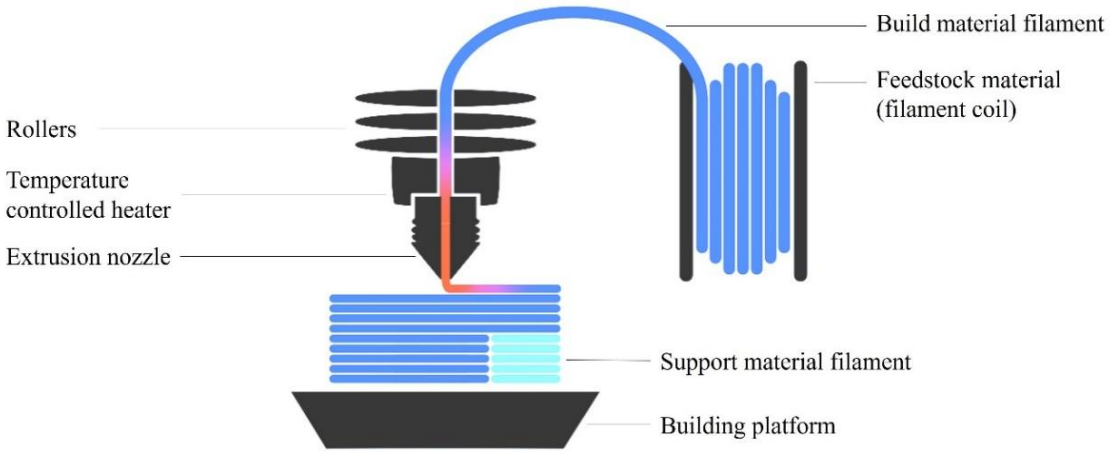

Figure 14. Schematic representation of MEX technology based on filament extrusion.

The quality of MEX products is influenced by various 3D printing parameters, such as infill method and percentage, raster angle and printing speed. Extrusion head and platform temperatures directly affect filament bonding and the resulting mechanical resistance [28]. Furthermore, compared to other AM processes, the accuracy of MEX elements is limited and strictly linked to nozzle dimension. Extrusion nozzles are available in various diameters, 0.25 mm to 0.8 mm, and determine the range of feasible layer height and extrusion width. A standard nozzle diameter (0.4 mm) allows to obtain theoretical layer height and extrusion width resolutions between 0.1-0.32 mm and 0.4-0.8 mm, respectively. The reduced resolution of MEX makes it ideal for applications where achieving high surface finishing is not necessary and the ridged effect is neglectable. Defects can be mitigated by chemical (solvent vapor exposition) and mechanical smoothing. Also, surface coatings might be applied to improve the surface finish and strengthen the mechanical behaviour of the components [29]. MEX inferior resolution compared to other AM printing technologies, makes it ideal for applications in which it is not necessary to achieve high accuracies and superficial finishes.

Besides, the affordability and simplicity of the system make MEX the most versatile technology. Common processed materials involved a wide range of thermoplastic polymers and plastics. Frequently used materials include: polylactic acid (PLA), acrylonitrile butadiene styrene (ABS), polycarbonate (PC), thermoplastic polyurethane (TPU) and Nylon. Also, the research literature is witnessing the successful use of ceramic, bio-glass and metallic materials [30]. Regarding the latter,

the process is known as Metal Material Extrusion (metal MEX) and the feedstock consists of a polymeric binder matrix, filled with evenly distributed metal particles [31].

The metal MEX process chain is schematised in Figure 15. Besides the extrusion (or shaping) of the material, the process comprises few additional activities to obtain the final metal part.

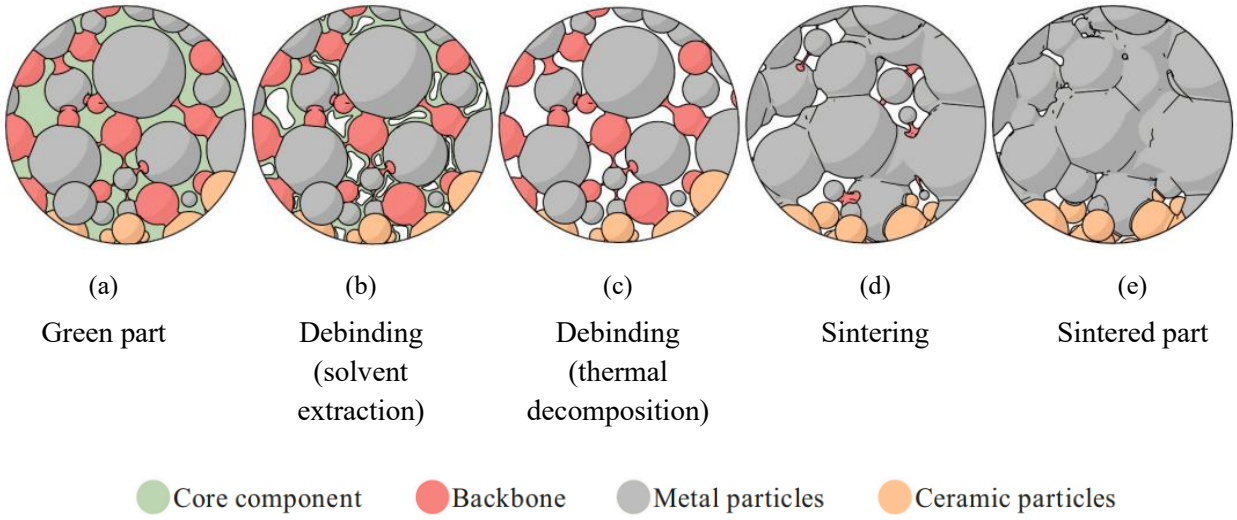

Figure 15. Representation of the material morphology during the shaping, debinding and sintering (SDS) activities of a metal component 3D printed with ceramic support element. (a) green part, as printed; (b) debinding, solvent extraction of the main binder component; (c) debinding, thermal decomposition of the residual backbone; (d) sintering, thermal densification of the metal particles of the brown part; (e) sintered part.

Firstly, the deposition process is followed by the debinding activity: removal of the binder polymer from the green part using solvents, catalysers and thermal decomposition. The main binder component is removed during the first debinding stage, while the backbone or the binder component accountable for holding the part shape is thermally decomposed.

Then, the brown parts are sintered through a cycle of thermal treatments applied to increase strength by bonding particles. The contact formation, known as neck (Figure 16), between adjacent particles occurs and then consolidation and voids closure take place (Figure 17).

Along with bonding, it is possible to induce densification and obtain a near fully densified metal component (96.0-99.8 % theoretically dense metal part) [32]. The sintering phase enhances the mechanical properties of the metal component, achieving values comparable to those typical of the metal base material. Nonetheless, the densification process might lead to shrinkage, which is highest along the building direction [33].

(a) (b)

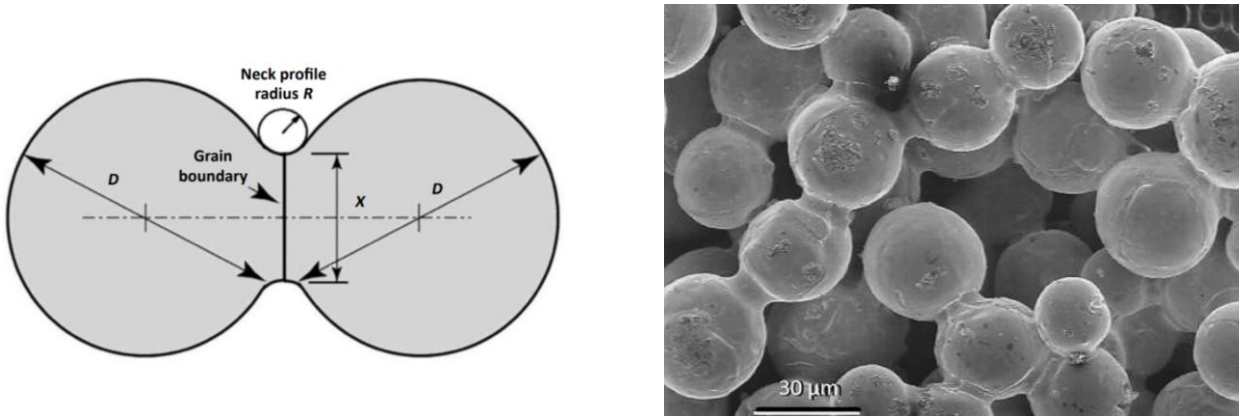

Figure 16. Schematic representation of two-particle sintering profile, where X is the neck diameter (a). Scanning Electron Microscope (SEM) image of neck formation between spherical bronze particles prior to full densification (b) [34].

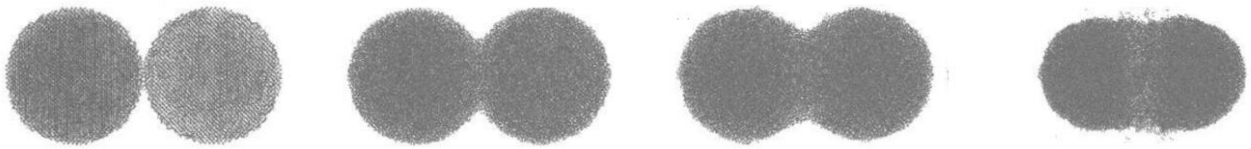

Figure 17. Molecular dynamics simulation of sintering process: spherical particles are brought closer by weak adhesive forces; initial bonds are formed through surface diffusion, causing the necks between the particles to grow. This leads to the rounding of pores within the element and, during the final grain growth, pores close [34].

1.3.3 Powder Bed Fusion

Powder Bed Fusion (PBF) processes are based on the concept of selective melting and bonding of powder particles.

As illustrated in Figure 18, the powder is dragged from the feed region and, through a levelling roller (blade or re-coater), it is evenly spread over the powder bed. To reduce residual stresses and improve adhesion, the building platform is preheated. Then, a focused energy source, such as a laser or electron beam, sinters (heating to a temperature below the melting point) or melts (heating to a temperature at or above the melting point) the powder particles to build the cross section of the component. The powder particles are selectively hit by the energy beam, meaning that fused and non-fused powder coexist on a single layer. Sometimes, un-melted powders serve as support for subsequent layers. The process takes place in a controlled atmosphere, the chamber is filled with inert gas (e.g., argon or nitrogen) to prevent oxidation.

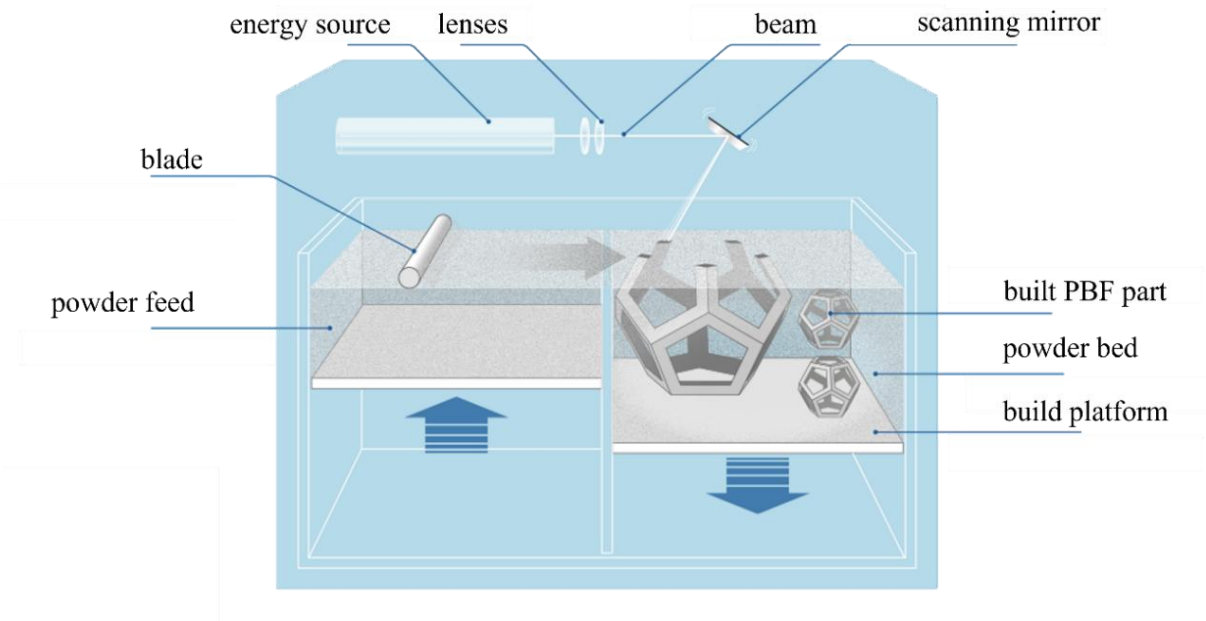

Figure 18. Schematic representation of PBF technology.

After the completion of a layer, the building platform is lowered by an amount equal to the layer thickness, a new layer of powder is deposited and levelled by the re-coater. Thin layers in the order of 50-200 µm are achievable, with some PBF systems it is possible to reach even 20-30 µm. Once the construction of the part is finished, a cooling period must be allowed to avoid deformations and defects due to uneven thermal contraction and oxygen diffusion. Finally, the component is retrieved from the powder bed and cleaned of any powder residue. After adequate treatment (i.e., sieving and drying), the un-melted powder may be added to virgin powder to be recycled. Post-processing operations (i.e., CNC machining) are required to achieve the desired dimensional accuracy and surface quality.

Selective laser sintering (SLS) was the first commercialised PBF process. The technology was patented in the 1980s at the University of Texas at Austin, USA, and was initially developed to produce polymer- or composite-based prototypes, then was later extended to the processing of metal materials [35]. Commonly used metal materials are stainless steel and several types of steels, titanium, aluminium and cobalt-chrome alloys. PBF technologies for metal fabrication can be distinguished in:

- Selective Laser Melting (SLM), in which metal powder particles are melted by a focused laser beam. The laser power is in the range of 100-1000 W and enables fine size features with good dimensional accuracy and roughness [36].
- Direct Metal Laser Sintering (DMLS), which employs a focused laser beam to sinter metal powder. Material particles are not fully melted owing to the fact that temperatures remain below the melting point. Thus, DMLS allows to combine different types of metal powders

(metal alloys), even incorporating polymeric powders. Although the DMLS is often referred to as a sintering technology, modern systems are operated at power levels to achieve full melting of metal powders [37], blurring the DMLS definition with SLM.

- Electron Beam Melting (EBM), in which metal particles bonding occurs by means of a focused electron beam. EBM was introduced to overcome the limitations, in terms of power and speed, of laser-based PBF technologies (LPBF). Specifically, EBM employs high-energy electron beam (3000-3500 W) [38]. However, it suffers from poorer dimensional accuracy and surface roughness [36].

Process parameters and powder characteristics are considered the most influential factors determining the quality of the final PBF products. The powder morphologies, such as the particle size distribution and shape (sphericity and uniformity), have significant effects on the bulk, surface and mechanical properties of powder as well as the final part. Coarser particles result in a rougher surface and lower density [39]. In addition, PBF parts are sensitive to beam-related parameters, such as beam size, input power, scan speed, scan spacing and scan pattern [40].

Besides surface roughness, one of the most critical defects related to PBF technology is porosity, with both irregular (keyhole or lack-of-fusion) or spherical shape (gas inclusions) defects, promoting early failure of the component (Figure 19 and Figure 20). Additionally, high residual stress is a widespread phenomenon, induced by the large thermal gradient during the local rapid melting and solidification process [36].

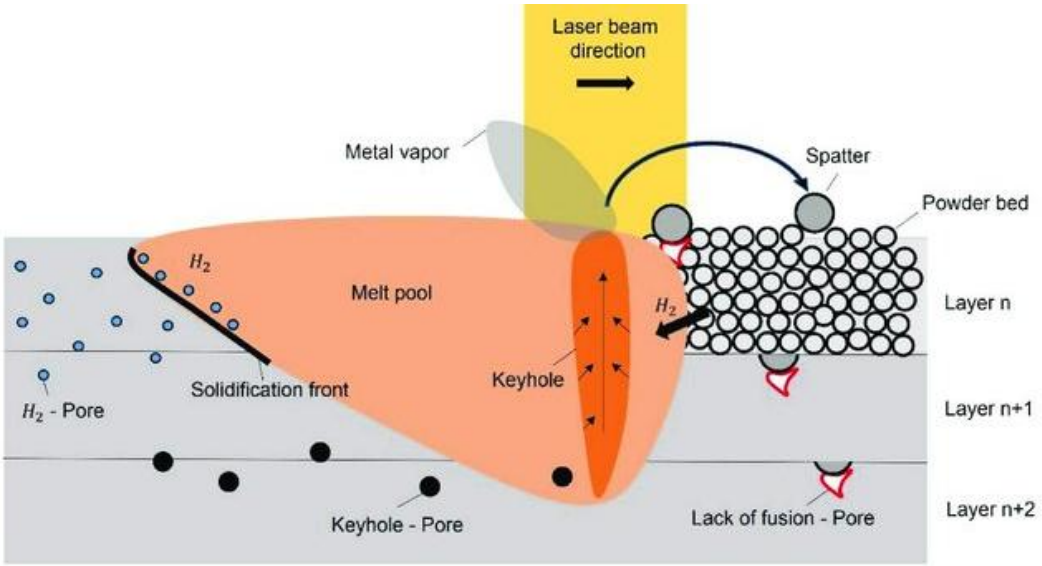

Figure 19. Schematic representation of the generation mechanism of H-induced, keyhole and lack-of-fusion pores in LPBF [41].

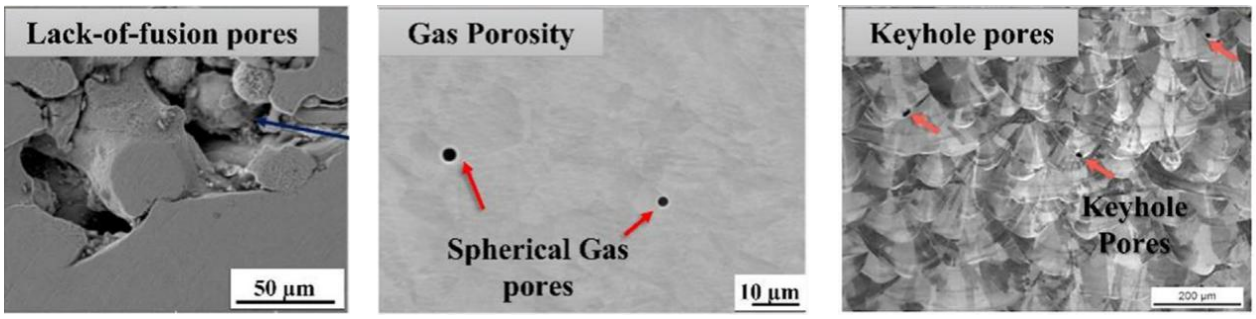

Figure 20. Representation of lack-of-fusion, gas and keyhole pores in AISI 316L samples produced via LPBF [42].

1.3.4 Binder Jetting

Binder Jetting (BJT) is an AM process that produces 3D elements starting from material powders, as in the case of PBF systems. Instead of melting material particles, BJT supports a printing head, also known as inkjet head, which selectively deposits liquid bonding agent to join powders of materials. BJT was initially invented in 1993 at the Massachusetts Institute of Technology. Later on, several industries have developed machines suitable for using a variety of different materials. In this respect, since BJT technology does not require a controlled atmosphere and high energy source, it offers considerable flexibility in processing materials, manufacturing a wide range of powders [43]. In fact, BJT is virtually compatible with any material powder. The technology provides printability of metal powders, such as stainless steel, Inconel, copper, nickel, titanium, and cobalt-chromium alloys [44]. Furthermore, the process is suitable for materials that do not melt and/or are difficult to be machined, such as ceramics and composite materials.

As depicted in Figure 21, the working principle of BJT is based on a printhead that moves horizontally (along the X- and Y-axes) over a powder bed and, selectively, releases the binder, which is typically a polymeric liquid. At the completion of each printed layer, the building platform lowers and a new layer of powder is spread over the powder bed through a roller. Typical layer thickness ranges from 50 to 300 µm [45]. When all the layers are built, the object, known as green part, is taken from the unbound powder for powder removal and further post-processing. The accuracy and strength of the resulting parts are closely related to powder and binder properties, printing parameters and subsequent treatments [46]. To ensure adequate powder-binder resistance during the 3D printing process, powder pre-treatment is necessary. However, even when powder-binder adhesion is good, the strength of the green part is relatively low due to the nature of BJT bonding method, which imparts characteristics to the material that do not always make it suitable for structural parts. Therefore, further processing is required. Just as in MEX metal production, green parts undergo curing and/or heating processes. The heat treatment involves sintering, consolidation and, sometimes, infiltration and burning of the

binder [47]. Indeed, binders are usually not the constituents of a final part and must be separated from the final part without altering its shape and size. After appropriate treatments, the desired parts are obtained.

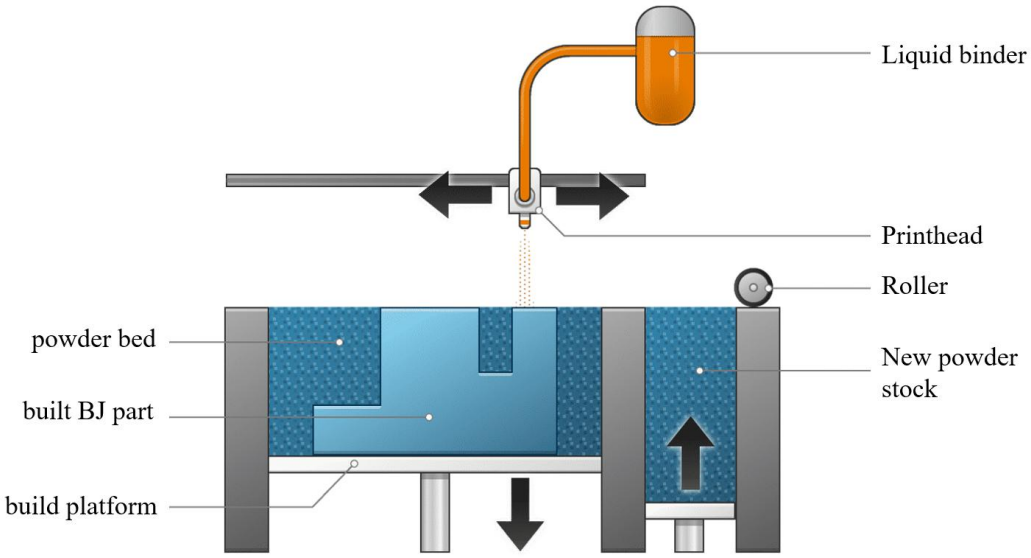

Figure 21. Schematic representation of BJT technology.

1.3.5 Material Jetting

The AM process known as Material Jetting (MJT) behaves similarly to the two-dimensional ink jet printing process: it uses arrays of nozzles that, moving horizontally on the build platform, deposit the material in successive layers, and an ultraviolet (UV) light source to cure or harden the laid material. Curing of each layer is performed in a single step with the deposition of the material. The described methodology requires the material to be deposited in droplets, which constrains the range of available materials, often limited to photosensitive polymers and waxes, due to their droplet-forming ability and viscosity.

The working principle of MJT is illustrated in Figure 22 and, depending on the ink-jet technique, the technology is divided into two main categories: continuous inkjet (CIJ) and Drop-On-Demand (DOD) (Figure 23). In CIJ, droplets of material are ejected continuously; whereas, in DOD, droplets of materials are ejected at a high frequency only when required, through the application of a thermal or piezoelectric signal waveform [48].

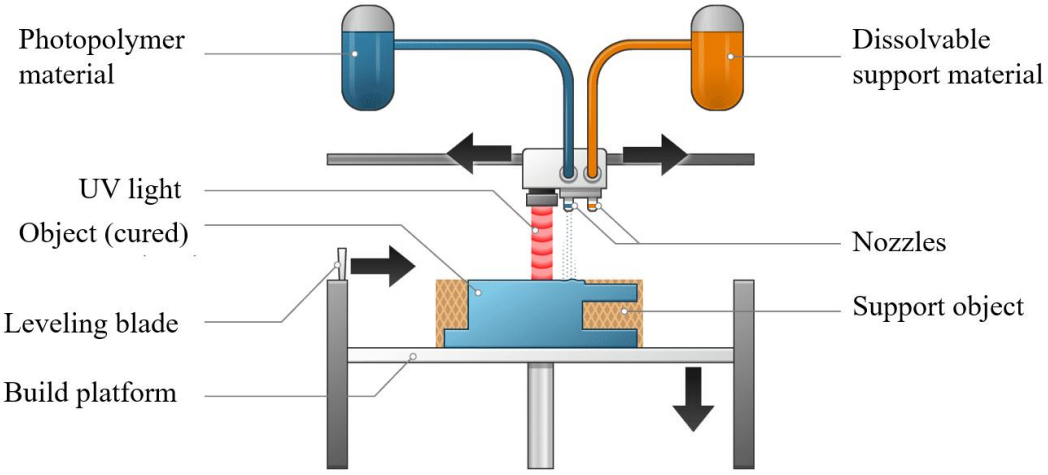

Figure 22. Schematic representation of MJ technology.

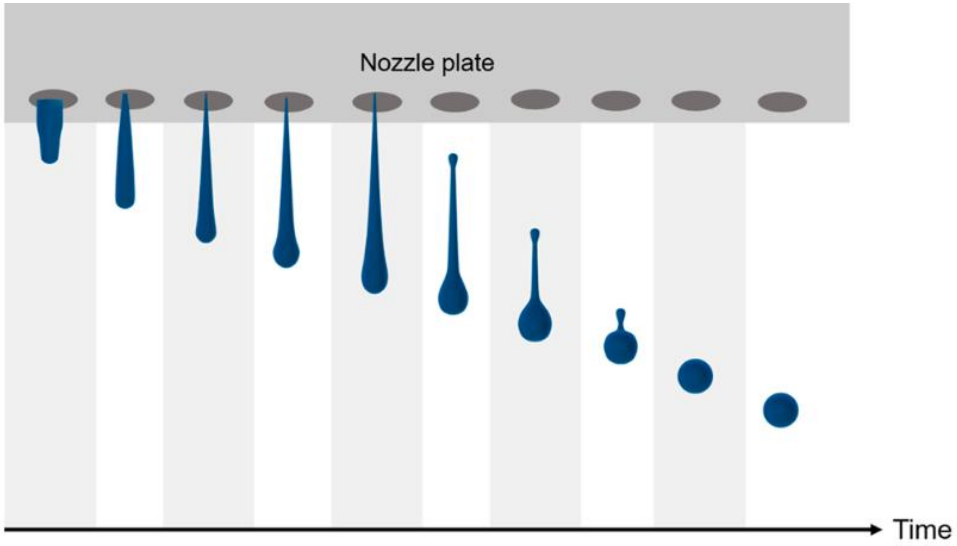

Figure 23. Illustration of the droplet formation of a viscoelastic fluid in DOD MJT (piezoelectric signal). The separation of the tail into two droplets and, thus, the formation of satellite droplets is prevented by the elastic effect.

The main advantages of MJT lie in the precision and surface quality. This technology allows to manufacture thin layers (in the tens of microns), resulting in parts with extremely smooth surfaces and highly accurate details.

As opposed to other AM technologies, the surface finish of MJT parts is not affected by the presence of support structures owing to their composition and removal methodology. Particularly, support structures are made of dissolvable support photosensitive polymers or waxes and are easily removable using an ultrasonic bath.

Moreover, MJT represents one of the few technologies capable of producing multi-colour and multi-material elements. This promotes the possibility of manufacturing more realistic prototypes, encompassing a variety of features, including diverse functional behaviours.

Though, the technology has some significant limitations related to the inferior mechanical properties of the resulting parts. This is explained by the inherently low mechanical and thermal performance of the commercially available photosensitive polymers and waxes [49]. Also, materials are limited in durability due to long-term aging and mechanical degradation prompted by the exposure to light and humidity [50]. These aspects constrain MJT suitability for applications where visual feature is prioritised over functionality and pushes research towards the development of more advanced materials, with a higher concentration of polymers or particles, and technologies capable of handling high-viscosity inks.

1.3.6 Sheet Lamination

Sheet Lamination (SHL) is an AM method involving the bonding of sheets of material to form a three-dimensional part. This is the only AM methodology based on the use of sheets of material (either paper, metal or polymer films) as feedstock material. Typically, the foil thickness ranges from 0.1 to 0.2 mm [47].

The process is outlined in Figure 24 and it consists of a mechanism that deposits sheets of material over a build platform and then heats, compresses, and cuts each layer to form the final three-dimensional element. The production process occurs either through bonding and then forming (bond-then-form) either through forming and then bonding (form-then-bond). The scrap material is diced into smaller pieces and left on the building platform acting as support structure.

Among the SHL processes, the most common are Laminated Object Manufacturing (LOM) and Ultrasonic Additive Manufacturing (UAM).

In LOM processes, polymeric or paper layers are bonded by means of adhesive, which is activated by heated roller and pressure, as shown in Figure 24. Then, successive layers are precisely cut by a laser or mechanical cutter. Instead, UAM is a class of LOM processes: the lamination process combines low-temperature ultrasonic seam welding (via a digitally controlled sonotrode) and CNC contour milling to manufacture metal components (Figure 25) [51]. The most used metal foils are aluminium, copper, stainless steel and titanium. The advantage of the process lies in the possibility of bonding different metals with a low energy request, as the feedstock material does not require to be melted since it is just subjected to a combination of ultrasonic vibration and pressure that create a solid-state weld between layers of metal foil. Also, among the benefits, the technique offers low processing temperature, solid-state bonding, reduced geometric distortion, retaining the surface

texture and the possibility of producing large scale parts [52]. Still, UAM processes require additional CNC machining and removal of the unbound metal during the welding process, making the extraction of unalloyed material quite intricate [53].

In general, SHL techniques are cost-effective, given the affordability of the feedstock material compared to other AM processes, and they have the ability to produce large scale structures. Limitations includes anisotropy of mechanical properties (grains are oriented and elongated along the rolling direction) and poor tensile properties owing to the weak interface joining [54]. Given these assumptions, SHL represents one of the least adopted technologies in the AM environment.

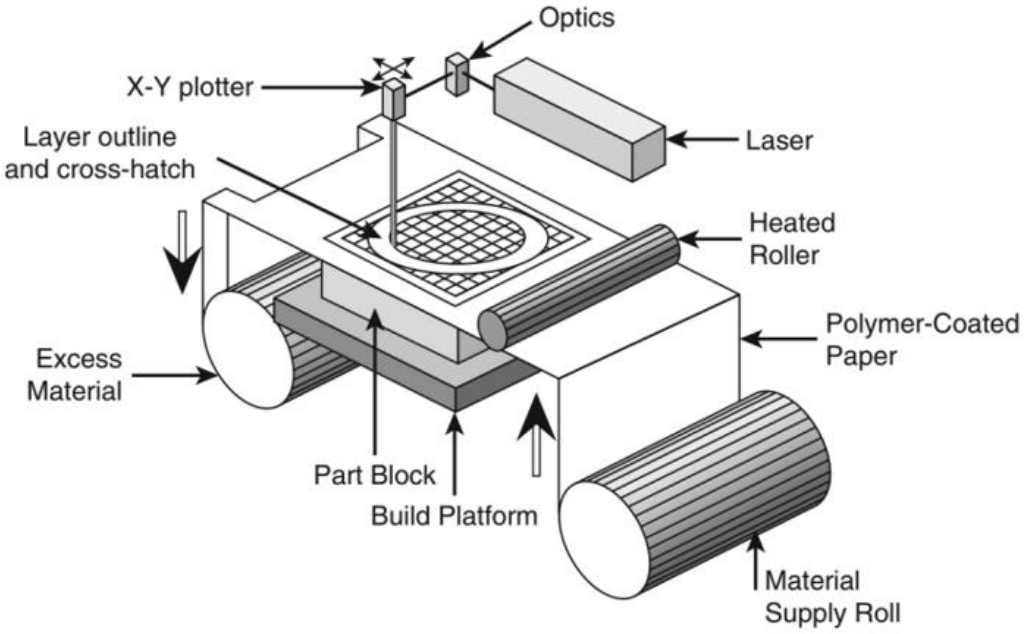

Figure 24. Schematic representation of SHL technology.

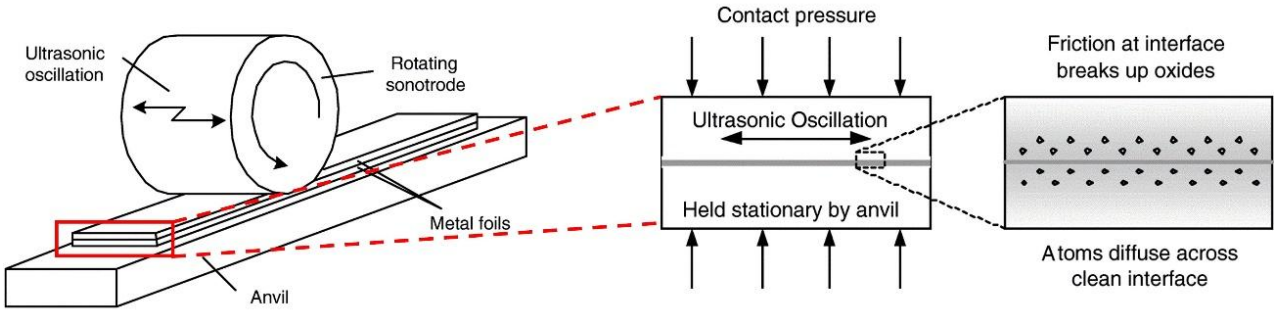

Figure 25. Schematic representation of the working principle of UAM, a SHL process.

1.3.7 Directed Energy Deposition

Directed Energy Deposition (DED) is an AM process in which a focused thermal energy source melts metal material as it is deposited. The deposition occurs onto a build surface, which can be either the build platform or an existing part. Owing to this distinct ability, DED technology has established itself as a tool for repairing and remanufacturing damaged components, as well as for applying coatings to existing surfaces [55].

The operating principle of DED process is illustrated in Figure 26. The technique leverages on a nozzle, which is mounted on a multi-axis appendage (4- and 5-axis machine) and it deposits the material from any angle by moving in different directions. The nozzle focuses on a substrate and its heat source (such as laser or electron beam or plasma/electric arc) delivers a high energy density, which generates a small melt pool. The molten pool is formed by the simultaneous melting of the feedstock material (powder or wire feedstock, Figure 26), delivered into the melt pool, and the substrate material. Then, the melt pool undergoes a rapid cooling, generally it ranges from 10^3 to 10^5 °C/s [56], concurring to the solidification of the layer.

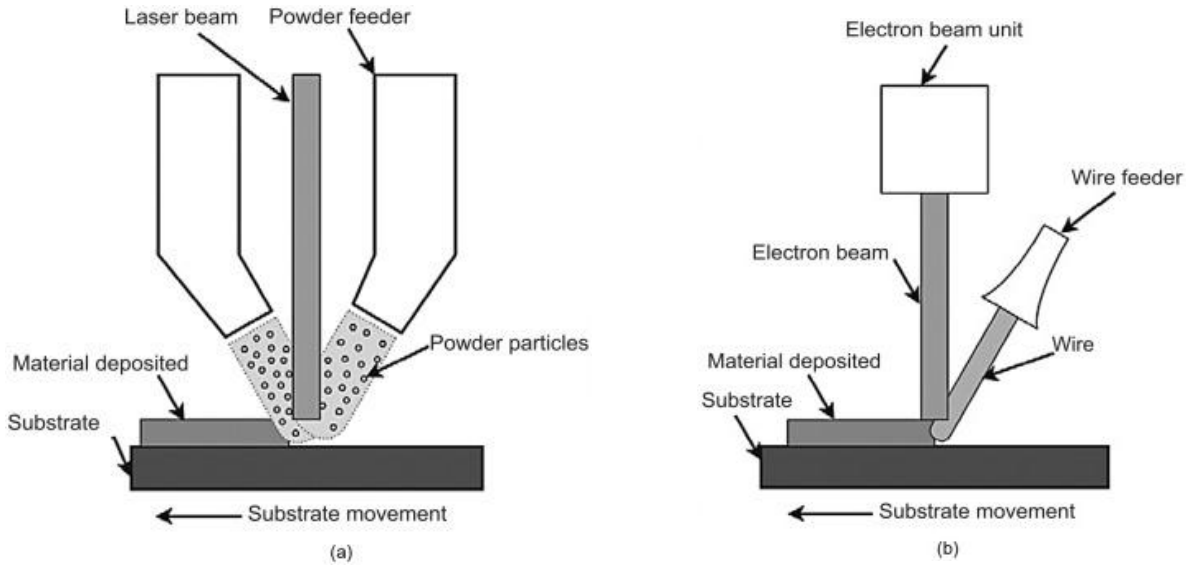

Figure 26. Schematic representation of DED technology. (a) Powder feeding DED system, the input material is metal powder; it allows greater precision and control of the final material properties. (b) Wire feeding DED system, the input material is a metal wire that is fed into the melting pool, allowing a reduction in material waste.

According to the distinct material feeding system and thermal energy source, several DED technologies are commercially available. The most popular ones are reported in the Table 3. All the mentioned DED processes typically take place in hermetically sealed chambers: LAM-DED, WAAM and WLAM use a protective gas to prevent oxidation during material deposition, while WEAM uses

a vacuum furnace. The 3D printing speed and layer thickness of wire-fed DED processes (WAAM, WLAM and WEAM) are significantly higher than those of powder-fed DED systems (LAM-DED); on the contrary, the dimensional accuracy and residual stress of the parts produced with wire-fed DED techniques are lower than those of powder-fed DED systems [56].

Material Feedstock	Thermal Energy	Classification	Deposition Mechanism
Powder	Laser	*Laser Additive Manufacturing Directed Energy Deposition* (LAM-DED)	Cladding
Wire	Electric Arc	*Wire Arc Additive Manufacturing* (WAAM)	Welding
	Plasma Arc		Welding
	Laser	*Wire Laser Additive Manufacturing* (WLAM)	Cladding and Welding

Table 3. Classification of the most popular DED technologies.

Materials commonly used in DED processes include a variety of high-performance metals, such as stainless steels, steel alloys, titanium-based alloys, cobalt-based alloys, nickel-based alloys, aluminium alloys, high-entropy alloys, intermetallic, shape memory alloys (SMAs), ceramics, composites and functionally graded materials (FGMs) [57].

In this regard, DED and PBF methodologies represent the most widely used AM techniques for the manufacturing of complex metal components, although they differ in terms of both manufacturing mechanism and material feeding systems, both production performance and quality. Compared to powder bed-based AM systems, DED processes operate at high printing rates, depositing huge volumes of material in extremely reduced times, thus allowing for large-scale printing [58]. Conversely, DED systems tend to have lower dimensional resolution and surface accuracy than PBF technologies. In fact, typical layer thickness and minimum feature size of LAM-DED elements are 200-500 μm and 380-1000 μm, respectively [56]. In addition, DED systems handle powders with larger particle sizes (in the order of 50-150 μm), which is an advantage in both economic and safety terms, although their recovery and reuse is more problematic and less effective than PBF systems.

Chapter 2. Additive Manufacturing and the medical sector

2.1 The evolution of Additive Manufacturing in the medical sector and its fields of application

Since the scientific innovations developed by Charles 'Chuck' Hull and successive researchers, the industrial landscape has been revolutionised. With its earliest introduction, in 1990s, AM has been widely studied and applied in a variety of fields, including the medical sector.

The historical evolution of the main AM techniques and technologies is illustrated in Figure 27 and it is complemented by several significant innovations in the healthcare field.

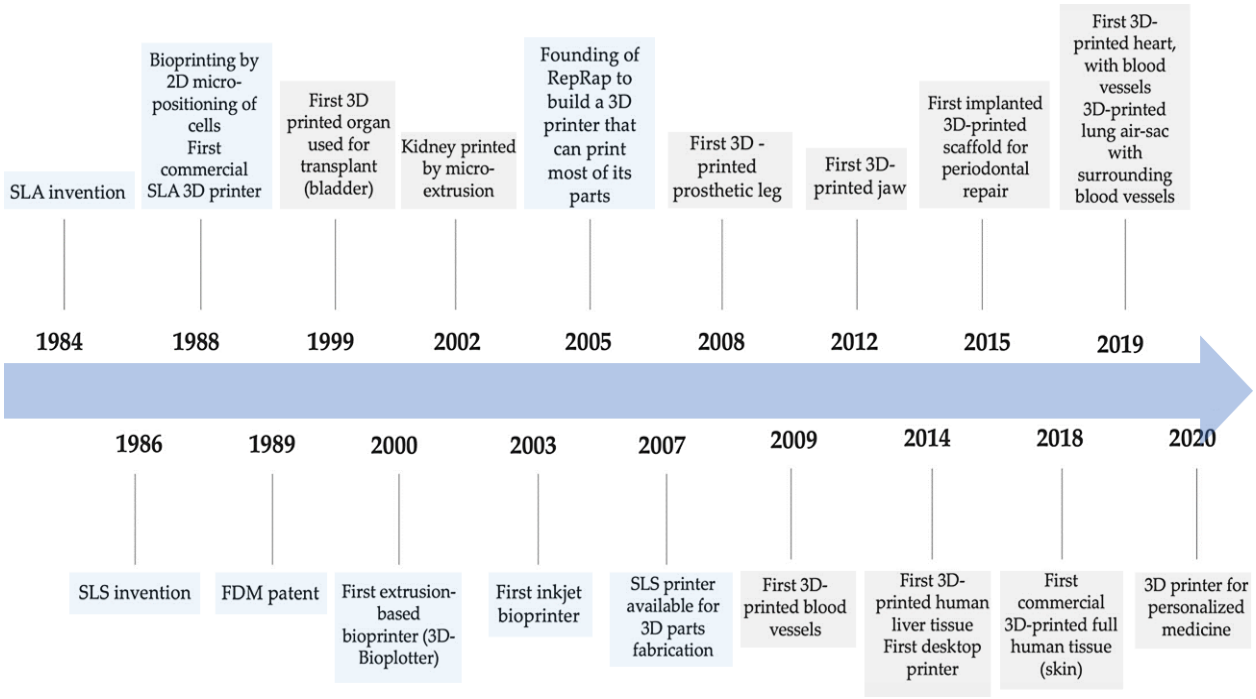

Figure 27. Milestones in the development of AM methodologies applied to the medical [59].

The progresses and potentialities of 3D printing over conventional manufacturing techniques provide the healthcare industry with new tools and therapies that are able to transform the way patients are being cured, moving towards a medicine that is tailored to the individual diagnostic case.

Several are the purposes of manufacturing medical applications leveraging on AM techniques. According to the Additive Manufacturing / 3D Printing (AM3DP) Medical Annual Report provided by the American Society of Mechanical Engineers (ASME) [60], between 2020 and 2022, there was a significant deployment of AM in the medical industry (Figure 28). In particular, an extensive use

of AM technologies for the production of anatomical models and for rapid prototyping was recorded. However, it is evident that more specific areas are showing increasing interest too.

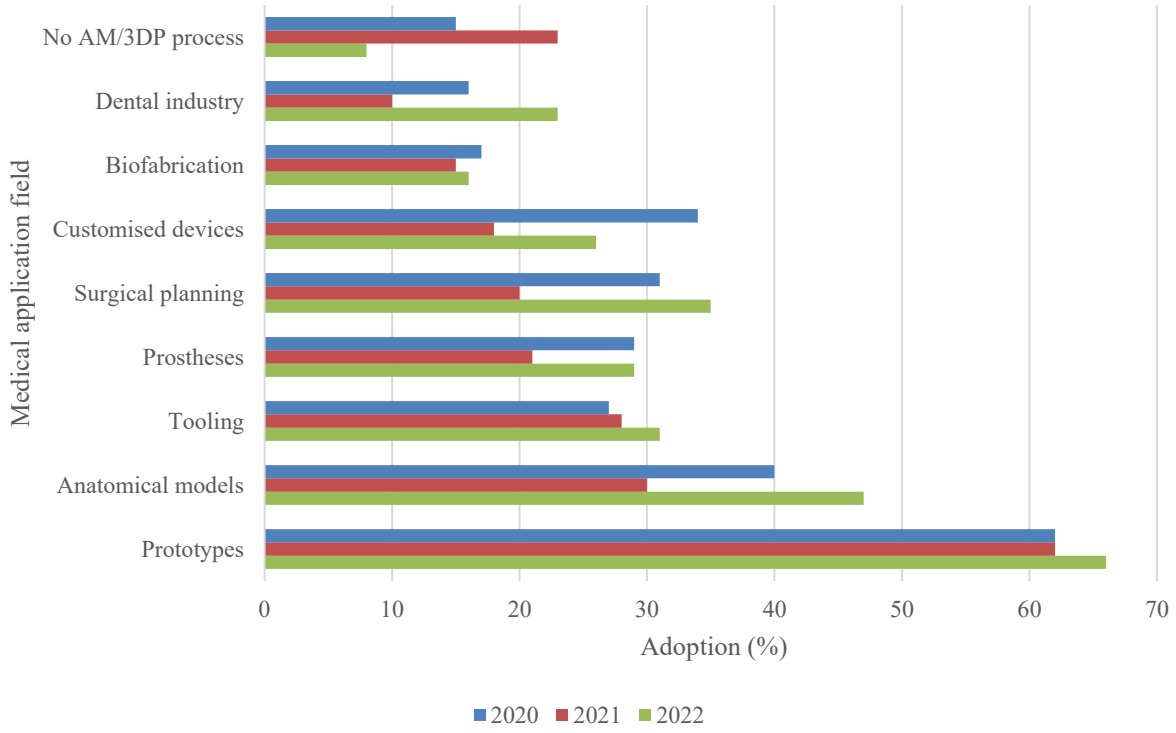

Figure 28. Adoption rate of AM in different medical applications by members of the AM3DP community [60].

AM presents a broad range of uses and purposes in the medical industry. Numerous classifications have been proposed in the literature, with some research identifying five major classes of 3D printed medical [61,62]. These include prototypes for surgical planning and educational intent, implants, prosthesis and orthosis devices, surgical instrumentation and biomanufacturing. The following sections focus on each item of the mentioned classification.

2.1.1 Anatomical models

Anatomical models are three-dimensional prototypes designed to reconstruct the patient's physiological or pathological morphology. The possibility of realising extremely accurate three-dimensional models of the interested anatomy allows the physician to identify and simulate the best surgical strategy in the pre-operative stage, as well as to train medical students. In addition, the possibility of having AM-printed anatomical models represents a preferred alternative to cadaver training, which is critical in terms of availability of the corpses and cost-effectiveness of the practice [63].

Although AM techniques enable to reproduce almost the exact copies, in terms of dimensional and geometric accuracy, of real anatomic districts and structures, the haptic perception of 3D printed models continues to pose significant challenges. The correspondence between the real model and 3D printed one, in terms of tactile and sensory characteristics, is not trivial and might be hampered if the 3D printed models lack material properties that closely replicate those of real human tissues [64]. For instance, in the process of reproducing an anatomical model of a blood vessel, whose modulus of elasticity might vary from 1 MPa to 10 MPa, the use of AM technologies such as MEX is not appropriate. This technology manufactures elements with significantly different mechanical properties, excessively rigid compared to the characteristics required for an accurate representation of blood vessels. This suggests that, not only the tactile sensation is compromised, but the behaviour of the model with respect to mechanical stresses does not correspond to that of real human tissue too. Instead, technologies, such as MJ, delivering softer and rubbery materials, might offer new prospects: multi-colour and multi-material abilities promote the creation of human anatomical models comprising diverse range of tissues [65].

In addition to the educational and surgical planning intent, anatomical models are visual and tangible solutions for informing the patient and his family too, making them aware of the diagnostic-therapeutic process and compliant to the medication schedule.

Figure 29 illustrates the percentage value of the different medical purposes of 3D printed anatomical models [66].

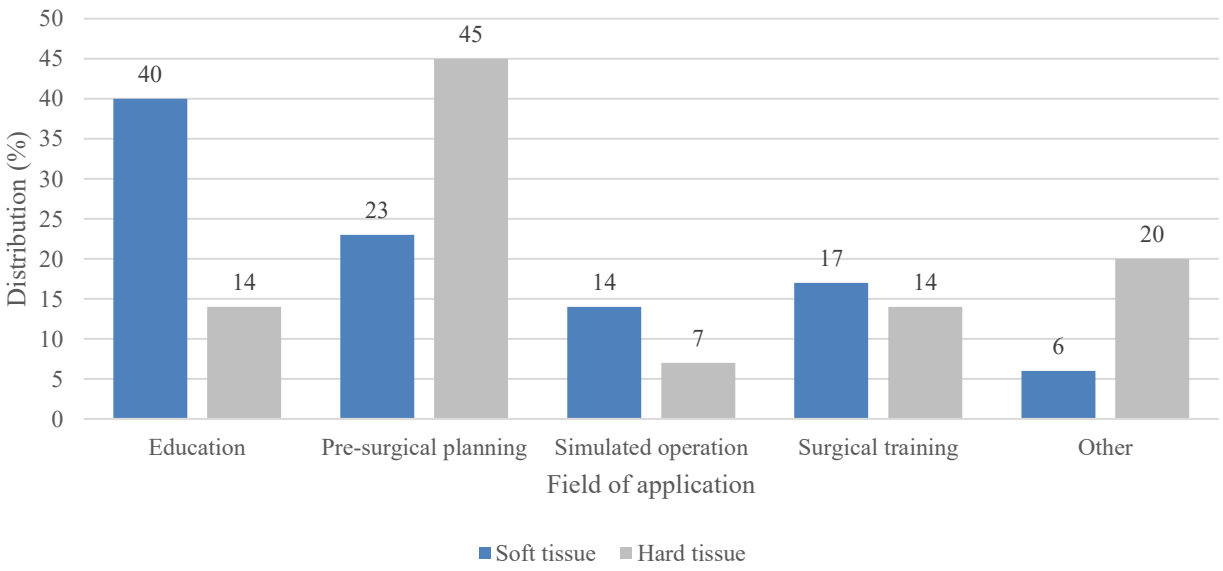

Figure 29. Distribution of AM-produced anatomical models for soft tissue and hard tissue applications [66].

2.1.2 Implants

As emerged from the previous section, there is a strong need to design and produce elements that not only perfectly reproduce the appearance of anatomical districts but provide adequate functional responses too. Hence, besides anatomical models, the integration of AM, imaging approaches, Reverse Engineering (RE) and digital modelling techniques, allows the production of almost any conceivable geometry of implant and implantable prosthesis.

An implant is a medical device designed to be surgically inserted into the human body, usually, permanently. This device replaces and supports a missing or damaged part of the body. Additively customised implants are widely spread in the orthopaedic field, especially in oncology and traumatology, where bone voids, resulting from the removal of primary and secondary skeletal tumours, are reconstructed through the insertion of patient-specific metal prosthetic implants [67]. In this way, the efficient and rapid design and production of custom-made prosthetic implants through AM techniques solves an obvious and persistent problem, namely when standard implants are no more satisfactory. Often, prosthetic implants are available in a small range of sizes and shapes, with medical professionals choosing the structure that best suits the clinical case under investigation. This situation may be appropriate in some cases, however, there are several circumstances in which implant customisation and the implementation of advanced geometrical features found to be highly advantageous. For instance, when patients have unique pathological features or complex conditions, or when the implant is required to fit the patient's anatomy perfectly, as in cranial or maxillofacial surgery [68]. In the case of the surgical operation dealing with fractures of the facial bones, traditionally, to adapt standard prosthetic implant to specific clinical requirements, it is necessary for the physician to manually manipulate the implant on the patient's bone during the surgical procedure itself. This, in turn, leads to a longer duration of the surgical procedure and an increased risk of complications [69].

Moreover, the ability of AM systems to generate implantable devices that exactly fit the morphology of the patient bridges the gap between biological matter and engineering design, producing devices that combine biocompatibility and biomechanical behaviour. This optimises the integration between the implant and the restoration of the surrounding tissue. In fact, in load-bearing implants, the mismatch of mechanical properties occurring between the prosthetic implant and the surrounding bone tissue results in an unbalanced load distribution in human kinematics [70]. The continuous uneven distribution of load stimulates bone resorption, which leads to osteoclast-driven alteration of the bone shape and dimension [71].

Bones are not static structures: they undergo continuous processes of change and adaptation throughout life. In response to an increase in load, bone progressively remodels itself to strengthen

and resist such stresses; conversely, a reduction in load induces a remodelling process that results in resorption of bone tissue. It is in the presence of an inadequately designed prosthesis, which does not ensure proper load distribution on the surrounding bone, that such resorption occurs. This phenomenon is known as stress-shielding effect: it is described by Wolff's law as the long-term adaptation response of bone structure and bone density to meet new mechanical demands, due to the alteration of the mechanical stimuli in the overall system [72]. Stress-shielding phenomenon induces various clinical complications, ranging from general pain and discomfort, to a reduction in the quality of the remaining bone or, even, to the fracture of the prosthetic implant.

As shown in Figure 30, the extreme variation in biomechanical behaviour of a healthy femur and a femur with prosthetic implant (titanium alloy) during a simulated walking gait highlights the necessity to develop solutions that are geometrically and functionally as similar as possible to the original structure.

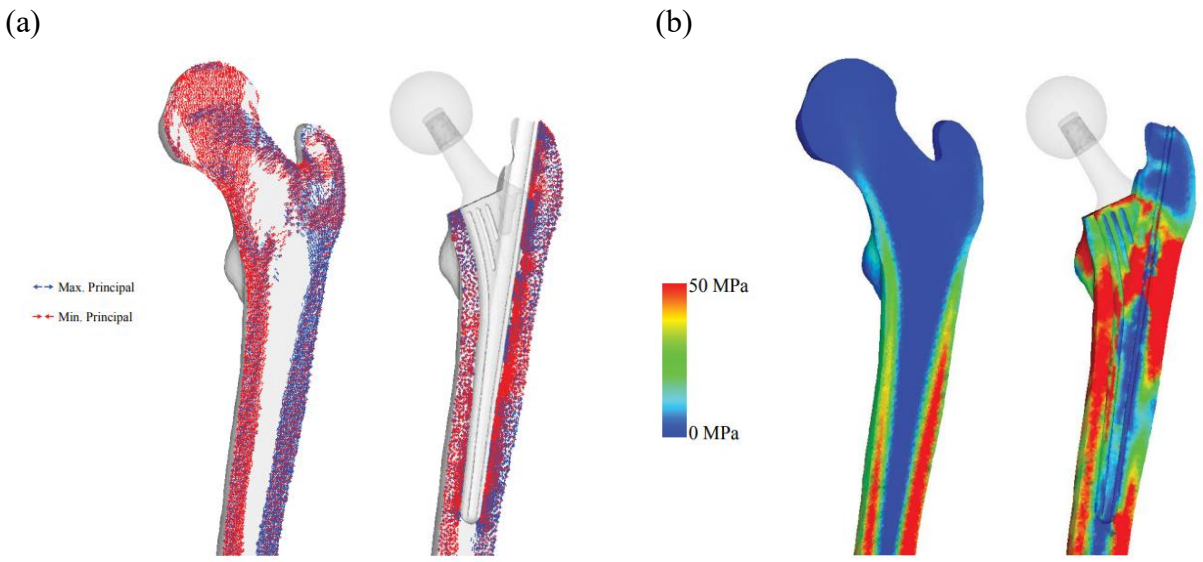

Figure 30. Finite Element Analysis (FEA) of a femur with an intact bone compared to a Total Hip Arthroplasty (THA) implant: simulation of the maximum loading experienced during a walking gait condition. (a) Principal stress projections in the intact bone and THA models (b) Drucker-Prager equivalent stress: THA model reveals that the proximal lateral section experiences high stress, while the distal lateral section experiences low stress [74].

The phenomenon of stress shielding is often induced by the different mechanical properties between the prosthetic implant and the bone. As shown in Table 4, the elastic moduli of metal implantable materials and the one of cancellous or cortical bone differ significantly. This is especially true in metal implants made of titanium, stainless steel, and cobalt chrome molybdenum alloys. Since metal alloys are ten times stiffer than human bone, they potentially absorb most of the mechanical load and

bring to a drastic reduction in the forces experienced by the bone, needed to maintain bone density and structure. As mentioned earlier, this leads to loss of density and weakening of the bone [73]. Remarkably, as opposed to traditional permanent metal implants, there are materials with bone-like properties. Specifically, magnesium alloys distinguish themselves for their higher mechanical affinity resulting from their ability to be reabsorbed by the human organism. However, the use of such materials is still limited as material resorption occurs at a higher rate than bone healing.

	Young's Modulus (GPa)	Yield Strength (MPa)	Compression Strength (MPa)	Tensile Strength (MPa)
Cortical bone	7–30		100–230	164–240
Cancellous bone	0.01–3		2–12	
Ti6Al4V (casted)	114	760–880		895–930
Ti6Al4V (wrought)	114	827–1103	896–1172	860–965
Stainless steel 316L	193	170–310	480–620	540–1000
CoCrMo Alloy	240	500–1500		900–1540
Mg (99.9%, casted)	41	21	40	87
Mg (99.9% wrought)	41	100	100–140	180

Table 4. Mechanical properties of metal material for implants compared to bone tissue (cortical and cancellous bone) [75,76].

In this framework, AM is successful in generating microstructural designs on the surface of the implant to decrease its stiffness.

An example of these kinds of surface structures is shown in Figure 31, the image shows the external surface of a titanium acetabular cup, the upper part of a total hip arthroplasty (THA) prosthesis, inserted into the cotyloid cavity at pelvis level. Another example is depicted in Figure 32 and Figure 33, representing respectively a pelvic implant and a magnification of its design structure.

These design elements are referred to as lattice, reticular, cellular and porous structures and, depending on the organisation of the baseline unit cell within the overall network, they distinguish into periodic or aperiodic geometries. The objective of these structures is to replicate the bone cellular matrix and, particularly, the aperiodic structures closely approximate the trabeculae of the bone. Aperiodic structures, also known as stochastic structures, are characterised by a random arrangement of the beams (struts) that compose the reticular network, creating an unordered lattice system. Among the most popular aperiodic structures is the Voronoi lattice, which is dependent on parameters such as the thickness of the Voronoi strut, the average distance between struts and a seed value to generate the points randomly.

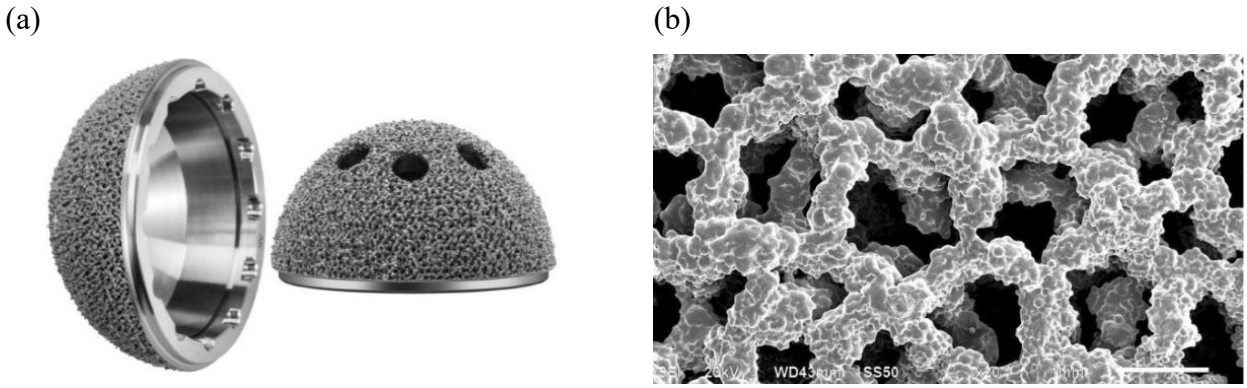

Figure 31. (a) EBM-produced titanium acetabular cup and (b) SEM image of the surface structure: trabecular structure, porous architecture based on a dodecahedron unit cell.

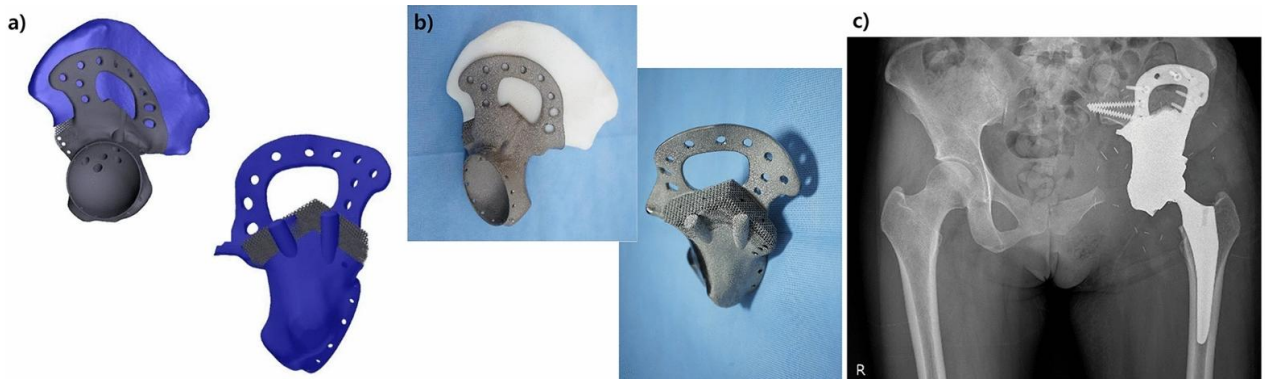

Figure 32. SLM-produced metal pelvic implant for Ewing's sarcoma surgery: (a) digital models of the implant on pelvic 3D scanning models (b); SLM-produced solid and reticular structures; (c) post-operative radiography of the applied prosthetic implant [77].

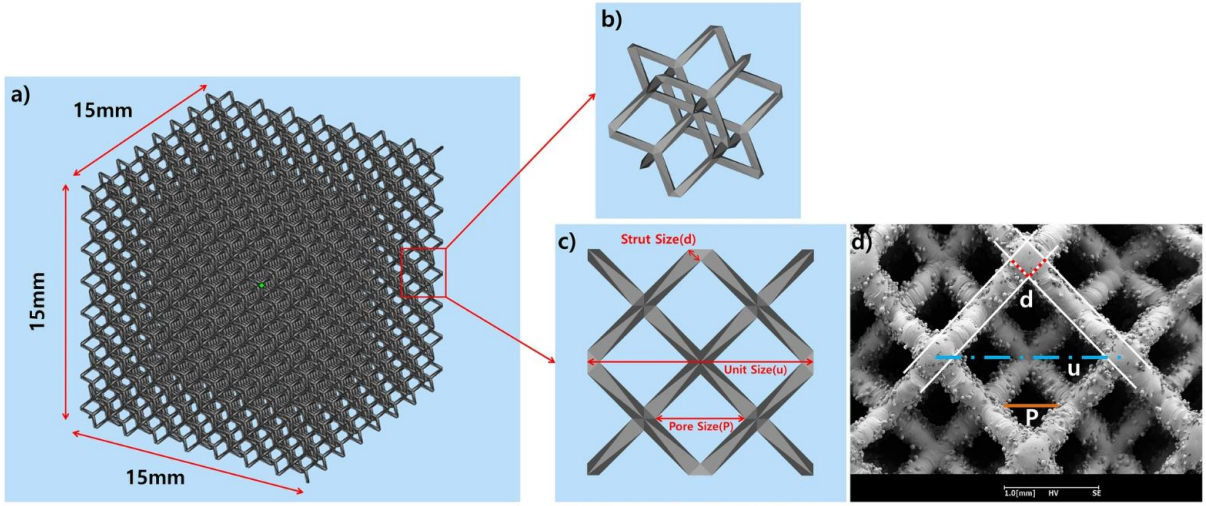

Figure 33. Detail of the structure implemented on the SLM-produced pelvic implant (a). The oblique (b) and top (c) views of the structure highlight the fundamental dimensional parameters: strut size, unit cell size and pore size. SEM image of the of the structure [77].

Hence, leveraging on AM methodologies, fine and intricate reticular structures are achieved. These possess numerous advantages in the field of implantable prostheses. First of all, lattice structures introduce the modulation of the elasticity (at a macroscopic level) of the solid implantable prosthesis and so, counteracts the stress-shielding effect induced by the greater stiffness of the solid implant compared to the natural bone. In addition, porous structures are able to promote osteointegration, namely the structural and functional connection between bone and implant [78]. In this respect, the porosity (intended as the volume fraction occupied by voids in relation to the total volume) and the pore size are factors that significantly influence cell invasion and angiogenesis, so the osteointegration activity [79].

Taking into account load-bearing prosthetic implants, especially THA acetabular cups or femoral stems, the optimal porosity values for bone growth is between 70% and 90% [80,81]. From the biological perspective, high porosity and pore connectivity favour cell migration and ingrowth into the prosthetic reticulum, promoting capillary formation and further facilitating cell migration and differentiation. In addition, enhanced porosity exhibits greater roughness, which stabilises the connection between the bone and the implant, preventing failure of the implant itself. Although the biological benefits appear potentially unlimited as porosity increases, the mechanical properties may be adversely affected. Specifically, the compressive strength of the implant decreases exponentially, making it more susceptible to failure under repeated stresses. Similar to porosity, also pore size and shape have direct influences on the osseointegration capacity of the implant, affecting nutrient transport, oxygen diffusion and metabolic waste elimination. Research studies agree that a pore size between 200 μm and 400 μm is an optimal range for bone growth [82–84]. Excessively small pores might hinder nutrient transport and prevent capillary growth and cartilage mineralisation, thus compromising implant stability. Moreover, scientific studies indicate that a pore diameter of at least 100 μm ensures adequate nutrient exchange [79,85].

Within the present context, PBF technologies, especially laser-beam PBF, are promising techniques for the fabrication of customised implants with intricate architectures and fine lattice structures [86,87]. Optimisation of the process parameters is essential to obtain high-performance implants.

2.1.3 Prostheses and Orthoses

A further medical application benefiting from AM technologies concerns prostheses, intended as the devices designed to be worn in contact with the patient's skin with the purpose of aesthetically substitute missing parts of the human body or replace impaired functions. This category includes, for example, the devices commonly used to restore the mobility of the upper and lower limbs, like sockets and artificial limbs. Also, the prosthetic segment comprises appliances such as eye and hearing aids.

Soft tissue prostheses can be produced too. Miechowicz et al. [88] produced a prototype of epitheses, an orbital prosthesis, with SLA and polyurethane (PU) photosensitive resins, after digitizing patient's face. Although SLA offered significant advantages in prostheses manufacturing, such as reduced time and cost, it has not completely solved the aforementioned issue, suggesting that further research in material science is required to optimise the fit to the defect.

Unlike prostheses, orthoses are external devices that do not substitute or replace body parts and their functionalities but rather sustain them. Specifically, orthoses are designed to support and correct the impaired physiological abilities. This category includes, for example, orthopaedic braces and insoles. Within this framework, MEX represents the predominant technique associated to AM-based customisation of orthoses; the most commonly used materials are thermoplastic polymer filaments, with recent experimentation with composite materials [89].

Conversely to implantable prosthetic systems, prostheses and orthoses are readily removable and replaceable. Their non-invasive nature makes them subjected to a less restrictive regulatory regime, thus, fostering experimentation with 3D printing technologies. This encourages the exploration towards innovative design solutions, characterised by an increased level of customisation, captivating designs, superior lightweight for equivalent strength and durability and greater comfort too. These personalised products are delivered in shorter production and consultation times, making them advantageous over the traditional process. Further confirmation of these statements comes from scientific studies, Ali et al. [90] demonstrated how ankle joint orthoses, manufactured from polymer and carbon fibre reinforced polymer (CFRP) using AM, offered superior performance at a lower cost than traditional materials.

2.1.4 Instruments

AM is also used to produce surgical and diagnostic instrumentation. Two are the major drivers for producing medical instrumentation by 3D printing. First and foremost is design freedom: conventional instrument designs might be revisited or completely revolutionised to accommodate the need for rare and uncommon medical operations. This aspect plays a key role since it provides the medical practitioners with improved tools and ensures safe and effective surgical operations. Additionally, the scientific literature justifies the choice of using AM methods given the considerable reduction in manufacturing costs [91,92]. This aspect brings to the cost-effectiveness of producing disposable, on-demand and patient-specific instruments. Customisation and cost-effectiveness, together, account for 50% of the reasons behind the choice of AM over conventional techniques for the production of medical instrumentation [91]. In addition to the growing trend of increased customisation, complexity and technical possibilities of AM-produced medical instruments, a further

application emerged: the production of tools designed to support people in developing countries or remote areas [91,93].

2.1.5 Latest trends

Biomanufacturing represents the latest application and the most advanced frontier of AM in the medical field. It is defined as the integration of AM technologies and tissue engineering [94]. This approach, originally called cytoscribing, was inspired by two-dimensional inkjet printers, as the ink droplets appear similar in form to biological products [95]. Then, technological advancement led to the development of bioprinters, namely 3D printing technologies capable of producing artificial and engineered biological tissues. These bioprinters are able to replicate cell aggregates ranging from small tissue constructs to complete organs and anatomical districts. The feedstock material used for these applications is known as bio-ink and consists of cells, taken directly from real organs, embedded in a matrix of biocompatible material, generally, hydrogel [96].

Biomanufacturing has the capability to transform the way transplants are performed, literally eliminating the necessity to conduct transplants from living donors or cadavers. Nonetheless, owing to its inherent complexity, bioprinting presents considerably more challenges than traditional 3D printing methods. A critical aspect concerns the need for the bio-ink to be cytocompatible, meaning that the bioprinted-produced element should not trigger harmful response in the host organism in order to maintain cell survival and viability. So, the effective production of bioprinted artificial organs relies on the appropriate selection of the bio-ink [97]. Another matter regards bioprinting conditions: it is essential to prevent contamination and ensure the purity of the process and so, the resulting product. The optimal management of printing parameters is vital to avoid inducing inappropriate stress conditions, such as excessive shear stress for cell survival.

The AM fields of application keep expanding and the technology itself is progressing, revolutionising its operating principle. Beyond traditional AM, technological innovation introduced the concept of 4D printing, where the fourth dimension is time [98]. 4D printing is defined as the 3D printing of smart materials (SMs) that, under the action of external or internal stimuli and within a required time frame, are able to control their geometric (shape, dimensions), structural (strength, stiffness) or functional properties [99]. SMs are designed to self-transform under thermal, mechanical, electrical or magnetic stimuli. This approach allows to produce medical applications able to automatically adapt to the patient's physiological conditions. Among the most popular applications are stents (expandable cylindrical nets that are inserted inside blood vessels to keep them leaky) and drug delivery systems, dynamically releasing pharmaceuticals based on the modification in patient's vital conditions [100].

Zhou et al. [101] showed that 4D printing can successfully produce drug-loaded vascular stents, capable of self-expanding in vivo.

Despite the positive progress, 4D printing is still limited with few SMs responding to a small range of triggers. Further research is required to better assess SMs interaction in the human environment.

To conclude, Figure 34 provides a glimpse on the discussed historical trends of AM technology applied to the medical field, outlining the future directions towards which it is heading.

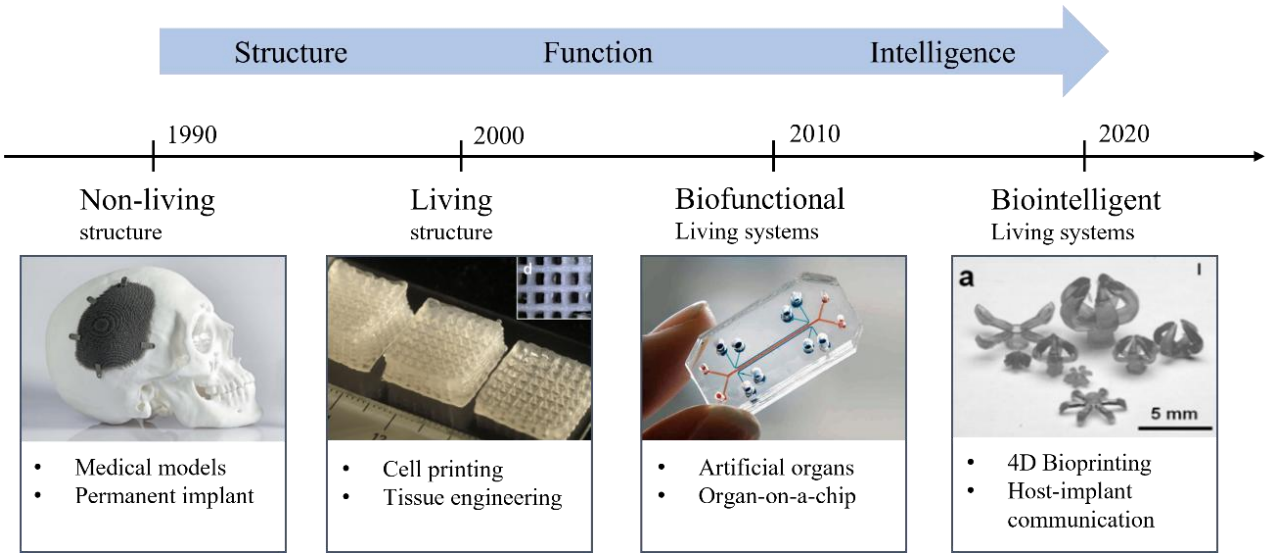

Figure 34. Roadmap of AM-produced medical applications, from non-living structures towards bio-intelligence [102,103].

2.2 Advantages and barriers

The present section examines the key advantages and opportunities of 3D printing in the field of medical production. The analysis includes the barriers and controversies associated with its implementation too.

Among the primary benefits of AM in medical applications, it stands out the ability to produce extremely customised solutions and equipment [104]. The high degree of personalisation attainable with AM is the aspect that initiated and stimulated the earliest research and experimentations in the clinical field. Customisation of medical applications allows medical solutions to be tailored to the patient's individual condition, offering significant advantages both for the patient, through reduced treatment times and recovery periods, and for the physician and hospital facilities, by improving the overall effectiveness of the diagnostic and therapeutic pathway.

Furthermore, beyond customisation, understood as the ability to produce patient-tailored prostheses and surgical instrumentation, AM enables the generation of intricate and articulated features. The

reachable degree of complexity is so high that these features are hardly feasible or economically viable using conventional manufacturing techniques. In addition to this, AM enables the design of optimised structures, improving the distribution of material within the element itself to meet specific constraints and performance requirements. In this way, medical devices show high robustness even with a significant reduction in weight [105].

Besides generating free-form and complex geometries, a further advantage of 3D printing is its ability to produce cost-effective medical elements. Although, as emerged, conventional manufacturing methodologies are convenient for large-scale volumes and standardised products, AM is becoming increasingly competitive for small series production and value-added products. This is beneficial in customised medical applications, which require single or limited production quantities [106]. Compared to traditional methods, AM significantly improves productivity, by fastening processing and delivery times. Cycle time is greatly reduced as a result of the flexibility in part modelling and design without having to invest time and resources in the preparation of customised equipment and tooling for the production of personalised medical devices. Whereas a prosthesis takes about a week to be manually produced and adapted to the patient anatomy, 3D printing reduces the time to one day, demonstrating the significant advantage of AM over conventional techniques [107].

Connected to this perspective, AM contributes to the reduction of production expenses by optimising the use of resources and minimising waste. In particular, AM is known for its aptitude in reducing waste and scarp materials. Indeed, the material is inherently used only where it is actually needed, the waste and scraps derive solely from the eventual use of support material (material that facilitates the truthful production of overhanging features and prevents part deformations during the 3D printing phase) and any post-processing treatments for finishing the element. As anticipated, the freedom of modelling allows to create lightweight designs, characterised by areas where the material is totally absent or lightened by advanced designs (reticular structures), and this aspect positively influences material savings.

Despite the numerous potential benefits associated with 3D printing, the over-optimistic expectations placed on this technology, at times, prevents from realising that there are several challenges associated with AM adoption in the clinical environment.

The healthcare industry is heavily regulated and requires rigorous testing by the regulatory authorities, like the Food and Drug Administration (FDA), for the certification of medical devices and instruments [108]. Clinical regulatory approval is a mandatory and critical step in the process of technological dissemination and adoption. Although some of the simpler additively produced medical devices have already been certified, meeting stricter regulatory requirements might hamper the diffusion of advanced medical applications. The need for extensive clinical and biological studies and

ethical and legal assessments further hinders the large-scale adoption of AM technologies and their solutions.

Commonly, regulation focuses on the final product. Nevertheless, AM methodology presents unique considerations that must be addressed to ensure the safety and effectiveness of the resulting parts, whether customised or mass-produced. This highlights the importance to take into consideration aspects such as the necessity to regulate, from a normative viewpoint, the AM processes.

Hence, it can be concluded that AM need strategic vision, economic investment and time to fully develop and reach its full potential [104]. Surely, 3D printing is democratising the design and production of medical application thanks to its increasing accessibility in terms of technological affordability and advances in engineering and material field. While recognising that the biomedical sector represents one of the most promising areas for 3D printing innovations, it is essential to appreciate the progress already achieved and move forward in an effort to facilitate the adoption of these technologies and products in the medical market.

Chapter 3. Material Extrusion and its application in the medical industry

In the current chapter, the AM technique known as Material Extrusion (MEX) is reviewed. The discussion focuses on exploring its applicability in the field of medicine, while, for details on the operating principles and technical characteristics, refer to Chapter 1, section 1.3.2.

Since the engineering of early MEX-based AM systems and, especially, over the past decade, significant technological advancements have occurred. MEX methodology widely expanded and it is being adopted by a broad spectrum of users, from amateurs (desktop 3D printers) to large-scale industrial professionals (industrial 3D printers). The growth in the adoption of MEX technology is such that, in 2021, the predominantly adopted 3D printing technologies found to be FDM and FFF, both based on the principle of extruding thermoplastic material from a nozzle [109]. There is a 100% prevalence among respondents who use or plan to adopt this technology. These data, complemented by those on the adoption rate of other AM techniques, are reported in Figure 35.

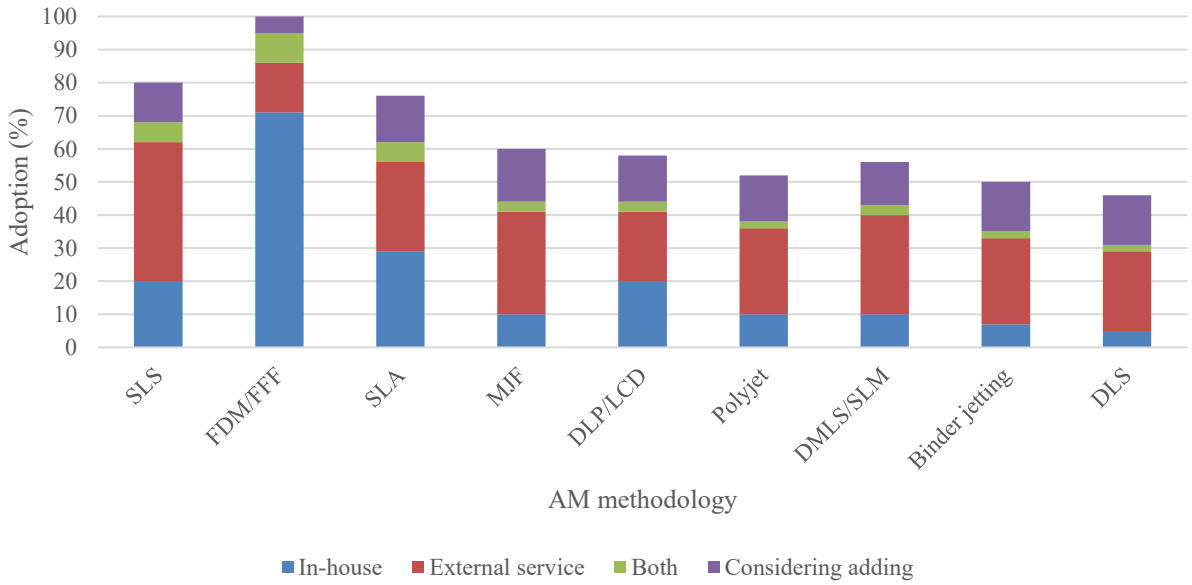

Figure 35. Distribution of the adoption of AM technologies distinguished by the modality of use (in-house, external service, both and considering AM adoption) and AM methodologies [109].

MEX distribution among diverse application areas is displayed in Figure 36. In 2020, the biomedical sector had a fair share, accounting for 21% of the US MEX market share [110]. The specific needs of biomedical applications, including high complexity, customisation and specific patient-physician

requirements, ease of processing, single or individual production quantities of high-value goods, are the driving forces behind MEX technology diffusion [111].

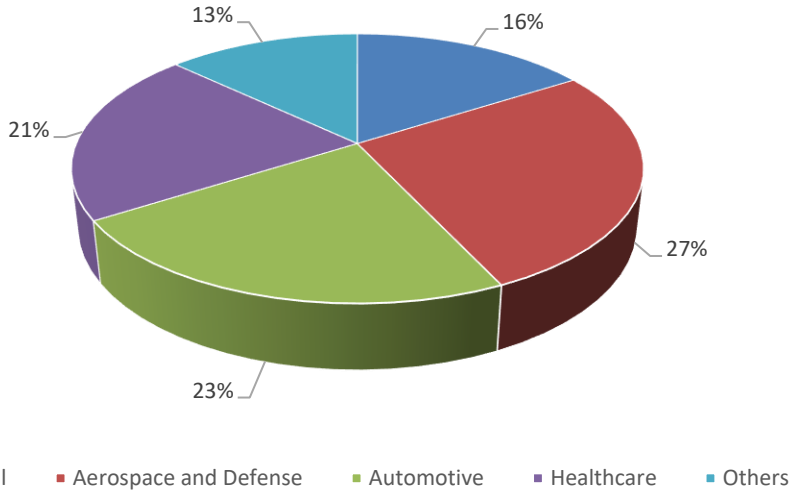

Figure 36. US Market share of MEX technology in various application areas [110].

3.1 Polymeric MEX-based medical components

Material Extrusion (MEX) technology was specifically conceived and designed for the extrusion of thermoplastic polymeric materials. Today, a wide range of polymers, especially under the shape of filament feedstocks, is available on the market.

Due to its affordability, ease of printing and biomechanical properties, such as biocompatibility and biodegradability, polylactic acid (PLA) still remains the dominant feedstock material in MEX manufacturing compared to other polymers.

PLA is a thermoplastic polymer with an elastic modulus between 2.5 and 3.4 GPa, suggesting a good stiffness. Typically, its tensile strength ranges between 45 and 70 MPa and it has a low elongation at break, usually less than 10%. With a 46% share of utilisation rate, PLA far exceeds all other polymers and composite materials; the second highest share is that of acrylonitrile butadiene styrene (ABS), with 27% [112].

Recent improvements in MEX printing equipment have expanded the range of available materials (Figure 37). Polymeric applications manufactured via MEX technology are widely adopted in the medical field, particularly for the creation of educational models and prototypes for surgical planning and training.

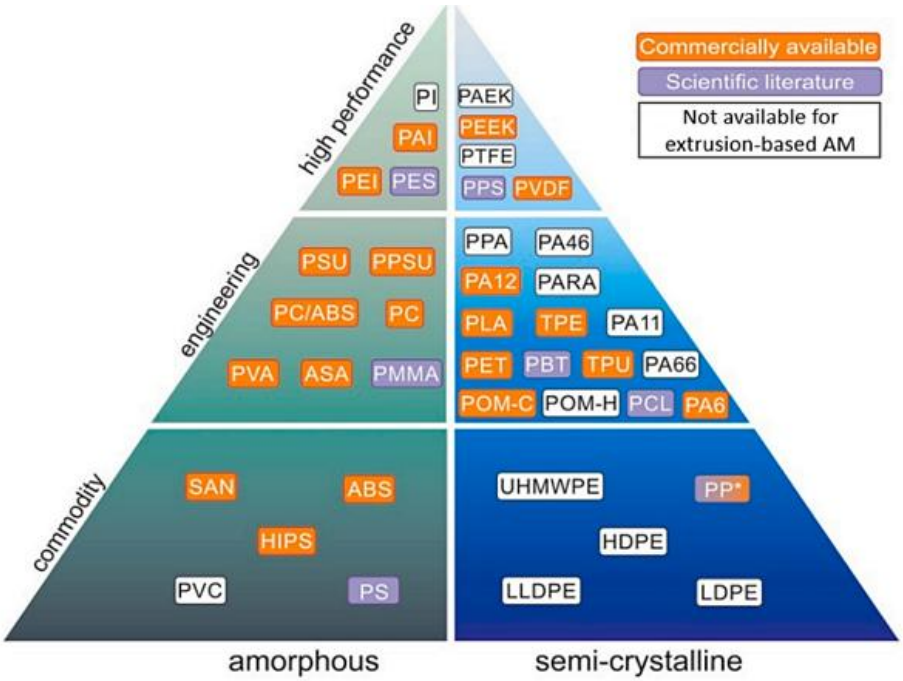

Figure 37. Amorphous and semi-crystalline polymeric materials, distinguished on the basis of their adoption in MEX-based AM: commodity, engineering and high performance use [113].

In these frameworks, there is an increasing demand for combining MEX with other techniques to integrate softer materials, such as silicones, within the thermoplastic rigid prototype. Again, this explains the thrust toward innovation in process and materials science. Additionally, Dave et al. [114] highlighted the potential of MEX technology as support or tooling process, i.e., for the production of moulds, dies, or negatives from which the positive model is subsequently derived. Indeed, MEX-based moulds are filled with softer materials in order to obtain prototypes with different properties.
In recent years there has been great interest in MEX-produced pharmaceutical dosage forms, such as tablets. In fact, the technology may deliver personalised and on-demand pharmacological products. Although the technology has the potential to produce personalised and on-demand pharmaceutical products, it must overcome numerous challenges to gain acceptance. These include the reduced availability of pharmacological polymers and biodegradable polymers, limited drug-polymer miscibility, the need for controlling printing temperatures to avoid drug degradation and the slow and partial drug release [115]. Despite these difficulties, McDonagh et al. [116] demonstrated how printing parameters, such as infill density and layer pattern, modulate drug release by successfully manufacturing dual-drug loaded polypills with simultaneous (paracetamol) and delayed (delodipine) release. While, Patel et al. [117] proved the feasibility of refining drug-polymer miscibility while significantly lowering the extrusion temperature of filaments by applying the principle of acid-base supersolubilisation to MEX-produced haloperidol tablets.

Nonetheless, in the context of technological innovation in the healthcare sector, one of the most promising applications of MEX is the engineering and manufacturing of prostheses and orthoses. The discussion on this latter topic is comprehensively addressed in the subsequent section.

3.1.1 Orthoses

As discussed in section 2.1.3, Chapter 2, orthoses are external devices designed with the purpose of supporting and ideally restoring the compromised functions of the human musculoskeletal system [118]. These medical devices are also commonly referred to as braces or splints.

Patients suffering from physical dysfunctions or disabilities, caused primarily by bone defects or muscle impairments (such as arthropathy and tendinopathy), as well as neurological disorders involving the brain, spinal cord and peripheral nerves, might require to use and wear orthoses. Depending on the individual clinical condition, orthoses for the upper limb (i.e., wrists, hands and elbows), lower limbs (i.e., hips, knees, ankles and feet) and orthoses for the spine (i.e., cervical, thoracic, lumbar and lumbosacral regions) are recommended. Based on this, the American Orthotics and Prosthetics Association adopted a scheme of naming orthoses according to the involved joints or spinal segments [119].

As established by current regulations [120], shared and standardised definitions of the therapeutic objectives and functional specifications associated with the design of orthoses are stated in Table 5. Beyond the categorisation, based on the involved body segment, orthoses distinguish themselves in prefabricated and customised.

Clinical objectives of orthotic treatment	Functional requirements of orthoses
• Relieve pain • Manage deformities • Prevent excessive range of joint motion • Increase range of joint motion • Compensate for abnormalities of body segment length and shape • Manage abnormal neuromuscular functions • Protect tissues • Promote healing	• Prevent, reduce and stabilise deformities • Modify range of joint motion • Alter length and shape of a body segment • Compensate and control for muscle inactivity or hyperactivity • Redistribute or reduce pressures and loads on tissues

Table 5. Fundamental therapeutic objectives and categories of functional specifications in orthotic treatment, according to ISO 8551:2020 [120].

Prefabricated orthoses are standardised medical device designed according to predefined specifications and they are readily available on the market to fit on a large population scale. They are available in a limited number of sizes and might be equipped with modular components, able to slightly adjust the device to patient anatomy. These aspects contribute to the cheapness of off-the-shelf orthoses [121]. Nevertheless, these solutions rarely adhere to the individual patient morphology optimally, requiring adjustments that are not always feasible. Besides, modifications may compromise the functionality of the orthosis and, consequently, hinder the therapeutic objectives. For instance, research related to orthotic therapy for wrist joint treatment [122–124] reported that the partial or total lack of control over wrist angle positioning in prefabricated orthoses resulted in adverse outcomes.

In response to the major disadvantages associated to the off-the-shelf orthoses, healthcare operators fabricate customised or personalised orthoses, tailor-designed and -made medical devices intended to perfectly fit the singularity of the patient.

Customisation procedure

The production of personalised orthoses, leveraging on conventional manufacturing methodologies, is a relatively demanding and cumbersome process, involving multiple steps to obtain the ultimate medical device [107]. It is performed by a trained medical professional and, sometimes, it may require the assistance of a second operator to ensure the correct positioning of the patient's body. The time required to design and produce an orthosis is primarily influenced by the extent of the anatomical area to be treated and the severity of the pathological condition. Yet, there are additional factors, such as patient requirements and preferences, that play a crucial role; for instance, in the case of high-performance athletic orthoses, the design, functionality and material superior requests may extend the processing timings. Generally speaking, the time required to complete this procedure might vary significantly, from a minimum of few days to several weeks, depending on the specific post-processing requirements too [125].

In the simplest conventional manufacturing instance, orthoses are developed from low-temperature thermoplastic (LTT) film of materials, softened in hot water (60°C to 80°C temperature), trimmed and directly moulded on patient’s body. However, it is often necessary to make a plaster cast of the anatomical region to obtain a negative mould from which a positive model of the anatomy is subsequently derived [126]. Plaster fluid fills the voids of the negative cast, left by the imprint of patient’s anatomy. Then, the positive model is adjusted to resemble the actual morphology of the patient and form the basis on which the detailed design of the orthosis takes place. Orthosis shaping is done entirely manually or leveraging on techniques like vacuum forming.

Although the fabrication of customised orthoses provides a unique and specific therapeutic treatment for the patient compared to the prefabricated orthoses, the approach is not free of flaws. The customised splinting process is strictly dependent on the preferences, expertise and experience of the healthcare operator [127], jeopardizing the entire quality of the medical device [122,128]. In fact, orthoses resulting from such procedures are often unsatisfactory, prompting thermal injuries and pressure-related complications (i.e., cutaneous diseases, compartment syndromes, bone and joint injuries) and difficulties in patient's adherence to the medical prescription [129]. Moreover, it is demonstrated that these complications are prevalent when the orthotic development is executed by less experienced practitioners [129].

Therefore, in the process of developing customised orthoses, it is evident that the design activity as well as the manufacturing process and materials exert a considerable influence on the effectiveness and overall performance of an orthosis [130].

In this framework, the introduction of 3D printing technologies and its auxiliary systems, such as Reverse Engineering (RE) and modelling systems, has the potential to bring significant benefits, while overcoming the drawbacks associated with the conventional manufacturing technologies. Indeed, AM offers the ability to capture the patient anatomical information with extreme precision, providing orthoses that exactly fit the specific clinical condition. Furthermore, it enables a rapid and cost-effective fabrication of mass-customised orthoses. Despite the promises, significant challenges need to be addressed. AM technology in the orthotic field is still in its preliminary development phase and extensive research is needed to explore and consolidate its potential.

The AM technologies that experienced the earliest utilisation in the orthotic field are based on MEX, VPP and PBF mechanisms [131,132]. Specifically, MEX technique found to be the most commonly adopted AM technique for the fabrication of customised orthoses. According to the literature revision conducted by Choo et al. [107], above the 73% of the analysed research articles, pertaining to orthotic manufacturing using AM technologies, employed MEX systems. The other adopted technologies were VPP, powder-based methods and systems whose methodology was not disclosed. From a clinical perspective, the review showed a predominant focus on limb function recovery, with a significant concentration on the lower limbs, accounting for 59% of the analysed studies, followed by the upper limbs at 36%. These results reflect the main areas of interest and progress in AM-based orthotic engineering. Moreover, the analyses compared personalised orthoses produced by traditional and AM techniques, stating that, generally, MEX-based orthoses are perceived as equivalent or superior to traditional solutions. Although there is still no unanimous consensus, opportunities and prospects, driving and supporting the research and development of MEX-based orthoses, emerged. These aspects are exhibited in detail below.

Manufacturing material

First and foremost, the choice of manufacturing material is a critical factor in the fabrication of orthoses, whether this process is performed via conventional or AM techniques.

In traditional manufacturing, material selection is often driven by orthosis affordability, availability and medical preferences. Nonetheless, to ensure that the orthoses meet functional and clinical requirements, there are numerous additional material properties that must be evaluated [130]. These characteristics are all reported in Table 6.

Material property	Description
Strength	Material quality to withstand an applied load without undergoing plastic deformation or failure. Orthoses characterised by higher degrees of strength are strong and resistant to great stress values. This characteristic is essential for medium and large orthoses, to adequately support joint weight, as well as for small orthoses, to ensure better stabilisation of the joint.
Stiffness	Stiffness is referred to the elastic modulus of a material, or the elastic response to an applied load. It measures the extent to which an orthosis is able to resist deformation in response to an applied force.
Hardness	Material quality to withstand localised (plastic) deformation provided by penetration or indentation. The choice of the hardness level of the orthotic device involves a trade-off: the inner part of an orthosis should exhibit a softer behaviour to increase patient comfort, while the outer part should exhibit increased hardness.
Durability	Material ability to maintain its properties within its lifecycle, without deteriorating, under ordinary conditions. In some orthotic instances, it is estimated via fatigue testing.
Processability	Material ease of handling, machining and working. Processability is intended both as formability and printability. In the first case, it is the ability of effortlessly shaping the material into an orthotic element while preserving quality standards. In the second case, it is the ability to smoothly extrude the material filament and reliably reconstruct, layer-by-layer, the orthosis.
Moisture resistance	Material ability to not alter its properties when exposed to moisture and liquids. Orthotic material should resist the effect of moisture, avoiding humidity absorption and material degradation.
Biocompatibility	Material ability to safely interact with the human body tissues, minimising the likelihood of cytotoxicity, sensitisation and irritation (intracutaneous

	reactivity). This definition of biocompatibility is in accordance with the intended material use and current medical standard for orthotic use [133].

Table 6. Definition of the material properties evaluated in the production process of customised orthoses.

In the production of conventional orthoses, the materials used in clinical settings are thermoplastic polymers, predominantly, semi-crystalline polypropylene (PP) and polyethylene (PE). They possess low density, thermal stability and chemical resistance. PP, having a slightly higher softening temperature than PE, is stiffer and more durable than PE [134]. Due to its superior mechanical properties, PP is commonly used for corrective orthoses.

The current personalised care trend, towards which medicine is heading, requires more precise modulation of material characteristics to better meet clinical objectives and patient satisfaction. It is not conceivable to identify a universal ideal orthotic material. In the long-term perspective, it is no more sustainable to rely solely on few traditional thermoplastic polymers. Likewise, it is not practicable to establish a unique optimal combination of parameters that accommodates every orthosis. As a matter of fact, the mechanical properties of distinct orthoses might require to vary significantly. For example, orthotic insoles are accommodative orthoses, designed to be comfortable and alleviate plantar pain, therefore they are made of soft and shock-absorbing materials; whilst, spine orthoses must provide support and correct spinal defects and, so, they are rigid in nature.

In the production of MEX orthoses, the most common used materials are thermoplastic filaments, including primarily PLA, ABS, and thermoplastic polyurethane (TPU) [135]. ABS is known for its high impact resistance, making it suitable for orthotic applications that require rigidity and robustness, and ease of processing [136]. TPU offers superior mechanical properties, like flexibility, tensile strength and abrasion resistance compared to similar thermoplastic elastomers [137]. Also, polyamide (PA) is becoming more and more popular given its enhanced strength, prolonged stability, chemical resistance and great versatility [138,139]. Particularly, Nouri et al. [130] proved that polyamide-12 (PA12) orthoses are a viable alternative to injected-moulded polyamide-6 (PA6) orthoses: the AM-finished items demonstrate competitive properties, in terms of robustness, adaptability and durability, compared to moulded elements.

Fibre-reinforced thermoplastic filaments constitute a more recent class of orthosis materials, providing practical and flexible solutions to improve the properties of thermoplastic filaments. Common synthetic reinforcements include glass, carbon and Kevlar fibres [130].

In this framework, it becomes more and more evident that MEX-based technologies have the potential to effortlessly manage a fair range of materials and modulate orthotic characteristics, offering well-defined and superior performances compared to traditional manufacturing processes and materials.

Furthermore, advances in material engineering and design made MEX-printed elements suitable for applications other than prototyping. These developments improved the functionality and reliability of MEX-produced orthoses for end applications too.

Contact interface and material selection

In conjunction with the benefits of using MEX technologies and thermoplastic filaments for orthotic manufacturing, another crucial aspect is the contact interface between the orthosis and the human body surface.

In most conventional custom orthoses, the fitting of the orthosis is done manually and human error might adversely affect it. The provision of an adequate offset is mandatory to avoid direct surface contact with bony protrusions or sensitive regions of the human body. If the therapeutic arrangement is not acceptable, the effective distribution of pressure on the involved skin and joints is endangered and, so, it is patient comfort. Under these circumstances, modifications to the orthosis to readjust the device to patient morphology must be made. To prevent undesirable effects, the healthcare professional has at his disposal few materials characterised by varying degrees of conformability, which is the ability of the material to adapt to the patient anatomy with minimal manual adjustments. Hence, when selecting the material for the manufacturing of the conventional personalised orthoses, the healthcare operator must critically balance its choices. The selection of less stiff materials facilitates shaping and prevents the need to apply excessive pressure on patients, who may have painful or compromised clinical conditions. However, these materials are not always suitable for all clinical conditions. Moreover, their processability tends to be problematic over large anatomical areas. As anticipated, erroneous shaping leads to inaccurate contact surfaces and uneven pressure distribution, in turn, hindering proper care and requiring further design modifications. In most cases, even if the traditional manufacturing process is flawless, orthoses still require post-fabrication adjustments.

Instead, the utilisation of MEX-based technologies prompts the optimisation of the contact surface between the orthosis and the interested body region. This possibility is facilitated by intensive experimentation in AM material and processing: optimisation of process parameters allows to produce MEX-based elements with distinct properties. Beyond that, the improvement in the adaptation of the custom orthosis to the morphology of the patient is certainly determined by the intrinsic nature of AM methodology: MEX orthoses, being precisely designed on the exact anatomy, do not require any adjustment to adapt to the patient morphology, theoretically.

Contact interface and Reverse Engineering techniques

In recent years, the introduction of various contactless acquisition systems of 3D anatomical surface information accelerated the dissemination of patient-specific AM orthoses [140].

In the field of orthosis modelling, Reverse Engineering (RE) initially used advanced medical imaging technologies, such as computed tomography (CT) and magnetic resonance imaging (MRI). However, because of the issues related to exposure to ionizing rays and the high cost of these assets, alternative solutions, not rigorously present in hospital settings, have been introduced.

RE of the human body segments might be accomplished via photogrammetry: it captures multiple images from different angles and merges them together to generate a complete representation of 3D models. A significant advantage of photogrammetry is the relatively reduced scanning time compared to other technologies, like structured light scanners or laser scanners, that requires that the patient remains motionless for a prolonged time [141,142]. Hence, photogrammetry is advantageous for critical categories of patients, such as paediatric individuals. Nevertheless, the processing time and computational requirements to reconstruct the 3D model might be quite elevated [140]. Whereas, structured light scanning projects patterns of light to capture the superficial coordinates of an element, it acquires textures too. Similar to laser scanner, structured light scanning provides higher-resolution data, such that it was found to be able to accurately reproduce fine anatomical features, even the complex curvature and nuances of the vertebral column [143]. However, since structured light scanning consists in capturing multiple images from different angles in a continuous flow, even minor motions of the body might hinder the quality of the resulting 3D model. Then, laser scanner represents another technology used for high-resolution surface scanning and it effectively supports the production of customised orthoses. Specifically, research is moving toward the development of 360-degree laser scanning systems able to capture the anatomy of the human upper and lower limb in a single shot, thus, extremely reducing scanning timings [140]. Early apparatus [144–146] encompass multiple cameras arranged in a circular frame. A similar approach [147] involved a single camera attached to a robotic arm rotating in a circular motion around the patient's limb.

Paoli et al. [148] demonstrated that optimal surface reconstructions, especially in terms of RE of upper limb extremities, were performed using handheld scanners, given their fast acquisition time. As discussed previously, in relation to materials for the development of MEX custom orthoses, the selection of the adequate methodology to acquire anatomical surface information strictly depends on the specific orthotic application and its requested level of accuracy [149,150]. Regardless of the adopted RE methodology, the deviation between digital geometry and 3D printed geometry is greatly reduced, if not totally nullified, when compared to orthoses obtained via traditional methods. Thus, enabling to accurately estimate the behaviour of the orthoses under ordinary conditions and predict

any inappropriately stressed anatomical area. This means that the responses and performances of the MEX-printed devices are predictable. This aspect, on the other hand, cannot be underestimated in the case of traditional custom orthoses.

Despite the benefits introduced by the integration of AM with RE systems, several challenges emerge and might limit the adoption of these technologies. These difficulties are related to the digitisation of the patient anatomy and orthotic modelling activities. As Baronio et al. [143] stated, AM represents only the final step of the whole process of orthotic customisation. RE is essential and, in the study, they emphasised the timing of this activity. As a result, although scanning (structured light scanner) and image alignment took 2 and 10 minutes, respectively, the modelling of a hand orthosis took 1.5 hours, highlighting the need to automate these operations to reduce overall process time. Similarly, Palousek et al. [151] digitised a full patient arm using passive photogrammetry in 12 minutes, however, the activities of polygon data processing and modelling took 3 and 6 hours, respectively. The study showed that this process requires a good knowledge of RE and a deep knowledge of CAD modelling software. Also, Kim et al. [152] reported that an expert CAD operator took 2.7 hours to model the frame of an arm orthosis. Moreover, as pointed out by Blaya et al. [153], the necessity of using multiple CAD software, to manage the conversion of the anatomical surface into a 3D printable orthosis model CAD, is not uncommon.

Given the discussed challenges and the potential advantages, the progresses in RE technologies are leading to faster, simpler, less invasive, affordable and more efficient tools [154]. Beyond that, the development of software able to support the integration of all of these technologies is required [155,156]. To avoid discouraging the implementation of AM in clinical settings, technological advances must be oriented towards the integration and automation of anatomical surface management and modelling activities.

Lightness and additional requirements

When developing patient-specific orthoses, beyond technical performances, it is essential to consider aspects valuable to the patient and whose relevance has a direct impact on patient acceptance, satisfaction, and compliance with his wearing schedule, rather than on pure technical characteristics. One of these factors is the material mass density and, consequently, the thickness and weight of the orthoses. A lightweight orthosis facilitates freedom of movement or simplifies wearing, improving the comfort during daily activities. Conventional customised orthoses might be shaped starting from perforated sheets of LTT materials, thus presenting patterns of micro- or/and macro-holes. Although these orthotic solutions promote lightness and air ventilation, these materials are difficult or pernicious to be processed. The uncontrolled hole enlargement and stretching, performed manually,

make the orthosis mechanical behaviour unpredictable [157]. On the other side, with 3D printing, the process of medical device lightening, though, for example, the modelling of uniform or topological optimised holes, provides predictable outcomes.

It is well known that AM supports a range of light-weighting approaches, including generative design techniques such as topological optimisation. Topological optimisation (TO) is a mathematical method extensively used in civil and mechanical engineering to design physical systems and mechanical structures by iteratively optimising the material distribution within a given design space. Driven by design engineering advances, TO has the ability to address diverse requirements, including the medical needs [158–163] related to the customisation of orthoses basing on the forces exerted on the device during its use [164]. TO explores diverse design solutions with organic forms that mimic the efficient natural structures.

Nonetheless, there is still a discrepancy between TO potentialities and its actual implementation in the medical field. The hindered adoption is not a consequence of the lack of data documenting functional outcomes and biomechanical performance of highly customised medical solutions. For example, Khan et al. [165] showed that the use of TO in ankle-foot orthoses (AFOs) led to significant weight reduction and improvements in terms of strength and flexibility, compared to standard orthoses. Similarly, Reis et al. [164] proposed a TO model of a resting hand orthosis that improved mechanical strength and reduced weight, the model provided thermal comfort too. As argued by Geoffroy et al [160], in the research on TO cranial orthosis for infantile plagiocephaly, it is essential to consider all the activities of the entire manufacturing process. This perspective highlights that, once the advantages of advanced modelling have been achieved, attention should shift towards prioritising production feasibility and process simplification. Indeed, according to Ambu et al. [166], research commitment should focus on developing a procedure, able to easily adapt patterns of predetermined TO ventilation holes to each unique design of orthosis. Moreover, it is erroneous to assume that functional designs, once modelled, can be effortlessly printed [167,168]. Although it is feasible to fabricate nearly any shape generated by TO software, if the optimisation is solely based on lightness, the risk is to compromise the overall efficiency of the AM process.

Hence, the hindered adoption is prompted by the absence of multi-factorial studies examining the integration of TO tool within the AM process chain. Furthermore, although the benefits arising from the creation of customised devices are supported by scientific evidence, it remains unclear whether the integration of this tool is compliant with existing systems, platforms, and infrastructure.

3.2 Metal MEX-produced medical components

The most popular techniques for producing AM metal components are powder fed and powder bed systems, which allow the manufacture of complex geometries with high density and precision. Especially, as exposed in Figure 38, the predominant adopted technology in the metal AM industrial market is Powder Bed Fusion (PBF) [169].

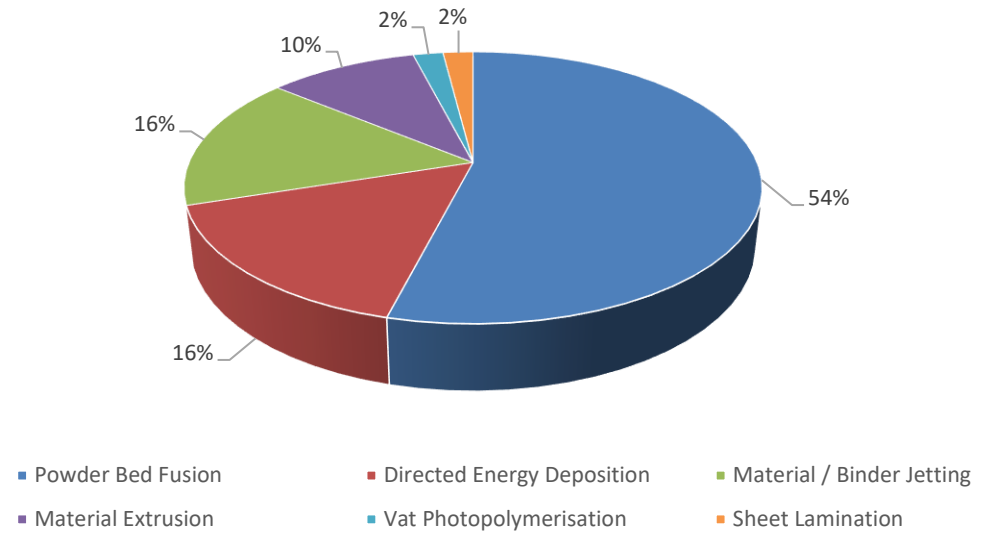

Figure 38. Adoption rate of metal AM technologies in 2020 [169].

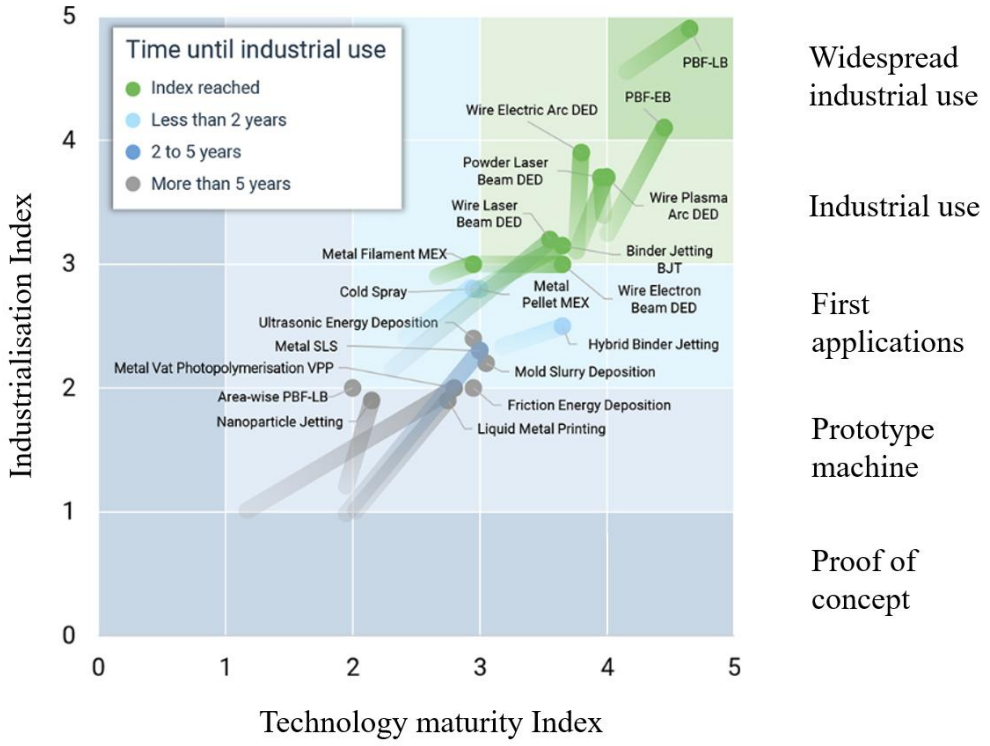

Figure 39. Maturity index of metal AM technologies, 2019-2023 [170].

In addition, Figure 39 presents a framework of the evolution and maturity of each distinct metal AM technology. This approach allows discernment between established and widely adopted technologies, emerging systems with potential for cost optimisation and niche technologies that are likely to maintain limited specialization. Recent improvements and increased knowledge in MEX processes have expanded their application to metal manufacturing, transforming MEX into an emerging and powerful alternative to powder bed and powder fed systems. Owing to the inherent simplicity of the extrusion process, MEX technology is characterised by a reduced technological investment, absence of high-power heat sources, reduced energy consumption and lower health and environmental risks associated with handling metal powders [171].

To manufacture metal components, MEX employs filaments, pastes or granules feedstocks based on metal powders combined with polymeric binders. Generally, the binder is multi-component to meet the required physical and mechanical properties for the printability of the green part. Besides binder formulation, the content, particle size and distribution of metal powders have an influence too.

Furthermore, the powder particle type plays a crucial role in determining either the processability of the material either the properties of the final element. Kukla et al. [172] reported that, in filament feedstocks produced with the same amount and kind of polymeric binder, the choice of powder affects the mechanical properties of the filaments. As shown in Figure 40, filaments containing stainless steel particles demonstrated the highest ultimate tensile strength (UTS) and elongation at break. Conversely, titanium powders resulted in lower tensile strength and flexibility, which adversely affected the spooling, feeding, and printability of the filament.

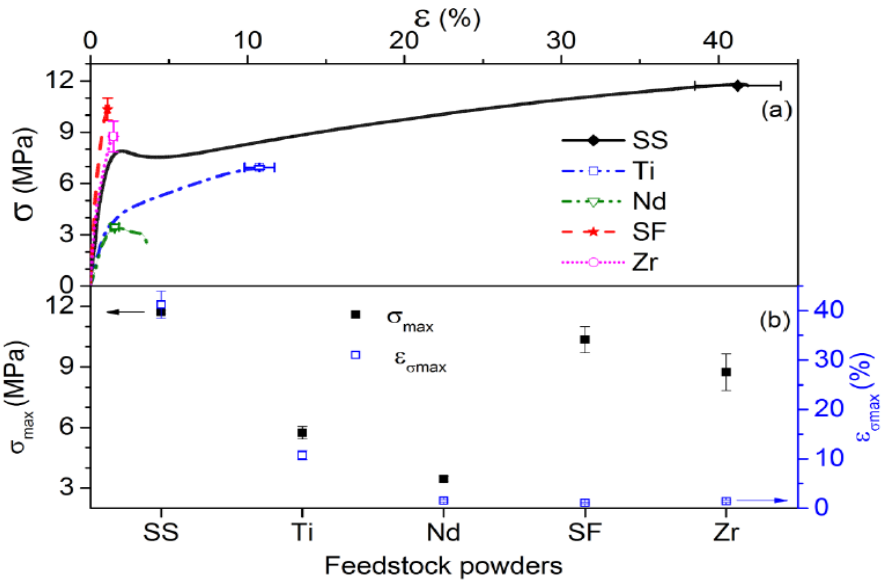

Figure 40. (a) ε-σ curves and (b) σmax and εσmax for MEX filaments loaded with different metal powder particles [172].

Owing to the complexity deriving from the feedstock formulation, a limited number of alloys have been developed and commercialised for MEX. As illustrated in Figure 41, among the most widely used alloys are AISI 316L and AISI 630, followed by Ti-6Al-4V and Nickel superalloys.

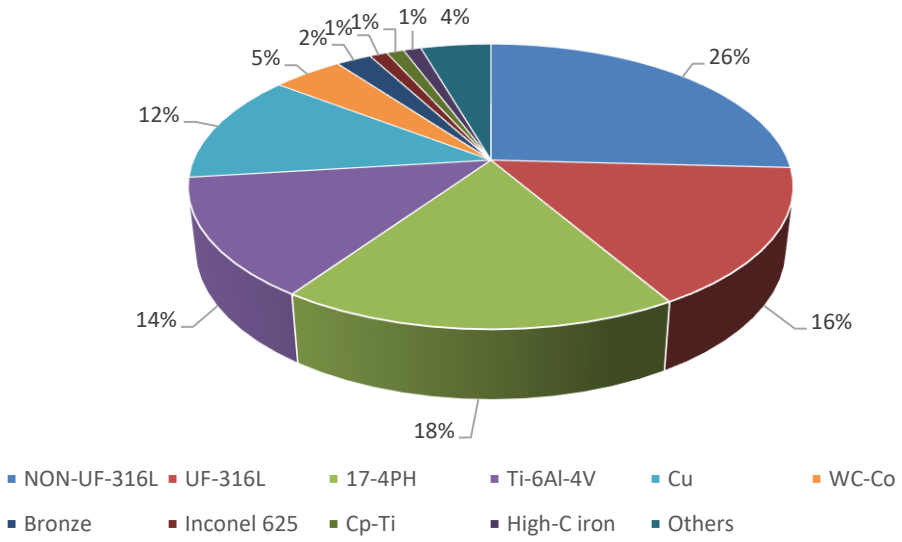

Figure 41. Metal alloys employed in MEX-based processes. Others include H3, M2, Ni-Cu and AZ91.

Despite efforts in the optimisation of feedstock shaping, generally, MEX-based components exhibit lower dimensional accuracy and strength compared to powder bed and powder fed AM technologies [173,174]. This phenomenon is mainly attributable to the lower density achieved in the final product. Carrozza et al. [175] distinguished two kinds of defect in MEX-produced specimens: micro-pores, or randomly distributed voids, and elongated macro-pores, characterised by a triangular or quadrilateral-shaped core periodically distributed throughout the specimen.

A critical factor in enhancing the physical and mechanical properties of MEX-fabricated metal components is to analyse the printing process targeting the elimination or reduction of the printing-induced voids.

To date, few methodologies have been investigated in scientific literature to improve densification:

- Control of the layer height, namely the thickness measurement along Z-direction of the deposited material layer. The influence of layer height on porosity is controversial in the literature. Some studies find little or no variation [176,177], while some others suggest an inverse relationship in which green part density tends to increase with smaller values of layer thickness [178,179].

- Increase of flow rate multiplier, parameter responsible for the volumetric amount of material extruded during printing. The default flow rate multiplier is set to 100%. In the research study conducted by Singh et al. [179], statistical analysis identified flow rate multiplier as the most relevant process variable influencing the void generation. An increase of this factor, bringing the value above 100%, reduced the gap between adjacent strands of extruded material and the overall porosity, improving the density of the green part. Likewise, Meng et al. [180] found that a high flow rate multiplier, over 100%, is essential to obtain highly dense components in the green state.
- Generation of an overlap between following strands of material. According to Côté et al. [181], an overlap of up to 5% reduced defects that were traditionally mitigated by lowering layer height. Increasing the overlap between 15% and 20% eliminated interlayer rhomboidal voids and minimise element dimensional deviations. While, overlap above 25% favoured the formation of macroscopic defects, reducing part quality.
- Control of printing speed, or feed rate parameter. Singh et al. [179], observed that reducing the printing speed facilitated a uniform extrusion and deposition of the feedstock, thereby decreasing the occurrence of large voids both within the strands and between consecutive layers.
- Regulation of raster angle, also known as hatch angle. It is the angle with which each strand, composing a layer, is deposited with respect to the X-axis of the building plate (Figure 42). It is denoted as the orientation angle of layers. Default raster angles are ± 45°, however variable or alternating angles are allowed too [182,183]. Numerous studies [176,183–185] demonstrated that the raster angle, together with part orientation, significantly impacts the mechanical properties of the component.

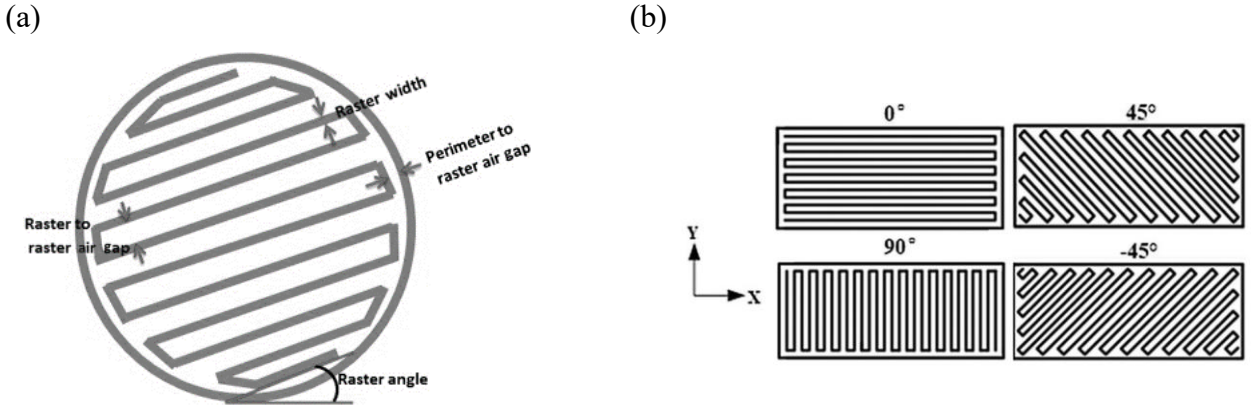

Figure 42. a) Representation of the raster path and raster angle in a cross section of a circular specimen, (b) examples of the most adopted raster path and angles.

Therefore, it is imperative to thoroughly consider all these variables to ensure optimal print quality. In addition to the parameters directly affecting void generation, it is advisable to study additional factors influencing the whole metal MEX process (Figure 43).

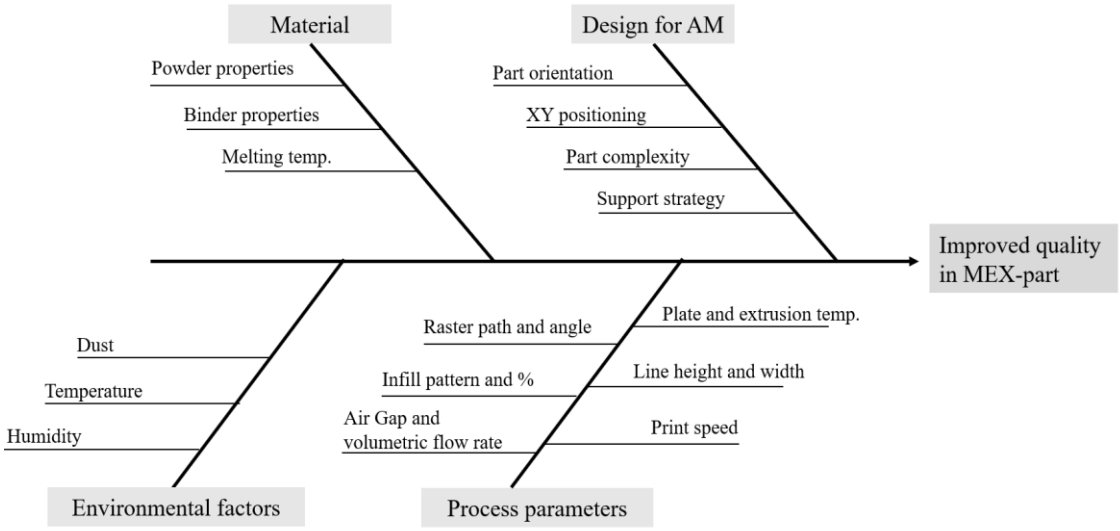

Figure 43. Ishikawa diagram of metal MEX process parameters.

This perspective is especially relevant when the application targets high-value industrial segments, such as the healthcare field, which requires compliance with stringent regulations. Therefore, it is critical to push research toward innovation and continuous improvement of MEX technology.

Currently, metal manufacturing via MEX represents an interesting approach for biomedical applications [31]. Indeed, recent studies [173,186,187] experimented Ti-6Al-4V manufacturing of diverse geometries with MEX. The sintered Ti-6Al-4V components exhibited a tensile strength of 875 ± 15 MPa and an elongation of 17 ± 3% with a relative density of 94.1 ± 0.1%, comparable to metal injection moulded (MIM) parts [188]. The promising results drive research toward medical applications such as customised implants. Shaikh et al. [189] investigated the feasibility and suitability of Ti-6Al-4V MEX-printing for patient-specific maxillofacial implant prototypes. However, the complexity of such geometries represented a significant obstacle in obtaining high-quality parts. In particular, a pronounced stair-step effect was observed contributing to high surface roughness at the macroscopic level. The surface roughness (Ra) corresponded to 18 ± 5 µm. In the sintered components, a relative density of 81 ± 4% was found, indicating a total porosity of 19%, of which 11% was interconnected open porosity. In addition, a Rockwell hardness of 6.5 ± 0.8 HRC was observed. Similarly, Garcìa de la Cruz et al. [190] explored MEX-produced CoCrMo alloys for prosthesis fabrication. Specimens showed high relative density, around 96%, and remarkable wear

resistance. Wear tests indicated that the obtained results are compatible with custom knee prostheses, offering enhanced wear resistance.

In conclusion, it is evident that research in the field of metal MEX is oriented on the in-depth analysis of the process and its printing parameters to optimise the mechanical properties and surface quality of the resulting MEX-based elements. This approach is vital for gaining detailed knowledge to facilitate, at a later stage, the development and production of intricate geometries, like those intended for medical applications.

3.3 Research Issue

The objective of the present manuscript is to provide an in-depth analysis of Additive Manufacturing (AM) methodologies and their applications in the healthcare industry. To this end, the study aims to evaluate, through an interdisciplinary approach, the factors influencing the integration of 3D printing technologies and the resulting solutions within medical settings. Specifically, the aspects include:

- Technical feasibility – This aspect concerns the capability of Additive Manufacturing (AM) technologies and their auxiliary systems to produce medical components with the required characteristics. Particular attention is given to alternative medical-grade materials and their processability with advanced AM technologies, as well as to the manufacturability of highly innovative designs that are often unattainable through conventional production methods. It should be noted that technical feasibility extends beyond the evaluation of AM technologies and their products, encompassing all operations within the AM process chain, with a specific focus on Reverse Engineering (RE) and modelling activities
- Process robustness – This element regards the flexibility of the AM process in addressing diverse clinical cases. It examines whether the investigated AM technology can reliably adapt to meet the specific needs of various patient and treatment scenarios, ensuring reliable outcomes across a range of medical applications.
- Economic sustainability – This aspect refers to the ability of the AM process to remain economically viable while continuously delivering medical device of high quality. The total costs of implementing the technology are considered, including both the initial investment associated with the acquisition of the necessary equipment and the recurring operating costs.
- Operational compatibility – Beyond the simplest form of compatibility, which concerns the consistency between the considered AM materials and their intended use (biocompatibility), other factors are taken into consideration. The integration of AM technology within existing clinical production and operational processes is evaluated. This aspect includes examinations of the consistency of the activities related and/or involved in the AM processes with respect

to the traditional clinical protocols. Moreover, the importance of analysing production times is observed too.

To systematically address the established objectives, the research activities focused on a distinct AM methodology, namely Material Extrusion (MEX) technology, available at the laboratories of the Department of Management, Information and Production Engineering of the University of Bergamo. MEX systems are widely adopted in the processing of polymeric materials and recent experimentations broadened its applicability to the printing of ceramic and metallic materials too. For this reason, the analysis of the applicability of MEX methodologies within the clinical framework develops along two strands. The first research branch, representing the most substantial and structured area of the study, focuses on the investigation of Material Extrusion (MEX) technology for the production of polymer-based medical applications. The second branch, which is still at an early stage of development, explores the flexibility of the technology for the fabrication of metal medical components.

In the first branch of the research activity, the objectives are addressed through the identification of a targeted clinical application, representing one of the most promising and strategic research directions: the production of patient-specific orthoses.

With regard to the topic of customised AM-produced orthosis, Figure 44 identifies the major areas of interest and gaps in existing research, as well as outlines potential future directions. The picture reports an analysis of the main research terms (keywords co-occurrence analysis), conducted on a final cluster of 132 engineering scientific articles. The analysis highlights the relevance of AM within the current scientific landscape, emphasizing its central role around which numerous equally significant research topics are developed. Moreover, the temporal distribution of the investigated subtopics, largely concentrated from 2016 onward, confirms the relatively young and rapidly growing nature of this research field. In particular, the most recent subtopics, such as “upper limb orthosis”, “process optimisation”, “polymer”, “3D scanning” and “human machine interface”, reflect the rise of innovative outlooks and facilitate the understanding of the thematic areas on which this study is structured.

In light of the foregoing discussion, the research focuses on the development of customised orthoses with an approach that, in a first step, aims at defining an alternative methodology to the traditional fabrication of orthoses and, specifically, orthoses for the treatment of upper limb joints. In this context, a multi-step procedure is proposed, laying the groundwork for evaluating the manufacturing feasibility of these devices. The process chain includes 3D scanning of the hand-wrist-arm district, semi-automated modelling of the anatomical surface into an orthotic model and, at last, fabrication of an orthotic prototype using MEX and biocompatible filaments.

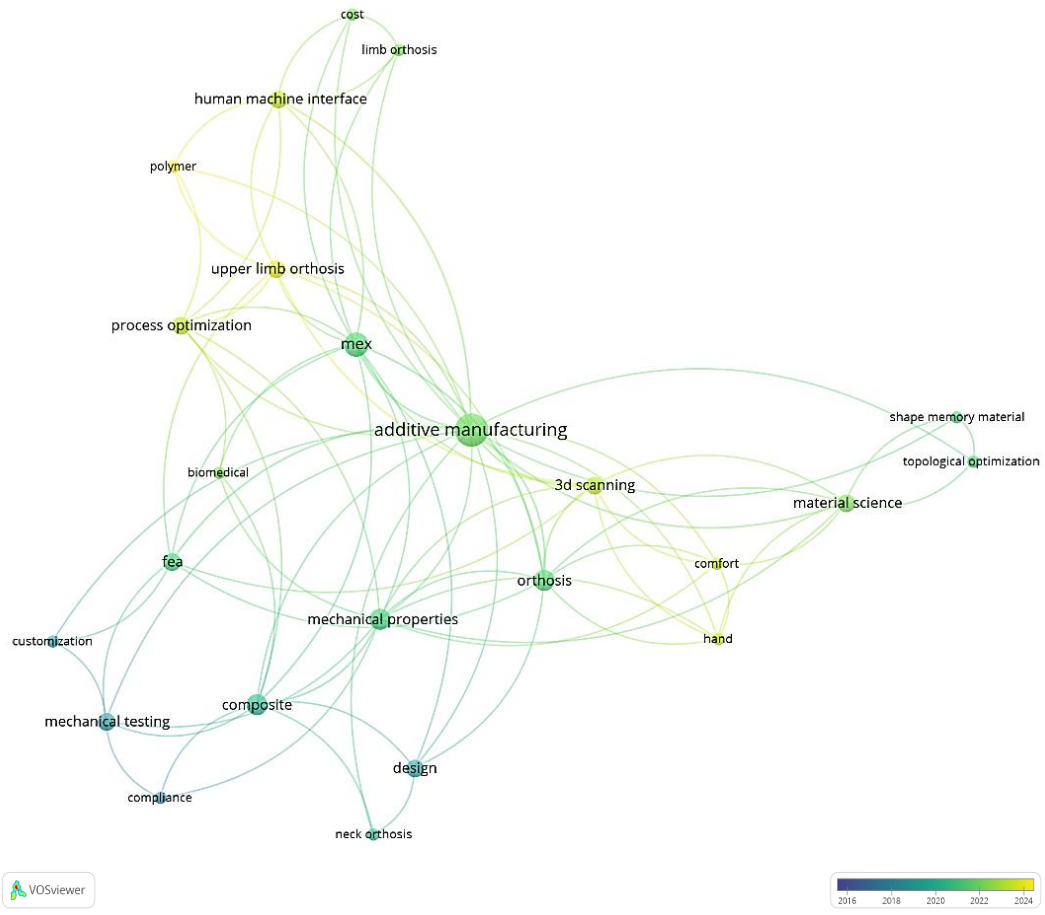

Figure 44. Keyword co-occurrence map based on bibliographic data (overlay visualization). The analysis was conducted using VOSviewer (version 1.6.19), a software for visualizing and analysing bibliometric networks, by considering the relationships between differ.

Alongside the delineation of the process chain to produce personalised upper-limb orthoses, a cost model is proposed. This provides an initial estimate of the costs associated with the devices obtained through the proposed methodology and enables an economic benchmark with traditional manufacturing processes.

Subsequent studies focus on expanding the analysis domain by experimenting with different materials, such as ABS, nylon, and PLA, and also estimating the technical performance of the devices. The heterogeneity of factors included in the evaluation aims at providing data and tools for healthcare operators to make informed and effective choices. In addition, the analyses encompass different anatomical structures, thereby verifying the stability and repeatability of the proposed methodology and its suitability for implementation across diverse clinical scenarios.

Ultimately, the integration of an advanced modelling technique into the AM process chain is presented. The impact of Topological Optimisation (TO), understood as a strategy of extreme customisation and lightening of medical devices, is studied. While technical analyses are often the

exclusive focus, this latest research evaluates economic, operational and practical aspects, offering a holistic perspective.

The second strand of the research activity is prompted by the recent advances in the combination of MEX technology, traditionally employed for 3D printing thermoplastic filaments, with metal powders. This integration opens new opportunities in the production of metal components, matching the versatility and cost-effectiveness of MEX technology with the high-performance potentialities of metals.

Compared to other metal AM methodologies, metal MEX is still in its early stage and its industrial application remains severely limited. The need to study and understand the relationship that links process parameters to the final behaviours and properties of metal MEX-produced elements is fundamental. This is even more important in the healthcare field, where strict regulations require medical devices to be performant, effective and safe.

Taking into consideration these assumptions, the research is oriented towards an initial technical evaluation of AISI 316L MEX-produced elements. Precisely, the optimal printing conditions that characterise the predominant AM technologies in the production of metal medical devices, namely Powder Bed Fusion (PBF) systems, were adapted and applied to MEX technology. This provides a deeper understanding of the research objectives: the feasibility of producing metal components for medical applications via MEX technology.

To conclude, the research project focuses on the analysis of MEX technology for medical applications, exploring both polymeric and metal components.

Nonetheless, the recent installation of a laser-based PBF (LPBF) system at the laboratories of the Department of Management, Information, and Production Engineering at the University of Bergamo has opened new research directions. Given that, to date, research on this topic has not yet produced sufficient results, it could not be included in the main body of this document. Therefore, the potential research directions regarding the suitability of LPBF for medical device manufacturing are briefly outlined in the concluding section.

Chapter 4. MEX-based manufacturing of customised medical applications: orthoses

4.1 Definition of the Additive Manufacturing workflow for the production of customised upper limb orthoses

This chapter is derived from the article "Sala, F.; Carminati, M.; D'Urso, G; Giardini, C. (2021). A feasibility analysis of a 3D customized upper limb orthosis".

DOI: 10.1016/j.procir.2022.06.038

I am grateful for the support received from my co-authors. I bear full responsibility for all the variations from the published version reported in the current chapter.

The present study contributes to the current research framework by proposing a standardised and structured procedure for the fabrication of customised upper limb orthoses for the management of chronic and non-acute conditions.

The proposed procedure is based on a multi-step methodology that integrates three main phases: Reverse Engineering (RE), digital modelling and Additive Manufacturing (AM).

In the existing scientific literature, several studies [143,151–153] have investigated the traditional fabrication process of customised upper limb orthoses and have examined the potential of advanced manufacturing techniques. Specifically, these contributions explored different methodologies to re-engineer medical devices for the treatment of acute conditions affecting the joints and bones of the hand-wrist-arm district. Although these technologies offer clear advantages, their benefits can be fully realised only when they are integrated within a structured workflow that enables rapid, automated, and consistent orthosis modelling.

Therefore, within this context, the present work revisits conventional manufacturing approaches for orthotic devices, aiming to overcome limitations related to comfort and functionality that characterise traditional orthoses. Moreover, the methodology seeks to reduce the variability associated with disparate levels of medical expertise too. Simultaneously, the work addresses the current challenges associated with modelling procedures, as identified and emphasised in the related scientific literature.

A software program, based on Python language, is developed with a user-friendly interface and a set

of intuitive commands that grant physicians a fair degree of arbitrariness in orthotic designing without requiring technical knowledge about CAD modelling.
The study is supplemented with a feasibility analysis, including an assessment of the time and cost of the implementation of the new methodology within the clinical framework. Specifically, the study includes the formulation of a cost model dedicated to the production of AM-based orthoses.

4.1.1 Methodology

Scanning Operation

High-speed data acquisition represents a critical step in ensuring accurate orthosis scanning, as the patient is required to remain motionless in the same position throughout the entire procedure. The optimal set-up involves positioning the patient in a seated posture, with the arm raised anteriorly to shoulder level. A support was placed under the middle phalanxes and the thumb was kept separately from the hand. The acquisition of the 3D shape was performed by means of the Hexagon Absolute Arm 7-Axis, equipped with RS6 Laser Scanner (Figure 45).

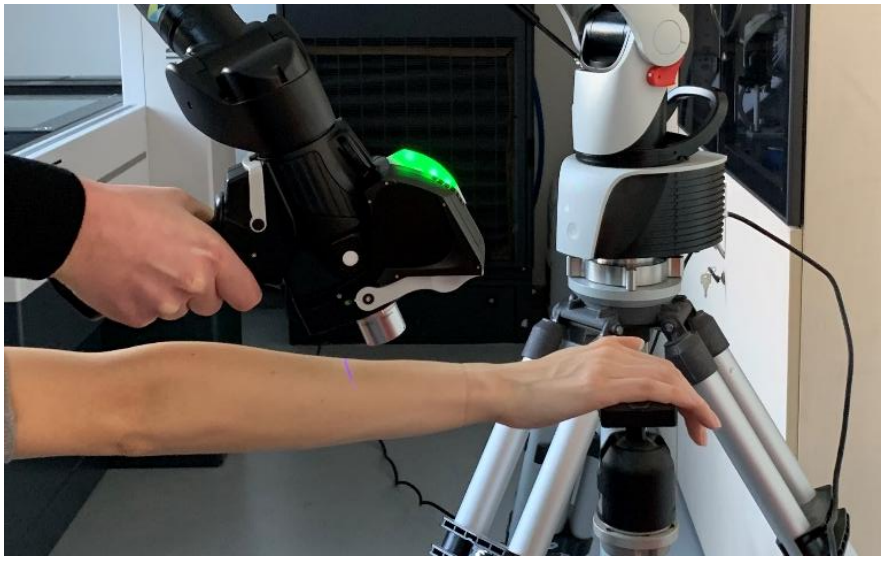

Figure 45. Optimal configuration of the 3D limb geometry acquisition with the Hexagon Absolute Arm 7-Axis equipped with RS6 Laser Scanner.

The scanning procedure was preceded by preliminary operations accomplished with Polyworks Inspector. A clipping plane, used to define and limit the region of interest, was established using a 6 mm touch probe. A point cloud was selected as extraction data type and a standard resolution was

chosen since details smaller than 1 mm in size were not necessary for the purposes of the activity. Then, a single 360° scansion around the patient's arm was acquired.

Surface elaboration

With PolyWorks Modeler, the digitised point cloud was transformed into a surface-based polygonal model, which is more accurate and less noisy. The software automatically detects and corrects the most evident topological errors, reconstructing the mesh and refining the surface triangulation. All the gaps and holes with a diameter lower than a target value were individually closed and all the detached elements were removed manually. The effectiveness of the described procedure largely depends on the operator's proficiency in using the software.

Thereafter, the STL file was exported to a commercial CAD software, where the limb surface-based model was manually processed into an orthotic solid-based model. Given the absence of a specific orientation in the exported model, the limb surface was aligned in a defined coordinate system. A smoothing action was applied to the limb surface and two offsets were generated. The first creates the 3D solid geometry, while the second ensures sufficient ease between the arm and the orthosis. Cut operations were applied to the orthosis extremities to preserve the shape of interest. A parametric pattern of holes was included to lighten the structure and the model was divided into two shells along the arm centre line.

CAD modelling

The procedure described in the previous section is not compatible with the time and cost constraints associated with the clinical production of orthoses. Furthermore, the process heavily depends on the operator's skill in converting the scanned point cloud into a printable STL file. These limitations highlight the need to develop an automated system that can reduce production time and facilitate the clinical workflow during the creation of the orthotic device. Hence, a CAD modelling system was designed and it was conceived as a simple and straightforward Graphical User Interface (GUI), composed of different commands that produce an accurate STL model of the orthosis from the 3D scanned forearm. Python language libraries such as PyQt5, Vtk and PyMeshLab were involved to automate the CAD modelling process.

The new modelling procedure requires the polygonal model to be imported into the GUI workspace. As opposed to the previously described procedure, the steps leading to the generation of an orthopaedic model are standardised and automated through the creation of functions, integrating multiple algorithms.

The function *fix_mesh* translates the model to the origin of the global reference system created in the environment and removes duplicated vertices and faces. The Quadric Edge Collapse Decimation algorithm simplifies the number of triangles in the textured mesh. The Ball Pivoting algorithm reconstructs surfaces using existing points without creating new ones. All the detached points are deleted and holes with diameters up to a defined measure are closed.
The function *smooth_mesh* enhances the surface of the model leveraging on the Laplacian Smooth feature, which is iterated with a sufficiently low number of repetitions to prevent mesh degeneration. After the levelling operation, the function *expand_mesh* creates an offset towards the outside of the surface model, fulfilling both the wearability and the immobilisation aspects of the orthotic device.
The function *hollow_mesh* creates a new mesh, which is a resampled version of the current one, using the Marching Cube algorithm that generates a solid shape with a customisable thickness.
The function *rotate_mesh* is responsible for the arbitrary rotation of the solid along the three Cartesian coordinates. This operation is exploited in conjunction with the function *crop_mesh*, The function *rotate_mesh* is responsible for the arbitrary rotation of the solid along the three Cartesian coordinates. This operation is exploited in conjunction with the function *crop_mesh*, utilised to remove the useless anatomic regions of the orthosis. Both operations are kept manual to allow the clinical staff to adjust the most critical anatomical areas.
The orthotic structure is emptied via ventilation holes, by means of the function *addholes_mesh*. The procedure necessitates the execution of a Boolean difference between two meshes, the current one and the one representative of the gaps shape. A library containing different holes designs is available and their actual positioning is performed manually at the discretion of the specific clinical case.
Furthermore, the *clamp_mesh* function manages the arbitrary insertion of the fastening systems, designed to join the two shells of the orthopaedic orthosis. The operation consists of a Boolean union among the current orthosis meshes and the joint system mesh (selected from a dedicated library).
Finally, the function *fork_mesh* divides the model into two orthotic shells, generating two STL files, each representing a half of the orthosis.

Additive Manufacturing

The customised orthosis can be fabricated using Material Extrusion (MEX), which is particularly suitable considering the complex geometry of the orthotic device and the constraints related to production cost and time.
The manufacturing process was carried out using an Ultimaker S5 printer equipped with a 0.8 mm nozzle, extruding an Acrylonitrile Butadiene Styrene (ABS) filament as the primary manufacturing material for the orthosis. ABS was chosen according to factors, including biological compatibility.

Given the alleged purposes and, in accordance with the standard [133], the materials required to be compatible only in terms of cytotoxicity, sensitization and irritation (or intracutaneous reactivity). Considerable attention was paid to the aspects of ease of printing and low purchase cost of materials. Ultimaker Breakaway was selected as the support material since it can be removed easily and manually from the orthosis after the end of the printing process.

The selected printing parameters for the ABS filament are a 250°C nozzle temperature and a printing speed of 60 mm/s. A layer height of 0.6 mm ensures a considerable time reduction of the printing process. The infill density rate was set to 100%.

The Ultimaker Cura 3D printing software was used to prepare the model and generate the G-code file to print.

Cost model

Based on existing cost assessments and valuations found in the literature [191,192], a comprehensive model for estimating the manufacturing costs of an AM orthosis was formulated. The parameters included in the analysis comprise the 3D printing (P) and 3D scanner (S) purchase costs and the costs related to their power consumption (E), the manufacturing material costs (M) and operator labour costs (L).

As shown in Eq. 1, P parameter was calculated as the product of the entire production time (Tp) and the purchase cost (Pp), standardised over its useful operating time, given by the utilisation rate (Kp) and useful life (Yp) of the technology. In particular, Tp corresponds to the deposition time (Td) plus non-deposition times (Tnd) or other times related to pre-print and post-print preparation (warm-up (Twu), set-up (Tsu) and cooling (Tc) times).

$$P = \frac{T_p \times P_p}{K_p \times Y_p} \qquad \text{Eq. 1}$$

The preceding mathematical expression was suitably modified to define S factor, as presented in Eq. 2. The scanning time (Ts) is a single component, directly assessed during the arm measurement activity.

$$S = \frac{T_s \times P_s}{K_s \times Y_s} \qquad \text{Eq. 2}$$

As shown in Eq. 3, E parameter is the energy consumption cost related to the 3D printing and 3D scanner technologies. Particularly, Pe stands for the cost of electricity and Ci for the power consumption measured during specific time intervals Ti (where i = {Td; Tnd; Ts}).

$$E = P_e \times (T_d \times C_{Td} + T_{nd} \times C_{Tnd} + T_s \times C_{Ts}) \quad \text{Eq. 3}$$

The M factor depends on the characteristics of the two extruded elements, the material (m) and the support material (ms). As displayed in Eq. 4, the parameters involved in the calculations are infill percentage (in), component volume (V), material density (ρ) and material cost (Pm and Pms). Specifically, Vm and Vms were derived from the values of the extruded wire length multiplied by the wire section surface.

$$M = in_m \times (\rho_m \times V_m \times P_m) + in_{ms} \times (\rho_{ms} \times V_{ms} \times P_{ms}) \quad \text{Eq. 4}$$

Lastly, Eq. 5 expresses the cost of labour parameter (L), simply given by the product of the hourly wage (Pl) and the working time (Tl) of the operator.

$$L = T_l \times P_l \quad \text{Eq. 5}$$

The overall cost to produce an AM orthosis is determined by the sum of the previous five equations as reported in Eq. 6.

$$C_{AM\ orthosis} = P + S + E + M + L \quad \text{Eq. 6}$$

4.1.2 Results

Scanning procedure and CAD modelling

The contactless acquisition of the arm shape, accomplished by an experienced operator following the procedure described in the methodology, took slightly less than 2 min (Table 7).

The developed GUI (Figure 46) is organised into five areas: menu, view bar, status bar, workspace and task bar. The menu (upper area) handles actions related to file management, such as uploading and saving the file. The view bar (right area) allows to interact with the virtual camera and display

the object from different perspectives. The status bar (bottom area) shows real-time information such as the execution time of the current operation, the coordinates and the number of faces and vertices of the model. The workspace (central area) represents the environment in which the polygonal model is processed. The generation of the final orthotic model is accomplished by nine primary commands reported in the operations bar (left area): model translation and pre-adjustment, surface smoothing, solid generation, rotation, cutting, ventilation holes creation, fastening systems implementation and model partitioning.

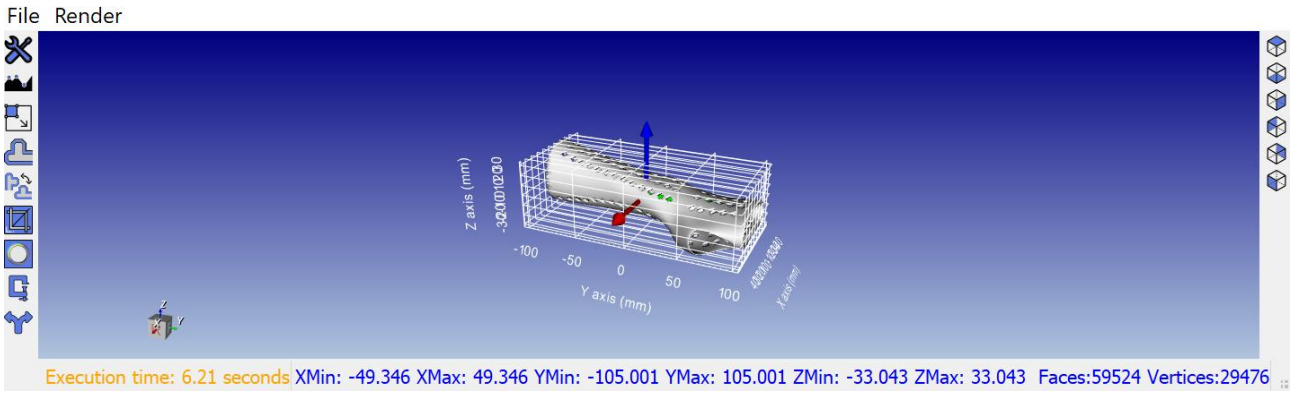

Figure 46. GUI.

Orthotic modelling operations are summarised in Table 7. The first operations that were performed on the limb scan concerned its translation in the workspace origin and the optimisation of the mesh (e.g., the closure of holes with diameter less than 50 mm). During surface smoothing, the Laplacian algorithm was iterated 50 times to avoid mesh degeneration. Two adjustable offsets were created: the first offset of 2 mm eases orthotic wearability, the second offset between 2-4 mm corresponds to the thickness generating the solid. The cutting operation, along with the rotation function, removed the upper and lower extremities and refined the area around the thumb. The orthotic solution was characterised by a ventilated structure, lightening the device and providing easy access to rehabilitative therapies (e.g., electrostimulation). Holes of rhomboidal shapes were selected to prevent material collapse during deposition, minimising support material usage to surface overhangs only and speeding up the time required for the support removal. In the present model, four rows of holes (spaced 10 mm apart) were introduced in the areas of the hand and forearm. Ultimately, the orthotic model was divided into two complementary shells joined by 12 fastening systems (6 per shell) enabling quick removability during medical inspection of the injured area.

The times of the operations to generate a new orthotic model via GUI are reported in Table 7. Standard deviations, computed on the execution of three tests, are provided as an indication of repeatability and reproducibility of the developed modelling system. The GUI procedure lasts approximately 15

min, reducing the elaboration times compared to the manual modelling executed by a CAD expertise (this one lasting more than 2.5 h).

Scanning procedure and modelling steps		Time and std [s]
	Acquisition of a single 360° scansion around the patient's arm	110.0
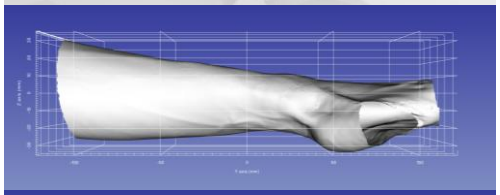	Primary processing (translation and pre-adjustment)	9.43 ± 0.05
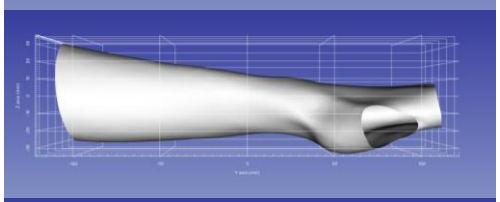	Surface smoothing	0.73 ± 0.01
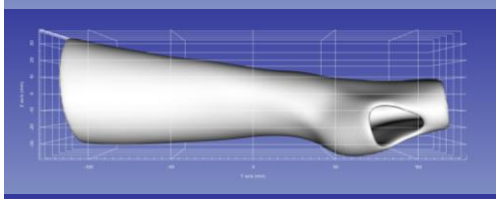	Offset creation	48.67 ± 0.38
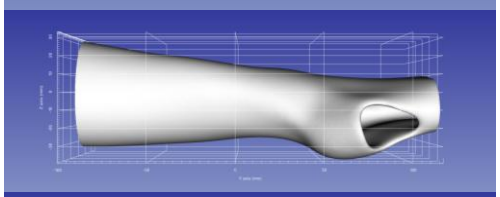	Rotation and cutting	3.94 ± 0.73
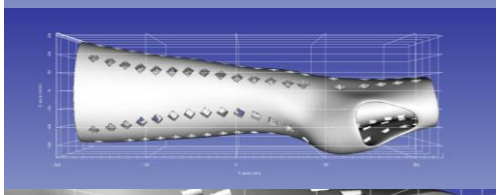	Creation of ventilation holes	737.31 ± 50.31
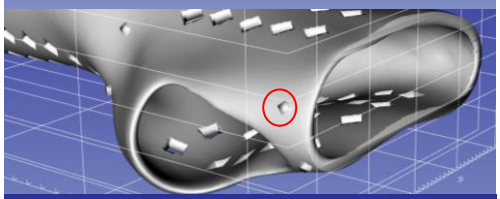	Implementation of fastening systems	63.92 ± 10.72
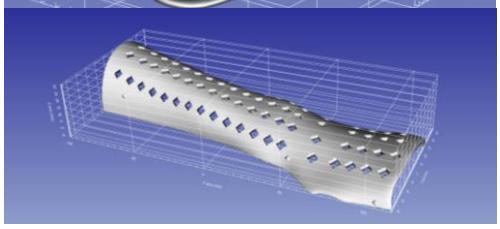	Model partitioning into two shells	2.23 ± 0.59

Table 7. Scanning procedure and operations for generating an orthotic model.

Orthosis fabrication

For the creation of the orthosis prototype (Figure 47), 85.5 cm^3 of ABS material was used. An additional 1.04 cm^3 of support material was added only in the upper region of the hand, for overhangs exceeding 88°. This angle reduced to a minimum the consumption of the support material and simultaneously provided the correct realisation of the product. No finishing treatment was performed, the study focused on assessing the feasibility analysis of the medical device realised with a semi-automated process.

Figure 47. Early prototype of the limb orthosis.

As reported in the methodology, a layer height of 0.6 mm was selected to lower the deposition time. Tensile tests [193] and three point bending tests [194] were carried out to verify a possible inverse relationship between the layers height of the samples and their mechanical properties. For each test, three samples with 0.1 mm layer height and three samples with 0.6 mm layer height were printed.
An analysis of variance (ANOVA) was performed and Table 8 reports the p-value obtained after the ANOVA. It is possible to observe that the layer height affected both the tensile and flexural strengths of the samples. Moreover, the layer height of 0.6 mm ensured higher levels of tensile and flexural strength (Table 9).

	Tensile strength	Flexural strength
p-value	0.000	0.016

Table 8. Influence of the layer height on the tensile and flexural strength.

	0.1 mm	0.6 mm
Mean tensile strength [MPa]	31.3	39.5
Mean flexural strength [MPa]	85.1	96.8

Table 9. Mean tensile and flexural strength as a function of the layer height.

Time-cost evaluation

The main parameters affecting the 3D printing cost are summarised in Table 10. Tp was derived from two contributions: the time spent actually extruding the material and the time required for all other operations. The deposition time (1.92 h) resulted from a 3D printer slicing program and it was dependent on the complexity of the STL file and the printing process parameters (e.g., layer height, layer width, printing speed). The non-deposition times, including warm-up (0.12 h), set-up (0.03 h) and cooling (0.13 h) times, were dependent on the properties of the selected material.

In addition to the 3D printing cost, which amounts to 0.60 €, the cost associated with the 3D scanning was similarly calculated, resulting in 0.24 € per orthosis. The detailed breakdown of the cost components of the latter is reported in Table 11.

Parameter	Symbol [unit]	Value
Production time	Tp [h]	2.20
Technology purchase cost	Pp [€]	6,000.00
Technology deployment	Kp [1]	0.50
Technology useful life	Yp [y]	5.00
3D printing cost	P [€]	0.60

Table 10. 3D printing parameters and cost.

Parameter	Symbol [unit]	Value
Scanning time	Ts [h]	0.03
Scanner purchase cost	Ps [€]	70,000.00
Scanner deployment	Ks [1]	0.10
Scanner useful life	Ys [y]	10.00
3D scanner cost	S [€]	0.24

Table 11. 3D scanner parameters and cost.

The energy cost depends entirely on the 3D printer parameters and resulted to be 0.14 €. The non-deposition phase is responsible for both nozzle and build plate heating and, consequently, requires higher power supply values than the actual deposition phase. On the other side, the scanner energetic

contribution can be considered negligible. The power supply parameters Ctd, Ctnd, and Cts were all measured with an electricity consumption sensor and are displayed in Table 12.

Parameter	Symbol [unit]	Value
Electricity cost	Pe [€/kWh]	0.26
Technology power consumption during *Td*	Ctd [kW]	0.23
Technology power consumption during *Tnd*	Ctnd [kW]	0.31
Scanner power consumption	Cts [kW]	0.19
Energy cost	E [€]	0.14

Table 12. Energy parameters and cost.

The parameters of material cost are shown in Table 13. The volume of a component was derived from the information on the wire area and the extruded wire length, obtained from the 3D printer slicing program. The extruded wire lengths were 13.51 m for the ABS and 0.16 m for the Breakaway. The overall material cost is 4.71 € while the cost of the support material is negligible.

Parameter	Symbol [unit]	Value
ABS infill percentage	inm [1]	1.00
ABS component volume	Vm [cm^3]	85.54
ABS density	ρm [g/cm^3]	1.10
ABS cost	Pm [€/kg]	50.00
Breakaway infill percentage	inms [1]	0.1
Breakaway volume	Vms [cm^3]	1.01
Breakaway density	ρms [g/cm^3]	1.22
Breakaway cost	Pms [€/kg]	72.67
Material cost	M [€]	4.71

Table 13. Material parameters and cost.

Parameter	Symbol [unit]	Value
Labour time	Tl [h]	0.50
Labour wage	Pl [€/h]	40.00
Labour cost	L [€]	20.00

Table 14. Labour parameters and cost.

The cost of labour is 20.00 € per orthoses (Table 14). Tl included the scanning time, non-deposition times and a fraction of the deposition time since the continuous presence of the operator is

unnecessary. Pl is a rough estimate and it is strongly dependent on the health care operator role and the facility in which he operates.

Combining P, S, E, M and L contributes, the total cost of a customised orthoses fabricated by means of AM results equal to 25.84 €. The analysis of the costs shows that the greater part of the orthotic fabrication cost is determined by the labour cost, accounting for 78% of the whole cost. The second most impactful parameter is material cost, representing 18% of the whole cost. Although the proposed approach requires dedicated equipment (high-speed and accurate 3D scanner, 3D printer and modelling software), the cost analysis highlights that this solution is competitive with respect to traditional customised orthoses. The total fabrication time (2.46 h) is given by the sum of the scanning acquisition, GUI modelling and 3D printing times. Time analysis shows that the most time-consuming phase is 3D printing, which lasts slightly more than two hours. Beyond that, the timing of the procedure proposed in the current study is compatible with the intended clinical practices: the treatment of non-emergency conditions affecting the joints and bones of the hand-wrist-arm district. In particular, the approach is advantageous with respect to vacuum forming, which may take up to several days owing to the negative and positive mould generation activities involved for fabricating a customised orthosis.

4.1.3 Conclusions

The present study was developed, proposing an alternative methodology to fabricate orthosis for the treatment of non-acute conditions of the hand-wrist-arm district via Reverse Engineering and Additive Manufacturing. The suggested methodology involved the design of a GUI, integrating a series of standardised and semi-automatic commands to support the healthcare operators in the modelling of the medical device.

The results of the analysis demonstrated the feasibility of the developed approach in terms of time and cost-effectiveness and, therefore, the viability of implementing the solution in clinical practice. An early prototype of the limb orthosis was printed using ABS by means of a desktop MEX machine. The proposed set-up ensured the fabrication of orthotic device even in healthcare facilities. The device cost was estimated to be around 26 €, requiring 0.03 h, 0.23 h and 2.20 h for its scanning, modelling and printing phases, respectively.

Future works will provide further evidence on the appropriateness in terms of cost, time and mechanical behaviour of the proposed medical solution by conducting experimental analyses aimed at expanding the portfolio of biocompatible materials that can be used for 3D printing orthoses. Besides, further information on patient acceptance and clinical efficacy of the AM customised solutions should be investigated too. Consideration should also be given to the aspect of comfort:

specific solutions to promote wearability should be investigated (e.g., orthotic surface smoothing treatment or development of soft sleeves internal to the orthosis).

4.2 Comparative evaluation of MEX-based orthoses for wrist immobilisation: efficiency, cost and technical performance

This chapter is derived from the article "Sala, F.; D'Urso, G; Giardini, C. (2023). Customized Wrist Immobilization Splints Produced via Additive Manufacturing—A Comprehensive Evaluation of the Viable Configurations".

DOI: 10.3390/prosthesis5030056

I am grateful for the support received from my co-authors. I bear full responsibility for all the variations from the published version reported in the current chapter.

The methodology reported in the previous study, namely the AM procedure for producing customised upper limb orthoses, and its findings are further explored in the present chapter. In fact, the present research refines the objectives and outlines the innovative methodology to fabricate patient-specific wrist immobilisation orthosis.

Upper extremity orthoses might be classified according to descriptive criteria, such as the primary purpose [195,196]. In compliance with the therapeutic target and clinical protocol established for a given pathological condition, orthoses distinguish themselves in mobilisation, immobilisation, restriction and torque transmission devices. The wrist is one of the upper extremity regions most frequently treated with orthotic devices. The use of wrist orthoses is often recommended for clinical conditions involving carpal tunnel syndrome, radial nerve injuries, tendinitis and tenosynovitis, rheumatoid arthritis, wrist fractures and sprains, complex regional pain syndrome type I and joint contractures. In treating these pathologies, therapists rely on a range of wrist immobilisation orthoses able to maintain wrist joint in the correct alignment while, concurrently, allowing a certain grade of finger mobility [197].

Once again, the proposed fabrication methodology addressed the variability induced by disparate levels of medical expertise by structuring and standardising the custom splinting process through the integration of advanced techniques and technologies in the traditional medical practice. The benefits from prefabricated and custom orthoses were brought together, so as to obtain devices characterised by a steady, high standard of quality and a great degree of customisation.

The emphasis was posed on the relevance of delivering optimal care by enhancing the individuality of the patient's requirements with non-traditional methodologies: lightness, strength, comfort, availability and affordability of the splint solutions were concomitantly valued and balanced in an effort to provide satisfactory outcomes. The analysis presented in the current study was built on this perspective. Accordingly, these factors were systematically evaluated on MEX-produced orthotic models, which differed in terms of thickness and manufacturing material (ABS, Nylon, PLA, PC, PA6-GF25, PA6-CF20).

A comprehensive analysis is performed to assess the applicability of the proposed methodology and the derived products in the clinical practice. The adequacy of the process is measured in terms of time and cost analyses, by focusing the attention on the minimisation of production times and material costs. Moreover, the compliance of the prototypes resulting from the discussed manufacturing process was assessed via a Finite Element Analyses (FEA): stresses and displacement distribution maps were presented. As anticipated, the FEA results were discussed in relation to the performance characteristics typically sought by clinicians during the splinting process.

Lastly, the present research quantified and displayed the outcomes of the conducted analysis as a comparative collection of distinct wrist immobilisation orthotic solutions that the physician has at his disposal in the treatment of the pathological wrist condition. The proposed approach represents a valid and effective tool to support informed clinical decision-making in the selection of wrist immobilisation orthoses. The heterogeneity of the factors considered in the benchmark resulted in a comprehensive evaluation of the wrist immobilisation orthoses configurations and, to date, such an assessment was not yet discussed in the literature.

4.2.1 Methodology

Reconstruction of the wrist geometry

The scanning procedure was performed using Hexagon Absolute Arm 7-Axis equipped with RS6 Laser Scanner. The contactless acquisition system consists of a handheld scanner (technical characteristics are shown in Table 15) set on a portable measuring arm.

The orientation and positioning of the patient's wrist depend on the diagnosis and therapeutic goals. In the present study, a neutral resting wrist position was adopted, as commonly recommended for the treatment of carpal tunnel syndrome. In practice, the patient was instructed to remain seated and motionless, with the arm raised anteriorly in such a way that the anatomical reference points of the shoulder and wrist joints were aligned along the same axis. The stability of the configuration was fostered by placing two supports of equal height in the proximity of the elbow joint and under the

fingertips. The conceived configuration optimally exposed the external geometry of the patient's upper limb, preventing shape distortion associated with arrangements that, instead, involve resting the arm on a surface. Additionally, the contactless systems avoid exposing the patient's limb to additional stresses and helped the patient in holding the correct position comfortably.

The position of the patient's during the reconstruction of the wrist morphology is represented in Figure 48. The scansion was executed as a single 360-degree acquisition around the patient's upper limb, avoiding unnecessary complications in merging multiple scans.

Several acquisition attempts were performed before selecting the finest result. Files presenting minor misalignments and/or discontinuities in the point cloud were further processed and properly elaborated. Whereas severely compromised files were discarded. The average scanning time required to acquire the current anatomical district was around 110 s but it is worth mentioning that this value may vary as it relies on the expertise of the operator.

Figure 48. Position of the patient during the reconstruction of the wrist geometry. The blue rectangles identify the position of the supports providing stability.

RS6 Laser Scanner	
Scanning technology	blue laser
Scanning accuracy	0.026 mm
Point acquisition rate	max. 1.2 million points/s
Points per line	max. 4000
Line rate	max. 300 Hz
Line width	150 mm

Table 15. RS6 Laser Scanner characteristics.

Design of the wrist immobilisation splint model

Starting from the 3D acquisition of the patient's wrist, an STL model of a circumferential splint was designed using a novel CAD software based on Python libraries. The software system, conceived to address the specific needs and challenges of the field, was introduced by the authors in a previous article [198]. The program optimises and streamlines the manual modelling workflow by translating it into a set of intuitive and user-friendly commands (Figure 49), specifically developed for use by clinical practitioners.

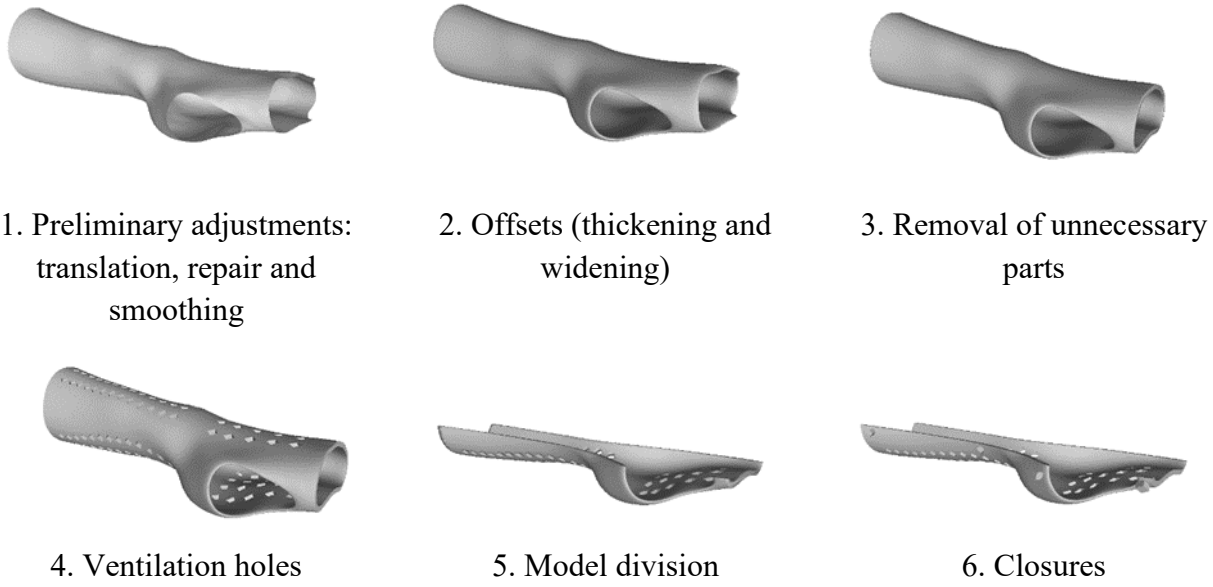

Figure 49. Flowchart of the guided modelling operations.

The first operation automates the translation of the model to the origin of the workspace reference system, the repair of mesh geometry defects (such as holes, gaps, intersections, and floating triangles) and surface smoothing operations. These activities improve the quality of the mesh, by addressing potential artefacts resulting from the 3D scanning process and by preparing the file for the subsequent modelling operations. Once the mesh geometry has been corrected, two offsets are applied: the first one expands the surface outward and is designed to ensure clearance between the arm and the inner surface of the device, while the second one defines the solid geometry by assigning a surface thickness. The user is required to input the offset values to ensure that the resulting orthotic device is tailored specifically to the needs of the patient. The cut and rotate commands refine the splint model, removing the non-functional areas. To accurately orient and section the model, the operator relies on the numerical values displayed by a protractor and millimetre grid. Ventilation holes are created to lighten the structure while providing sufficient strength. From a library that includes ventilation holes

with distinct shapes, the user selects the preferred geometry and applies it to the model either by clicking on a specific location or by generating a pattern of evenly spaced holes. In the final stages of the modelling activity, the splint model is divided into two complementary shells and integrated with fastening systems. Given the circumferential design of the medical device, these operations are necessary to ensure that the patient is able to fit the splint and lock it in place. The algorithms and, consequently, the interfaces of the division and closure commands are conceptually consistent with those used for removing unnecessary regions and generating ventilation holes, respectively. The outputs of the modelling activity consist of two STL files representing the two halves of the medical device.

Production of the splint prototype

The splint prototype was conceived to be realised with an instrument able to easily fabricate customised and intricate geometries. Material Extrusion (MEX) represents the appropriate process for the intended purpose, as well as being easily implementable in any health care setting. The considered printer was an Ultimaker S5 desktop-FDM, with a working chamber of 330 x 240 x 300 mm. The technology is equipped with a dual-extrusion print head: one extruding the primary material and the other extruding the support material. Different set of print cores were used depending on the print material.

The manufacturing materials were chosen in compliance with the biocompatibility requirements. Splints are medical devices that interface superficially with the patient's body, maintaining prolonged contact with intact skin. The indications to which this type of medical device is subjected during the biological evaluation include assessing issues related to cytotoxicity, sensitisation and intra-cutaneous irritation or reactivity [133]. For this type of medical application, some materials identified by the FDA as low-risk materials do not require any testing for pre-market submission [199] and, consequently, were considered in the study. Additional materials, not included in the aforementioned category, were also considered. In particular, composites such as glass-fibre- and carbon-fibre-reinforced polymers, were included in the study given their enhanced properties: high stiffness and strength combined with low weight.

ABS, Nylon, PLA and PC filaments were provided by Ultimaker, while PA6-GF25 and PA6-CF20 filaments were provided by Polymaker. The chosen support material was Ultimaker Breakaway, a filament composed of a mixture of PLA and TPU. Besides being compatible with the majority of the selected materials, Ultimaker Breakaway is quickly and manually removable at the end of the printing process.

Polymeric filaments, including the support filament, necessitated the utilisation of a regular print core (AA-type), which comes with a nozzle size of up to 0.8 mm. Conversely, composite filaments mandate the use of hardened steel print cores (CC-type), designed for handling abrasive or composite materials. These print cores are available with a maximum nozzle size of 0.6 mm.

Time and cost analysis

The overall process time for producing a customised splint device via AM included the execution of the activities of limb scanning, splint CAD-model development and splint printing.

The 3D printing task, identified as the most time-consuming stage of the process, was estimated from the STL model of the medical device using a 3D slicing application for 3D printers (Ultimaker Cura). The calculation of the time for printing a splint prototype was performed using specific printing parameters for each selected material filament (Table 16), in accordance with the recommended processing settings [200–206].

	ABS	Nylon	PLA	PC	PA6-GF25	PA6-CF20
Nozzle diameter	0.8 mm	0.8 mm	0.8 mm	0.8 mm	0.6 mm	0.6 mm
Layer height	0.6 mm	0.6 mm	0.6 mm	0.6 mm	0.45 mm	0.45 mm
Infill density	100%	100 %	100%	100%	100%	100%
Infill pattern	Line	Line	Line	Line	Line	Line
Nozzle temperature	250 °C	245 °C	210 °C	265 °C	300 °C	300 °C
Build plate temperature	85 °C	70 °C	60 °C	110 °C	50 °C	50 °C
Print speed	50 mm/s	35 mm/s	45 mm/s	70 mm/s	60 mm/s	60 mm/s

Table 16. FDM filaments printing parameters.

The diameter size of the head nozzle extruding the primary material was chosen to maximise the volume of the deposited layers: a 0.8 mm head nozzle was selected for polymeric filaments, while a 0.6 mm was selected for the composite materials. The chosen layer height, 0.6 mm and 0.45 mm respectively, implied a considerable reduction in printing time and a rougher surface compatible with the intended solution. The infill density was set at a constant level of 100%, whilst the infill pattern type was set as lines. The chosen printing speed was the default one.

The minimum angle of overhangs for which support material was added was 80°, which allowed to reduce to a minimum the utilization of the support material by depositing it just in correspondence of the opening dedicated to the thumb finger. Furthermore, the support material infill density was reduced to 10% and the pattern type was set as triangles.

The two complementary shells of the splint model were positioned vertically on the build platform to further reduce printing time and minimise the consumption of the support material.

Based on existing models specifically developed for estimating the costs involved in the fabrication process of customised orthotics [198], the main cost drivers were identified. The total cost of a tailor-made orthosis is driven by labour cost and material cost. Machining costs, including technologies purchase cost (3D scanner and 3D printer) and energy consumption cost, represent only a fraction of the overall cost. Besides labour cost, the most impactful cost component is material cost, which can be derived from the unit price of the material and the quantity consumed during the 3D printing process. The 3D slicing software for 3D printers, Ultimaker Cura, provided the length value of material extruded during printing. The estimate came from the printing arrangements presented in Table 16, which, in addition to shortening printing times, optimised the amount of extruded filaments reducing the cost of raw material. In the present research, the computation of material cost component did not include adjustments for factors such as material waste and scrap and fluctuation in raw material prices.

Both time and cost analysis followed the programming of the experiments, Design of Experiment (DOE), in which two factors, splint thickness and manufacturing material, were varied on 3 and 6 levels, respectively.

Technical analysis

The commercial availability of different thermoplastic materials allows the physician to further tailor the splint, keeping in mind that the selection of the optimal material involves comparing the therapeutic targets with the technical characteristics of the manufacturing material. Conformability, flexibility, durability, rigidity and design appearance (e.g., ventilation, colour, thickness and finish) [197] are the technical characteristics sought by the medical personnel.

Mechanical properties of the medical devices produced with the designed AM procedure were evaluated through the execution of Finite Element Analyses (FEA) using Abaqus. Splint STL models, differing in surface thickness, were developed during the CAD modelling phase and loaded in Abaqus working space. The models were subjected to a free technique meshing process: the algorithm automatically adapts the size and shape of the elements to accurately represent the local features, ensuring great flexibility in capturing the complexity of the current geometry. Models were discretised using tetrahedral elements, characterised by an approximate global size ranging from 2.5 mm to 5.5 mm depending on the necessity to cope with possible convergence and numerical instability problems during the execution of the simulation. The resulting mesh consisted of a total of 86 743 elements for splint model of 2 mm, 127 455 for splint model of 3 mm and 140 326 elements

for splint model of 4 mm. The number of nodes was 164 583 for splint model of 2 mm, 217 929 for splint model of 3 mm and 234 339 for splint model of 4 mm.

The mechanical properties of the splint model were tested according to different manufacturing materials. The selected materials were the standard and fibre-reinforced polymeric materials presented in Table 16 and the simulations were set up with the material properties [204,205,207–210] reported in Table 17.

	ABS	Nylon	PLA	PC	PA6-GF25	PA6-CF20
Mass density [g/cm^3]	1.10	1.14	1.24	1.20	1.20	1.17
Young's modulus [MPa]	1 682	579	2 347	1 904	4 431	7 453
Poisson ratio [1]	0.35	0.39	0.33	0.36	0.40	0.38
UTS [MPa]	33.9	34.3	45.6	53.7	84.0	105.0

Table 17. Mechanical properties of the manufacturing materials.

As noted in other bibliographical research [146,211,212], explicit strength requirements for upper limb splints are currently lacking. Moreover, these devices are not typically subjected to specific or high mechanical loads; therefore, the present study simulated an unintentional mechanical impact condition. The simulation specifically focused on recreating the collision of the palm region of the medical device against a surface during a patient fall episode while wearing the designed device. Load and constraint conditions were carefully established to ensure an accurate representation of the aforementioned scenario. The test was performed by constraining the displacements and rotations of the nodes describing the region close to the distal part of the ulna and imposing a pressure uniformly distributed over the palm surface (with a total magnitude of 500 N). The minimum thickness demonstrating sufficient strength was identified for each material. Additionally, displacements affecting the wrist area were reported. The recorded results were attributable to the system consisting of the mere splint, meaning that the tests were performed without simulating the presence of the arm inside the medical device.

4.2.2 Results and discussions

Results

Following the methodology, from a single 3D acquisition, three splint models were designed. All the splint models include a pattern of rhomboidal holes, designed to facilitate the ventilation function and lighten the entire structure. The modelling parameters during the CAD stage were kept unchanged,

except for the offset parameter, which is responsible for creating the solid shape of the scanned surface. Therefore, the three splint models present the same general conformation, while the surface thickness was varied on 2, 3 and 4 mm, respectively. Time, cost and technical analyses were based on the use of 6 different manufacturing materials, thus, resulting in a total of 18 splint combinations. The splint models were evaluated in terms of time and costs, leveraging on Ultimaker Cura slicing software. The printing time (Figure 50) and the amount of extruded material (Table 18 and Table 19) of the 18 splint combinations were simulated. From the information on the extruded material, the material weight and material cost (Figure 51) were derived. The material weight considered only the manufacturing material, whilst the material cost included also the cost component of support material.

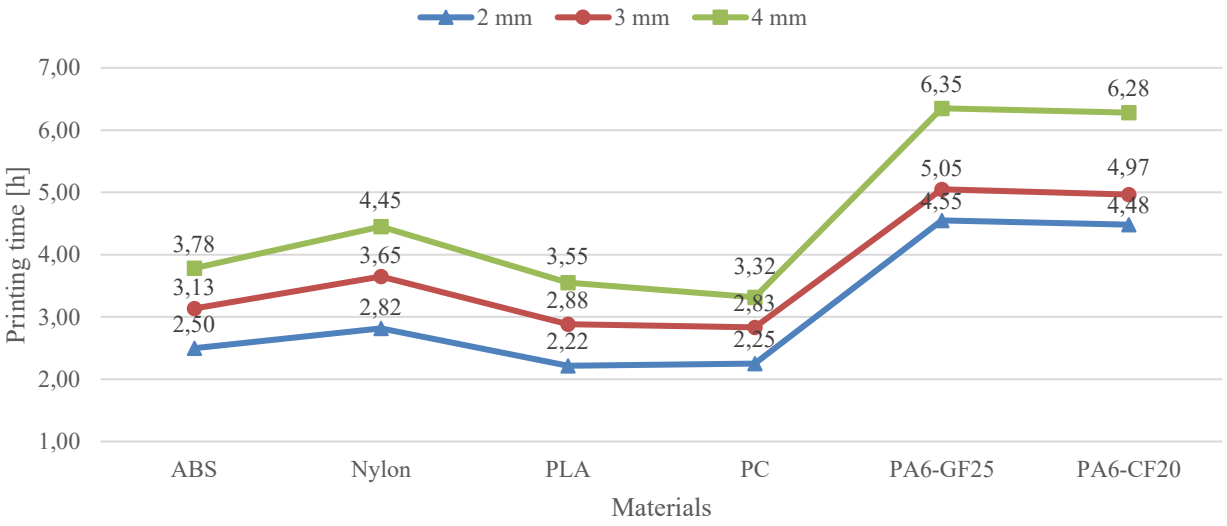

Figure 50. Printing times for producing a customised wrist immobilisation splint as a function of the material type and thickness. ABS, Nylon, PLA and PC filaments used a head nozzle of 0.8 mm diameter, while PA6-GF25 and PA6-CF20 used a head nozzle of 0.6 mm diameter.

	ABS	Nylon	PLA	PC	PA6-GF25	PA6-CF20
Material consumption, 2 mm	10.9 m	10.9 m	10.9 m	11.1 m	10.9 m	10.8 m
Material consumption, 3 mm	16.5 m	16.5 m	16.6 m	16.7 m	16.8 m	16.7 m
Material consumption, 4 mm	22.6 m	22.6 m	22.7 m	22.8 m	22.9 m	22.8 m
Material price	0.58 €/m	0.92 €/m	0.57 €/m	0.90 €/m	1.38 €/m	1.64 €/m

Table 18. Manufacturing material consumptions and manufacturing material prices (support material is not included).

	For ABS	For Nylon	For PLA	For PC	For PA6-GF25	For PA6-CF20
Support consumption, 2 mm	0.21 m	0.28 m	0.23 m	0.20 m	2.39 m	2.39 m
Support consumption, 3 mm	0.20 m	0.21 m	0.19 m	0.20 m	0.90 m	0.90 m
Support consumption, 4 mm	0.20 m	0.20 m	0.22 m	0.16 m	0.97 m	0.96 m
Support price	0.92 €/m	0.92 €/m	0.92 €/m	0.92 €/m	0.92 €/m	0.92 €/m

Table 19. Support material consumption and support material price. Ultimaker Breakaway was used as support material.

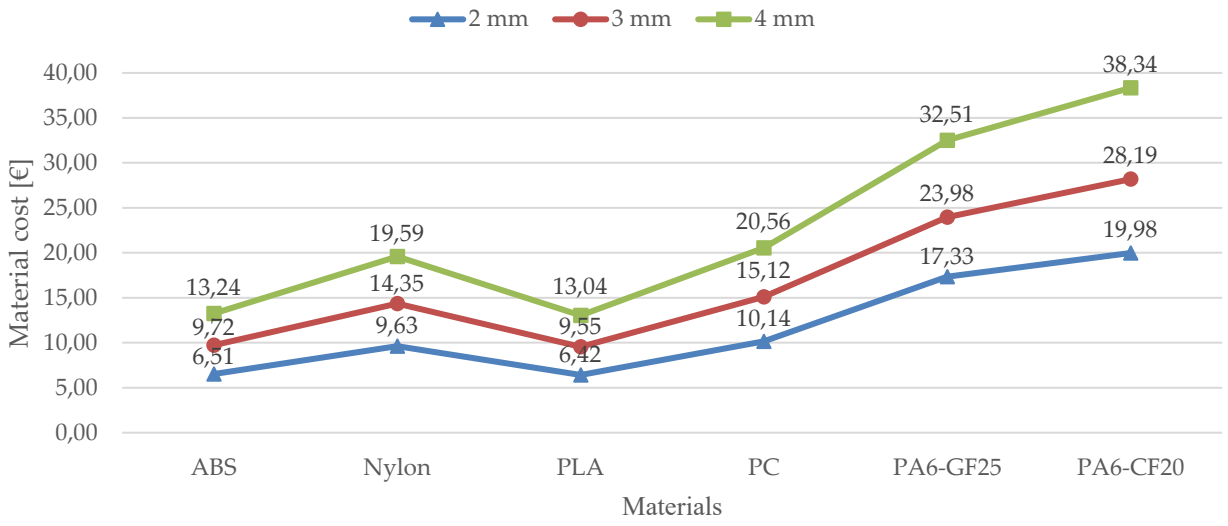

Figure 51. Total material cost for producing a customised wrist immobilisation splint as a function of the material type and thickness (the values include both the manufacturing material component both the support material component).

Technical analysis was performed: FEA provided the predicted stresses and displacement distribution maps of the wrist immobilisation splint which were consistent across all scenarios given their sole dependence on geometric factors. For each simulation, the maximum stress was recorded at the opening designed for the thumb, as illustrated in Figure 52. The maximum values of stress were averaged to 64 MPa for splint configuration of 2 mm, 28 MPa for splint configuration of 3 mm and 18 MPa for splint configuration of 4 mm. The results are collected in Figure 53, where they were compared to the UTS of each manufacturing material in order to identify splint combinations capable of withstanding the simulated accidental mechanical impact: the maximum stress values exceeding the material UTS result in splint failure. It is critical to mention that all the 18 splint combinations, near the apexes of the ventilation holes, showed a stress intensification effect which might be mitigated by introducing a fillet radius at each corner of the rhomboidal holes.

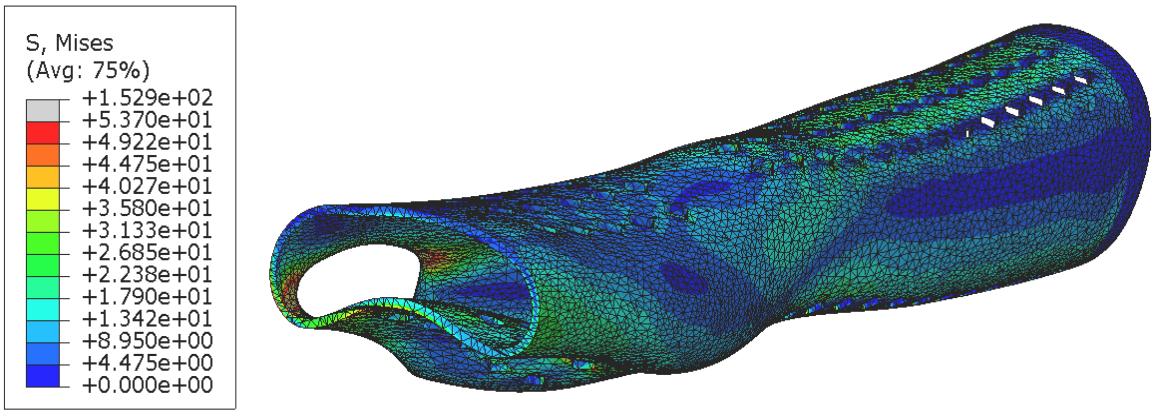

Figure 52. Von Mises stress distribution for PC splint with a 2 mm thickness.

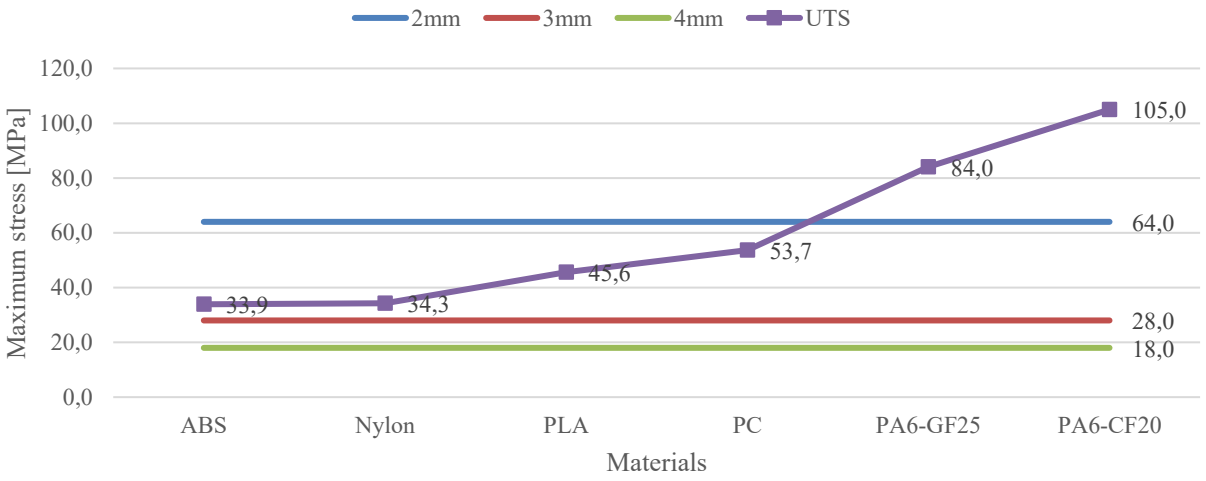

Figure 53. Maximum value of stress experienced by the splint model according to splint thickness (2, 3, 4 mm), compared to the UTS of each material type (ABS, Nylon, PLA, PC, PA6-GF25, PA6-CF20).

Concerning displacements, the distribution maps of the 18 splint combinations followed a pattern like the one depicted in Figure 54. The largest displacement magnitudes were consistently observed in the areas corresponding to the hand and the palm, whereas the wrist region experienced comparatively smaller movements. Table 20 reports the range of displacement values impacting only on the wrist area.

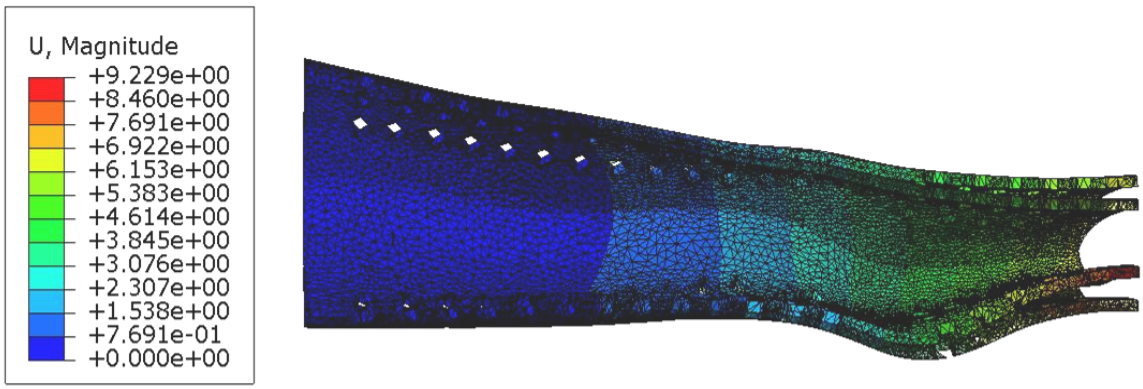

Figure 54. Displacements distribution for PC splint with a 3 mm thickness.

	2 mm	3 mm	4 mm
ABS	3.9 – 7.8 mm	2.6 – 4.4 mm	1.8 – 2.9 mm
Nylon	11.3 – 22.6 mm	7.6 – 12.6 mm	5.1 – 8.5 mm
PLA	2.8 – 5.6 mm	1.9 – 3.1 mm	1.3 – 2.1 mm
PC	3.1 – 6.1 mm	2.3 – 3.8 mm	1.6 – 2.6 mm
PA6-GF25	1.5 – 2.9 mm	1.0 – 1.6 mm	0.7 – 1.1 mm
PA6-CF20	0.9 – 1.8 mm	0.6 – 1.0 mm	0.4 – 0.7 mm

Table 20. Range of displacement according to material filament and splint thickness.

Last, Figure 55 summarises the key characteristics taken into consideration in the analysis: material cost, weight, printing time, UTS and rigidity. The figure represents a collection of customised polymer and composite wrist splints in AM, characterised by the minimum thickness that allows the part to resist to the simulated accidental impact. Precisely, the considered splint configurations were ABS and Nylon with 4 mm surface thickness, PLA and PC with 3 mm surface thickness and PA6-GF25 and PA6-CF20 with 2 mm thickness. The final selection of the six different combinations of materials and thicknesses was based on a safety factor, a numerical value calculated by dividing the UTS of the material by the maximum expected stress experienced by the medical device (respectively to 64 MPa for splint configuration of 2 mm, 28 MPa for splint configuration of 3 mm and 18 MPa for splint configuration of 4 mm). The considered safety factor was 1.25 and, according to some literature studies [164,213], it was identified as the appropriate minimum value for rehabilitation devices. Regarding Nylon splint, this arrangement was included for comparative purposes only, given the unsatisfactory results observed in the displacement distribution maps.

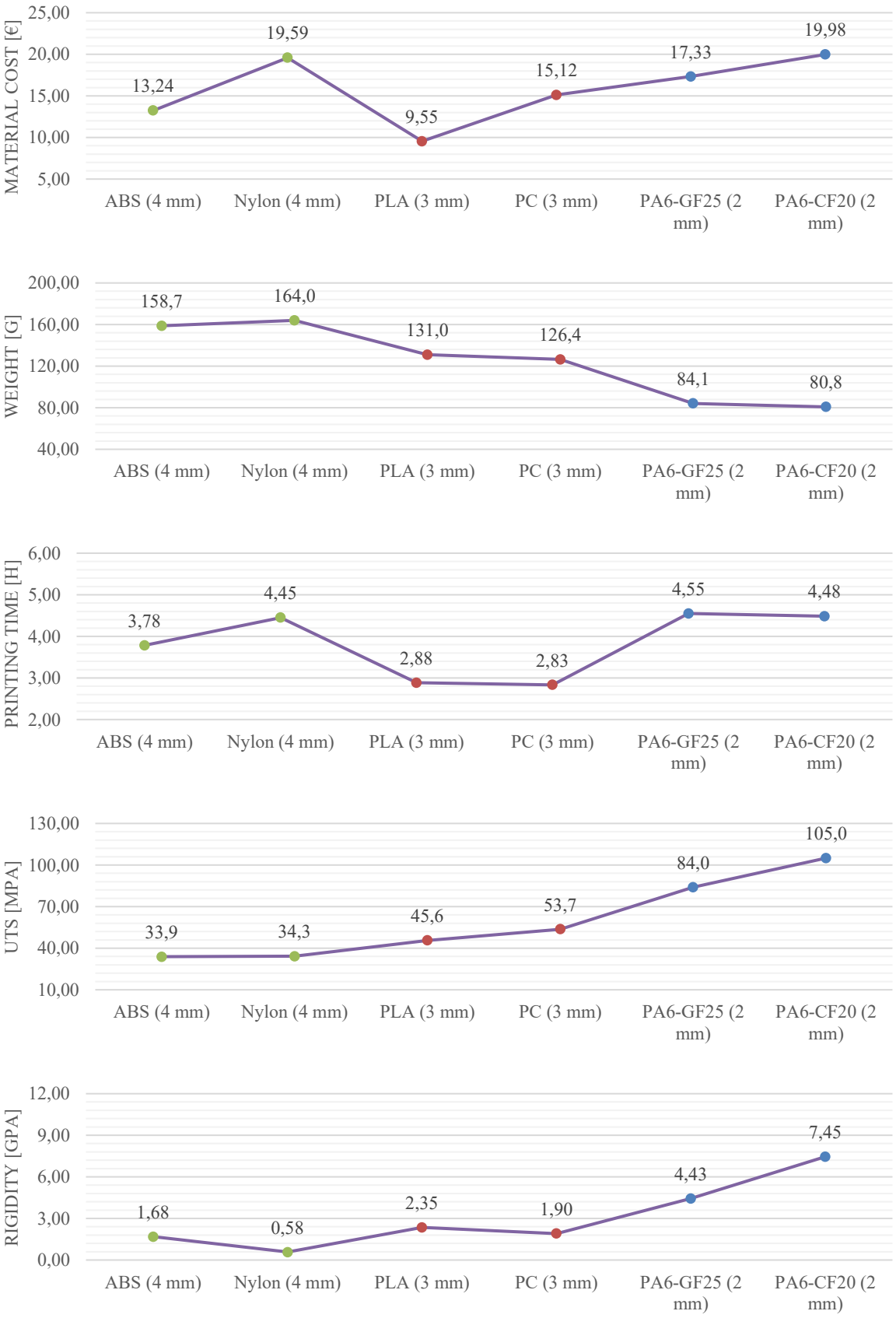

Figure 55. Comparison of the main characteristics of the wrist immobilisation splint made in polymeric and composite materials.

Discussion

The analyses conducted on the printing times of wrist immobilisation splints showed that, with the considered 3D printing technology, the material deposition time varied significantly depending on the selected material type and layer thickness. In particular, the material deposition time ranged from a minimum of 2.2 h and a maximum of 6.4 h.

The analysis conducted through the slicing software demonstrated that the estimated times were the result of the sum of multiple processing components and the overall time value was attributable to a few leading time components, such as outer and inner walls deposition and retractions (movement of the head nozzle with the function of avoiding the stringing effect). The time component related to the deposition of the support material did not fit into the aforementioned leading time components since its value was modest as a result of the optimised printing parameters (support overhang angle = 80°) and optimised printing orientation (vertical orientation in the top right quadrant of the printing plane). In fact, for each splint configuration, the recorded support value was always below 8% of the whole printing time.

The composite materials, PA6-GF25 and PA6-CF20, presented by far the highest printing values due to a technical constraint: a narrower FDM nozzle diameter resulted in a reduction of the deposited layer height from 0.6 mm to 0.45 mm. Thus, composite materials demanded a printing time of at least 4.5 h just to realise the thinnest thickness (2 mm). In contrast, for the same level of thickness, polymeric materials required a shorter printing time, ranging from 2.2 h to 2.8 h. Additionally, the composite printing time is lengthened by the post-printing annealing: it is recommended to anneal (oven at 90 °C for 2 h) the composite prototypes to improve their mechanical and thermal properties. Polymeric prototypes do not require any annealing process.

With respect to the cost analysis, the value of the total material cost was given by the sum of the manufacturing material and support material cost components. The aggregate material cost ranged from 6 €, in 2 mm thickness wrist splints manufactured in ABS or PLA, to over 30 €, in 4 mm thickness wrist splints made of composite material.

Comparably to the above-mentioned discussion on the deposition time of the support material, the contribution of the support material component to the total material cost was almost negligible as the amount of support material extruded was minimised. The amount of deposited support material might be subjected to variations since its close dependence on the model geometry resulting from the scanning and modelling activities. In the present instance, the deposition of support material occurred only at the closures and the opening area dedicated to the thumb finger. Following designs of fastening systems should focus on the realisation of systems involving elements that do not protrude from the primary splint structure (i.e., interlocking closure on the interaction surfaces of the two splint

shells). Further adjustments of the opening dedicated to the thumb finger are desirable: the shape of the thumb opening must limit the creation of downward-facing surfaces. These improvements would assure the complete removal of the supporting material, thus, eliminating all the issues related to the use of the support material, primarily the prolonged printing time and the rougher surface finish of the areas in contact with the support. Although the support material was used, still, the main structure of the wrist immobilisation splint was able to self-support during the 3D printing activity.

As a result of the cost and time assessments on the innovative methodology, an advantage in terms of material cost was evident compared to traditional splinting, both off-the-shelf splints and tailor-made splints. Concerning production time, 3D printing times were substantial, thus, making the innovative methodology less favourable compared to conventional solutions at first glance. This limitation could be mitigated through the adoption of more advanced Additive Manufacturing technologies, capable of reducing material deposition times. Notwithstanding, when comparing production times of the traditional procedure with the AM methodology, additional remarks, that deviates from the mere amount of time, should be made. In particular, it should be noted that the medical application under investigation addressed non-emergency clinical conditions (such as carpal tunnel syndrome, tendinitis and arthritis). Therefore, from a clinical point of view, there are no real drawbacks associated with the prolonged production time. With no time constraint, the medical solution might be delivered to the patient at a later time (i.e., after an election visit or after a surgical operation), following limb scanning and splint design. In support of this thesis, it must be noted that the physician contribution lies in the scanning and modelling activities. In fact, the active presence of the physician during the 3D printing phase is not mandatory (except for the start-up and the shutdown of the AM machine) as the process is fully automated.

Alongside the discussion on the applicability and sustainability of the AM splinting process in clinical practice, evaluated in terms of production time and material costs, technical aspects related to the feasibility and functionality of the resulting medical devices were also considered. Finite element simulations identified the opening area dedicated to the thumb finger as the areas of potential fracture. Wrist splint configurations unable to withstand accidental mechanical impact (500 N) were excluded as inadequate in providing a sufficient immobilisation function of the wrist joint. The prototypes fabricated with composite materials (PA6-GF25 and PA6-CF20) were the only splint configurations able to resist to the simulated mechanical impact in every surface thickness. As for prototypes fabricated with polymeric material (ABS, Nylon, PLA, PC), splint configurations with the smallest surface thickness (2 mm) were not achievable because the maximum recorded stress value exceeded the material UTS. By increasing the thickness to 3 mm, all polymeric prototypes were able to withstand the impact. However, it should be noted that in some cases, like the ABS and Nylon

prototypes, the maximum stress values were not so different from their UTS, such that it is preferable to discard these solutions in favour of wrist splint configurations characterised by a greater thickness. From the stress distribution assessment, the selected splint configurations were ABS and Nylon with 4 mm surface thickness, PLA and PC with 3 mm surface thickness and PA6-GF25 and PA6-CF20 with 2 mm surface thickness.

In addition to the simulations that determine whether the wrist immobilisation splint undergoes rupture, considerable importance was paid to the displacement parameter. The ability of the device to provide effective immobilisation depends on maintaining minimal displacements of the elements from their initial positions during the application of the simulated mechanical impact. Technical evaluations reported that the greatest displacement was recorded in correspondence to the extremity of the palm, with considerably less impact on the wrist area. As expected, lower surface thickness exhibited greater displacements. Under the same value of surface thickness, materials characterised by greater flexibility exhibited greater displacements. Specifically, excessive displacement values were registered in customised wrist splints made of Nylon (including the configuration presenting a surface thickness of 4 mm), thus, undermining their effective immobilisation functionality.

Along with the stress and displacement distribution maps, other technical aspects (generally sought by the physician during the traditional fabrication of a customised splint) were involved in the discussion. Observations were made on the conformability and design appearance (e.g., ventilation and thickness) aspects.

Conformability, or the ability of the splint to fit intimately the patient's arm, no longer depends on the choice of LTT material and the physician expertise. Conformability is intrinsic to the process as the customised device is nothing more than a replica of the morphology of the patient's arm.

Another aspect concerned the perforations, which are intended to favour air exchange while, simultaneously, reducing the weight of the medical device. Although several LTT materials with various perforation patterns are commercially available, the use of these materials requires extra precaution (e.g., LTT stretching should be limited to not distort hole pattern nor impact the forecasted pressure and strength distribution). The implementation of ventilation holes was both facilitated and standardised in the design of a customised splint in AM. Considering the study objectives and the observation that stress concentrations were primarily localised around small regions of the holes, a configuration with rhomboid-shaped ventilation holes was adopted. Other geometries of ventilation holes, such as ellipsoidal or rectangular holes with rounded corners, effectively reduced these local stress concentrations. However, it should be envisaged that these configurations require the use of additional support material near the holes to avoid the collapse of the structure during printing, thus increasing the 3D printing time. The pattern of rhomboid-shaped ventilation holes was distributed

over the front and back surface of the wrist immobilization splint, away from the joining zone of the two halves. Future research should consider the possibility of optimising the hole distribution according to topological criteria, so that the configuration maximises lightness as a function of the required mechanical strength.

A last consideration regarded surface thickness: commonly, the thickness of a film of LTT material is about 3 mm, even if thicknesses of 2 and 4 mm are available as well. Customised AM wrist splints achieved thicknesses comparable to those realised with LTT materials, with the advantage that the choice of thickness depended only on the desired level of strength and not on the expertise of the medical operator. Conversely, regarding customised orthoses with LTT materials, it is recommended that physicians with less experience use greater thicknesses as these are more easily mouldable.

As anticipated in the result section (Figure 55), all the quantitative outcomes derived from the analyses were gathered together in a comprehensive diagram that may assist medical operators in the process of selecting the most appropriate configuration of wrist splint according to some key characteristics: material cost, weight, printing time, UTS and rigidity. Although, from the comparative analysis of each variable, differences in the splint configuration chosen were visible, in reality, there was no splint configuration that prevailed in absolute terms; each presented distinct and optimal performance. To conclude, a first 3D printed prototype of wrist splint immobilisation is presented in Figure 56: the shells were not subject to surface treatments and the closure system was integrated with elastomer rings.

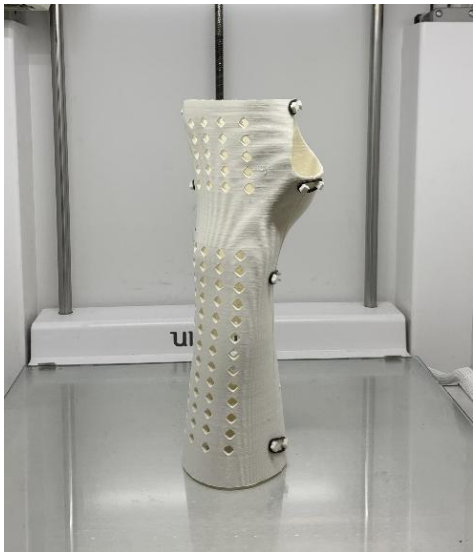

Figure 56. Prototype of wrist immobilisation splint made in PLA with a 3 mm surface thickness.

4.2.3 Conclusions

The present study developed an innovative manufacturing technique for designing and fabricating highly customised immobilisation wrist splint. The process integrated the concepts of reverse engineering and AM to overcome the issues associated with conventional pre-fabricated and tailor-made splints and their manufacturing techniques. In particular, the newly developed methodology addresses the variability induced by different levels of medical expertise by structuring and standardising the splinting process, while providing medical devices characterised by a steady high standard of quality and a high degree of customisation.

The commercial availability of different thermoplastic materials enabled physicians to further tailor the splints, keeping in mind that the selection of the most suitable material required balancing the therapeutic objectives (specific to a pathological wrist condition) with a range of additional factors, including cost-time dimensions and technical performance. In this regard, the present study proposed a model for conducting comparisons of different wrist immobilisation configuration that may assist medical operators in choosing the most suitable solution. From the comparative analysis, no splint configuration prevailed over the others. Additionally, cost analyses demonstrated the competitivity of the proposed methodology and medical solutions compared to the traditional procedure, while advantages related to production time were arguable.

Future works will focus on the aspect of product optimisation. Specifically, refining of the wrist immobilisation splint will be investigated through the execution of topological optimisation; starting from an initial design, simulation will be aimed at minimising the overall weight or volume of the wrist splint while ensuring mechanical strength.

4.3 Robustness analysis of the process for producing MEX-based customised upper limb orthoses

This chapter is derived from the article “Sala, F.; Quarto, M.; D’Urso, G; Giardini, C. (2023). Preliminary evaluation of an additive manufacturing procedure for producing patient-specific upper-limb orthotic devices”.

DOI: 10.21741/9781644902714-13

I am grateful for the support received from my co-authors. I bear full responsibility for all the variations from the published version reported in the current chapter.

In the present study, the reliability, effectiveness and flexibility of the methodology, defined for producing MEX-based customised upper limb orthoses, are investigated. The research proposes an analysis of the production process aimed at testing whether, in the presence of variability from the standard operating conditions, it is possible to achieve consistent outcomes that meet the desired specifications.

To accomplish the research objectives, three anatomical regions of different size and level of detail were used as test objects for the evaluation of the validity and repeatability of the manufacturing process under investigation. The anatomical regions involved the upper extremities of the limbs, particularly the wrist and finger joints.

Pathological conditions affecting the wrist joint may require the use of orthoses that immobilise the wrist joint, while enabling full mobility of the metacarpophalangeal (MP) joint and thumb. Clinicians might rely on a variety of wrist orthotic patterns depending on the anatomical region along which they extend: volar, dorsal, ulnar and circumferential. As the name suggests, circumferential devices completely envelop the wrist joint, bringing greater stability, and are especially indicated in fractures and complex regional pain syndrome.

On the basis of the medical consultation, pathological conditions affecting the fingers may require a medical device designed to support or protect only the affected finger, or alternatively, to stabilise the entire hand. Diagnoses such as, finger sprains, mallet finger, boutonniere and swan-neck deformities, may require finger-based orthoses to constrain only the movement of the proximal interphalangeal (PIP) and/or distal interphalangeal (DIP) joint under investigation, thus leaving the metacarpophalangeal (MP) joint unrestricted and allowing the mobility of the other digits. On the other side, other clinical conditions, like osteoarthritis and traumatic injuries of the thumb, may require more structured orthopaedic devices, that, as opposed to finger-based splints, cross the entire palm and dorsum of the hand. This is the case of hand-based thumb orthoses, which constrain both interphalangeal (IP) and metacarpophalangeal (MP) thumb joints, allowing for wrist and other digits mobility.

Hence, from the present research, three medical devices, characterised by a different degree of complexity, were developed using MEX technology and PLA filaments. Orthoses model for the wrist, hand (thumb finger) and finger (index finger) are developed. Also, for each orthotic application, different designs are developed exploiting two lightening strategies. One of these strategies is Topological Optimisation (TO).

Product feasibility, along with the entire process consistency, is assessed through a preliminary evaluation on 3D printing costs and times. Potential advantages and drawbacks of the procedure are illustrated, as well as initial remarks on lightening strategies of medical devices.

4.3.1 Methodology

Acquisition of the anatomical regions

The fabrication of patient-specific orthoses started with the acquisition of the surface geometry data from the anatomical area requiring treatment. The acquisition was carried out by means of a handheld 3D scanner, in particular, the technology was Hexagon Absolute Arm 7-Axis equipped with an RS6 Laser Scanner. The instrumentation provides contactless, rapid (max 1.2 million points/s point acquisition rate, max. 300 Hz line rate) and detailed (0.026 mm precision) scans, in accordance with the current clinical requirements [148].

The three anatomical regions were acquired through a single scan in the form of a point cloud, directly exportable to STL-format. The scanning parameters were kept constant across all scenarios, while the acquisition set-up was adapted to the dimension and level of detail of the specific anatomical region and, critically, aligned with the intended therapeutic goal. This implies that, in the presence of injuries that prevent active movement of the joint under consideration, it is essential for the physician to passively relocate the patient's joint in the correct alignment in order to scan a physiological joint and prevent the unsuccessful development of a pathological scan. This consideration safely applies to the pathologies to which the present research refers. Key information concerning the 3D scanning set-up of the different anatomical regions of the upper extremities is presented in Table 21.

Upper limb region	Joints	Number of stabilisers	Scanning configuration
Wrist	Radiocarpal, ulnocarpal and distal radioulnar joints	3	The arm is positioned horizontally and stabilised by three supports at: radius head; index, middle, and ring fingers middle phalanges; thumb distal phalanx.
Thumb	Interphalangeal (IP) and/or metacarpophalangeal (MP) joints	3	The hand is positioned horizontally and stabilised by three supports at: ulna head; index, middle, and ring fingers middle phalanges; thumb distal phalanx.
Finger (Index)	Proximal interphalangeal (PIP) and distal interphalangeal (DIP) joints	2	The (index) finger is positioned horizontally and stabilised by two supports at: metacarpals; (index) finger distal phalanx.

Table 21. 3D scanning set-up of the three applications.

Elaboration of the customised anatomical regions into orthotic models

The 3D scans were imported into a software developed with the purpose of converting the surface anatomical data into a solid orthosis model. The program was originally designed for a particular application, namely arm modelling [198], and partially automates its manual modelling process in a series of simple steps (described in Table 22) based on Python language. In the present research, the use of this software was extended to additional atomic regions of the upper-limb extremities in order to evaluate its adequacy.

Function	Description
Centring	Translation of the STL scan from its original reference system to a new reference system with (0;0;0) origin.
Fixing	Removal of duplicated/isolated vertices/faces, edge repair, hole closure, normal correction, mesh reconstruction and simplification.
Smoothing	Homogenisation of the surface texture.
Expanding	Shift of the faces along their normal and towards the outside to arbitrarily expand the mesh.
Solid creation	Converting the surface into a solid through the generation of a thickness of arbitrary size.
Cutting	Removal of the element extremities through cuts perpendicular to Cartesian axes. Cuts in different directions are executed by orienting the orthotic element accordingly.
Lightening	Creation of holes (of arbitrary shape and dimension) along the solid structure to reduce the weight and volume of the orthotic element.
Dividing	Splitting the model into two halves.
Combining	Creation of connection points on the external surfaces of the two halves and implementation of elements that prevent slippage of the union surfaces during the assembly of the two halves.

Table 22. Operations of the modelling software.

From the software, two orthotic designs per anatomical application were retrieved: a full model and a lightened model. The latter design presented a pattern of rhomboid-shaped holes, realised through the lightening operation.

An additional orthotic design was developed from the full model. Simulations were performed using the optimisation module of the finite-element analysis (FEA) software Abaqus to lighten the structure.

As opposed to the lightening operation performed in the previous model, the current activity considers reasonable forces acting on the orthotic element during the rehabilitation pathway.

Static simulations simplified the patient-device system by focusing exclusively on the orthotic component. Loading conditions were conceived to replicate joint flexion relevant to each clinical application and, in the present optimisation study, were represented as follows:

- Wrist – Application of a torque (with F = 200 N and d = 100 mm) on the distal perpendicular surface of the orthosis (in the proximity of the fingers), forcing the proximal perpendicular surface of the orthosis with an encastre constraint.
- Thumb – Application of a torque (with F = 30 N and d = 100 mm) on the perpendicular thumb surface of the orthosis, forcing with an encastre constraint the perpendicular surface of the orthosis near the wrist.
- Finger (Index) - Application of a torque (with F = 30 N and d = 60 mm) on the distal perpendicular surface of the index finger, forcing with an encastre constraint the proximal perpendicular surface of the index finger.

The optimisation process determined a new material distribution based on the minimisation of the strain energy, while satisfying a volume (below the 60% of the original volume) and geometric constraint (preservation of the load and boundary condition areas).

Additive manufacturing of the orthotic models

The orthotic models were manufactured by Ultimaker S5 desktop Material Extrusion (MEX) machine, an additive manufacturing (AM) technology based on heating and extrusion of a thermoplastic filament from a nozzle to a building platform.

The selected polymeric filament was polylactic acid (PLA) and, besides being one the most commonly used material in 3D printing, it combined the needs for cost-effectiveness too [214]. The mechanical properties (Table 23) and printing settings (extra fast modality, Table 24) of Ultimaker PLA were retrieved from the technical data sheets. Beyond the use of the manufacturing material, the use of support material was kept to a minimum: only orthotic models characterised by large overhangs and hanging features necessitated the use of Ultimaker Breakaway support material (the minimum overhang value for which the support was printed was 65°).

	Density	Elastic modulus	Ultimate tensile strength	Poisson ratio
PLA	1.24 g/cm^3	2347 MPa	46 MPa	0.33

Table 23. Mechanical properties of Ultimaker PLA.

	Layer height	Infill %, pattern	Printing temperature	Printing speed
PLA	0.6 mm	100%, line	210°C	70 mm/s

Table 24. Printing settings of Ultimaker PLA (extra fast modality).

4.3.2 Results and discussion

Process evaluation

The production process of customised orthoses for upper limb rehabilitation progressed according to the three stages stated in the methodology.

Scans of the three anatomical regions under investigation were acquired in multiple attempts owing to the high resolution of the scanning device (RS6 Laser Scanner), which inevitably captured involuntary muscle contractions, resulting in minor misalignment artifacts in the mesh. The resulting scans were of excellent quality and the meshes were extremely dense (i.e., the arm scan featured over 150,000 nodes).

Subsequently, the scans were imported into the modelling software. By subjecting the arm scan to the modelling commands, orthotic models (full and lightened designs) for wrist rehabilitation were obtained flawlessly.

Also, the software responded positively to the generation of orthotic models of a different shape and geometry, indeed, orthotic models for rehabilitation of the thumb finger and index finger were successfully obtained. Nevertheless, two remarks concerning the development of the latter two orthotic models should be made. These scans were not processed with the fixing command, as this algorithm, when combined with the smoothing function, tended to excessively shrink the original mesh in an attempt to optimise the number of nodes and triangles. This effect is visible in Figure 57, representing the different profiles of the models of the index finger application. One further remark uniquely concerned the orthotic model for the treatment of the index finger; dividing and combining operations were not necessary since the orthosis could be modelled as a single part.

Different designs for the three applications were developed:

- Model 1 – full model.
- Model 2 – lightened model obtained with the lightening function.
- Model 3 – lightened model obtained with the optimisation module of Abaqus.

An overview of the structures of orthotic model for wrist, hand and index finger is shown in Table 25, Table 26 and Table 27.

Regarding model 3, at the completion of the topological optimisation process, the resulting geometry was definitely rough such that extra edge refinements are necessary. Particularly, the finishes would

be functional to facilitate the 3D printing process, besides providing practical wearability. Depending on the extension and medical function of the specific anatomical region, different orthotic thicknesses were made: the wrist and thumb orthoses were built with a thickness of 2 mm, whilst the index finger orthosis of 1 mm. The thicknesses conformed to medical indications and are slightly thinner than traditional devices.

The medical prototypes were printed in PLA using MEX technology (Ultimaker S5). In almost every instance the use of support material (Ultimaker Breakaway) was necessary, with the only exception of models 1 and 2 of the index finger orthosis. Models derived from topological optimisation (model 3) resulted in the greatest use of support material.

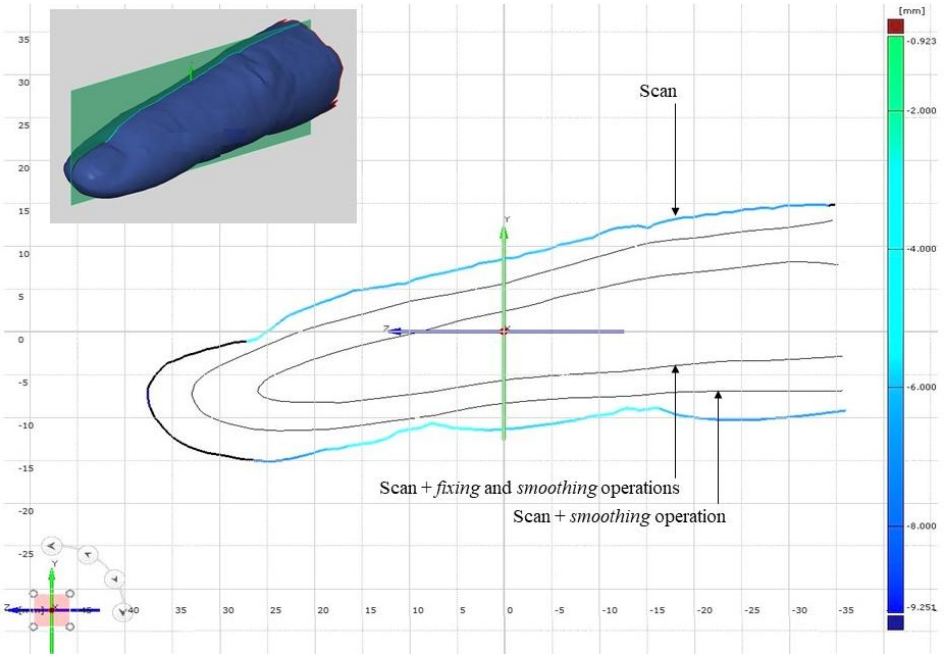

Figure 57. Graphication of the error (mm) between the finger original scan and the finger model which was developed using the fixing command. In the upper left quadrant measurement section was reported.

Product evaluation

The current procedure was complemented with a time-cost valuation of the medical devices. Time analysis comprised the estimation of the production time, intended as material deposition time, through the use of the Ultimaker Cura slicing program. Cost analysis involved the cost of the materials used to produce the prototypes, thus, the manufacturing material (PLA, about 0.57 €/m) and the support material (Breakaway, about 0.92 €/m). Cost analysis was based on the length of deposited filament, captured through the Ultimaker Cura slicing software.

Also, the analysis was supplemented with the information on prototype weight and mechanical behaviour under reasonable working condition to assess the feasibility of the two strategies of volume reduction.

The mentioned information is discussed below and reported in Table 25, Table 26, Table 27.

In terms of time, across all medical application, the progressive lightening of the device was associated with an increase in printing time, primarily prompted by the need of employing support material for the manufacturing of geometries characterised by large overhangs and thin-walled structures. The effect was particularly pronounced in the topologically optimised models (model 3), whose designs were required printing times at least twice as long as those of the full models (model 1). From a relative perspective, the worst-case scenario was the orthosis dedicated to the rehabilitation of the index finger conditions: the printing time of the orthotic model 3 was 2.6 times longer than the printing time of the orthotic model 1. In absolute terms model 1 was produced in 12 min, while model 3 in 31 min.

	Wrist – Model 1	Wrist – Model 2	Wrist - Model 3
	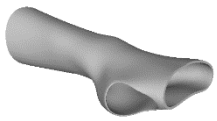		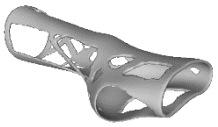
Printing time	122 min	176 min	294 min
Material cost	7.07 €	8.27 €	11.66 €
Weight	95 g	92 g	64 g
Max. stress	30 MPa	31 MPa	32 MPa
Max. displacement	2.7 mm	3.2 mm	4.0 mm

Table 25. Assessment of the wrist orthotic models.

	Thumb – Model 1	Thumb – Model 2	Thumb - Model 3
			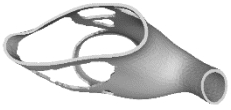
Printing time	74 min	95 min	151 min
Material cost	4.95 €	5.43 €	6.71 €
Weight	64 g	62 g	42 g
Max. stress	11 MPa	11 MPa	11 MPa
Max. Displacement	0.5 mm	0.5 mm	0.5 mm

Table 26. Assessment of the thumb orthotic models.

	Finger – Model 1	Finger – Model 2	Finger - Model 3
	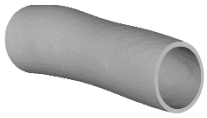	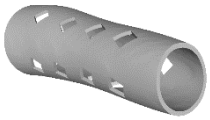	
Printing time	12 min	14 min	31 min
Material cost	0.40 €	0.35 €	0.80 €
Weight	6 g	5 g	3 g
Max. stress	14 MPa	24 MPa	25 MPa
Max. Displacement	0.5 mm	0.6 mm	0.5 mm

Table 27. Assessment of the (index) finger orthotic models.

A similar trend is shown in the cost analysis too. Indeed, in each medical application, the progressive lightening of the device led to a rise in material cost. The implication of the above consideration was that the manufacturing material cost saved through the volume reduction strategy (particularly that referring to topological optimisation) was totally recovered by the use of support material (which for the same quantity has a higher purchase price than PLA). The worst-case scenario was, once again, the orthosis dedicated to the treatment of the index finger: cost of model 3 was twice as much as model 1, however, in absolute terms, the cost was moving from € 0.40 to € 0.80.

From a mechanical behaviour perspective, FEA simulations demonstrated that all medical applications and corresponding design variants satisfied the requirements in terms of tensile strength and deformation. The maximum stress values recorded were consistently below the UTS of the manufacturing material, thus, preventing failure under service conditions. In terms of deformations, the highest displacement values were observed in the case of the orthosis dedicated to the wrist joint care: these values were slightly more than 3 mm, but were still considered acceptable as they occur near the distal end of the device, thus, leaving the wrist area almost unaffected; displacements of the wrist region varied from 0.5 mm to 1.1 mm. Regarding the thumb and the index finger orthoses, the maximum displacements were definitely contained, making the proposed solutions viable.

Considering all the factors mentioned above, some observations emerged. Firstly, production time emerged as a significant variable in the evaluation process of the analysed methodology. Production times were non-negligible (especially for large volume applications) and might be prolonged by additional time variables that were not taken into account in the current study (i.e., acquisition and modelling times). Under these circumstances, it is unlikely to guarantee ready-to-use devices and, therefore, it would be necessary to adopt some measures to streamline the overall process time. Although the time analysis did not reveal a distinct advantage, sources of competitiveness did emerge from the cost evaluation. Indeed, the estimated material cost for 3D production was significantly lower than the cost of material used in the production of conventional orthoses (i.e., LTT materials).

The strategy of reducing the volume of orthotic models with the aim of optimising the production process did not achieve the desired results in terms of time and cost (except for the finger index orthosis model 2, whose output might be a considerable alternative). Even more dubious was the role of volume reduction implemented through topological optimisation. Indeed, there was also evidence of an even greater increase in material cost and production time: the irregular shapes derived from the topological optimisation simulation required an immoderate amount of support material, which drastically affected the material deposition process. In contrast, from the mechanical performance perspective, satisfactory stress and displacement values were ensured for moderate volume (and weight) reduction in both strategies. Notably, topological optimisation, whose fundamental objective is to determine the optimal material distribution under specific operating conditions, proved to be a pivotal design strategy, enabling the development of significantly lighter yet mechanically compliant solutions.

Certainly, through the illustrated methodology, it was possible to make extremely customised and lightweight geometries able, at the same time, to ensure adequate mechanical strength, which up to date it is not possible with traditional splinting techniques.

4.3.3 Conclusions

The present research evaluated the process of customised splinting for the treatment of upper limb pathologies through the utilisation of advanced techniques, specifically Reverse Engineering and Additive Manufacturing (AM).

The manufacturing process of patient-specific orthoses, analysed in the current study, was considered functional and straightforward. Some general observations may be drawn. Regarding the acquisition activity, although the scanning laser under consideration was highly performant, it is advisable to evaluate technologies that facilitate the scanning operation for the medical worker.

Inherent to the modelling activity, the software originally developed to convert the arm surface geometry into an arm orthosis proved to be highly versatile, as it successfully generated medical devices for various anatomical regions. This capability demonstrates the potential of using a single application for modelling diverse anatomical areas, without the need for dedicated, case-specific tools. Optimisation of the software algorithms would allow even more efficient and agile handling of meshes of different sizes and complexities.

On the 3D printing side, there was an emerging need to optimise printing time, for instance using higher-performance 3D printers. In addition, post-printing surface finishing treatments of the devices should be considered too.

Lastly, two volume-reduction approaches were investigated by developing lightened orthotic models. Nevertheless, from the current product evaluation, the most competitive design in terms of cost, time and mechanical behaviour resulted to be the standard full prototype (model 1). Thus, the role of the two emptying strategies found to be still uncertain: the costs and production times associated with the deployment of these approaches must be justified by the value and specificity of the considered application.

Surely, the use of the topological optimisation technique is a powerful tool, able to greatly lighten medical devices while ensuring higher mechanical performances. However, in some cases the role of topological optimisation compared to the volume reduction performed with the lightening command worth further investigation (i.e., in the case of model 3 of the wrist and thumb orthoses improved lightness was achieved and mechanical performance simulations suggested that lighter structures can be further realised). Whilst, in some other cases, it was clearly the option to be discarded (i.e., in the case of model 3 of the index finger orthosis, whose efforts would not bring additional value compared to model 2).

To conclude, the present study provided a preliminary yet structured analysis of the consistency and robustness of the AM process for producing customised orthoses. The assessment evaluated factors such as production cost, time and mechanical behaviour. Future research needs to be conducted to provide a more exhaustive assessment, especially regarding topological optimised orthoses.

4.4 Evaluation of customisation in the production process of orthoses: the role of topological optimisation

This chapter is derived from the article “Sala, F.; D’Urso, G; Giardini, C. (2024). Evaluation of the Integration of Topological Optimisation in the Process Chain for Manufacturing Customised Orthopaedic Devices via Additive Manufacturing”.

DOI: 10.3390/prosthesis6060109

I am grateful for the support received from my co-authors. I bear full responsibility for all the variations from the published version reported in the current chapter.

Within the framework of medical device customisation, the concept of Topological Optimisation (TO) represents a valuable instrument, able to redesign the basic structure of prefabricated orthoses, enhancing the conventional idea of tailored-made medical devices. Simultaneously, the tool realises lightweight elements without limiting their reliability and functionality [215–218].

TO is a mathematical method widely used in civil and mechanical engineering in the design of physical systems and mechanical structures [219]. The traditional TO approach based on density-method consists in the discretisation of a defined area into a grid of finite elements (e), described as isotropic solid microstructure and characterised by a density distribution function of material (ρ) within the design domain [220]. The binary assignment of material determines a discrete density distribution, where $\rho(e) = 1$ when material is present and $\rho(e) = 0$ when material is removed. To promote analysis stability, continuous density distribution is introduced: intermediate level of densities, $\rho_{min} < \rho(e) < 1$, are assigned to each element and a penalty factor (p) is adopted to limit the presence of intermediate density elements, fostering structural stiffness [221–223]. The study of the optimal allocation of material of the elements of defined areas is dependent on the definition of objective functions and constraints.

Therefore, the present research aims at investigating the use of TO strategy as a methodology for customising medical devices with the aim of further lightening the structure while preserving the strength characteristics of the device. In the present research, TO is not considered solely as a design tool for material redistribution, but as a comprehensive methodological framework enabling a broader evaluation of the AM process. In fact, such an analysis encompasses multiple variables and factors influencing production, thereby extending its relevance beyond mere structural optimisation. The tool was analysed with respect to the entire manufacturing process of orthopaedic devices, highlighting potential advantages and disadvantages associated with its implementation.

The study is based on an orthopaedic device belonging to the class of orthoses, also known under the name of splints and braces, which are elements worn in direct contact with the patient's skin. The selected orthosis is responsible for the treatment of motor dysfunction of the wrist joints in rehabilitation programs.

The adopted methodology outlines the most significant activities to manufacture AM-based orthosis devices and it delves into the TO topic: the study is conducted with Simulia Tosca, an optimisation suite based on simulations executed with Abaqus FEM. Software is used with the intent of progressively lightening the orthosis, developing four different models with decreased percentage of residual volume fraction.

Primarily, the feasibility of customising TO orthoses, either in terms of digital modelling either in terms of 3D printing, is examined. Furthermore, the strength and deformation behaviours are investigated in relation to the gradual lightening of the medical device. The structural and functional integrity of the orthoses during patient remission was evaluated too. Insights and recommendations on the adequacy of TO, in terms of production time and production costs, are presented.

4.4.1 Methodology

Currently, in the landscape of design and fabrication of upper-limb orthotic devices, traditional manufacturing methods, often characterised by labour-intensive processes [130], are predominant. The progress of advanced orthotic modelling and manufacturing is still largely confined to the prototyping stage. This limited clinical translation may be attributed to the absence of clear regulatory frameworks and professional guidelines supporting the integration of advanced technologies in clinical practice. Additionally, the wide range of available techniques and materials requires systematic investigation and validation.

The modelling and manufacturing technique for orthotic devices dedicated to the upper limb joints, presented in the current research, explores advanced techniques, specifically Reverse Engineering (RE) and Additive Manufacturing (AM).

The RE phase encompasses the processes required to generate the final digital solid model of the medical device, starting from the anatomical data acquired, for instance, through a 3D scanning system. At this stage, great relevance is paid to the activities involved in the modelling of the raw information with CAD software to transform the anatomical surface into a truly wearable orthosis model. Once the desired digital model is obtained, the following task involves fabrication using AM techniques.

The computational instrument being investigated in this paper, namely Topology Optimisation (TO), places itself in the RE activity chain. In particular, it lies outside of digital modelling and requires numerical simulations to identify the regions of the orthosis model to be reshaped. The entire workflow is illustrated in Figure 58 and outlined in the following paragraphs.

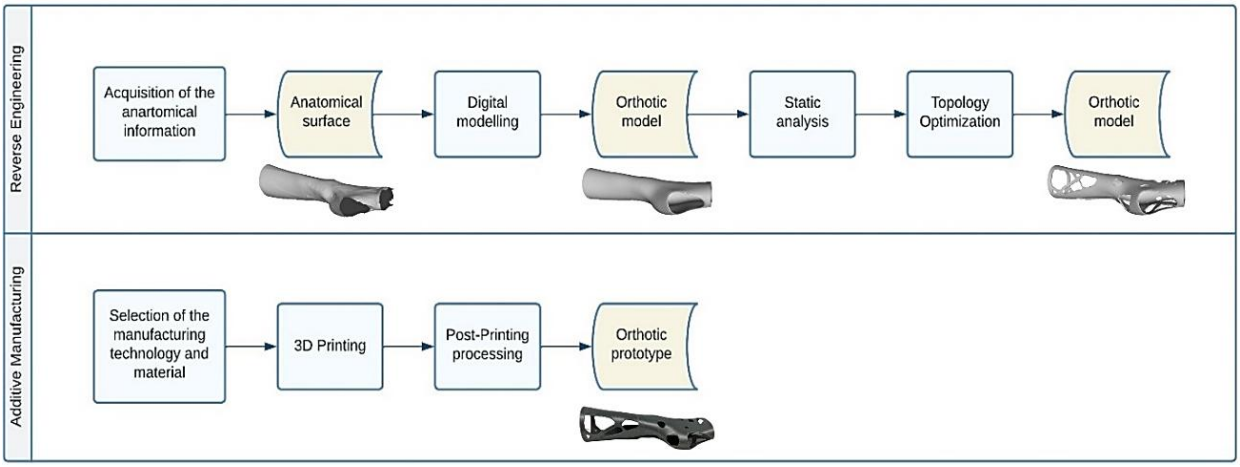

Figure 58. Flow chart of the activities for manufacturing customised orthoses for the treatment of the wrist joint.

Digital modelling

The need to individualise treatment requires orthopaedic devices to be tailored to the specific therapeutic targets and anatomical characteristics of each patient. To comply with these specifications, a medical prototype was modelled from the geometry of the patient, which was captured through a laser scanner (Hexagon Absolute Arm 7-Axis equipped with RS6 Laser Scanner). The anatomical surface was acquired in the form of a point cloud, converted into a format that is compatible with CAD and AM technologies and modelled into a solid.

As a consequence of the uniqueness of each clinical case, the transformation of the surface information into a 3D digital model of the orthopaedic device often involves performing a series of manual editing operations [126,224,225]. Although general CAD software that caters to the demands of image processing is available, advanced programs [198,212,226] able to accelerate and streamline the modelling activity in an effort to automate the procedure were found to be essential. The orthosis modelling activity presented in this research is based on one of these approaches [198].

The modelling process developed an orthotic prototype resembling the design of the traditional circumferential wrist immobilisation pattern. The device consisted of two shells that join along the central axes of the structure and completely envelop the wrist joint, the thumb and the fingers.

Static Analysis

At this stage, numerical analysis was conducted to evaluate the operating behaviour of the designed medical device, anticipating and correcting any design flaws or inefficiencies. Numerical simulations were conducted with Abaqus, a finite element method (FEM) suite involved in the study of the mechanical, thermal, and electromagnetic behaviour of structures and materials. Given the absence of specific mechanical tests designed to examine the standard behaviour of the considered medical device and considering that the device is not subjected to particular loads during its use, the present research simulated an accidental mechanical impact. Specifically, the present analysis was intended to represent the unintentional impact of the orthosis against a rigid surface.

The experimental conditions were simplified, and two assumptions were made:

- The static analysis was performed without accounting for the presence of the forearm inside the orthotic device;
- The static analysis was carried out on the device as a whole; disregarding the connections between the interacting interfaces of the two shells.

Based on these assumptions, the orthotic model was imported into the Abaqus simulation environment. The model was discretised into 40,680 quadratic tetrahedral elements with an approximate global size of 5 mm. Also, control over the minimum size of the mesh feature was

defined as a fraction of 0.1, meaning that the minimum element size was set to 0.5 mm. A curvature control with a maximum deviation factor of 0.1 was applied to ensure that the mesh accurately captured the model's surface geometry, minimising excessive approximations. In conclusion, the total number of nodes was 81,897. This discretisation provided a high-resolution representation of the orthosis. Indeed, the defined parameters were validated by performing mesh size-dependency tests, ensuring that the accuracy and reliability of the results were not compromised.

The orthosis was defined as a homogenous linear elastic structure with Young Modulus and Poisson's ratio of the selected thermoplastic material. The boundary and load condition were established as depicted in Figure 59. The distal end of the orthotic model (set of 450 nodes) was fixed with an encastre constraint. A load of 400 N was exerted as a pressure uniformly distributed over the palm of the hand (surface of 2259 faces). The simulation was performed and the stress and displacement distributions, under the current experimental condition, were monitored.

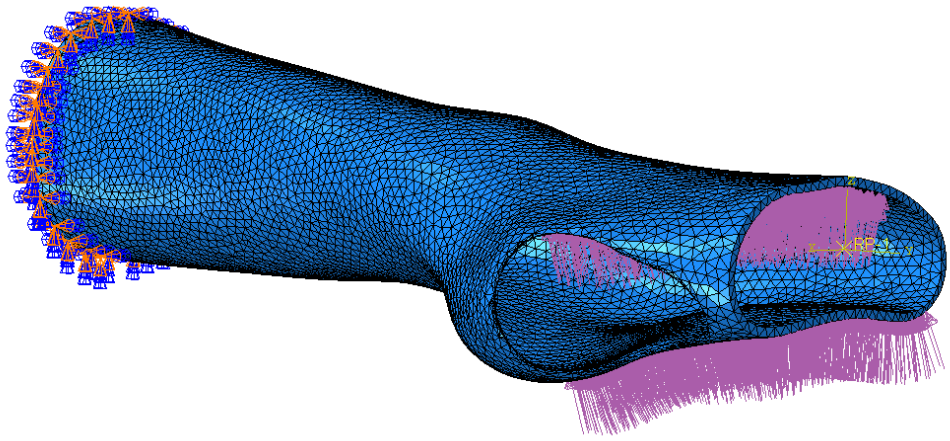

Figure 59. Load and Boundary conditions applied to the orthosis model for the execution of the static analysis.

Topology Optimisation

The mechanical behaviour of the orthosis was further investigated through Topology Optimisation (TO) analysis, enabling the development of innovative orthopaedic device designs. The study was performed with Simulia Tosca, an optimisation suite based on Abaqus FEM simulations. Indeed, from the analysis of the prescribed conditions of the FEM model, the software was able to determine the areas subjected to elevated loads and propose a geometry that optimised the overall stiffness of the structure.

The optimisation task used the general algorithm, partly described by Bendsøe et al. [227]. Given the purpose of the study, namely the lightening of the orthotic structure, the whole model was selected

as the design area. Two design responses were determined as follows: the energy stiffness measure identified the objective function, while the volume measure identified the optimisation constraint. Under the specified design responses, the optimisation task involved the minimisation of the energy stiffness measure respecting the requirement of structural volume. Four experimental conditions were planned; these comprised a volume reduction minor or equal to a percentage fraction of the initial volume, identified as 90%, 80%, 70% and 60%, respectively. A geometric constraint was introduced to further guide the TO process, specifically preserving the edges of the orthotic model as frozen areas (4 822 elements). The maximum number of iterations to be performed was set to 50, which proved sufficient for the algorithm to converge to a stable solution.

3D Printing

The customised orthotic designs were 3D-printed using Material Extrusion (MEX) technology, Ultimaker S5. Thermoplastic polymeric filaments, with a diameter of 2.85 ± 0.10 mm, were employed. Specifically, PLA (properties reported in Table 28) was selected due to its suitability for the current medical application and its faster printing times compared with alternative materials. This makes it a practical choice both timewise and economically.

The models were sliced, and their printing settings (Table 29) were defined in Ultimaker Cura (v5.3.0). The prototypes were 3D-printed with a 100% infill density and a 0.8 mm head nozzle, capable of realising a layer height of 0.6 mm. Some features of the prototypes required the use of support material (PLA or Ultimaker Breakaway, a mixture of PLA and TPU), extruded from a second printhead with a 0.8 mm head nozzle and 0.6 mm layer height.

	Mass density	Elastic modulus (E)	Ultimate tensile strength (UTS) after 3D printing	Poisson's ratio
PLA	1.24 g/cm^3	3,292 ± 101 MPa	56.0 ± 1.5 MPa	0.33

Table 28. Material properties of PLA filament.

	Nozzle temperature	Build plate temperature	Print speed
PLA single extrusion	210° C	60° C	45 mm/s
PLA dual extrusion	210° C	60° C	45 mm/s
PLA dual extrusion with Ultimaker Breakaway	200° C / 225° C	60° C	35 mm/s

Table 29. 3D printing parameters of PLA and Ultimaker Breakaway filaments in the different extrusion modalities.

4.4.2 Results and discussion

Design of the optimised models

This section presents the results of the topological optimisation, with particular emphasis on their implications for medical device design; furthermore, the geometric properties of the resulting structures were systematically analysed.

Digital modelling led to the construction of an orthotic prototype (see full model, pictures of Table 30) for the treatment of wrist pathologies. The element has a dimension of 94 × 82 × 228 mm^3. The subsequent activities of static analysis and TO resulted in the creation of five solid models, which differed according to the fraction of residual volume (RVF) (see Model 1, Model 2, Model 3 and Model 4, line 1–2 of Table 30). Material was removed from specific regions where it did not significantly contribute to the structural strength and overall performance of the system, as reported in Table 30. The upper portion of the forearm and the wrist were less susceptible to material removal.

	Full Model	Model 1	Model 2	Model 3	Model 4
Target RVF	100%	90%	80%	70%	60%
Target RV	82 299 mm^3	74 069 mm^3	65 839 mm^3	57 609 mm^3	49 379 mm^3
Measured RVF	100%	91%	85%	77 %	68%
Measured RV	82 299 mm^3	76 962 mm^3	70 472 mm^3	63 333 mm^3	56 137 mm^3
Front view					
Back view	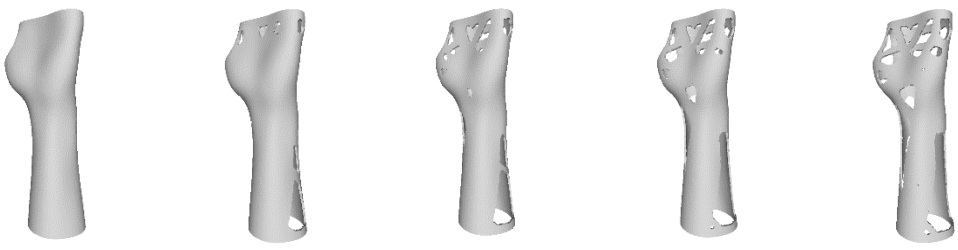				

Table 30. Orthotic models and their geometrical properties.

The structures of Model 1, Model 2, Model 3, and Model 4 attained convergence and stability at the 24th, 30th, 33rd, and 41st iteration cycles, respectively, thus requiring fewer iterations than the predefined maximum value of 50 design cycles. The final structures were taken from the last iteration step, guaranteeing that the selected configurations corresponded to the stable, converged states achieved at the end of the optimisation process. In every instance, the volume constraint was satisfied, and, for the last iteration step, was always slightly below the target volume constraint value (0.0004% deviation). It is worth noting that, when exporting the topological optimised model from Abaqus, the software may simplify and/or approximate the geometry to ensure part realisability, resulting in slight variations in the final models. This explains the discrepancy between the target RVF or RV (i.e., the volume values set up as constraints in Abaqus) and the measured RVF or RV (i.e., the volume values measured in the exported files using other 3D file processing software).

The logic of material preservation is determined by the TO algorithm utilised. The progressive reduction in material occurs through the creation of new holes and/or enlargement of the holes created during the previous TO iterations. The holes created in the structure are characterised by an asymmetrical and irregular shape as a result of the material redistribution aimed at reducing the volume of the structure without constraining it to a predetermined or preestablished shape. Therefore, given that TO provides only an indication of how the structure should be revised, geometrical modifications to adjust the holes or adapt them to specific manufacturing constraints are required during post-processing. This necessity opens up opportunities for exploring innovative approaches to manage the voided areas identified by TO during the modelling phases, for example, by employing lattice geometries to fill the voids and mitigate practical design inefficiencies.

Mechanical performances of the optimised models

The mechanical properties of the medical device models were investigated by conducting analyses of Von Mises stress distributions and deformations (measured in terms of displacements from the initial undeformed configuration). The results were derived from the static analysis described in the methodology section.

Table 31 provides information on the stress state to which each model of orthosis was subjected under the specified load. The equivalent stress values of the structures of the full model and Model 1, Model 2, Model 3 and Model 4 consistently remained below the UTS of the manufacturing material (56.0 MPa). Moreover, on average, the stress did not exceed 30 MPa, except in a localised region near the opening intended for the thumb finger, where the maximum stress value was recorded. This indicates that the volume reduction strategy, even in the lightest configurations, did not adversely affect the structural integrity of the component. In fact, the models presented satisfactory safety factor values

(summarised in Table 33), compatible to the safety factors identified for medical devices of the same kind [164,213,228].

		Von Mises Stress (front view)	Von Mises Stress (back view)
Full Model	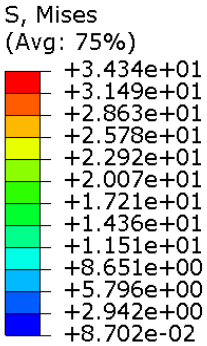		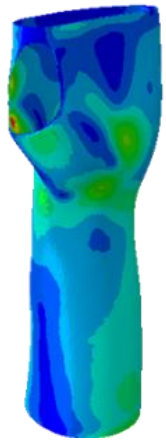
Model 1	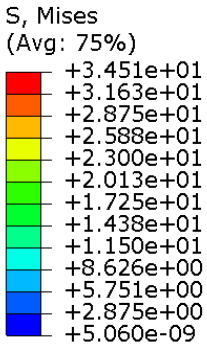		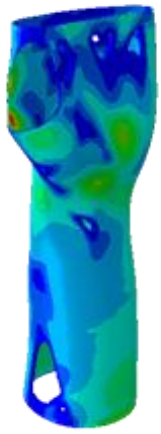
Model 2	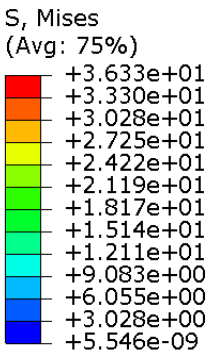	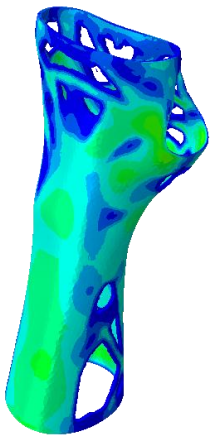	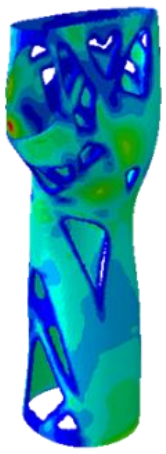

Model 3	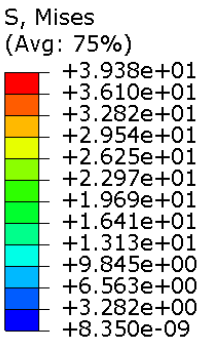	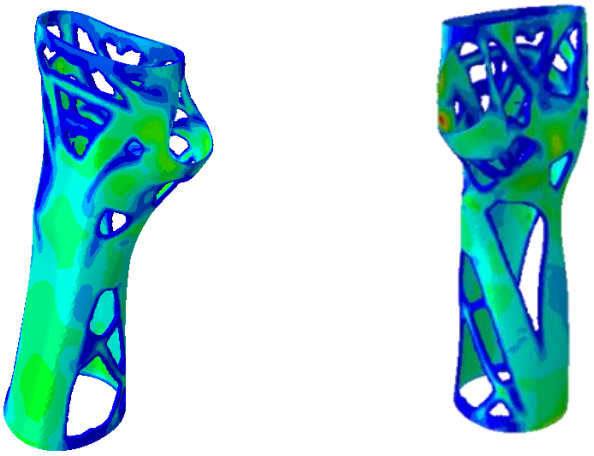
Model 4	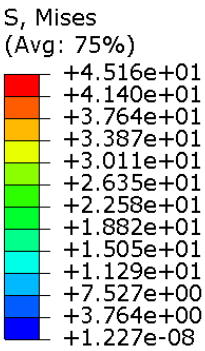	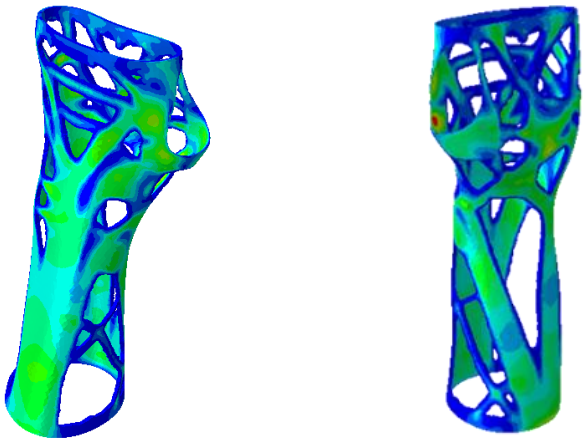

Table 31. Static analysis results: Von Mises stress.

Table 32 presents an analysis of the magnitude of the displacement. The maximum displacement values were recorded on the upper edge of the medical device, close to the hand area; these range from 7 mm (full model) to almost 12 mm (lightest model, Model 4). It is worth noting that the critical displacement values are the ones affecting the area of the wrist joint: the displacement values recorded in this area were around 3 mm (full model) and around 6 mm (Model 4). Considering the functionality that the medical device must achieve, the deformation values obtained were not entirely negligible in the lightest configuration.

		Displacements (front view)	Displacements (back view)
Full Model	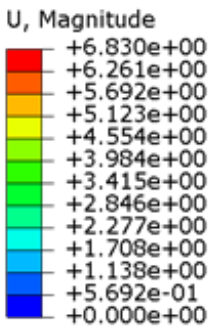	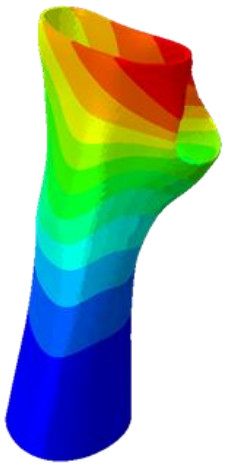	
Model 1	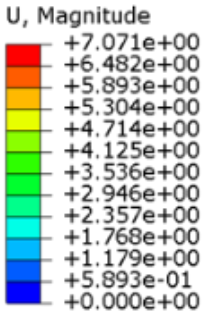	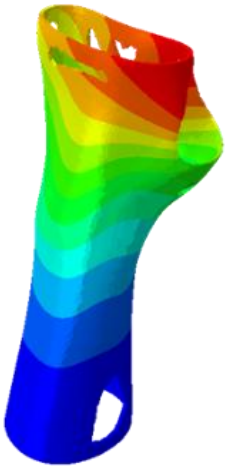	
Model 2	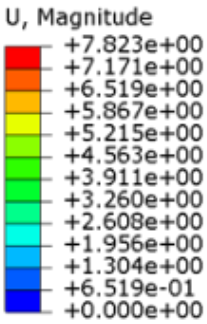	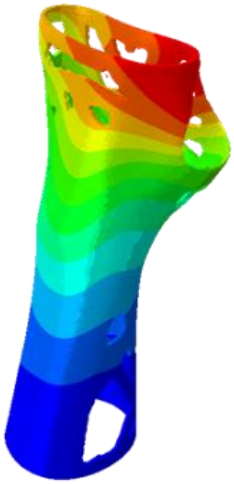	

Model 3	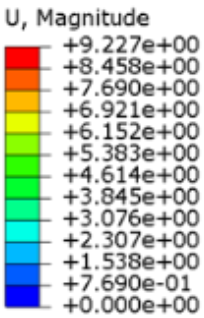	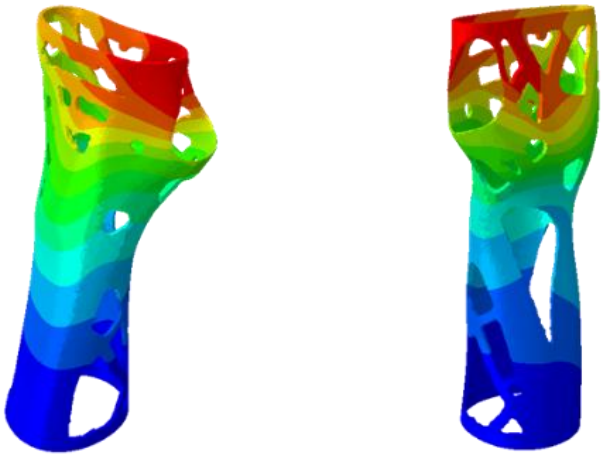
Model 4	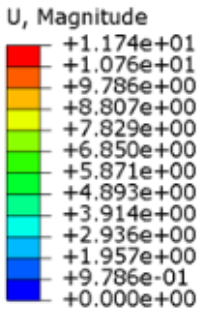	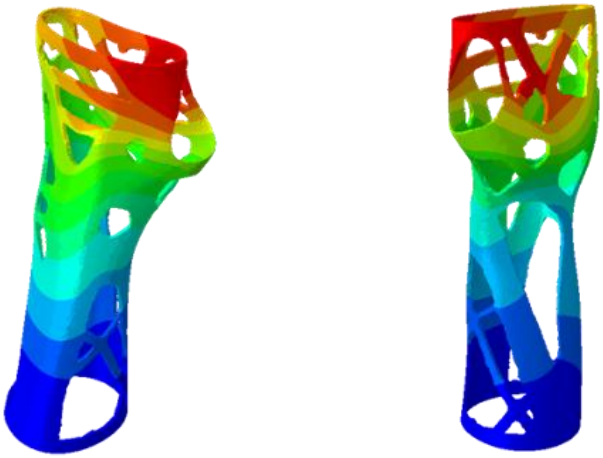

Table 32. Static analysis results: Displacements.

	Target RVF	Max. Displacement	Max. Stress	Safety Factor based on Max. Stress
Full Model	100%	7 mm	34 MPa	1.65
Model 1	90%	7 mm	35 MPa	1.60
Model 2	80%	8 mm	36 MPa	1.56
Model 3	70%	9 mm	39 MPa	1.44
Model 4	60%	12 mm	45 MPa	1.24

Table 33. Static analysis summarised results: maximum displacement and maximum Von Mises stress.

The main results related to the mechanical characteristics, considered in terms of von Mises stress and displacement with respect to variations in the volumetric dimensions of the medical device achieved through topological optimisation (TO), are summarised in Table 33.

Further analyses of the mechanical behaviour of the four TO orthosis models (Model 1 to 4) were conducted to simulate the structural response to wrist movements. Specifically, the simulations focused on wrist flexion and ulnar deviation (see Figure 60). Although extension and radial deviation are also significant, these movements typically involve a restricted range of motion and generate

forces characterised by lower intensity compared to flexion and ulnar deviation. Furthermore, they are less relevant in daily wrist activities.

(a)

Ulnar deviation—wrist movement causing the hand to shift medially toward the ulna

Flexion—wrist movement causing the hand to bend down toward the palm

(b)

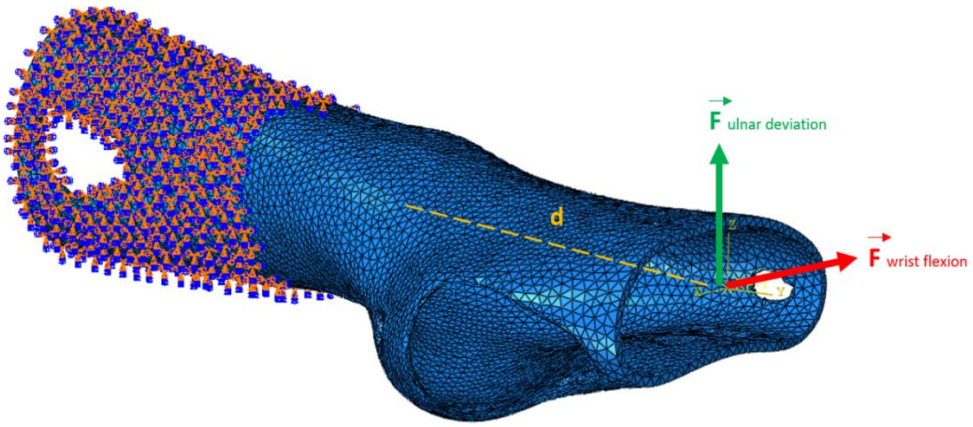

Figure 60. Illustration of the wrist movements (a) and schematic representation of the load and boundary conditions applied to the orthosis (Model 1) (b). Note: flexion and ulnar deviation forces are graphed in the same picture but are applied separately in the analysis.

The simulations were performed in accordance with the procedure already defined in the methodology section. In these analyses, ulnar deviation and flexion movements were modelled as moment loads, applied to the distal perpendicular surface of the orthosis (near the fingers), while the proximal region of the orthosis was constrained with an encastre boundary condition. The applied forces in both scenarios were chosen to represent conditions compatible with joints in the late stages of rehabilitation, during which the patient requires minimal support from the device and is capable of

exerting moderate forces. Specifically, for ulnar deviation, force F = 30 N and lever arm d = 75 mm were used, while for wrist flexion, F = 50 N and d = 75 mm were applied.

The mechanical response of the orthosis, in terms of Von Mises stress and displacement, to the applied moment load is illustrated in Figure 61, representing Model 1. As expected, during ulnar deviation, the orthosis structure experiences elevated lateral stresses due to the concentration of forces along the sides of the device. In contrast, during wrist flexion, the loads are primarily distributed across the dorsal and palmar surfaces. The behaviour of Models 2, 3 and 4 is consistent with that of Model 1, differing only in exhibiting increased displacements and stress concentrations near the apex of the voids generated by TO process.

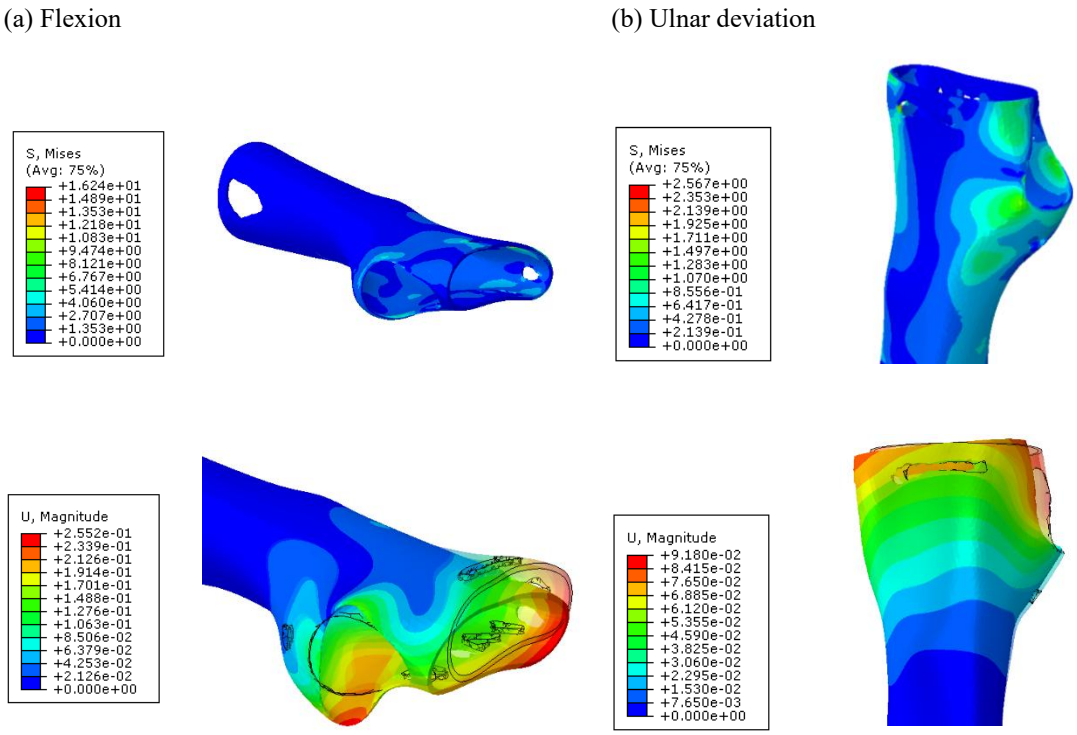

Figure 61. Additional static analysis results: Von Mises stress and displacement of the flexion (a) and ulnar deviation (b) movement. Note: displacement analysis illustrates both the original structure (outlined in black) and the deformed structure under torsional loading (solid coloured structure). The deformed shape is scaled by a factor of +50% for flexion and +100% for ulnar deviation to enhance visibility of displacements that would otherwise be imperceptible.

The results, measured in terms of Von Mises stress and displacement, are summarised in Table 34. The stresses are consistently below the material UTS. The deformations, quantified as global measures of displacements, are insignificant. Also, it is worth noting that the displacements along the specific directional components of the wrist movement (i.e., lateral direction for ulnar deviation and

vertical direction for flexion) are lower than the global displacement values obtained by considering all three axial components combined (U, magnitude).

The findings suggest that the orthosis designs maintain their structural integrity and functionality even during the patient's rehabilitation phase.

	Target RVF	Max. Displacement (U. magnitude)	Max. Stress (S. Von Mises)
Flexion			
Model 1	90%	0.3 mm	16 MPa
Model 2	80%	0.4 mm	22 MPa
Model 3	70%	0.5 mm	38 MPa
Model 4	60%	0.7 mm	28 MPa
Ulnare Deviation			
Model 1	90%	< 0.1 mm	3 MPa
Model 2	80%	0.1 mm	4 MPa
Model 3	70%	0.2 mm	7 MPa
Model 4	60%	0.2 mm	7 MPa

Table 34. Additional static analysis summarised results: maximum displacement and maximum Von Mises stress.

Rapid Prototyping of the optimised models

In the present section, an analysis focusing on manufacturing time and cost was conducted with the objective of assessing the impact of TO activities on rapid prototyping. Specifically, the benefits derived from the material redistribution were observed from the production process perspective.

Originally, the prototypes were produced using the default optimal printing parameters: the model was 3D-printed in PLA (~0.57 EUR /m) with dual extrusion to realise the default support structures in Ultimaker Breakaway (~0.92 EUR /m). All the models were manufactured successfully without experiencing difficulties. By examining the production cost, expressed in terms of raw material, and the production time required to fabricate the products, the critical issues associated with the volume reduction strategy implemented via TO became evident (Figure 62).

The incremental growth in the complexity of geometries in TO models, characterised by large overhangs and irregular holes, required a significant increase in the use of support material to prevent the collapse of the articulated features. Thus, production time extended and, in the present instance, almost doubled by moving from 2.8 h for realising the full model to 5.2 h for the lightest one. As shown in Figure 63, the advantageous cost effect of reducing the use of manufacturing material with

TO was nullified. Specifically, the overall production cost of Model4 doubled and its support material cost component increased seven-fold compared with the full model.

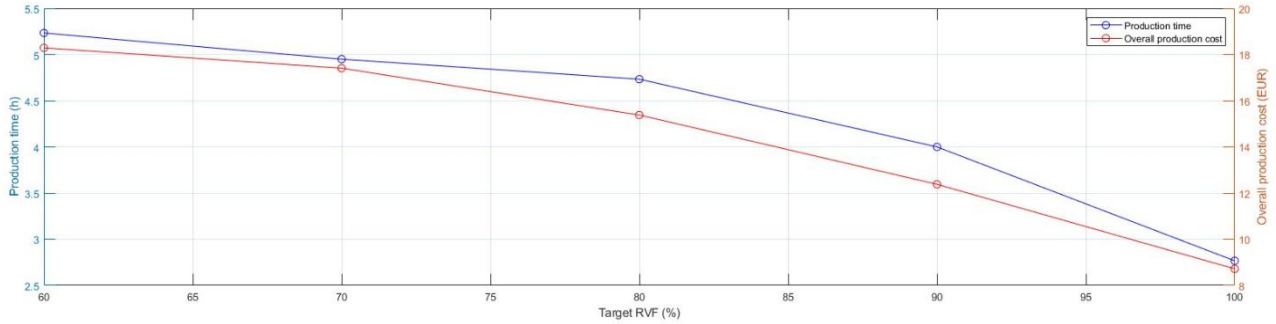

Figure 62. Overall production cost (EUR) and production time (h) over the different values of Target Residual Volume Fraction (%).

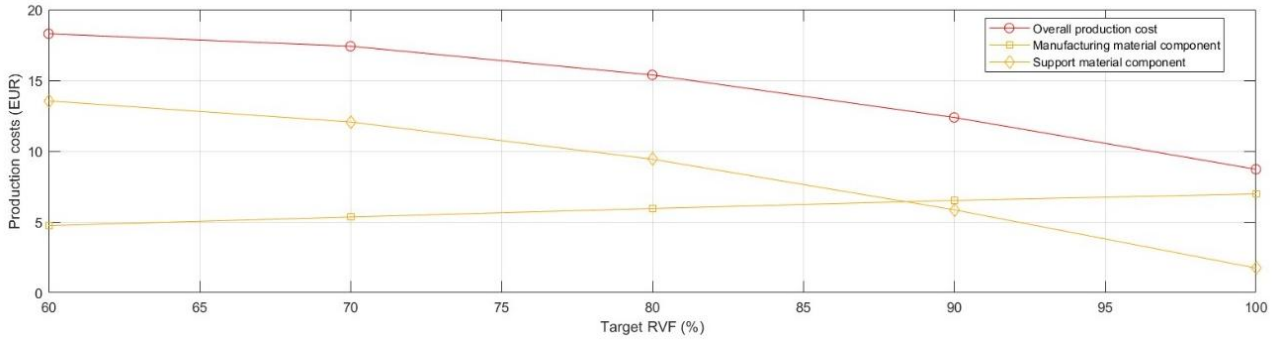

Figure 63. Breakdown of the overall production cost (EUR) in manufacturing material component (EUR) and support material component (EUR) over the different values of Target Residual Volume Fraction (%).

To mitigate the observed growth in production cost and time, a more detailed analysis of the support structures was required, particularly focusing on the optimisation of design and printing parameters of the support structures, together with the support material selection.

Following a Design of Experiment (DOE) plan, a series of tests were established to observe variations in production time and cost over the different values of the Target RVF. The first aspect considered the support material, which was distinguished into the recommended standard support material (Ultimaker Breakway, a mixture of TPU and PLA) and a support material equal to the structuring material (PLA). Using Ultimaker Breakaway allows for better surface accuracy by swiftly and cleanly detaching the support parts from the 3D-printed element. Using the same material filament (PLA) for both the support part and the structuring part may require post-production processing to improve surface quality, yet it allowed to examine the transition from dual-extrusion mode (two printheads)

to single-extrusion mode (one printhead). Further, the design of the support structure was analysed: the tree support structure (individually developed with Meshmixer software, with an overhang angle of 45°) replaced the default structure provided by the slicing software Cura (linear support with an overhang angle of 45°).

Hence, the experimental design plan (Table 35) was structured as follow:

- Ultimaker Cura Default support structure (test1, test2 and test3) and tree support structure (test4, test5 and test6);
- Ultimaker Breakaway support material (test1 and test4) and PLA support material (test2, test3, test5 and test6);
- For the tests employing the same material (PLA) for both the structuring part and the support part, dual extrusion (test2 and test5) and single extrusion (test3 and test6). Note, that processes involving different materials (test1 and test4), by principle, use the dual extrusion mechanism.

	Support structure	Support material	No. Extruders
Test1	Default	Breakaway	Dual
Test2	Default	PLA	Dual
Test3	Default	PLA	Single
Test4	Tree	Breakaway	Dual
Test5	Tree	PLA	Dual
Test6	Tree	PLA	Single

Table 35. Experimental design plan.

Prototypes, corresponding to the different tests, were 3D printed to ensure feasibility in the production process. The results of the performed tests were collected in Figure 64 and Figure 65, which respectively illustrate the evolution of manufacturing time and cost curves as a function of medical device lightening. It can be observed that the use of tree-structured supports and a single material for both the support and structural parts, extruded from a single nozzle, significantly reduces 3D printing time. Furthermore, as a result of the improved design of support structures, it is also possible to observe an overall flattening of the curves of production times as the volumetric reduction of the device progressed. Comparably, a reduction in the overall production cost was observed. The optimal result, measured in terms of production time and production cost, was test6.

At last, Table 36 and Table 37 summarise the outcomes of the default printing strategy (test1), which returned the least favourable outcomes, and the optimal printing strategy, which can be identified in test6. Besides the absolute values, the percentage values are reported with respect to the default strategy for manufacturing the full model.

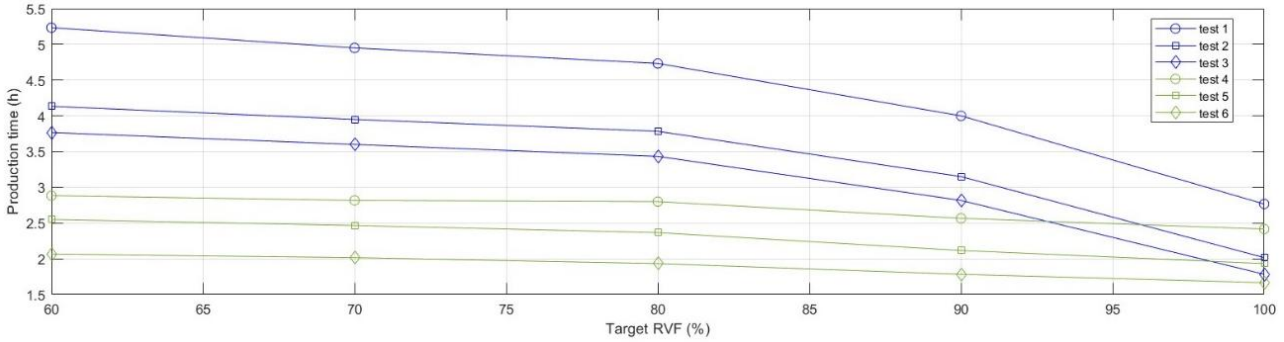

Figure 64. Production time (h) of the six tests over the different values of Target Volume Fraction (%).

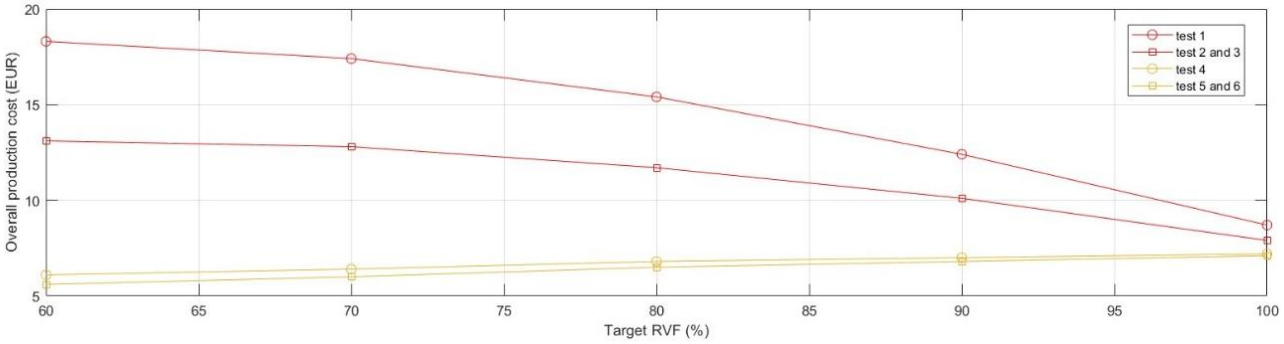

Figure 65. Overall production cost (EUR) of the six tests over the different values of Target Volume Fraction (%).

		Default printing strategy (*test1*)	Optimised strategy (*test6*)
	Target RVF	100 %	100 %
	Printing Time	2.8h	1.7h
	Material Cost	8.72€	7.14€

Table 36. Default printing strategy (test1) and optimised printed strategy (test6) of full model.

		Default printing strategy (*test1*)	Optimised strategy (*test6*)
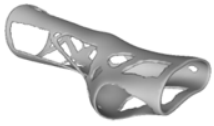	Target RVF	60 %	60 %
	Printing Time	5.2h	2.1h
	Material Cost	18.29€	5.56€

Table 37. Default printing strategy (test1) and optimised printed strategy (test6) of Model4.

4.4.3 Conclusions

The present research explores the implementation of Topology Optimisation (TO) as a design-driven framework for the development of patient-specific orthopaedic devices, with emphasis on orthoses and splints for wrist joint stabilisation. TO was performed through the Simulia Tosca optimisation suite of Abaqus software with the objective of lightening a predetermined model of the medical device, by ensuring an extremely customised design that was satisfactory to the patient's individual preferences and conformed to their wearing schedule. The goal of the study was to examine the effects of TO strategy through a multi-factorial assessment, that extended beyond a product-centred viewpoint to incorporate variables associated with the entire process chain.

Finite Element Analysis (FEA) results indicated that stress levels remained within acceptable limits for all configurations. Moreover, the regions experiencing peak stress consistently exhibited a safety factor exceeding 1.2. Displacements were not excessive, although their magnitude was not entirely negligible. While the structural advantages derived from the application of TO were clearly observable, the benefits from a manufacturing standpoint were initially less evident. The introduction of lighter and more geometrically complex configurations led to increased production time and costs, primarily due to the greater demand for support material required to fabricate the articulated geometries. Thus, a targeted optimisation of the process parameters, especially the parameters related to the support material, was undertaken. After optimising the 3D-printing strategy, the material cost of the lightest model (model4) was lowered by 22% compared to the full model, thereby providing tangible evidence of the economic potential. In terms of fabrication time, the increase was partially contained; the production time difference between the full model and the lightest model (model4) was reduced to +24%, compared with a +86% increase observed under the non-optimised printing conditions.

In summary, TO demonstrated significant potential as an approach for the advanced customisation of orthopaedic devices. Although it primarily functions as a conceptual design tool, generating an initial structural layout rather than a fully refined final geometry, all optimised lightweight models were successfully fabricated without major issues. Further refinement of the modelling stage, including adjustment and smoothing of the topology-derived geometries as well as appropriate finishing treatments, would likely improve both manufacturing performance and device usability. Such enhancements could positively influence production efficiency while also supporting patient comfort and adherence to prescribed wearing schedules.

Chapter 5. MEX-based production of metal medical components

5.1 The effect of hatch angle variation on metal MEX-based components for medical application

This chapter is derived from the article "Sala, F.; Nani, L.; Quarto, M.; D'Urso, G. (2024). Preliminary assessment of material extrusion (MEX) for medical applications: The effect of hatch angle".

DOI: 10.21741/9781644903131-21

I am grateful for the support received from my co-authors. I bear full responsibility for all the variations from the published version reported in the current chapter.

Also, I would like to extend my gratitude to the Scientific Association for material FORming (ESAFORM) for the received recognition, Best Communication Award 2024.

Metal AM technologies belonging to the class of Powder Bed Fusion (PBF) or Directed Energy Deposition (DED) benefit from widespread adoption in medical research and industry. In contrast, Material Extrusion (MEX) still requires extensive investigation to expand its applicability in this field.

In the present research, the optimal printing conditions characterising LPBF technology are adequately transferred to MEX technology, with the aim of evaluating the influence of the printing parameters over the material properties. At the same time, the purpose is to provide a better understanding of the fabrication of medical metal parts via MEX.

Optimising and adjusting LPBF parameters has significant influences on the quality of the printed parts and the required densification, microstructure and mechanical properties [229–231]. Hence, the accomplishment of satisfactory outcomes in LPBF manufacturing relies on the balance of several factors, including laser power, scanning speed, layer thickness, hatch distance and angle.

Among the process parameters, the hatch angle represents the angle of rotation related to the element growth axis at which scanning vectors, belonging to successive layers, are melted. For LPBF technologies, the optimal configuration corresponds to 67°. Thus, 67°k scanning strategy, where k indicates the number of layers, involves the rotation of each layer by 67°, creating a structure that minimises the overlap of scanning vectors belonging to alternating layers.

Generally, the most common deposition strategy adopted by MEX processes is ±45° and it involves the deposition of material lines oriented at +45° on even layers and -45° on odd layers, commonly resulting in the overlapping phenomenon [175]. This pattern generates an envelope of porosity, creating continuous pores that follow the intersections of the layers along the growth direction [7].

Therefore, the objective of the following study was to assess the impact of applying the optimal scanning strategy, typical of LPBF technologies, on the key properties of components produced using a different AM method, namely MEX.

Hence, the current research focused on the evaluation of the influence of two different deposition strategies over MEX-built elements, considering tensile and hardness properties as well as defect distribution (porosity). The results were analysed statistically.

The evaluations were performed on AISI 316L specimens. Stainless steel alloys are well known for their low cost and good mechanical properties, heat resistance and biocompatibility [232,233]. This material is primarily used in the fabrication of surgical instrumentation. Though, it is relevant to note that its applications extend to orthopaedic implants and fixators, artificial heart valves, syringe needles and numerous other medical tools too [234].

The research is summarised below in the form of a graphical abstract (Figure 66), which was presented and awarded during the 2024 ESAFORM conference, held in Toulouse, France.

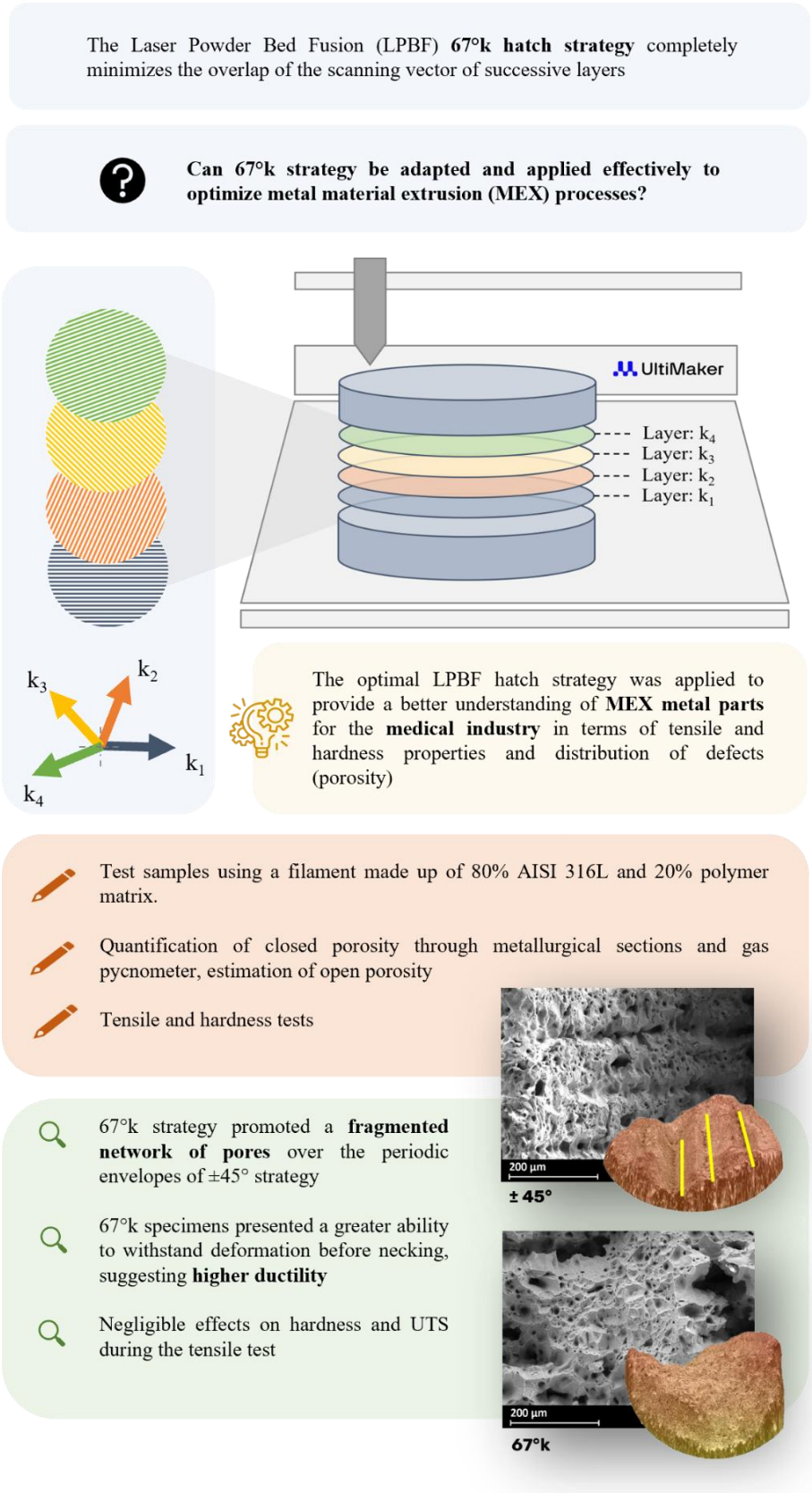

Figure 66. Modified graphical abstract of the study: Preliminary assessment of material extrusion (MEX) for medical applications: The effect of hatch angle. Sala, F.; Nani, L.; Quarto, M.; D'Urso, G. (2024).

5.1.1 Methodology

Sample preparation

The test samples were manufactured by means of an Ultimaker S5 MEX technology, using a filament with a diameter of 2.85 mm provided by BASF Ultrafuse 316L. The filament consisted of 80% austenitic stainless steel (AISI 316L) and 20% polymer binder (polyoxymethylene (POM)), which acted as thermoplastic matrix, enabling processing through MEX technology. A print core CC 0.6 equipped with a hardened steel nozzle was employed to extrude the filament.

The geometry of the specimen was developed in compliance with the international standards related to the mechanical tests to be performed, as further described in the following sections.

Then, the sample geometries were uploaded into the slicing software Ultimaker Cura, where the processing parameters (Table 38) were configured according to optimisation criteria, with respect to density and shrinkage, as identified in prior studies [235]. Print speed was slightly increased to minimise delamination in the initial deposited layers, a phenomenon associated with the geometry of the tensile specimens.

	Layer height	Infill density	Infill pattern	Nozzle temperature	Build plate temperature	Print Speed
± 45°	0.1 mm	100%	± 45°	240°	100°	40 mm/s
67° k	0.1 mm	100%	67° k	240°	100°	40 mm/s

Table 38. Selected process parameters for the MEX-built specimens.

The specimens were fabricated following a Design of Experiment (DOE) with a single factor, aimed at investigating the effect of two distinct deposition approaches. Specifically, the hatch angle, or the angle defined between the infill lines of one layer and the subsequent one, was set at two different configurations: ± 45° and 67°k, where k denotes the layer number. Figure 67 provides a layer-by-layer schematic comparison of the two deposition strategies for the cross-section of the MEX-built specimens.

As anticipated, in LPBF processes, the 67°k scanning strategy is known for completely minimising the overlap of the scanning vector of successive layers. With the adoption of the LPBF optimal strategy in MEX processes, the variation in the deposition strategy was achieved by modifying the infill pattern value during the configuration of the process settings.

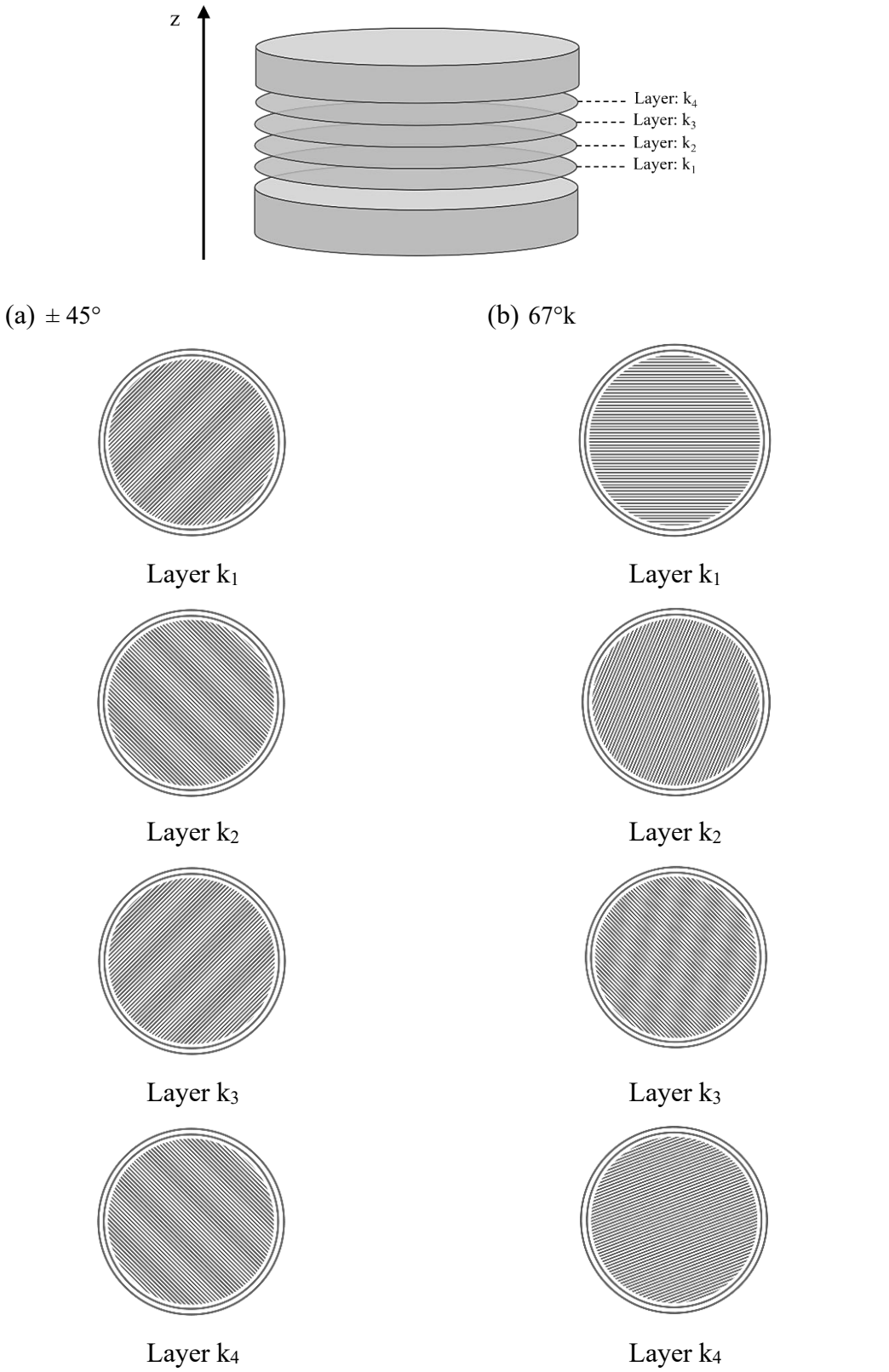

Figure 67. Layer-by-layer schematic representation of the different deposition strategies. (a) Variation of the hatch angle in four subsequent layers (+45° odd layers, -45° even layers) in ± 45° cylindrical specimen. (b) Constant variation of the hatch angle (steady rotation of 67°) in the 67°k cylindrical specimen.

After the 3D printing stage, the green parts underwent debinding and sintering processes, leading first to the formation of the brown part and eventually to the fully dense metal component. During the debinding phase, the majority of the polymeric component is removed from the green part through a combined catalytic and thermal process carried out at 120°C with HNO_3 (98% concentration). During the sintering cycle, which is performed in an argon atmosphere, the brown part is subjected to three thermal ramps (Table 39). All post-processing treatments were performed by an external service provider.

Two sets of samples were produced and their properties were compared with reference data reported in literature, as well as with values provided in technical datasheets for AISI 316L specimens produced using LPBF powder-based technologies [236–240].

	Initial temperature	Final temperature	Ramp rate	Holding time
1st Ramp	Room temperature	600°C	5°C/min	1 h
2nd Ramp	600°C	1380°C	5°C/min	3 h
3rd Ramp	1380°C	Room temperature	Furnace cooling	

Table 39. Thermal ramps of the sintering cycle.

Porosity analysis

Compared to LPBF deposition processes, MEX generates structures characterised by reduced bulk density due to the presence of defects (i.e., open and closed porosity). In the present study, defect analysis was performed on cylindrical specimens with dimension 15 mm diameter and 5 mm height, in three separate stages.

First, porosity was evaluated on cross-section taken perpendicular to the deposition lines (Figure 68). The surfaces were metallographically prepared and polished to a 1 µm finish using a diamond suspension. The prepared sample sections were examined using a Keyence VHX-7100 digital-optical microscope and the porosity content was quantified through image analysis, ImageJ software.

The metallurgical sections provide only an indication of the porosity distribution, which is limited to the specific cross-section being examined. Since MEX processes, unlike LPBF, tend to generate interconnected defect networks across successive layers rather than isolated spherical pores, additional investigations are therefore necessary to achieve a more comprehensive characterisation. For this reason, to adequately quantify the amount of closed porosity on the whole specimen, a gas pycnometer was used. In particular, the pycnometer estimated the average value of the volume occupied by the printed part, namely the volume of the material, and the close porosity; then, knowing the density of the material, it is possible to estimate the closed porosity as reported in Eq.1 and Eq.2.

$$\delta_{\text{bulk}} = \frac{weight}{V_{pycnometer}} \quad \text{Eq.1}$$

$$cp = \frac{\delta_{material} - \delta_{bulk}}{\delta material} \quad \text{Eq.2}$$

Where δ_{bulk} and $\delta_{material}$ represent the mass density of the printed part and the material used for the printing process (8 g/cm^3) respectively; $weight$ corresponds to the mass of the printed part, $V_{pycnometer}$ is the volume of the part measured using the gas pycnometer and cp denotes the fraction of closed porosity.

In a subsequent step, the open porosity was estimated using the total volume calculated from the sample's external dimensions. In particular, the amount of open porosity (*op*) was computed as the difference between the overall volume and the volume defined by the gas pycnometer.

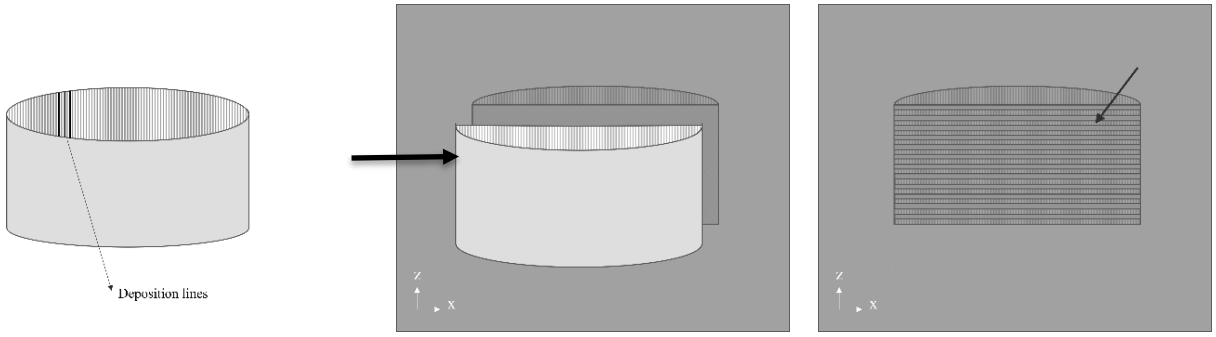

Figure 68. Schematic representation of the considered plane (cross-section parallel to the growth direction of the specimen) for the analysis of porosity.

Tensile test

According to ASTM F3122-14 [241], the procedure outlined in the test method UNI EN ISO 6892-1:2020 [193] defines how to conduct a tensile test on metal materials and determine mechanical properties, including elongation at break (A%) and ultimate tensile strengths (UTS). The procedure was performed on specimens characterised by a circular section, with a calibrated length of 30 mm and a diameter of 6 mm. Tensile tests were conducted using a Galdabini testing machine with a 50kN load cell. The tests were conducted perpendicular to the growth direction of the layers, under deformation control 2.5 x 10^{-4} s^{-1} and a preload of 400N. The procedure was carried out on tensile specimens and repeated four times for each variation of the deposition pattern.

Hardness test

ASTM F3122-14 specifies UNI EN ISO 6507-1:2018 [242] as a standard for the Vickers hardness (HV) of additive-manufactured parts. The top surface of cylindrical specimen was polished up to 1µm with diamond suspension. A 5x5 grid was drawn on the internal section, obtaining 25 uniformly spaced indentations. The procedure involved applying a 1kgf load for 15s. The tests were performed one time per each deposition pattern variation.

5.1.2 Results and discussion

Porosity analysis

The porosity analysis based on metallographic sections is presented in Figure 69. Image analysis enabled the identification of pore areas, revealing a porosity of 1.99% for ±45° infill pattern and 1.47% for 67°k. For both deposition strategies, the measured porosity percentage values were lower compared to those reported in the literature. This result may be attributed to the specificity of the measurement, as the values reflect a single cross-section and may not directly represent the overall specimen.

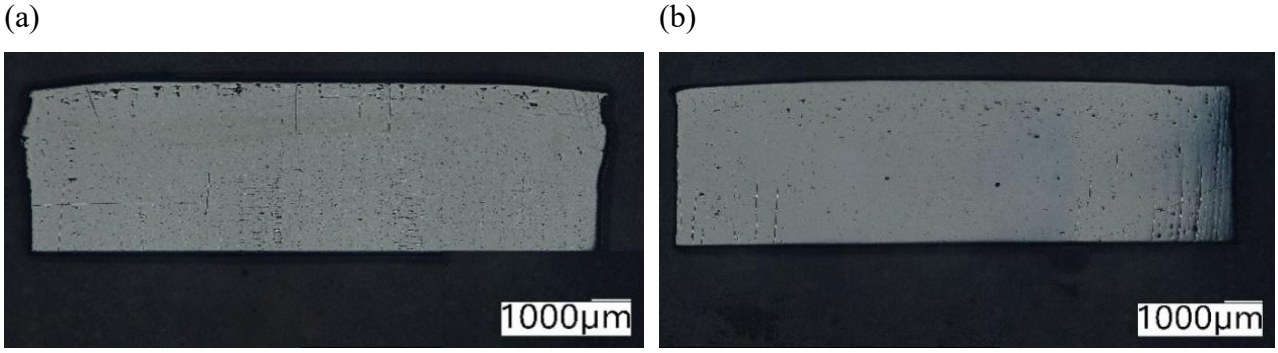

Figure 69. Metallurgical section for the two deposition strategies. (a) ±45° Infill pattern and (b) 67°k infill pattern.

The image investigation was complemented by the pycnometer analysis, which provided the aggregate value of closed porosity. The information related to the extension of the porosity along the depth dimension was captured. The pycnometer confirmed the adherence of the obtained porosity values to the conservative literature results. Furthermore, comparing the volume estimated by the gas pycnometer and the nominal part volume, the percentage of open porosity were estimated too.

The results showed that samples characterised by ± 45° infill pattern had closed porosity values of 1.29% and open porosity of 12.95%; whilst 67°k infill pattern had closed porosity values of 2.79%

and open porosity of 3.70%. Although shifting from the ± 45° deposition strategy to the 67°k indicated an increase in closed porosity, there was a corresponding decrease in open porosity, suggesting that the 67°k pattern is more effective at interrupting the continuity of the porosity network. Still, the porosity values recorded in MEX-built specimens are not comparable to the LPBF ones, capable of providing densities greater than 99%.

Tensile test

To assess the impact of the infill pattern on mechanical strength, a statistical analysis was conducted on the outcomes of tensile tests (Table 40).

Infill pattern	Repetition	A%	UTS
± 45°	1	50.5%	479 MPa
	2	47.2%	433 MPa
	3	48.4%	393 MPa
	4	40.1%	453 MPa
67°k	1	54.3%	471 MPa
	2	61.9%	439 MPa
	1	50.5%	479 MPa
	2	47.2%	433 MPa

Table 40. Mechanical properties of tensile specimens.

The Analysis of Variance (ANOVA) revealed that the infill pattern influenced elongation (A%), whereas it appeared to have no significant effect on Ultimate Tensile Strength (UTS). Notably, the elongation demonstrated a *p*-value of 0.042, which is below the predetermined confidence level of 5%. Conversely, the UTS exhibited a *p*-value of 0.951, emphasizing the absence of any substantial effect.

As shown in Figure 70, the elongation was higher for 67°k samples, suggesting that samples 3D printed with a 67°k infill pattern may undergo greater deformation before reaching the point of rupture. In other words, this suggested a higher ductile behaviour and greater ability to withstand deformation before necking under stress. This behaviour could be advantageous for applications where material deformability is critical. For example, in medical applications, where the increased ductility may translate into improved mechanical reliability.

Furthermore, the observed result could be correlated with the arrangement of pores, particularly with the breaking of the envelopes caused by the continuous rotation of the pattern 67°k. This finding is corroborated by the fracture surface images in Figure 71, showing distinct pore arrangements depending on the infill pattern. It is evident that in the ± 45° infill pattern, pores are aligned in

columns, indicating preferential paths for crack propagation, whereas in the 67°k pattern, pores are more uniformly distributed across the surface.

(a) (b)

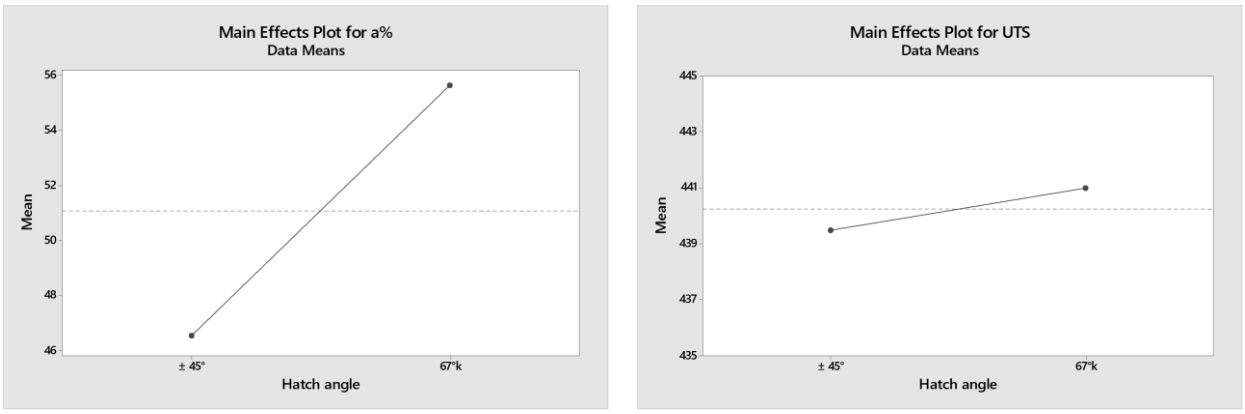

Figure 70. Main effect plot for (a) elongation at break (A%) and (b) UTS.

(a) ± 45° (b) 67°k

Figure 71. Reconstructions of the fracture surfaces via optical microscope. a) ± 45° Tensile specimen. b) 67° k Tensile specimen.

	MEX (± 45°)	MEX (67° k)	LPBF
Elongation at break	46.6 ± 4.5 %	55.6 ± 5.4 %	57 %
UTS	439.5 ± 36 MPa	441.0 ± 30 MPa	Up to 700 MPa

Table 41. Comparison of the main tensile properties measured on MEX and LPBF elements.

Hardness test

In Table 42, the average values and the standard deviation of the HV_{1000} for both infill patterns were reported. It is possible to note that there is not an appreciable difference in the values, this is probably related to the dimension of the indentation and the part structure. Specifically, the indentation is typically made on a single material strand, making it unlikely to involve two adjacent strands. As a

result, the measured hardness closely reflects that of the monolithic material and exhibits a relatively low standard deviation across the entire surface.

	MEX (± 45°)	MEX (67° k)	LPBF
HV_{1000} / HV	124±6 HV	131±3 HV	230 HV

Table 42. Comparison of the average hardness values measured on MEX and LPBF elements.

5.1.3 Conclusions

Based on the optimised strategy reported in literature for LPBF process, the present work investigated whether, with the appropriate adaptations, the concept of an infill pattern characterised by a continuous rotation of the layers improves the structure of the parts 3D printed with metal-MEX technology. A 67° rotation per layer was compared with the ±45° deposition strategy, which remains the most used approach in MEX processes.

Cylindrical and tensile samples were manufactured by varying only the deposition strategy through the infill pattern. The main differences in terms of porosity, tensile strength and hardness were investigated to assess the effectiveness of the LPBF-inspired scanning strategy (67°k). The tested hypothesis consisted in the possibility of interrupting the porosity envelopes induced by the ±45° strategy.

The relevant outcomes of the present research are summarised as follow:

- The investigated deposition strategies produced specimens with similar overall porosity; however, the structure of the porous network was strongly affected by the deposition pattern. The ±45° strategy produced a periodic and semi-continuous network, while 67°k strategy led to a more fragmented pore distribution.
- The differences in the morphology of the porous network had negligible effects on UTS and hardness.
- A significant effect was observed on elongation at break, where 67°k specimens withstood greater deformation before rupture. This suggested a higher ductility derived from the 67°k deposition strategy and, thus, beneficial results for applications, such as the medical ones, requiring greater predictability of fracture behaviour. Additional investigations are required to confirm the hypothesis.

General conclusions

The present doctoral research investigates Additive Manufacturing (AM) processes through the analysis of their implementation in the healthcare sector.

The objective of the research is pursued by focusing on a promising AM technology, Material Extrusion (MEX), which is based on the principle of heating and selectively depositing material through a nozzle. This system, originally developed for the extrusion of polymeric materials, can process any material capable of continuously flowing through a nozzle and subsequently solidifying, including metal materials. Owing to the flexibility and versatility of this technology, the study examines both polymeric and metal medical components.

The main conclusions arisen from each section of this work are presented below:

- The feasibility of producing tailor-made orthoses through an innovative methodology based on Reverse Engineering (RE) and Additive Manufacturing (AM) is confirmed. The implementation of the proposed methodology in orthosis clinical practice demonstrates considerable potential. Multidisciplinary research has proven essential to deepen the understanding of the factors that facilitate its effective and seamless integration into existing healthcare workflows.
    - Overall, MEX emerges as a highly functional and innovative manufacturing system for medical devices. Despite its considerable potential in orthotic applications, the successful implementation of MEX requires a well-structured framework encompassing all supporting activities within the 3D printing value chain. In particular, the conducted research highlights that Reverse Engineering (RE) processes and related technologies require significant attention to ensure the effective and comprehensive exploitation of Additive Manufacturing (AM) capabilities.
    - One of the key challenges in implementing MEX for customised orthosis production lies in the requirement for specialised engineering expertise in the proper acquisition, processing and modelling of patient data. Regarding data acquisition, healthcare professionals might rely on a wide range of professional technologies for data acquisition, beyond those typically available in hospital settings. Among the key criteria for technology selection are accuracy, acquisition speed, and the contactless nature of the system. Based on these factors, this research identifies laser scanning as an optimal solution. The most critical limitations, however, concern data processing and modelling. The current digital workflow requires advanced CAD expertise and

significant design time, restricting accessibility in clinical practice. To address this issue, the present work proposes and develops a dedicated and unique approach, supported by an intuitive Graphical User Interface (GUI), that integrates a series of semi-automatic commands to effortlessly, easily and rapidly transform anatomic scans into digital orthoses. Moreover, the approach extremely cuts down the modelling time. The proposed software also demonstrates high versatility, enabling the generation of medical device models for anatomical regions beyond those initially targeted. Overall, the approach contributes to the democratisation of engineering technologies in healthcare, promoting broader and more autonomous use by clinical professionals.

- The conducted studies underline the potential of the proposed methodology as a cost-effective solution for the production of customised orthotic devices. The economic viability of the approach is rigorously evaluated through the conceptualisation of a cost model, that is subsequently applied to an initial prototype of MEX-based upper limb orthosis made of ABS. The resulting cost is remarkably low compared to that of conventional customised orthoses. Within the cost structure, labour emerges as the predominant component, accounting for 78% of the total, followed by material costs at 18%. Costs associated with Reverse Engineering (RE) and Additive Manufacturing (AM) systems are minimal, and ongoing technological advancements in these domains are expected to further diminish their economic impact. These findings corroborate the hypothesis that the challenges associated with RE and AM adoption lie in a realm that is distinct from the economic one.
- In addition to the cost assessment, the research includes analyses of production times. Despite the current and projected technological advancements in MEX systems, the printing phase is identified as the most critical and time-intensive stage of the overall process. It may give rise to concerns regarding the adoption of AM technology in the clinical practice. Hence, it is essential to recognise that certain therapies may not benefit substantially from AM when rapid production is a priority. Identifying and prioritising the treatments for which the proposed methodology is both suitable and competitive, such as non-urgent or elective interventions, is therefore crucial. Beyond this, the challenges posed by extended printing durations have guided the research, highlighting the incorporation of production time as a key variable in the optimisation of MEX printing parameters.
- The mechanical performances of the customised orthoses fabricated with the proposed methodology are validated via technical simulation based on FEM. The boundary and

loading conditions are faithfully replicated to simulate the performance of the orthotic device, including scenarios such as accidental impacts or typical joint movements during the rehabilitation phase. In addition to the evaluations of material strength, it is essential to assess shape distortions as well. Indeed, although the safety factors of the orthotic designs are deemed adequate, it is crucial to ensure that shape distortions do not negatively interfere with the ability of the medical devices to maintain proper joint alignment. In general, the adopted methodology proves its ability to produce resilient and high-performance structures, showcasing its effectiveness for advanced engineering and medical applications.

- The robustness of the proposed methodology, defined for producing MEX-based customised upper limb orthoses, is systematically verified. The procedure successfully manages the variability resulting from the development of orthoses for three anatomical regions differing in size, shape and level of detail. The manufacturing workflow adapts seamlessly to the production of wrist, hand, and finger orthoses, requiring only minimal adjustments to achieve optimal results.
- The studies seek to promote the integration of the innovative methodology into clinical practice by designing and producing a series of customised orthoses, optimised in terms of lightness, strength, comfort, availability and affordability too. This resulted in a set of orthoses, with varying features, including thicknesses (2-4 mm) and manufacturing materials (ABS, nylon, PLA, PC, PA6-GF25, PA6-CF20). Beyond producing individual devices, the work establishes a robust framework that enables healthcare providers to make informed, patient-specific decisions, effectively bridging engineering innovation and clinical application.
- Lastly, the document also investigates the advanced customisation of orthotic devices through the study of weight reduction strategies. These approaches include the creation of hole patterns as well as more sophisticated methodologies, such as Topological Optimisation (TO). Reducing the weight of orthoses is highly valued by both healthcare professionals and patients, as it enhances comfort while maintaining, if properly designed, the required mechanical strength and durability. In this context, feasibility, intended as the ability of realising the device and the simplicity with which medical operators can carry out its fabrication, represents a fundamental aspect. Whilst the implementation of basic patterns of ventilation hole patterns are successfully automated in the developed software program (GUI), advanced and most promising modelling techniques, like TO, remain challenging. Moreover, in this latter case, the

need for accounting manufacturing aspects during the weight reduction activity gains prominence. Specifically, optimising process parameters (i.e., build orientation, infill density, pattern, layer thickness, wall thickness, and support material strategies) is essential to ensure efficient fabrication of orthoses with complex geometries, articulated holes, and minimal thicknesses.

- Ultimately, the present research brings more clarity to the feasibility of implementing metal MEX technology in medical device manufacturing, offering a powerful alternative to the most widely adopted metal AM technologies, namely the PBF and DED methods. Hence, the conducted work expands the understanding of metal MEX by studying and optimising its printing parameters and providing a deeper comprehension of the mechanical and structural behaviour of metal MEX components.
    - Compared to components produced using PBF and DED technologies, MEX-based elements exhibit lower dimensional accuracy and mechanical strength, primarily due to a reduced density in the final metal structure. This limitation poses a significant challenge to the implementation of metal MEX manufacturing, especially in high-value industrial applications such as the medical sector.
    - In the current research, the topic is addressed by studying and optimising a specific MEX printing parameter, known as raster angle (or hatch angle), for AISI 316L specimens. The selected alloy is well-known for its biocompatibility and excellent corrosion resistance, especially in biological environments. The research demonstrated that the hatch strategy commonly employed in LPBF processes (67°k) can be successfully adapted and applied to metal MEX processes too, prompting a uniform, fragmented porous network and disrupting the periodic porosity observed with the default ±45° strategy. Furthermore, the 67°k strategy significantly improved the elongation at break, indicating a higher ductile behaviour and greater ability to withstand deformation before necking. These findings improve the predictability of the fracture behaviour of MEX component, a critical advantage for medical applications.
    - Current research is focusing on the exploration of titanium-based MEX components. Titanium owns an excellent biocompatibility, combined with great mechanical properties, and the use of MEX technology might potentially simplify and economise the production process of Ti components. Currently, the experiments focus on finding the optimum process parameters for the production, via extrusion, of titanium-filled

filament (commercially pure titanium particles immersed in a polymer binder matrix), and processability, via 3D printing, of green parts.

Beyond the developments in polymer and metal applications of MEX technology, ongoing research is extending to other AM technologies, in particular Laser Powder Bed Fusion (LPBF), which employs a laser to selectively melt or fuse metal powders.

In collaboration with the University of Birmingham, this research is centred on the development of customised metal implants for the treatment of sagittal craniosynostosis, a craniofacial developmental anomaly that affects infants. Generally, this condition is attributed to the premature fusion of the sagittal suture, leading to abnormal cranial growth characterised by an elongation of the skull in the anterior-posterior direction and a simultaneous reduction in its bilateral dimensions. The current conventional treatment involves a two-stage surgical approach: initially springs are implanted to maintain patency and, then, during a second surgery, springs are removed upon completion of the treatment. The focus of the present research consists in the development of novel Ti-6Al-4V implants that can be permanently implanted within the cranial structure, thereby obviating the need for a subsequent removal surgery.

Multiple implant designs have been conceptualised and printed, from basic honeycomb structures to more sophisticated assembly structures. The design optimisation process is being guided by the stringent mechanical criteria, particularly the requirement for a great transverse expansion under a limited longitudinal load. Previous investigations have determined that an optimal Poisson's ratio for these implants is approximately 3.

To conclude, the numerous emerging research directions indicate that the medical sector remains one of the most fertile fields for innovation in 3D printing. The versatility and adaptability of AM technologies offer unprecedented opportunities to tackle challenges in medical device manufacturing, enabling customised designs and enhanced mechanical and material performance. As demonstrated in the present work, even the simplest of the AM technology was able to address diverse medical applications, yielding valuable insights. As the advantages of these technologies become increasingly evident, it is equally critical to develop supporting systems and workflows to ensure their seamless integration into clinical practice. Without such a holistic approach, the full potential of AM technologies risks being underutilised, remaining fragmented innovations rather than transformative solutions for modern healthcare. Therefore, it is imperative to pursue continuous research and development to maximise achievable benefits of AM technologies, while fostering their adoption in the industrial and healthcare world.

List of figures

List of tables

References

1. Chattopadhyay, S.; Mahapatra, S.D.; Mandal, N.K. Advancements and Challenges in Additive Manufacturing: A Comprehensive Review. *Eng. Res. Express* **2024**, *6*, doi:10.1088/2631-8695/ad30b1.
2. Gibson, I.; Rosen, D.; Stucker, B. Additive Manufacturing Technologies: 3D Printing, Rapid Prototyping, and Direct Digital Manufacturing, Second Edition. *Addit. Manuf. Technol. 3D Printing, Rapid Prototyping, Direct Digit. Manuf. Second Ed.* **2015**, 1–498, doi:10.1007/978-1-4939-2113-3/COVER.
3. ICTC Distribution of Sales Revenue of the Additive Manufacturing Market Worldwide in 2019, by Industry 2021.
4. Calignano, F.; Mercurio, V. An Overview of the Impact of Additive Manufacturing on Supply Chain, Reshoring, and Sustainability. *Clean. Logist. Supply Chain* **2023**, *7*, 100103, doi:10.1016/j.clscn.2023.100103.
5. Rouf, S.; Malik, A.; Singh, N.; Raina, A.; Naveed, N.; Siddiqui, M.I.H.; Haq, M.I.U. Additive Manufacturing Technologies: Industrial and Medical Applications. *Sustain. Oper. Comput.* **2022**, *3*, 258–274, doi:10.1016/j.susoc.2022.05.001.
6. Industrytoday Global 3D Printing Products and Services Market Size from 2020 to 2026 (in Billion U.S. Dollars) 2021.
7. In Statista Projected Global Additive Manufacturing Market Growth between 2020 and 2026 2021.
8. Zhou, L.; Miller, J.; Vezza, J.; Mayster, M.; Raffay, M.; Justice, Q.; Al Tamimi, Z.; Hansotte, G.; Sunkara, L.D.. Additive Manufacturing: A Comprehensive Review. *Sensors* **2024**, *24*, doi:https://doi.org/10.3390/s24092668.
9. Tu, J.; Yeoh, G.-H.; Liu, C. CFD Solution Analysis: Essentials. *Comput. Fluid Dyn.* **2018**, 211–253, doi:10.1016/B978-0-08-101127-0.00006-4.
10. Patil, H.; Jeyakarthikeyan, P. V. Mesh Convergence Study and Estimation of Discretization Error of Hub in Clutch Disc with Integration of ANSYS. *IOP Conf. Ser. Mater. Sci. Eng.* **2018**, *402*, doi:10.1088/1757-899X/402/1/012065.

11. Birosz, M.T.; Safranyik, F.; Andó, M. Build Orientation Optimization of Additive Manufactured Parts for Better Mechanical Performance by Utilizing the Principal Stress Directions. *J. Manuf. Process.* **2022**, *84*, 1094–1102, doi:10.1016/j.jmapro.2022.10.038.

12. Das, P.; Mhapsekar, K.; Chowdhury, S.; Samant, R.; Anand, S. Selection of Build Orientation for Optimal Support Structures and Minimum Part Errors in Additive Manufacturing. *Comput. Aided. Des. Appl.* **2017**, *14*, 1–13, doi:10.1080/16864360.2017.1308074.

13. Tavares, T.M.; Ganga, G.M.D.; Godinho Filho, M.; Rodrigues, V.P. The Benefits and Barriers of Additive Manufacturing for Circular Economy: A Framework Proposal. *Sustain. Prod. Consum.* **2023**, *37*, 369–388, doi:10.1016/J.SPC.2023.03.006.

14. C. B. Carolo, L.; Cooper O., R.E. A Review on the Influence of Process Variables on the Surface Roughness of Ti-6Al-4V by Electron Beam Powder Bed Fusion. *Addit. Manuf.* **2022**, *59*, 103103, doi:10.1016/J.ADDMA.2022.103103.

15. Brooks, H.L.; Rennie, A.E.W.; Abram, T.N.; McGovern, J.; Caron, F. Variable Fused Deposition Modelling - Analysis of Benefits, Concept Design and Tool Path Generation. *Innov. Dev. Virtual Phys. Prototyp. - Proc. 5th Int. Conf. Adv. Res. Rapid Prototyp.* **2012**, 511–517, doi:10.1201/b11341-83.

16. Delli, U.; Chang, S. Automated Process Monitoring in 3D Printing Using Supervised Machine Learning. *Procedia Manuf.* **2018**, *26*, 865–870, doi:10.1016/j.promfg.2018.07.111.

17. Kumar, V.P.; Jebaraj, A.V. Comprehensive Review on Residual Stress Control Strategies in Laser - Based Powder Bed Fusion Process – Challenges. *Lasers Manuf. Mater. Process.* **2023**, 400–442, doi:10.1007/s40516-023-00217-6.

18. Li, C.; Liu, J.F.; Fang, X.Y.; Guo, Y.B. Efficient Predictive Model of Part Distortion and Residual Stress in Selective Laser Melting. *Addit. Manuf.* **2017**, *17*, 157–168, doi:10.1016/J.ADDMA.2017.08.014.

19. Jiménez, M.; Romero, L.; Domínguez, I.A.; Espinosa, M.D.M.; Domínguez, M. Additive Manufacturing Technologies: An Overview about 3D Printing Methods and Future Prospects. *Complexity* **2019**, *2019*, 9656938, doi:10.1155/2019/9656938.

20. International Organization for Standardization. UNI EN ISO/ASTM 52900:2022 - Additive Manufacturing - Principi Generali - Terminologia 2022.

21. Bártolo, P.J. *Stereolithography: Materials, Processes and Applications*; Springer Science & Business Media, Ed.; 2011;

22. Pagac, M.; Hajnys, J.; Ma, Q.P.; Jancar, L.; Jansa, J.; Stefek, P.; Mesicek, J. A Review of Vat Photopolymerization Technology: Materials, Applications, Challenges, and Future Trends of 3d Printing. *Polymers (Basel).* **2021**, *13*, 1–20, doi:10.3390/polym13040598.

23. Chua, C.K.; Leong, K.F.; Lim, C.S. (Chu S. Rapid Prototyping: Principles and Applications. **2010**, 512.

24. Taormina, G.; Sciancalepore, C.; Messori, M.; Bondioli, F. 3D Printing Processes for Photocurable Polymeric Materials: Technologies, Materials, and Future Trends. *J. Appl. Biomater. Funct. Mater.* **2018**, *16*, 151–160, doi:10.1177/2280800018764770.

25. Tumbleston, J.R.; Shirvanyants, D.; Ermoshkin, N.; Janusziewicz, R.; Johnson, A.R.; Kelly, D.; Chen, K.; Pinschmidt, R.; Rolland, J.P.; Ermoshkin, A.; et al. Continuous Liquid Interface Production of 3D Objects. *Science (80-.).* **2015**, *347*, 1349–1352.

26. Gonzalez-Gutierrez, J.; Cano, S.; Schuschnigg, S.; Kukla, C.; Sapkota, J.; Holzer, C. Additive Manufacturing of Metallic and Ceramic Components by the Material Extrusion of Highly-Filled Polymers: A Review and Future Perspectives. *Materials (Basel).* **2018**, *11*, doi:10.3390/ma11050840.

27. Gleadall, A.; Visscher, D.; Yang, J.; Thomas, D.; Segal, J. Review of Additive Manufactured Tissue Engineering Scaffolds: Relationship between Geometry and Performance. *Burn. Trauma* **2018**, *6*, 1–16, doi:10.1186/s41038-018-0121-4.

28. Popescu, D.; Zapciu, A.; Amza, C.; Baciu, F.; Marinescu, R. FDM Process Parameters Influence over the Mechanical Properties of Polymer Specimens: A Review. *Polym. Test.* **2018**, *69*, 157–166, doi:10.1016/j.polymertesting.2018.05.020.

29. Turner, B.N.; Strong, R.; Gold, S.A. A Review of Melt Extrusion Additive Manufacturing Processes: I. Process Design and Modeling. *Rapid Prototyp. J.* **2014**, *20*, 192–204, doi:10.1108/RPJ-01-2013-0012.

30. Singh, S.; Singh, G.; Prakash, C.; Ramakrishna, S. Current Status and Future Directions of Fused Filament Fabrication. *J. Manuf. Process.* **2020**, *55*, 288–306, doi:10.1016/j.jmapro.2020.04.049.

31. Suwanpreecha, C.; Manonukul, A. A Review on Material Extrusion Additive Manufacturing of Metal and How It Compares with Metal Injection Moulding. *Metals (Basel).* **2022**, *12*, doi:10.3390/met12030429.

32. Armstrong, M.; Mehrabi, H.; Naveed, N. An Overview of Modern Metal Additive

Manufacturing Technology. *J. Manuf. Process.* **2022**, *84*, 1001–1029, doi:10.1016/j.jmapro.2022.10.060.

33. Quarto, M.; Carminati, M.; D'Urso, G.; Giardini, C.; Maccarini, G. Processability of Metal-Filament through Polymer FDM Machine. *ESAFORM 2021 - 24th Int. Conf. Mater. Form.* **2021**, *13*, 1–11, doi:10.25518/esaform21.2114.

34. German, R. Thinking about Metal Binder Jetting or FFF ? *Met. AM* **2019**, *5*, 127–139.

35. Gibson, I.; Rosen, D.; Stucker, B. Powder Bed Fusion Processes. *Addit. Manuf. Technol.* **2015**, 107–145, doi:10.1007/978-1-4939-2113-3_5.

36. Dejene, N.D.; Lemu, H.G. Current Status and Challenges of Powder Bed Fusion-Based Metal Additive Manufacturing: Literature Review. *Metals (Basel).* **2023**, *13*, doi:10.3390/met13020424.

37. Mower, T.M.; Long, M.J. Mechanical Behavior of Additive Manufactured, Powder-Bed Laser-Fused Materials. *Mater. Sci. Eng. A* **2016**, *651*, 198–213, doi:10.1016/j.msea.2015.10.068.

38. Ladani, L.; Sadeghilaridjani, M. Review of Powder Bed Fusion Additive Manufacturing for Metals. *Metals (Basel).* **2021**, *11*, doi:10.3390/met11091391.

39. Spierings, A.; Herres NTB Buchs, N.; Levy, G. Influence of the Particle Size Distribution on Surface Quality and Mechanical Properties in AM Steel Parts., doi:10.1108/13552541111124770.

40. Pfaff, A.; Jäcklein, M.; Schlager, M.; Harwick, W.; Hoschke, K.; Balle, F. An Empirical Approach for the Development of Process Parameters for Laser Powder Bed Fusion. *Mater. 2020, Vol. 13, Page 5400* **2020**, *13*, 5400, doi:10.3390/MA13235400.

41. Nudelis, N.; Mayr, P. A Novel Classification Method for Pores in Laser Powder Bed Fusion. *Metals (Basel).* **2021**, *11*, doi:10.3390/MET11121912.

42. Vukkum, V.B.; Gupta, R.K. Review on Corrosion Performance of Laser Powder-Bed Fusion Printed 316L Stainless Steel: Effect of Processing Parameters, Manufacturing Defects, Post-Processing, Feedstock, and Microstructure. *Mater. Des.* **2022**, *221*, 110874, doi:10.1016/J.MATDES.2022.110874.

43. Lv, X.; Ye, F.; Cheng, L.; Fan, S.; Liu, Y. Binder Jetting of Ceramics: Powders, Binders, Printing Parameters, Equipment, and Post-Treatment. *Ceram. Int.* **2019**, *45*, 12609–12624, doi:10.1016/J.CERAMINT.2019.04.012.

44. Mirzaali, M.J.; Shahriari, N.; Zhou, J.; Zadpoor, A.A. *Quality of AM Implants in Biomedical Application*; Elsevier, 2022; ISBN 9780323886642.

45. Mostafaei, A.; Elliott, A.M.; Barnes, J.E.; Li, F.; Tan, W.; Cramer, C.L.; Nandwana, P.; Chmielus, M. Progress in Materials Science Binder Jet 3D Printing — Process Parameters , Materials , Properties ,. *Prog. Mater. Sci.* **2021**, *119*, 100707.

46. Ziaee, M.; Crane, N.B. Binder Jetting: A Review of Process, Materials, and Methods. *Addit. Manuf.* **2019**, *28*, 781–801, doi:10.1016/j.addma.2019.05.031.

47. Zhang, Y.; Jarosinski, W.; Jung, Y.G.; Zhang, J. Additive Manufacturing Processes and Equipment. *Addit. Manuf. Mater. Process. Quantif. Appl.* **2018**, 39–51, doi:10.1016/B978-0-12-812155-9.00002-5.

48. Elkaseer, A.; Chen, K.J.; Janhsen, J.C.; Refle, O.; Hagenmeyer, V.; Scholz, S.G. Material Jetting for Advanced Applications: A State-of-the-Art Review, Gaps and Future Directions. *Addit. Manuf.* **2022**, *60*, 103270, doi:10.1016/j.addma.2022.103270.

49. Gülcan, O.; Günaydın, K.; Tamer, A. The State of the Art of Material Jetting—a Critical Review. *Polymers (Basel).* **2021**, *13*, doi:10.3390/polym13162829.

50. Högström, P.-A.; Karlsson, S.; Gedde, U.W. Effect of Aging on the Mechanical Properties of UV Curable Optical Fiber Coatings. *Int. J. Polym. Mater. Polym. Biomater.* **2000**, *46*, 403–421, doi:10.1080/00914030008033884.

51. Kumar, A.; Dixit, A.R.; Sreenivasa, S. Mechanical Properties of Additively Manufactured Polymeric Composites Using Sheet Lamination Technique and Fused Deposition Modeling: A Review. *Polym. Adv. Technol.* **2024**, *35*, doi:10.1002/pat.6396.

52. Pattnaik, A.; Sanket, A.S.; Pradhan, S.; Sahoo, R.; Das, S.; Pany, S.; Douglas, T.E.L.; Dandela, R.; Liu, Q.; Rajadas, J.; et al. Designing of Gradient Scaffolds and Their Applications in Tissue Regeneration. *Biomaterials* **2023**, *296*, 122078, doi:10.1016/j.biomaterials.2023.122078.

53. Pirozzi, M.A.; Jacob, D.; Pálsson, T.; Gargiulo, P.; Helgason, T.; Jónsson, H. State of the Art in 3D Printing. *Handb. Surg. Plan. 3D Print. Appl. Integr. New Dir.* **2023**, 3–36, doi:10.1016/B978-0-323-90850-4.00014-4.

54. Badoniya, P.; Srivastava, M.; Jain, P.K.; Rathee, S. *A State-of-the-Art Review on Metal Additive Manufacturing: Milestones, Trends, Challenges and Perspectives*; Springer Berlin Heidelberg, 2024; Vol. 46; ISBN 0123456789.

55. Saboori, A.; Aversa, A.; Marchese, G.; Biamino, S.; Lombardi, M.; Fino, P. Application of

Directed Energy Deposition-Based Additive Manufacturing in Repair. *Appl. Sci.* **2019**, *9*, doi:10.3390/app9163316.

56. Ahn, D.G. *Directed Energy Deposition (DED) Process: State of the Art*; Korean Society for Precision Engineering, 2021; Vol. 8; ISBN 4068402000.

57. Svetlizky, D.; Das, M.; Zheng, B.; Vyatskikh, A.L.; Bose, S.; Bandyopadhyay, A.; Schoenung, J.M.; Lavernia, E.J.; Eliaz, N. Directed Energy Deposition (DED) Additive Manufacturing: Physical Characteristics, Defects, Challenges and Applications. *Mater. Today* **2021**, *49*, 271–295, doi:10.1016/j.mattod.2021.03.020.

58. Ji, W.; Zhou, R.; Vivegananthan, P.; See Wu, M.; Gao, H.; Zhou, K. Recent Progress in Gradient-Structured Metals and Alloys. *Prog. Mater. Sci.* **2023**, *140*, 101194, doi:10.1016/j.pmatsci.2023.101194.

59. Sufaru, I.G.; Macovei, G.; Stoleriu, S.; Martu, M.A.; Luchian, I.; Kappenberg-Nitescu, D.C.; Solomon, S.M. 3D Printed and Bioprinted Membranes and Scaffolds for the Periodontal Tissue Regeneration: A Narrative Review. *Membranes (Basel).* **2022**, *12*, doi:10.3390/membranes12090902.

60. American Society of Mechanical Engineers (ASME) Additive Manufacturing 3d Printing Year in Review 2022, Report of AM Contributions to Medical Field 2022.

61. Salmi, M. Additive Manufacturing Processes in Medical Applications. *Materials (Basel).* **2021**, *14*, 1–16, doi:10.3390/ma14010191.

62. Tuomi, J.; Paloheimo, K.; Björkstrand, R.; Salmi, M.; Paloheimo, M.; Mäkitie, A.A. Medical Applications of Rapid Prototyping - From Applications to Classification. *Innov. Dev. Des. Manuf. - Adv. Res. Virtual Rapid Prototyp.* **2010**, 701–704, doi:10.1201/9780203859476-121.

63. Banks, J. Adding Value in Additive Manufacturing: Researchers in the United Kingdom and Europe Look to 3D Printing for Customization. *IEEE Pulse* **2013**, *4*, 22–26, doi:10.1109/MPUL.2013.2279617.

64. Goh, G.D.; Sing, S.L.; Lim, Y.F.; Thong, J.L.J.; Peh, Z.K.; Mogali, S.R.; Yeong, W.Y. Machine Learning for 3D Printed Multi-Materials Tissue-Mimicking Anatomical Models. *Mater. Des.* **2021**, *211*, 110125, doi:10.1016/j.matdes.2021.110125.

65. Mogali, S.R.; Yeong, W.Y.; Tan, H.K.J.; Tan, G.J.S.; Abrahams, P.H.; Zary, N.; Low-Beer, N.; Ferenczi, M.A. Evaluation by Medical Students of the Educational Value of Multi-Material and Multi-Colored Three-Dimensional Printed Models of the Upper Limb for Anatomical

Education. *Anat. Sci. Educ.* **2018**, *11*, 54–64, doi:10.1002/ASE.1703.

66. Żukowska, M.; Rad, M.A.; Górski, F. Additive Manufacturing of 3D Anatomical Models—Review of Processes, Materials and Applications. *Materials (Basel).* **2023**, *16*, doi:10.3390/ma16020880.

67. Zoccali, C.; Luzzati, A.; Di Bella, S.; Attala, D.; Demitri, S.; Orsini, U.; Angelini, A.; Magnan, B.; Moretti, B.; Ruggeri, P.; et al. *La Stampa 3D in Ortopedia: Indicazioni e Limiti 3D Printing Products in Orthopedics: Indications and Limits*; 2017; Vol. 43;.

68. Vecchi, G.; Atzeni, E.; Salmi, A.; Iuliano, L. Prosthesis Customization in Maxillofacial Surgery by Means of Additive Manufacturing. *Procedia CIRP* **2023**, *118*, 781–786, doi:10.1016/j.procir.2023.06.134.

69. Jardini, A.L.L.; Najar Lopes, É.S.S.; Gabriel, L.P.; Calderoni, D.; Maciel Filho, R.; Kharmandayan, P. Bone Reconstruction Surgery of Complex Craniomaxillofacial Deformities Using Additive Manufacturing Customized Implants - a Case Report. *Rapid Prototyp. J.* **2021**, *27*, 872–878, doi:10.1108/RPJ-07-2020-0169.

70. Cortis, G.; Mileti, I.; Nalli, F.; Palermo, E.; Cortese, L. Additive Manufacturing Structural Redesign of Hip Prostheses for Stress-Shielding Reduction and Improved Functionality and Safety. *Mech. Mater.* **2022**, *165*, 104173, doi:10.1016/J.MECHMAT.2021.104173.

71. McNamara, L. Bone as a Material. *Compr. Biomater.* **2011**, 169–186, doi:10.1016/B978-0-08-055294-1.00068-4.

72. Huiskes, R.; Research®, H.W.-… and R.; 1992, undefined The Relationship between Stress Shielding and Bone Resorption around Total Hip Stems and the Effects of Flexible Materials. *journals.lww.com*.

73. Prasad, K.; Bazaka, O.; Chua, M.; Rochford, M.; Fedrick, L.; Spoor, J.; Symes, R.; Tieppo, M.; Collins, C.; Cao, A.; et al. Metallic Biomaterials: Current Challenges and Opportunities. *Materials (Basel).* **2017**, *10*, doi:10.3390/ma10080884.

74. Kosei, F.; Mitsugu, T. Analysis of Principal Stress Projection in Femur with Total Hip Arthroplasty Using CT-Image Based Finite Element Method. *Int. Arch. Orthop. Surg.* **2018**, *1*, doi:10.23937/IAOS-2017/1710003.

75. Bowen, P.K.; Shearier, E.R.; Zhao, S.; Guillory, R.J.; Zhao, F.; Goldman, J.; Drelich, J.W. Biodegradable Metals for Cardiovascular Stents: From Clinical Concerns to Recent Zn-Alloys. *Adv. Healthc. Mater.* **2016**, *5*, 1121–1140, doi:10.1002/ADHM.201501019.

76. Paxton, N.C.; Powell, S.K.; Woodruff, M.A. Biofabrication: The Future of Regenerative Medicine. *Tech. Orthop.* **2016**, *31*, 190–203, doi:10.1097/BTO.0000000000000184.

77. Park, J.W.; Park, H.; Kim, J.H.; Kim, H.M.; Yoo, C.H.; Kang, H.G. Fabrication of a Lattice Structure with Periodic Open Pores through Three-Dimensional Printing for Bone Ingrowth. *Sci. Reports 2022 121* **2022**, *12*, 1–8, doi:10.1038/s41598-022-22292-z.

78. Schwartz, Z.; Lotz, E.M.; Berger, M.B.; Boyan, B.D. The Effect of Substrate Microtopography on Osteointegration of Titanium Implants. *Compr. Biomater. II* **2017**, 429–443, doi:10.1016/B978-0-12-803581-8.10218-8.

79. Zheng, Y.; Han, Q.; Wang, J.; Li, D.; Song, Z.; Yu, J. Promotion of Osseointegration between Implant and Bone Interface by Titanium Alloy Porous Scaffolds Prepared by 3D Printing. *ACS Biomater. Sci. Eng.* **2020**, *6*, 5181–5190, doi:10.1021/ACSBIOMATERIALS.0C00662.

80. Cheng, A.; Humayun, A.; Cohen, D.J.; Boyan, B.D.; Schwartz, Z. Additively Manufactured 3D Porous Ti-6Al-4V Constructs Mimic Trabecular Bone Structure and Regulate Osteoblast Proliferation, Differentiation and Local Factor Production in a Porosity and Surface Roughness Dependent Manner. *Biofabrication* **2014**, *6*, doi:10.1088/1758-5082/6/4/045007.

81. Li, J.P.; Habibovic, P.; van den Doel, M.; Wilson, C.E.; de Wijn, J.R.; van Blitterswijk, C.A.; de Groot, K. Bone Ingrowth in Porous Titanium Implants Produced by 3D Fiber Deposition. *Biomaterials* **2007**, *28*, 2810–2820, doi:10.1016/J.BIOMATERIALS.2007.02.020.

82. Wang, X.; Xu, S.; Zhou, S.; Xu, W.; Leary, M.; Choong, P.; Qian, M.; Brandt, M.; Xie, Y.M. Topological Design and Additive Manufacturing of Porous Metals for Bone Scaffolds and Orthopaedic Implants: A Review. *Biomaterials* **2016**, *83*, 127–141, doi:10.1016/J.BIOMATERIALS.2016.01.012.

83. Li, G.; Wang, L.; Pan, W.; Yang, F.; Jiang, W.; Wu, X.; Kong, X.; Dai, K.; Hao, Y. In Vitro and in Vivo Study of Additive Manufactured Porous Ti6Al4V Scaffolds for Repairing Bone Defects. *Sci. Rep.* **2016**, *6*, 1–11, doi:10.1038/srep34072.

84. Distefano, F.; Pasta, S.; Epasto, G. Titanium Lattice Structures Produced via Additive Manufacturing for a Bone Scaffold: A Review. *J. Funct. Biomater.* **2023**, *14*, doi:10.3390/jfb14030125.

85. Polo-Corrales, L.; Latorre-Esteves, M.; Ramirez-Vick, J.E. Scaffold Design for Bone Regeneration. *J. Nanosci. Nanotechnol.* **2014**, *14*, 15–56, doi:10.1166/JNN.2014.9127.

86. Sing, S.L.; An, J.; Yeong, W.Y.; Wiria, F.E. Laser and Electron-Beam Powder-Bed Additive

Manufacturing of Metallic Implants: A Review on Processes, Materials and Designs. *J. Orthop. Res.* **2016**, *34*, 369–385, doi:10.1002/JOR.23075.

87. Velu, R.; Calais, T.; Jayakumar, A.; Raspall, F. A Comprehensive Review on Bio-Nanomaterials for Medical Implants and Feasibility Studies on Fabrication of Such Implants by Additive Manufacturing Technique. *Mater. 2020, Vol. 13, Page 92* **2019**, *13*, 92, doi:10.3390/MA13010092.

88. Miechowicz, S.; Wojnarowska, W.; Majkut, S.; Trybulec, J.; Pijanka, D.; Piecuch, T.; Sochacki, M.; Kudasik, T. Method of Designing and Manufacturing Craniofacial Soft Tissue Prostheses Using Additive Manufacturing: A Case Study. *Biocybern. Biomed. Eng.* **2021**, *41*, 854–865, doi:10.1016/J.BBE.2021.05.008.

89. Patel, P.; Proceedings, P.G.-M.T.; 2022, undefined Custom Orthotics Development Process Based on Additive Manufacturing. *ElsevierP Patel, P GohilMaterials Today Proceedings, 2022•Elsevier*.

90. Ali, M.H.; Smagulov, Z.; Otepbergenov, T. Finite Element Analysis of the CFRP-Based 3D Printed Ankle-Foot Orthosis. *Procedia Comput. Sci.* **2021**, *179*, 55–62, doi:10.1016/J.PROCS.2020.12.008.

91. Culmone, C.; Smit, G.; Breedveld, P. Additive Manufacturing of Medical Instruments: A State-of-the-Art Review. *Addit. Manuf.* 2019, *27*, 461–473.

92. Ulmeanu, M.E.; Doicin, C. V.; Baila, D.I.; Rennie, A.E.W.; Neagu, C.; Laha, S. Comparative Evaluation of Optimum Additive Manufacturing Technology to Fabricate Bespoke Medical Prototypes of Composite Materials. *Mater. Plast.* **2015**, *52*, 416–422.

93. Dotz, A.D. A Pilot of 3D Printing of Medical Devices in Haiti. *Technol. Dev.* **2015**, 33–44, doi:10.1007/978-3-319-16247-8_4.

94. Bártolo, P.J.; Chua, C.K.; Almeida, H.A.; Chou, S.M.; Lim, A.S.C. Biomanufacturing for Tissue Engineering: Present and Future Trends. *Virtual Phys. Prototyp.* **2009**, *4*, 203–216, doi:10.1080/17452750903476288.

95. Hospodiuk, M.; Dey, M.; Sosnoski, D.; Ozbolat, I.T. The Bioink: A Comprehensive Review on Bioprintable Materials. *Biotechnol. Adv.* **2017**, *35*, 217–239, doi:10.1016/j.biotechadv.2016.12.006.

96. Rezvani Ghomi, E.; Khosravi, F.; Neisiany, R.E.; Singh, S.; Ramakrishna, S. Future of Additive Manufacturing in Healthcare. *Curr. Opin. Biomed. Eng.* 2021, *17*, 100255.

97. Amaya-Rivas, J.L.; Perero, B.S.; Helguero, C.G.; Hurel, J.L.; Peralta, J.M.; Flores, F.A.; Alvarado, J.D. Future Trends of Additive Manufacturing in Medical Applications: An Overview. *Heliyon* **2024**, *10*, e26641, doi:10.1016/j.heliyon.2024.e26641.

98. Kumar, S.; Singh, R.; Singh, T.P.; Batish, A. PLA Composite Matrix as Functional Prototypes for Four Dimensional Applications. *Encycl. Mater. Compos.* **2019**, *1*, 1091–1100, doi:10.1016/B978-0-12-803581-8.11595-4.

99. Salimon, A.I.; Senatov, F.S.; Kalyaev, V.A.; Korsunsky, A.M. Shape Memory Polymer Blends and Composites for 3D and 4D Printing Applications. *3D 4D Print. Polym. Nanocomposite Mater. Process. Appl. Challenges* **2020**, 161–189, doi:10.1016/B978-0-12-816805-9.00006-5.

100. Gazzaniga, A.; Foppoli, A.; Cerea, M.; Palugan, L.; Cirilli, M.; Moutaharrik, S.; Melocchi, A.; Maroni, A. Towards 4D Printing in Pharmaceutics. *Int. J. Pharm. X* **2023**, *5*, 100171, doi:10.1016/J.IJPX.2023.100171.

101. Zhou, Y.; Zhou, D.; Cao, P.; Zhang, X.; Wang, Q.; Wang, T.; Li, Z.; He, W.; Ju, J.; Zhang, Y. 4D Printing of Shape Memory Vascular Stent Based on BCD-g-Polycaprolactone. *Macromol. Rapid Commun.* **2021**, *42*, 1–9, doi:10.1002/marc.202100176.

102. Tian, X.; Wu, L.; Gu, D.; Yuan, S.; Zhao, Y.; Li, X.; Ouyang, L.; Song, B.; Gao, T.; He, J.; et al. Roadmap for Additive Manufacturing: Toward Intellectualization and Industrialization. *Chinese J. Mech. Eng. Addit. Manuf. Front.* **2022**, *1*, 100014, doi:10.1016/J.CJMEAM.2022.100014.

103. Ge, Q.; Sakhaei, A.H.; Lee, H.; Dunn, C.K.; Fang, N.X.; Dunn, M.L. Multimaterial 4D Printing with Tailorable Shape Memory Polymers. *Sci. Reports 2016 61* **2016**, *6*, 1–11, doi:10.1038/srep31110.

104. Lee Ventola, C. Medical Applications for 3D Printing: Current and Projected Uses. *Pharm. Ther.* **2014**, *39*, 704.

105. Wu, N.; Li, S.; Zhang, B.; Wang, C.; Chen, B.; Han, Q.; Wang, J. The Advances of Topology Optimization Techniques in Orthopedic Implants: A Review. *Med. Biol. Eng. Comput.* **2021**, *59*, 1673–1689, doi:10.1007/s11517-021-02361-7.

106. Tyagi, V.; Kumar, R.; Singh, P.L.; Shakkarwal, P. Barriers in Designing and Developing Products by Additive Manufacturing for Bio-Mechanics Systems in Healthcare Sector. *Mater. Today Proc.* **2021**, *50*, 1123–1128, doi:10.1016/j.matpr.2021.08.020.

107. Choo, Y.J.; Boudier-Revéret, M.; Chang, M.C. 3D Printing Technology Applied to Orthosis

Manufacturing: Narrative Review. *Ann. Palliat. Med.* **2020**, *9*, 4262270–4264270, doi:10.21037/APM-20-1185.

108. Shim, K.W. Medical Applications of 3D Printing and Standardization Issues. *Brain Tumor Res. Treat.* **2023**, *11*, 159, doi:10.14791/BTRT.2023.0001.

109. In Statista Which 3D Printing Technologies Do You Use? 2021.

110. *Global 3D Printing Filament Market Share Report, 2020-2027*;

111. Rajan, K.; Samykano, M.; Kadirgama, K.; Harun, W.S.W.; Rahman, M.M. *Fused Deposition Modeling: Process, Materials, Parameters, Properties, and Applications*; Springer London, 2022; Vol. 120; ISBN 0017002208860.

112. Ching, Y.C.; Udenni Gunathilake, T.M.S.; Ching, K.Y.; Chuah, C.H.; Sandu, V.; Singh, R.; Liou, N.S. Effects of High Temperature and Ultraviolet Radiation on Polymer Composites. *Durab. Life Predict. Biocomposites, Fibre-Reinforced Compos. Hybrid Compos.* **2019**, 407–426, doi:10.1016/B978-0-08-102290-0.00018-0.

113. Altıparmak, S.C.; Yardley, V.A.; Shi, Z.; Lin, J. Extrusion-Based Additive Manufacturing Technologies: State of the Art and Future Perspectives. *J. Manuf. Process.* **2022**, *83*, 607–636, doi:10.1016/j.jmapro.2022.09.032.

114. *Fused Deposition Modeling Based 3D Printing*; Dave, H.K., Davim, J.P., Eds.; Materials Forming, Machining and Tribology; Springer International Publishing: Cham, 2021; ISBN 978-3-030-68023-7.

115. Lakkala, P.; Munnangi, S.R.; Bandari, S.; Repka, M. Additive Manufacturing Technologies with Emphasis on Stereolithography 3D Printing in Pharmaceutical and Medical Applications: A Review. *Int. J. Pharm. X* **2023**, *5*, doi:10.1016/J.IJPX.2023.100159.

116. McDonagh, T.; Belton, P.; Qi, S. Manipulating Drug Release from 3D Printed Dual-Drug Loaded Polypills Using Challenging Polymer Compositions. *Int. J. Pharm.* **2023**, *637*, 122895, doi:10.1016/j.ijpharm.2023.122895.

117. Patel, N.G.; Serajuddin, A.T.M. Development of FDM 3D-Printed Tablets with Rapid Drug Release, High Drug-Polymer Miscibility and Reduced Printing Temperature by Applying the Acid-Base Supersolubilization (ABS) Principle. *Int. J. Pharm.* **2021**, *600*, 120524, doi:10.1016/J.IJPHARM.2021.120524.

118. Anderson, K.; Anderson, L.E.; Glanze, W.D. *Mosby's Medical, Nursing, & Allied Health Dictionary*; Mosby, 1998; ISBN 0815148003.

119. Braverman, S.E. Orthotics for the Fighting Force. *Phys. Med. Rehabil. Clin. N. Am.* **2002**, *13*, 159–173, doi:10.1016/S1047-9651(03)00076-7.

120. International Organization for Standardization. ISO 8551:2020 - Prosthetics and Orthotics - Functional Deficiencies - Description of the Person to Be Treated with an Orthosis, Clinical Objectives of Treatment, and Functional Requirements of the Orthosis 2020.

121. Tran, K.; Spry, C. Custom-Made Foot Orthoses versus Prefabricated Foot Orthoses: A Review of Clinical Effectiveness and Cost-Effectiveness. *Ottawa Can. Agency Drugs Technol. Heal.* **2019**, 1–16.

122. Boyd, A.S.; Benjamin, H.J.; Asplund, C. Principles of Casting and Splinting. *Am. Fam. Physician* **2009**, *79*.

123. Paterson, A.M.; Bibb, R.; Campbell, R.I.; Bingham, G. Comparing Additive Manufacturing Technologies for Customised Wrist Splints. *undefined* **2015**, *21*, 230–243, doi:10.1108/RPJ-10-2013-0099.

124. Althoff, A.D.; Reeves, R.A. *Splinting*; StatPearls Publishing, 2022;

125. Mian, S.H.; Abouel Nasr, E.; Moiduddin, K.; Saleh, M.; Abidi, M.H.; Alkhalefah, H. Assessment of Consolidative Multi-Criteria Decision Making (C-MCDM) Algorithms for Optimal Mapping of Polymer Materials in Additive Manufacturing: A Case Study of Orthotic Application. *Heliyon* **2024**, *10*, e30867, doi:10.1016/J.HELIYON.2024.E30867.

126. Chen, R.K.; Jin, Y. an; Wensman, J.; Shih, A. Additive Manufacturing of Custom Orthoses and Prostheses—A Review. *Addit. Manuf.* **2016**, *12*, 77–89, doi:10.1016/J.ADDMA.2016.04.002.

127. Wang, Y.; Tan, Q.; Pu, F.; Boone, D.; Zhang, M. A Review of the Application of Additive Manufacturing in Prosthetic and Orthotic Clinics from a Biomechanical Perspective. *Engineering* **2020**, *6*, 1258–1266, doi:10.1016/J.ENG.2020.07.019.

128. Paterson, A.M.; Bibb, R.; Campbell, R.I.; Bingham, G. Comparing Additive Manufacturing Technologies for Customised Wrist Splints. *Rapid Prototyp. J.* **2015**, *21*, 230–243, doi:10.1108/RPJ-10-2013-0099.

129. Halanski, M.; Noonan, K.J. Cast and Splint Immobilization: Complications. *J. Am. Acad. Orthop. Surg.* **2008**, *16*, 30–40, doi:10.5435/00124635-200801000-00005.

130. Nouri, A.; Wang, L.; Li, Y.; Wen, C. Materials and Manufacturing for Ankle–Foot Orthoses: A Review. *Adv. Eng. Mater.* **2023**, *25*, doi:10.1002/adem.202300238.

131. Alqahtani, M.S.; Al-Tamimi, A.A.; Hassan, M.H.; Liu, F.; Bartolo, P. Optimization of a Patient-Specific External Fixation Device for Lower Limb Injuries. *Polymers (Basel).* **2021**, *13*, doi:10.3390/POLYM13162661.

132. Vasiliauskaite, E.; Ielapi, A.; De Beule, M.; Van Paepegem, W.; Deckers, J.P.; Vermandel, M.; Forward, M.; Plasschaert, F. A Comparative Analysis between Conventional Manufacturing and Additive Manufacturing of Ankle-Foot Orthosis. *Appl. Sci. Eng. Prog.* **2020**, *13*, 96–103, doi:10.1080/17483107.2019.1629114.

133. ISO 10993-1:2018 - Biological Evaluation of Medical Devices.

134. Bohinc, K.; Abram, A.; Zore, A.; Štukelj, R.; Lenarčič, A.; Vidrih, R.; Škapin, A.S. Biophysical Properties of Foamed and Solid Polymers Used in Orthotics and Prosthetics. *Materials (Basel).* **2021**, *14*, 6877, doi:10.3390/MA14226877/S1.

135. Mian, S.H.; Abouel Nasr, E.; Moiduddin, K.; Saleh, M.; Alkhalefah, H. An Insight into the Characteristics of 3D Printed Polymer Materials for Orthoses Applications: Experimental Study. *Polym. 2024, Vol. 16, Page 403* **2024**, *16*, 403, doi:10.3390/POLYM16030403.

136. Memarian, F.; Fereidoon, A.; Ghorbanzadeh Ahangari, M. Effect of Acrylonitrile Butadiene Styrene on the Shape Memory, Mechanical, and Thermal Properties of Thermoplastic Polyurethane. *J. Vinyl Addit. Technol.* **2018**, *24*, E96–E104, doi:10.1002/VNL.21601.

137. Xu, T.; Shen, W.; Lin, X.; Xie, Y.M. Mechanical Properties of Additively Manufactured Thermoplastic Polyurethane (TPU) Material Affected by Various Processing Parameters. *Polym. 2020, Vol. 12, Page 3010* **2020**, *12*, 3010, doi:10.3390/POLYM12123010.

138. Deckers, J.P.; Vermandel, M.; Geldhof, J.; Vasiliauskaite, E.; Forward, M.; Plasschaert, F. Development and Clinical Evaluation of Laser-Sintered Ankle Foot Orthoses. *https://doi.org/10.1080/14658011.2017.1413760* **2018**, *47*, 42–46, doi:10.1080/14658011.2017.1413760.

139. Turek, P.; Bazan, A.; Zakrecki, A. Influence of Post-Processing Treatment on the Surface Roughness of Polyamide PA12 Samples Manufactured Using Additive Methods in the Context of the Production of Orthoses. *Proc. Inst. Mech. Eng. Part B J. Eng. Manuf.* **2023**, doi:10.1177/09544054231202423.

140. Silva, R.; Silva, B.; Fernandes, C.; Morouço, P.; Alves, N.; Veloso, A. A Review on 3D Scanners Studies for Producing Customized Orthoses. *Sensors 2024, Vol. 24, Page 1373* **2024**, *24*, 1373, doi:10.3390/S24051373.

141. Ciobanu, O.; Ciobanu, G.; Rotariu, M. Photogrammetric Scanning Technique and Rapid Prototyping Used for Prostheses and Ortheses Fabrication. *Appl. Mech. Mater.* **2013**, *371*, 230–234, doi:10.4028/WWW.SCIENTIFIC.NET/AMM.371.230.

142. Dal Maso, A.; Cosmi, F. 3D-Printed Ankle-Foot Orthosis: A Design Method. *Mater. Today Proc.* **2019**, *12*, 252–261, doi:10.1016/J.MATPR.2019.03.122.

143. Baronio, G.; Harran, S.; Signoroni, A. A Critical Analysis of a Hand Orthosis Reverse Engineering and 3D Printing Process. *Appl. Bionics Biomech.* **2016**, *2016*, doi:10.1155/2016/8347478.

144. TUDelft 3D Handscanner Available online: https://www.tudelft.nl/en/ide/research/research-labs/applied-labs/3d-handscanner.

145. Carfagni, M.; Furferi, R.; Governi, L.; Servi, M.; Uccheddu, F.; Volpe, Y.; Mcgreevy, K. Fast and Low Cost Acquisition and Reconstruction System for Human Hand-Wrist-Arm Anatomy. *Procedia Manuf.* **2017**, *11*, 1600–1608, doi:10.1016/J.PROMFG.2017.07.306.

146. Buonamici, F.; Furferi, R.; Governi, L.; Lazzeri, S.; McGreevy, K.S.; Servi, M.; Talanti, E.; Uccheddu, F.; Volpe, Y. A Practical Methodology for Computer-Aided Design of Custom 3D Printable Casts for Wrist Fractures. *Vis. Comput.* **2020**, *36*, 375–390, doi:10.1007/S00371-018-01624-Z.

147. Li, J.; Tanaka, H. Feasibility Study Applying a Parametric Model as the Design Generator for 3D–Printed Orthosis for Fracture Immobilization. *3D Print. Med. 2018 41* **2018**, *4*, 1–15, doi:10.1186/S41205-017-0024-1.

148. Paoli, A.; Neri, P.; Razionale, A. V.; Tamburrino, F.; Barone, S. Sensor Architectures and Technologies for Upper Limb 3d Surface Reconstruction: A Review. *Sensors (Switzerland)* **2020**, *20*, 1–33, doi:10.3390/S20226584.

149. Nam, H.S.; Seo, C.H.; Joo, S.Y.; Kim, D.H.; Park, D.S. The Application of Three-Dimensional Printed Finger Splints for Post Hand Burn Patients: A Case Series Investigation. *Ann. Rehabil. Med.* **2018**, *42*, 634–638, doi:10.5535/ARM.2018.42.4.634.

150. Rogati, G.; Leardini, A.; Ortolani, M.; Caravaggi, P. Validation of a Novel Kinect-Based Device for 3D Scanning of the Foot Plantar Surface in Weight-Bearing. *J. Foot Ankle Res.* **2019**, *12*, doi:10.1186/S13047-019-0357-7.

151. Palousek, D.; Rosicky, J.; Koutny, D.; Stoklásek, P.; Navrat, T. Pilot Study of the Wrist Orthosis Design Process. *Rapid Prototyp. J.* **2014**, *20*, 27–32, doi:10.1108/RPJ-03-2012-0027.

152. Kim, H.; Jeong, S. Case Study: Hybrid Model for the Customized Wrist Orthosis Using 3D Printing. *J. Mech. Sci. Technol. 2015 2912* **2015**, *29*, 5151–5156, doi:10.1007/S12206-015-1115-9.

153. Blaya, F.; Pedro, P.S.; Silva, J.L.; D'Amato, R.; Heras, E.S.; Juanes, J.A. Design of an Orthopedic Product by Using Additive Manufacturing Technology: The Arm Splint. *J. Med. Syst.* **2018**, *42*, doi:10.1007/S10916-018-0909-6.

154. Parry, E.J.; Best, J.M.; Banks, C.E. Three-Dimensional (3D) Scanning and Additive Manufacturing (AM) Allows the Fabrication of Customised Crutch Grips. *Mater. Today Commun.* **2020**, *25*, 101225, doi:10.1016/J.MTCOMM.2020.101225.

155. Cirello, A.; Ingrassia, T.; Marannano, G.; Mirulla, A.I.; Nigrelli, V.; Petrucci, G.; Ricotta, V. A New Automatic Process Based on Generative Design for CAD Modeling and Manufacturing of Customized Orthosis. *Appl. Sci.* **2024**, *14*, doi:10.3390/APP14146231.

156. Wang, X.V.; Xu, P.; Cui, M.; Yu, X.; Wang, L. A Literature Survey of Smart Manufacturing Systems for Medical Applications. *J. Manuf. Syst.* **2024**, *76*, 502–519, doi:10.1016/J.JMSY.2024.08.017.

157. Anderson, D.M. *Mosby's Medical, Nursing, & Allied Health Dictionary*; Mosby, 2002; ISBN 0323014305.

158. Fey, N.P.; South, B.J.; Seepersad, C.C.; Neptune, R.R. Topology Optimization and Freeform Fabrication Framework for Developing Prosthetic Feet. *20th Annu. Int. Solid Free. Fabr. Symp. SFF 2009* **2009**, 607–619.

159. Pallari, J.H.P.; Dalgarno, K.W.; Woodburn, J. Mass Customization of Foot Orthoses for Rheumatoid Arthritis Using Selective Laser Sintering. *IEEE Trans. Biomed. Eng.* **2010**, *57*, 1750–1756, doi:10.1109/TBME.2010.2044178.

160. Geoffroy, M.; Gardan, J.; Asadollahiyazdi, E.; Laurent, S.; Lapotre, J.; Goodnough, J.; Mattie, J.; Wright, J.; Bates, S. Cranial Remodeling Orthosis for Infantile Plagiocephaly Created through a 3D Scan, Topological Optimization, and 3D Printing Process. *J. Prosthetics Orthot.* **2018**, *30*, 247–258, doi:10.1097/JPO.0000000000000190.

161. Sotola, M.; Stareczek, D.; Rybansky, D.; Prokop, J.; Marsalek, P. New Design Procedure of Transtibial ProsthesisBed Stump Using Topological Optimization Method. *Symmetry 2020, Vol. 12, Page 1837* **2020**, *12*, 1837, doi:10.3390/SYM12111837.

162. Zolfagharian, A.; Gregory, T.M.; Bodaghi, M.; Gharaie, S.; Fay, P. Patient-Specific 3D-

Printed Splint for Mallet Finger Injury. *Int. J. Bioprinting* **2020**, *6*, 1–13, doi:10.18063/IJB.V6I2.259.

163. Hanafusa, A.; Jamaludin, M.S.; Tuan, L. Van; Ikebata, H.; Suzuki, R.; Kawamura, T.; Yamamoto, S. ichiro; Agarie, Y.; Otsuka, H.; Ohnishi, K. Introduction of Prosthesis and Orthosis Evaluation System That Utilizes Human Models. *IFMBE Proc.* **2021**, *82*, 93–101, doi:10.1007/978-3-030-66169-4_13.

164. Reis, P.; Volpini, M.; Pimenta Maia, J.; Batista Guimarães, I.; Evelise, C.; Monteiro, M.; Carlos Campos Rubio, J. Resting Hand Splint Model from Topology Optimization to Be Produced by Additive Manufacturing. *Rapid Prototypying J.* **2021**, doi:10.1108/RPJ-07-2020-0176.

165. Khan, S.F.; Radzmi, I. Design and Analysis of Various Thermoplastic for Optimized Ankle Foot Orthosis. *J. Phys. Conf. Ser.* **2021**, *2051*, 012034, doi:10.1088/1742-6596/2051/1/012034.

166. Ambu, R.; Oliveri, S.M.; Calì, M. Neck Orthosis Design for 3D Printing with User Enhanced Comfort Features. *Int. J. Interact. Des. Manuf.* **2023**, doi:10.1007/S12008-023-01507-1.

167. Popescu, D.; Lăptoiu, D.; Căruțașu, N.L. Considerations on the Design, Printability and Usability of Customized 3D-Printed Upper Limb Orthoses. *Appl. Sci.* **2024**, *14*, doi:10.3390/APP14146157.

168. Michalec, P.; Schusser, M.; Weidner, R.; Brandstötter, M. Designing Hand Orthoses: Advances and Challenges in Material Extrusion. *Appl. Sci.* **2024**, *14*, doi:10.3390/APP14209543.

169. Vafadar, A.; Guzzomi, F.; Rassau, A.; Hayward, K. Advances in Metal Additive Manufacturing: A Review of Common Processes, Industrial Applications, and Current Challenges. *Appl. Sci. 2021, Vol. 11, Page 1213* **2021**, *11*, 1213, doi:10.3390/APP11031213.

170. AMPower Metal Additive Manufacturing's Journey to Industrialisation 2023.

171. Arrizubieta, J.I.; Ukar, O.; Ostolaza, M.; Mugica, A. Study of the Environmental Implications of Using Metal Powder in Additive Manufacturing and Its Handling. *Met. 2020, Vol. 10, Page 261* **2020**, *10*, 261, doi:10.3390/MET10020261.

172. Kukla, C.; Gonzalez-Gutierrez, J.; Cano, S.; Hampel, S. Fused Filament Fabrication (FFF) of PIM Feedstocks. *Proc. VI Congr. Nac. Pulvimetalurgia y I Congr. Iberoam. Pulvimetalurgia, Ciudad Real, Spain* **2017**, 7–9.

173. Singh, P.; Balla, V.K.; Tofangchi, A.; Atre, S. V.; Kate, K.H. Printability Studies of Ti-6Al-4V by Metal Fused Filament Fabrication (MF3). *Int. J. Refract. Met. Hard Mater.* **2020**, *91*, doi:10.1016/J.IJRMHM.2020.105249.

174. Thompson, Y.; Gonzalez-Gutierrez, J.; Kukla, C.; Felfer, P. Fused Filament Fabrication, Debinding and Sintering as a Low Cost Additive Manufacturing Method of 316L Stainless Steel. *Addit. Manuf.* **2019**, *30*, doi:10.1016/J.ADDMA.2019.100861.

175. Carrozza, A.; Lorenzi, S.; Carugo, F.; Fest-Santini, S.; Santini, M.; Marchese, G.; Barbieri, G.; Cognini, F.; Cabrini, M.; Pastore, T. A Comparative Analysis between Material Extrusion and Other Additive Manufacturing Techniques: Defects, Microstructure and Corrosion Behavior in Nickel Alloy 625. *Mater. Des.* **2023**, *225*, 111545, doi:10.1016/J.MATDES.2022.111545.

176. Brackett, J.; Cauthen, D.; Condon, J.; Smith, T.; Gallego, N.; Kunc, V.; Duty, C. The Impact of Infill Percentage and Layer Height in Small-Scale Material Extrusion on Porosity and Tensile Properties. *Addit. Manuf.* **2022**, *58*, 103063, doi:10.1016/J.ADDMA.2022.103063.

177. Singh, P.; Balla, V.K.; Atre, S. V.; German, R.M.; Kate, K.H. Factors Affecting Properties of Ti-6Al-4V Alloy Additive Manufactured by Metal Fused Filament Fabrication. *Powder Technol.* **2021**, *386*, 9–19, doi:10.1016/J.POWTEC.2021.03.026.

178. Naim, M.; Chemkhi, M.; Kauffmann, J.; Alhussein, A. Taguchi DoE Analysis and Characterization of 17-4 PH Stainless Steel Parts Produced by Material Extrusion (MEX) Process. *Adv. Ind. Manuf. Eng.* **2024**, *8*, 100138, doi:10.1016/J.AIME.2024.100138.

179. Singh, G.; Missiaen, J.M.; Bouvard, D.; Chaix, J.M. Copper Extrusion 3D Printing Using Metal Injection Moulding Feedstock: Analysis of Process Parameters for Green Density and Surface Roughness Optimization. *Addit. Manuf.* **2021**, *38*, doi:10.1016/J.ADDMA.2020.101778.

180. Meng, F.; Beretta, M.; Selema, A.; Sergeant, P.; Vleugels, J.; Desplentere, F.; Ferraris, E. Production and Characterisation of Filament-Based Material Extrusion (MEX) Additively Manufactured Copper Parts. *Procedia CIRP* **2024**, *121*, 234–239, doi:10.1016/J.PROCIR.2023.09.253.

181. Côté, R.; Demers, V.; Demarquette, N.R.; Charlon, S.; Soulestin, J. A Strategy to Eliminate Interbead Defects and Improve Dimensional Accuracy in Material Extrusion 3D Printing of Highly Filled Polymer. *Addit. Manuf.* **2023**, *68*, 103509, doi:10.1016/J.ADDMA.2023.103509.

182. Masood, S.H. Advances in Fused Deposition Modeling. *Compr. Mater. Process. Thirteen Vol. Set* **2014**, *10*, 69–91, doi:10.1016/B978-0-08-096532-1.01002-5.

183. Gordelier, T.J.; Thies, P.R.; Turner, L.; Johanning, L. Optimising the FDM Additive Manufacturing Process to Achieve Maximum Tensile Strength: A State-of-the-Art Review. *Rapid Prototyp. J.* **2019**, *25*, 953–971, doi:10.1108/RPJ-07-2018-0183.

184. Iyer, S.; Mcintosh, J.; Bandyopadhyay, A.; Langrana, N.; Safari, A.; Danforth, S.C.; Clancy, R.B.; Gasdaska, C.; Whalen, P.J. Microstructural Characterization and Mechanical Properties of Si3N4 Formed by Fused Deposition of Ceramics. *Int. J. Appl. Ceram. Technol.* **2008**, *5*, 127–137, doi:10.1111/J.1744-7402.2008.02193.X.

185. Liu, Z.; Lei, Q.; Xing, S. Mechanical Characteristics of Wood, Ceramic, Metal and Carbon Fiber-Based PLA Composites Fabricated by FDM. *J. Mater. Res. Technol.* **2019**, *8*, 3743–3753, doi:10.1016/J.JMRT.2019.06.034.

186. Shaikh, M.Q.; Lavertu, P.Y.; Kate, K.H.; Atre, S. V. Process Sensitivity and Significant Parameters Investigation in Metal Fused Filament Fabrication of Ti-6Al-4V. *J. Mater. Eng. Perform.* **2021**, *30*, 5118–5134, doi:10.1007/S11665-021-05666-8/TABLES/7.

187. Shaikh, M.Q.; Singh, P.; Kate, K.H.; Freese, M.; Atre, S. V. Finite Element-Based Simulation of Metal Fused Filament Fabrication Process: Distortion Prediction and Experimental Verification. *J. Mater. Eng. Perform.* **2021**, *30*, 5135–5149, doi:10.1007/S11665-021-05733-0/FIGURES/14.

188. Singh, P.; Balla, V.K.; Gokce, A.; Atre, S. V.; Kate, K.H. Additive Manufacturing of Ti-6Al-4V Alloy by Metal Fused Filament Fabrication (MF3): Producing Parts Comparable to That of Metal Injection Molding. *Prog. Addit. Manuf.* **2021**, *6*, 593–606, doi:10.1007/S40964-021-00167-5/FIGURES/8.

189. Shaikh, M.Q.; Nath, S.D.; Akilan, A.A.; Khanjar, S.; Balla, V.K.; Grant, G.T.; Atre, S.V. Investigation of Patient-Specific Maxillofacial Implant Prototype Development by Metal Fused Filament Fabrication (MF3) of Ti-6Al-4V. *Dent. J. 2021, Vol. 9, Page 109* **2021**, *9*, 109, doi:10.3390/DJ9100109.

190. García de la Cruz, L.; Alvaredo, P.; Torralba, J.M.; Campos, M. Material Extrusion: A Promising Tool for Processing CoCrMo Alloy with Excellent Wear Resistance for Biomedical Applications. *Mater. Des.* **2024**, *244*, 113089, doi:10.1016/J.MATDES.2024.113089.

191. Yim, S.; Rosen, D. Build Time and Cost Models for Additive Manufacturing Process

Selection. *Proc. ASME Des. Eng. Tech. Conf.* **2012**, *2*, 375–382, doi:10.1115/DETC2012-70940.

192. Ruffo, M.; Hague, R. Cost Estimation for Rapid Manufacturing - Simultaneous Production of Mixed Components Using Laser Sintering. *Proc. Inst. Mech. Eng. Part B J. Eng. Manuf.* **2007**, *221*, 1585–1591, doi:10.1243/09544054JEM894.

193. International Organization for Standardization. UNI EN ISO 6892-1:2020 - Metallic Materials - Tensile Testing - Part 1: Method of Test at Room Temperature. 2020.

194. International Organization for Standardardization. EN ISO 7438:2020 - Metallic Materials - Bend Tests 2020.

195. American Society of Hand Therapies *Splint Classification System*; The American Society of Hand Therapists: Garner, NC, 1992;

196. Bailey, J.; Cannon, N.; Colditz, J.; Fess, E.; Gettle, K.; DeMott, L. *Splint Classification System*; The American Society of Hand Therapists, 1992;

197. Coppard, B.M.; Lohman, H. *Introduction to Splinting : A Clinical Reasoning and Problem-Solving Approach*; Mosby, 2008; ISBN 0323033849.

198. Sala, F.; Carminati, M.; D'Urso, G.; Giardini, C. A Feasibility Analysis of a 3D Customized Upper Limb Orthosis. *Procedia CIRP* **2022**, *110*, 207–212, doi:10.1016/J.PROCIR.2022.06.038.

199. Cber, C. Use of International Standard ISO 10993-1, "Biological Evaluation of Medical Devices-Part 1: Evaluation and Testing within a Risk Management Process" Guidance for Industry and Food and Drug Administration Staff Preface Public Comment. **2020**.

200. Ultimaker Recommended Printing Settings and Configurations for Ultimaker ABS Available online: https://support.makerbot.com/s/article/1667337602935.

201. Ultimaker Recommended Printing Settings and Configurations for Ultimaker Nylon Available online: https://support.makerbot.com/s/article/1667337602768.

202. Ultimaker Reccomended Printing Settings and Configurations for Ultimaker PLA Available online: https://support.makerbot.com/s/article/1667337611872.

203. Ultimaker Recommended Printing Settings and Configurations for Ultimaker PC Available online: https://support.makerbot.com/s/article/1667337602519.

204. Polymaker PolyMide PA6-GF - Technical Data Sheet Available online: https://c-

3d.niceshops.com/upload/file/PolyMide_PA6_GF_TDS_V5.1.pdf.

205. Polymaker PolyMide PA6-CF - Technical Data Sheet Available online: https://c-3d.niceshops.com/upload/file/PolyMide_PA6_CF_TDS_V5.1.pdf.

206. Ultimaker Ultimaker Breakaway - Technical Data Sheet Available online: https://ultimaker.my.salesforce.com/sfc/p/#j0000000HOnW/a/5b000004Udwf/FxKwB7aukJUO6tPWfTUYr089QQMY3u1bPhreKFrXDs4.

207. Ultimaker Ultimaker ABS - Technical Data Sheet Available online: https://ultimaker.my.salesforce.com/sfc/p/#j0000000HOnW/a/5b000004UX1e/ymaTcu23yezPH0a2.9qJEJYtA_pvXVnTcQMeWNRiIaY.

208. Ultimaker Ultimaker Nylon - Technical Data Sheet Available online: https://ultimaker.my.salesforce.com/sfc/p/#j0000000HOnW/a/5b000004UiEo/LIYV6VDfKlwDuaqc.9FhLVGIN0sN96YivUwV0fu7ylA.

209. Ultimaker Ultimaker PLA - Technical Data Sheet Available online: https://ultimaker.my.salesforce.com/sfc/p/#j0000000HOnW/a/5b000004Uiac/95CBv380plulni.oGx.QVyYZTOIJAc6d_BypJjAmeok.

210. Ultimaker Ultimaker PC - Technical Data Sheet Available online: https://ultimaker.my.salesforce.com/sfc/p/#j0000000HOnW/a/5b000004TlDg/NmLGE1iImMnHn_5T0YLumlngSpw3CsXc3.ge1aCf_mE.

211. Chen, Y.-J.; Lin, H.; Zhang, X.; Huang, W.; Shi, L.; Wang, D. Application of 3D-Printed and Patient-Specific Cast for the Treatment of Distal Radius Fractures: Initial Experience., doi:10.1186/s41205-017-0019-y.

212. Lin, H.; Shi, L.; Wang, D. A Rapid and Intelligent Designing Technique for Patient-Specific and 3D-Printed Orthopedic Cast. *3D Print. Med. 2016 21* **2016**, *2*, 1–10, doi:10.1186/S41205-016-0007-7.

213. Brett, A.M. Failure Analysis and Prevention, Fatigue Failures. *ASM Int. Handb.* **2002**, *11*.

214. DeStefano, V.; Khan, S.; Tabada, A. Applications of PLA in Modern Medicine. *Eng. Regen.* **2020**, *1*, 76–87, doi:10.1016/J.ENGREG.2020.08.002.

215. Sabyrov, N.; Sotsial, Z.; Abilgaziyev, A.; Adair, D.; Ali, M.H. Design of a Flexible Neck Orthosis on Fused Deposition Modeling Printer for Rehabilitation on Regular Usage. *Procedia Comput. Sci.* **2021**, *179*, 63–71, doi:10.1016/J.PROCS.2020.12.009.

216. Mali, H.S.; Vasistha, S. Fabrication of Customized Ankle Foot Orthosis (AFO) by Reverse

Engineering Using Fused Deposition Modelling. *Lect. Notes Multidiscip. Ind. Eng.* **2020**, *Part F164*, 3–15, doi:10.1007/978-981-32-9433-2_1/FIGURES/12.

217. Liu, S.; Li, Q.; Liu, J.; Chen, W.; Zhang, Y. A Realization Method for Transforming a Topology Optimization Design into Additive Manufacturing Structures. *Engineering* **2018**, *4*, 277–285, doi:10.1016/j.eng.2017.09.002.

218. Yan, W.; Ding, M.; Kong, B.; Xi, X.B.; Zhou, M. Lightweight Splint Design for Individualized Treatment of Distal Radius Fracture. *J. Med. Syst.* **2019**, *43*, doi:10.1007/S10916-019-1404-4.

219. Sigmund, O.; Maute, K. Topology Optimization Approaches: A Comparative Review. *Struct. Multidiscip. Optim.* **2013**, *48*, 1031–1055, doi:10.1007/S00158-013-0978-6/FIGURES/2.

220. Bendsøe, M.P.; Kikuchi, N. Generating Optimal Topologies in Structural Design Using a Homogenization Method. *Comput. Methods Appl. Mech. Eng.* **1988**, *71*, 197–224, doi:10.1016/0045-7825(88)90086-2.

221. Bendsøe, M.P. Optimal Shape Design as a Material Distribution Problem. *Struct. Optim.* **1989**, *1*, 193–202, doi:10.1007/BF01650949/METRICS.

222. Zhou, M.; Rozvany, G.I.N. The COC Algorithm, Part II: Topological, Geometrical and Generalized Shape Optimization. *Comput. Methods Appl. Mech. Eng.* **1991**, *89*, 309–336, doi:10.1016/0045-7825(91)90046-9.

223. Mlejnek, H.P. Some Aspects of the Genesis of Structures. *Struct. Optim.* **1992**, *5*, 64–69, doi:10.1007/BF01744697/METRICS.

224. Schwartz, D.A.; Schofield, K.A. Utilization of 3D Printed Orthoses for Musculoskeletal Conditions of the Upper Extremity: A Systematic Review. *J. Hand Ther.* **2021**, doi:10.1016/J.JHT.2021.10.005.

225. Jin, Z.; Li, Y.; Yu, K.; Liu, L.; Fu, J.; Yao, X.; Zhang, A.; He, Y. 3D Printing of Physical Organ Models: Recent Developments and Challenges. *Adv. Sci.* **2021**, *8*, doi:10.1002/ADVS.202101394.

226. Li, J.; Tanaka, H. Rapid Customization System for 3D-Printed Splint Using Programmable Modeling Technique – a Practical Approach. *3D Print. Med. 2018 41* **2018**, *4*, 1–21, doi:10.1186/S41205-018-0027-6.

227. Bendsøe, M.P.; Sigmund, O. Topology Optimization. *Topol. Optim.* **2004**, doi:10.1007/978-3-662-05086-6.

228. Sala, F.; D'Urso, G.; Giardini, C. Customized Wrist Immobilization Splints Produced via

Additive Manufacturing—A Comprehensive Evaluation of the Viable Configurations. *Prosthes. 2023, Vol. 5, Pages 792-808* **2023**, *5*, 792–808, doi:10.3390/PROSTHESIS5030056.

229. Ahmed, N.; Barsoum, I.; Haidemenopoulos, G.; Al-Rub, R.K.A. Process Parameter Selection and Optimization of Laser Powder Bed Fusion for 316L Stainless Steel: A Review. *J. Manuf. Process.* **2022**, *75*, 415–434, doi:10.1016/j.jmapro.2021.12.064.

230. Jia, H.; Sun, H.; Wang, H.; Wu, Y.; Wang, H. Scanning Strategy in Selective Laser Melting (SLM): A Review. *Int. J. Adv. Manuf. Technol.* **2021**, *113*, 2413–2435, doi:10.1007/s00170-021-06810-3.

231. Robinson, J.H.; Robert, I.; Ashton, T.; Jones, E.; Fox, P.; Sutcliffe, C. The Effect of Hatch Angle Rotation on Parts Manufactured Using Selective Laser Melting., doi:10.1108/RPJ-06-2017-0111.

232. Singh, R. Welding Corrosion Resistant Alloys – Stainless Steel. *Appl. Weld. Eng.* **2012**, 191–214, doi:10.1016/B978-0-12-391916-8.00018-2.

233. Yang, K.; Ren, Y. Nickel-Free Austenitic Stainless Steels for Medical Applications. *Sci. Technol. Adv. Mater.* **2010**, *11*, 014105, doi:10.1088/1468-6996/11/1/014105.

234. Chua, K.; Khan, I.; Malhotra, R.; Zhu, D. Additive Manufacturing and 3D Printing of Metallic Biomaterials. *Eng. Regen.* **2021**, *2*, 288–299, doi:10.1016/J.ENGREG.2021.11.002.

235. Quarto, M.; Carminati, M.; D'Urso, G. Density and Shrinkage Evaluation of AISI 316L Parts Printed via FDM Process. *Mater. Manuf. Process.* **2021**, *36*, 1535–1543, doi:10.1080/10426914.2021.1905830.

236. D'Andrea, D. Additive Manufacturing of AISI 316L Stainless Steel: A Review. *Met. 2023, Vol. 13, Page 1370* **2023**, *13*, 1370, doi:10.3390/MET13081370.

237. Suryawanshi, J.; Prashanth, K.G.; Ramamurty, U. Mechanical Behavior of Selective Laser Melted 316L Stainless Steel. *Mater. Sci. Eng. A* **2017**, *696*, 113–121, doi:10.1016/J.MSEA.2017.04.058.

238. Gatões, D.; Alves, R.; Alves, B.; Vieira, M.T. Selective Laser Melting and Mechanical Properties of Stainless Steels. *Materials (Basel).* **2022**, *15*, doi:10.3390/ma15217575.

239. Xu, M.; Guo, H.; Wang, Y.; Hou, Y.; Dong, Z.; Zhang, L. Mechanical Properties and Microstructural Characteristics of 316L Stainless Steel Fabricated by Laser Powder Bed Fusion and Binder Jetting. *J. Mater. Res. Technol.* **2023**, *24*, 4427–4439, doi:10.1016/J.JMRT.2023.04.069.

240. Huang, G.; Wei, K.; Deng, J.; Liu, M.; Zeng, X. High-Power Laser Powder Bed Fusion of 316L Stainless Steel: Defects, Microstructure, and Mechanical Properties. *J. Manuf. Process.* **2022**, *83*, 235–245, doi:10.1016/J.JMAPRO.2022.08.066.

241. ASTM International. ASTM F3122-14 - Standard Guide for Evaluating Mechanical Properties of Metal Materials Made via Additive Manufacturing Processes 2014.

242. International Organization for Standardization. UNI EN ISO 6507-1:2018 - Metallic Materials - Vickers Hardness Test - Part 1: Test Method. 2018.